# Boundary Shear Stress Along Vegetated Streambanks

Leslie Clark Hopkinson

Dissertation submitted to the faculty of the Virginia Polytechnic Institute and State University in partial fulfillment of the requirements for the degree of

Doctor of Philosophy

In

Biological Systems Engineering

Theresa M. Wynn
W. Cully Hession
Panos Diplas
Clinton L. Dancey
C. Andy Dolloff

October 20, 2009
Blacksburg, Virginia

Keywords: Streambank erosion, Reynolds stress, streambank vegetation, turbulent kinetic energy, vegetated flow

# Boundary Shear Stress Along Vegetated Streambanks

Leslie Clark Hopkinson

## Abstract

This research is intended to determine the role of riparian vegetation in stream morphology. This experiment examined the effects of riparian vegetation on boundary shear stress (BSS) by completing the following objectives: (1) evaluating the effects of streambank vegetation on near-bank velocity and turbulence; (2) determining a method for measuring BSS; and, (3) examining the effects of streambank vegetation on BSS using an existing model.

A second order prototype stream, with individual reaches dominated by the three vegetation types (trees, shrubs, and grass) was modeled using a fixed-bed Froude-scale modeling technique. One model streambank of the prototype stream was constructed for each vegetation type in addition to one bank with only grain roughness. Velocity profiles were measured using an acoustic Doppler velocimeter (ADV) and a miniature propeller (MP). A flush-mounted Dantec MiniCTA system was used to measure shear stress at the streambank wall.

The addition of vegetation on a sloping streambank increased the streamwise free stream velocity and decreased the near-bank streamwise velocity. The turbulence caused by the upright shrub treatment increased turbulent kinetic energy and Reynolds stresses near the streambank toe, an area susceptible to fluvial erosion. The presence of dense, semi-rigid vegetation may encourage the formation of a wider channel with a vertical streambank.

The small range of CTA shear stress measurements (0.02–2.14 Pa) suggested that one estimate can describe a streambank. The law of the wall technique is not appropriate because the velocity profiles did not follow the necessary logarithmic shape. Vegetative roughness present in channels created secondary flow; turbulence characteristics more appropriately estimated BSS.

The BSS model predicted velocity fields in similar distribution to that measured by the ADV and MP. BSS calculated using the ray-isovel method for both velocity measurement devices were different than the measured BSS values, likely due to distortions in the measured velocity field. In general, the predicted BSS distribution increased with water depth and decreased with increasing vegetation density. The predicted BSS at the shrub toe indicated a spike in shear stress consistent with TKE estimates.

## Grant Information

This publication was developed under a STAR Research Assistance Agreement No. FP-91695301-0 awarded by the U.S. Environmental Protection Agency. It has not been formally reviewed by the EPA. The views expressed in this document are solely those of Leslie Hopkinson and Theresa Wynn and the EPA does not endorse any products or commercial services mentioned in this publication. Funds for this research were also provided by the Cunningham Fellowship and the Virginia Tech Graduate School.

## Dedication

I dedicate this work to my new family, Dave and Sully.

## Acknowledgements

I would like to thank my advisor, Tess Wynn, for all her support throughout my dissertation program. I would also like to thank the members of my committee, Cully Hession, Andy Dolloff, Panos Diplas, and Clint Dancey for their input and support. I am incredibly grateful for the lab help from Laura Teany. She always seemed to have an answer when I was having a breakdown. I would like to thank my two great undergraduate researchers: Gina Hayes and Annette Sparks. Gina did a great job with some tedious data processing. Annette Sparks helped me find all the errors with my data collection technique. I am also grateful to Jason Kean with the USGS for helping me with the use of his BSS model.

I cannot imagine grad school without all the great graduate student support. First, I would like to thank the all the grad students that have moved on to exciting things: Rhonda, Amanda, Ray, and Marc. Thanks for making my first years in Blacksburg so memorable. Also, I would like to thank all the support from the TWOSWEET students. They were always around when I needed help. Thanks to the HH crew for listening and being there on Fridays. I would like to give a special thanks to Candice Piercy and Barb Utley who helped with their long-distance encouragement. Thanks to Jess Kozarek for being a great roomie and friend since my first day in Blacksburg.

I would also like to acknowledge my family for their love and support. I would especially like to thank my husband, Dave, for his patience and heavy lifting help. I would like to give a special thanks to my parents, Dan and Carla Clark, and for their encouragement even outside of my mom's three-hour radius. Thanks to my brother Daniel for his phone advice. I cannot forget my furry friend, Sully, who allowed me to share his desk to finish writing.

## Table of Contents

## List of Figures

## List of Tables

## List of Abbreviations

A……..……..…….Cross-sectional area
$A_r$…….Projected plant area
$A_b$……..…Total flow area per unit length
a……....Exponent in excess shear stress equation (assumed equal to1)
ADV…..……...……...Acoustic Doppler velocimeter
B ……..……Flow blockage by vegetation (%)
BF…….Bankfull
BSS……..Boundary shear stress (Pa)
$C_1$ ……..……..Proportionality constant for the TKE method (0.19-0.21)
$C_2$……Proportionality constant for the TKE method (0.90)
$C_D$ ……..……..Drag coefficient
$C_D$'……. Vegetation drag coefficient
CTA……Constant temperature anemometry
D ……..……..…Perpendicular distance to the stream boundary (m)
$D_{50}$ …..……Median particle size (mm)
$D_{84}$ ……Particle size of the 84$^{th}$ percentile (mm)
$D_{fp}$……..Depth of flow in the floodplain (m)
$D_{mc}$ ……..……Depth of flow in the main channel
DPIV……Digital particle image velocimetry
$D_s$ ……..……...……Average stem diameter
du/dy……...Velocity gradient
$D_{veg}$ ……..……...…Vegetation relative submergence
F……..…….Hydrostatic force
Fr……Froude number
fst……..…...FST-hemisphere density (g/cm$^3$)
$F_{stems}$ ……Drag force per unit volume due riparian vegetation
g ……..……....Acceleration due to gravity (m/s$^2$)
H……...……Water depth (m)
J ……..……Vegetation Flexibility
K……..Relative roughness
k ……..……Von Karman constant (0.41)
$k_d$ ……..……Soil erodibility coefficient (m$^3$/N·s)
$K_{eddy}$…….. Kinematic eddy viscosity
$k_{s, bed}$ ……..Bed grain roughness (mm)
$k_{s,bank}$ …..…….....Bank grain roughness (mm)
l ……..……..Length of control volume
$K_t$……..……... Kinematic eddy viscosity for vegetated regions
$K_o$……Channel scale eddy viscosity
$K_{eddy}$…….. Kinematic eddy viscosity
L……Flume width
LDV……..……...……Laser Doppler velocimeter
$l_m$ …..……..Mixing length
LOW …..……..Law of the wall

$L_v$ ……...……...Nondimensional vegetation parameter
LWD……...Large woody debris
M……...……...Density distribution of vegetation on a channel bed
n ……...……...Number of stems per unit area
$n_M$……...Manning's n
P……....Wetted perimeter
PIV……...Particle image velocimetry
Q……..Flow discharge ($m^3/s$)
R……Reynolds number
$R_{bank}$ .....Relative bank grain roughness
$R_{bed}$ ……..……Relative bed grain roughness
$R_h$ ……..Hydraulic radius (m)
$RMS_u$ .....Downstream turbulence intensity
$RMS_v$……..……Lateral turbulence intensity
$RMS_w$ ……..……Vertical turbulence intensity
S……...Slope of the energy grade line (m/m)
$S_{bank}$ .....Bank Slope (m/m)
$S_{bed}$ ……Channel bed slope (m/m)
SNR ……..……...…Signal to noise ratio
$S_w$……Water surface slope
TKE……Turbulent kinetic energy
$\overline{u}$ ……..……Time-averaged velocity (m/s)
u……...Water velocity in the downstream direction (m/s)
u'……Velocity fluctuations in the streamwise direction
U……Depth averaged velocity in the downstream direction
u*……Shear velocity
$u_{ref}$ ……..……...Reference velocity
v'……Velocity fluctuations in the vertical direction
v ……..……Water velocity in the lateral direction (m/s)
$\nu$……..……Kinematic viscosity
V ……..……Time-averaged CTA voltage (V)
V*……..……Squared voltage normalized by the temperature difference
$v_e$……Eddy viscosity
$V_{fp}$……..Average velocity of the floodplain (m/s)
$V_{mc}$……..……Average velocity of the main channel
w'……..……..Velocity fluctuations in the lateral direction
w ……Water velocity in the vertical direction (m/s)
W ……Weight of fluid
x ……..……Downstream distance (m)
y ……..……..Vertical axis
z ……..……Lateral axis
$z_0$ ……..……..Roughness height (m)
$z_1$ ……..……..……Distance from the wall
$<\tau_{xy}>$ ……..……..Spatially averaged transverse shear stress
ΔV ……..……..Operating temperature of the sensor minus the water temperature °C
Θ……Bank slope angle ($^o$)

$\alpha$ ..... vegetation density
$\varepsilon$ ..... Erosion rate (m/s)
$\gamma$ ..... Specific weight of water
$\delta p$ ..... Length of wetted perimeter
$\delta p_b$ ..... Incremental length of wetted perimeter
$\lambda$ ..... Average stem spacing
$\mu$ ..... Dynamic viscosity of water ($N \cdot s/m^2$)
$\lambda_p$ ..... Vegetation density
$\theta$ ..... Angle of bed slope
$\rho$ ..... Water density ($m^3/s$)
$\tau$ ..... Local shear stress (Pa)
$\tau_a$ ..... Applied shear stress (Pa)
$\tau_{avg}$ ..... Average boundary shear stress
$\tau_{avg,bank}$ ..... Average boundary shear stress on a sloping bank
$\tau_{avg,bank,H}$ ..... Average boundary shear stress on a sloping bank calculated with H
$\tau_{avg,bank,RH}$ ..... Average boundary shear stress on a sloping bank calculated with $R_h$
$\tau_{avg,H}$ ..... Average boundary shear stress calculated with H
$\tau_{avg,Rh,}$ ..... Average boundary shear stress calculated with $R_h$
$\tau_{bed}$ ..... Total bed shear stress
$\tau_c$ ..... Critical shear stress (Pa)
$\tau_{fst}$ ..... Shear stress measured with fst-hemispheres
$\tau_{Isovel}$ ..... Shear stress calculated form isovels (Pa)
$\tau_{LOW}$ ..... Boundary shear stress calculated by the law of the wall (Pa)
$\tau_{LOW,ADV}$ ..... BSS calculated by the law of the wall and ADV (Pa)
$\tau_{LOW,ADV,20\%}$ ..... BSS calculated by the law of the wall, ADV, and 20% of the profile(Pa)
$\tau_{LOW,MP}$ ..... BSS calculated by the law of the wall and MP (Pa)
$\tau_{LOW,MP}$ ..... BSS calculated by the law of the wall, MP, and 20% of the profile (Pa)
$\tau_{mc/fp}$ ..... Shear stress at the main channel/floodplain interface (Pa)
$\tau_{Prandtl}$ ..... Prandtl's turbulent shear stress (Pa)
$\tau_{TKE}$ ..... Stress from TKE
$\tau_{TKE,2cm}$ ..... Stress from TKE calculated 2 cm from the streambank
$\tau_{TKE,4cm}$ ..... Stress from TKE calculated 4 cm from the streambank
$\tau_{TKE,w}$ ..... Stress from TKE in the vertical direction
$\tau_{uv,extrap}$ ..... Component of Reynolds stress from extrapolated velocity profile
$\tau_{uv,2cm}$ ..... Component of Reynolds stress calculated 2 cm from the streambank
$\tau_{uv,4cm}$ ..... Component of Reynolds stress calculated 4 cm from the streambank
$\tau_{uv}$ ..... Component of Reynolds stress
$\tau_{uw}$ ..... Component of Reynolds stress
$\tau_{uw,2cm}$ ..... Component of Reynolds stress calculated 2 cm from the streambank
$\tau_{uw,4cm}$ ..... Component of Reynolds stress calculated 4 cm from the streambank
$\tau_{uw,extrap}$ ..... Component of Reynolds stress from extrapolated velocity profile
$\tau_{vw}$ ..... Component of Reynolds stress
$\tau_{vw,2cm}$ ..... Component of Reynolds stress calculated 2 cm from the streambank
$\tau_{vw,4cm}$ ..... Component of Reynolds stress calculated 4 cm from the streambank

$\tau_{vw,extrap}$ ……..Component of Reynolds stress from extrapolated velocity profile

# Chapter 1 Introduction

## 1.1 Introduction

Sediment is one of the leading causes of water quality impairment for rivers, polluting 31% of declared impaired stream miles (USEPA, 2002). Sediment damages aquatic ecosystems, suffocates bottom dwelling organisms, and interferes with recreational use and water treatment processes. Damages associated with sediment pollution in North America cost roughly $16 billion annually (ARS, 2003). In response to the habitat and water quality impacts of channel instability, approximately $1 billion/year was spent during 1990-2003 to restore degraded streams (Bernhardt et al., 2005). While agriculture, urban runoff, construction, and forestry are significant sources of sediment (USEPA, 2002), streambank retreat is a source that is largely ignored. In certain systems, streambank retreat can contribute as much as 85% of the total watershed sediment yield (Trimble, 1997a; Wallbrink et al., 1998; Prosser et al., 2000), making it an important sediment source to study. Bank retreat negatively impacts riparian ecosystems, stream-side structures, and road crossings. The dominate processes causing bank retreat must be identified and understood to lessen the impacts. The most common stream technique used to control streambank retreat involves reshaping streambanks to a stable angle and then establishing riparian vegetation on the streambank face and floodplain (Bernhardt et al., 2005, 2007; Bernhardt and Palmer, 2007). Because vegetation is a significant element in restoration designs, the impact of vegetation on bank retreat needs to be understood.

While considerable research has been conducted on the role of vegetation in reducing streambank failures (Abernethy and Rutherfurd, 2001; Simon and Collison, 2002; Simon et al., 2006; Pollen, 2007), less is known about the influence of vegetation on flow turbulence and boundary shear stress, particularly for the case of a vegetated, sloping bank. This stream form is commonly created to control streambank retreat. The effects of vegetation on flow have been explored for submerged vegetation (Ghisalberti and Nepf, 2002; Jarvela, 2002; Ghisalberti and Nepf, 2006; Liu et al., 2008; Nepf and Ghisalberti, 2008) and emergent vegetation (Nepf, 1999; Nepf and Vivoni, 2000; Jarvela, 2002; Thompson et al. 2004, Liu et al., 2008) when placed on the channel bed. The effects of vegetation on turbulence structure with vegetation on the floodplain (Thornton et al., 2000; McBride et al., 2007; Yang et al., 2007) and as streamside

vegetation (White and Nepf, 2007) have been examined; however, the effects of vegetation on sloping streambanks have not been analyzed.

The excess shear stress equation, which relates the streambank erosion rate to the difference between the boundary shear stress (BSS) and the soil critical shear stress, predicts the erosion rate of fine grain soils due to stream channel scour (Osman and Thorne, 1988; Hanson and Simon, 2001). Julian and Torres (2006) used the excess shear stress equation to model bank erosion for cohesive banks. The equation is also used to predict channel erosion in models such as HEC-6, SWAT, and HSPF (USACE, 1993; Allen et al., 1997; Bicknell et al., 1997).

BSS on the channel boundary is commonly calculated based on flow depth and slope (Chang, 2002), but this method can cause major errors in soil detachment calculations when resistance (e.g. vegetation) is substantial (Thompson et al., 2004). While techniques exist to determine BSS (e.g. law of the wall, Reynolds stresses, turbulent kinetic energy, FST-hemispheres, Prandtl's mixing length theory, and average boundary shear stress), those models do not consider the impact of vegetation; therefore, research is needed to quantify the influence of riparian vegetation on BSS.

Kean and Smith (2004) adapted a model developed by Houjou et al. (1990) that calculates velocity and shear stress fields using ray-isovel turbulence closure to include drag effects of vegetated banks. This model expanded ray-isovel approach developed by Leighly (1932). Isovels are lines of constant velocity, and rays, perpendicular to the isovels, range from the channel boundary to the water surface. The area between two rays at the boundary represents shear stress on the bank (Kean and Smith, 2004; Wobus et al, 2008). The model has been applied to flume studies (Kean and Smith, 2004) and geomorphically stable natural channels (Griffin et al., 2005; Kean and Smith, 2005), with an additional erosion component (Wobus et al., 2008) and with small-scale topographic features on the channel boundary (Kean and Smith, 2006a and 2006b). The model can be used to better understand the impact of vegetation on BSS.

### 1.2 Goals and Objectives

This research is intended to determine the role of riparian vegetation in streambank retreat, providing insight to the type and density of vegetation that offers the greatest protection against streambank erosion. The overall goal of this experiment was to examine the effects of riparian vegetation on BSS to improve stream restoration design and to assess the impacts of

riparian management on channel stability. This goal was met by completing the following objectives:

1. Evaluate the effects of streambank vegetation on near-bank three-dimensional velocity structure and turbulence characteristics (Ch. 4);
2. Determine a method for measuring BSS in the field along hydraulically rough streambanks (Ch. 5); and
3. Examine the effects of streambank vegetation on BSS using an existing boundary shear stress model (i.e. Kean and Smith, 2004; Ch. 6).

### 1.3 Study Design

A flume experiment was conducted, comparing four distinct streambank vegetation types: no vegetation (bare), grass, shrubs, and trees. A second order prototype stream (Tom's Creek in Blacksburg, VA), with individual reaches dominated by the three vegetation types was modeled using a fixed-bed Froude-scale modeling technique. One model streambank of the prototype stream was constructed for each vegetation type in addition to one bank with only grain roughness, resulting in four model streambanks. Simulated vegetation (e.g. wooden dowels and a woven grass mat) were attached in the locations identified in a field survey.

Velocity profiles perpendicular to the flume model boundary were measured using a three-dimensional acoustic Doppler velocimeter and a miniature propeller. A Dantec MiniCTA system with a flush-mounted hot-film probe (55R46) was used to measure shear stress at the streambank wall, and measurements were considered representative of the actual boundary shear stress. Three-dimensional velocity and turbulence characteristics (Reynolds stress, turbulent intensities, and TKE) were examined to characterize the near bank flow. Both BSS measurement theory and instruments for field use were studied to determine a field method to measure boundary shear stress along hydraulically rough streambanks. The flume results were used to model shear stress distributions using an existing boundary shear stress model (Kean and Smith, 2004) to compare direct measurements of shear stress to model results. Each research objective is addressed in a separate chapter, presenting the methodology, results and discussion.

# Chapter 2 Review of streambank retreat and boundary shear stress

## 2.1 Bank Retreat

Bank retreat occurs from a combination of subaerial processes and erosion, fluvial erosion, mass failure, and basal clean-out (Thorne, 1982; 1990). Because bank retreat occurs due to a combination of processes, bank protection plans must identify the causes and effects of bank retreat (Thorne, 1982). Geomorphology, hydrology, and hydraulic characteristics can provide insight to the dominant processes (Lawler et al., 1997).

### *2.1.1 Subaerial Processes and Erosion*

Bank retreat is influenced by climate-driven processes known as subaerial processes (e.g. shrink-swell and freeze-thaw processes) that reduce soil strength. These processes are independent of stream flow, are influenced by climate and bank composition, and make banks more susceptible to erosion by fluvial entrainment and cause direct soil deposition (Thorne, 1982).

Soil moisture conditions reduce inner bank strength (Thorne, 1982; Lawler et al., 1997). Bank strength is weakened by positive pore water pressure in poorly drained banks occurring after extended precipitation or snowmelt. Streambank soils may swell and shrink as the banks become saturated and dried. This cycling causes cracks and fissures in the bank, making the bank susceptible to erosion. Bank strength is also weakened by the increased weight of saturated soil (Thorne, 1982).

Freezing water in the pores of streambank material also causes cracks, leading to loosening of bank material (Thorne, 1982). Vegetation can minimize erosion by ice by maintaining a more constant temperature on the bank and promoting quick thawing; maintaining a constant temperature minimizes freeze-thaw cycling (USDA-NRCS, 1996). The movement of soil water weakens the soil; removal of fines reduces soil cohesion and leads to bank weakening (Thorne, 1982).

### *2.1.2 Fluvial Entrainment*

Fluvial scour causes bank retreat by entraining material from the bank and transporting the material downstream. Flow generates shear stress along the streambank. When the bank material does not exert an equal and opposite shear stress (lift and drag forces overcome the forces holding the grain or aggregate in place), fluvial entrainment of bank material occurs

(Thorne, 1982; Lawler et al., 1997). Subaerial processes often weaken the soil, increasing the erosion caused by fluvial entrainment (Lawler et. al., 1997).

Aggregates are entrained in the flow from cohesive banks, while individual particles are entrained from noncohesive banks. In nature, fluvial entrainment acts on both of noncohesive and cohesive banks. Due to vegetation and porewater effects, banks with coarse material can exhibit cohesive properties in natural systems (Lawler et al., 1997).

Partheniades (1965) conducted a flume study that related erosion rates to shear stress for two clay types: remolded natural material (San Francisco bay mud) at field moisture and a flocculated bed. Erosion rates depended strongly on shear stress and increased after stresses reach a critical limit. Initially proposed by Partheniades (1965), the excess shear stress equation relates the streambank erosion rate to the difference between the applied shear stress ($\tau_a$) and the soil critical shear stress ($\tau_c$). This equation predicts the erosion rate of fine grain soils due to stream channel scour, as follows (Partheniades, 1965; Osman and Thorne, 1988; Hanson and Cook, 1997; Hanson and Simon, 2001):

$$\varepsilon = k_d(\tau_a - \tau_c)^a \qquad [2.1]$$

where $\varepsilon$ is the erosion rate (m/s), $k_d$ is the soil erodibility coefficient ($m^3/N \cdot s$), a is an exponent typically assumed to be 1, $\tau_a$ is the applied shear stress on the soil boundary (Pa), and $\tau_c$ is the critical shear stress (Pa).

Julian and Torres (2006) used the excess shear stress equation to model bank erosion for cohesive banks. The equation is also used to predict channel erosion in models such as HEC-6, SWAT, and HSPF (USACE, 1993; Allen et al., 1997; Bicknell et al., 1997). As with all models, there are limitations to the expression: the effective shear stress can be related to flow hydraulics, and the soil parameters, $\tau_c$ and $k_d$, must be estimated or measured based on soil properties. Many factors, such as soil moisture content, clay content and type, and soil structure, contribute to the erosion of fine grained sediments, making $\tau_c$ and $k_d$ difficult to quantify (Grissinger, 1982).

An understanding of $\tau_c$ is required to correctly model and understand erosion (Owoputi and Stolte, 1995); following the excess shear stress equation, erosion occurs when the effective stress exceeds the critical shear stress. The critical shear stress is defined as the stress at which

detachment begins or the condition that begins soil detachment. If the critical stress is higher than the effective stress, the erosion rate is considered zero (Osman and Thorne, 1988; Nearing et al., 1989; Hanson, 1990a; Hanson et al., 2002). There are several approaches to determining $\tau_c$. Critical shear stress can be estimated based on particle size and specific gravity by Shield's diagram (Hann, et al., 1994; Temple and Hanson, 1994), estimated based on particle size only (Smerdon and Beasley, 1961), estimated based on soil characteristics (Smerdon and Beasley, 1961; Temple, 1980, 1983, and 1985; Julian and Torres, 2006), estimated based on soil specific gravity, particle size and water depth by Neill's equation (Neill, 1967; ESRD, 2004), assumed zero (Foster et al., 1977; Hanson, 1990b; Temple 1992; Hanson et al., 1999), determined in flume studies (Dunn, 1959; Smerdon and Beasley, 1961; Kamphuis and Hall, 1983; Hanson et al., 1999), or measured *in situ* with a submerged jet test device (Blaisdell et al., 1981; Hanson and Simon, 2001). Clark and Wynn (2007) evaluated five empirical methods to estimate $\tau_c$ and ultimately recommended $\tau_c$ be measured *in situ*.

Soil erodibility describes the rate at which soil is detached, once erosion starts (Hanson et al., 2002). Although simple relationships between $k_d$ and soil properties are not available, two empirical methods (i.e. Osman and Thorne, 1988; Hanson and Simon, 2001) exist for estimating $k_d$, if $\tau_c$ can be determined. However, Clark and Wynn (2007) analyzed the two empirical methods to estimate $k_d$ and concluded that the empirical methods resulted in statistically similar $k_d$ values. The calculated $k_d$ estimates were two orders of magnitude less than the $k_d$ estimated by the jet test measurements, suggesting field validation over a range of soil types to develop a method to measure $k_d$ is needed. Wynn and Mostaghimi (2006b) reported $k_d$ was also influenced by vegetation; $k_d$ decreased with increasing large root density (diameters 2 to 20 mm).

Total applied shear stress on the channel boundary is commonly calculated based on flow depth and slope (Chang, 2002), but this method can cause major errors in soil detachment calculations when resistance is substantial (Thompson et al., 2001, 2004). Shear stress calculation at the soil-water boundary is needed for transport calculations (Giffin et al., 2005). Additionally, a better prediction of the applied boundary shear stress is required to quantify and predict the erosion of vegetated streambanks (ASCE, 1998b). Shear stress has also been related to channel stability (Temple, 1980, 1983, and 1985) and is important for the design of stable channels where the applied shear stress cannot exceed the critical shear for motion by channel scour (Chang, 2002).

### *2.1.3 Bank Failure*

Streambank failure occurs in response to geotechnical instability, resulting in a mass of bank material sliding or falling to the bank toe. Failure occurs when gravitational forces overcome the mechanical strength of the bank material (Lawler et al., 1997). The weight of vegetation can promote bank retreat by mass wasting (Thorne, 1990), but a study by Abernethy and Rutherfurd (2000) showed vegetation surcharge was not sufficient to cause bank destabilization.

Mass failure occurs differently for cohesive, noncohesive, and composite streambanks. Because shear strength increases less quickly than mechanical shear stress with bank depth for cohesive soils, streambanks composed of cohesive soils often experience deep seated failures. Fluvial entrainment enhances failure by increasing the bank height and angle. When the critical height and angle are reached, failure occurs. Block mass increases with increasing moisture content and may accelerate advance bank retreat by mass wasting (Lawler et al., 1997).

### *2.1.4 Basal Endpoint Control*

Bank failure transports bank material to the basal area, the portion of the bed and the lower banks that surrounds the bank toe. The material either disappears due to fluvial entrainment or accumulates, forming a protective wedge. The movement of the material depends on the energy of the stream (Thorne, 1982), and sediment delivered from upstream (Lawler et al., 1997). Bank retreat adjusts to the state of the sediment. If the sediment mass delivered from upstream exceeds the stream transport capacity, the sediment will be deposited in the basal area. If the sediment amount equals the stream transport capacity, the stream will be in equilibrium. If the sediment amount is less than the stream transport capacity, scouring of the bank toe will occur (Thorne, 1982; Thorne, 1990; Lawler et al., 1997). Vegetation present on streambanks promotes sediment deposition, especially in densely vegetated areas (USDA-NRCS, 1996).

Understanding fluvial entrainment is critical for bank stability. Fluvial entrainment accelerates mass wasting by scouring material in the basal area; scouring increases bank angle and height (Thorne, 1982). Julian and Torres (2006) found fluvial entrainment was the main factor contributing to bank retreat in a study of cohesive streambank erosion, indicating a need to further understand the process of fluvial entrainment.

## 2.2 Shear Stress Measurement Techniques

Average applied shear stress on the channel boundary is commonly calculated based on flow depth and slope (Chang, 2002), but this calculation does not account for vegetative roughness. A better prediction of the local applied boundary shear stress is necessary to quantify and predict the erosion of vegetated streambanks (ASCE, 1998b). Several theories exist to quantify shear stress, and these methods require different types of field measurements and instruments (Table 2.1). The methods are discussed in the following sections.

### *2.2.1 Average boundary shear stress*

Average boundary shear stress, the force per unit area in the flow direction on the channel boundary, is commonly calculated based on flow depth and slope (Chang, 2002). Applying the momentum equation to a uniform flow control volume in the direction of flow results in the following equation (Munson et al., 1998):

$$\sum F_x = \rho Q(U_2 - U_1) \qquad [2.2]$$

where ρ is the fluid density, Q is discharge, and U is the depth-averaged water velocity.

Assuming $U_1$=$U_2$ for uniform flow and no acceleration of the fluid, the sum of forces in the x-direction equals zero. The equation then is represented in the following form (Munson et al., 1998):

$$F_1 - F_2 - \tau_{avg} Pl + W \sin\theta = 0 \qquad [2.3]$$

where P is the wetted perimeter, l is the length of control volume, F is the hydrostatic force, θ is the angle of bed slope, and W is the weight of water in control volume.

**Table 2.1. Review of methods to estimate boundary shear stress, including field requirements for each method**

| Method | Equation[1] | Measurement Requirements |
|---|---|---|
| Average Boundary Shear Stress | $\tau_{avg} = \gamma R_h S$<br>$\tau_{avg} = \gamma HS$ (wide stream)<br>$\tau_{avg,bank} = \gamma HS \cos\Theta$ (sloping bank) | $R_h$, S, H, and/or $\Theta$ |
| Law of the Wall | $\frac{u}{u*} = \frac{1}{k}\ln\frac{z}{z_0}$ | 1D velocity profiles near boundary (<20% flow depth) or depth-averaged velocity and an estimate of roughness ($z_0$) |
| Reynolds Stresses | $\tau_{uv} \cong -\rho\overline{u'v'}$ | 3D velocity measurements and instantaneous velocity fluctuations |
| Prandtl's Mixing Length Theory | $\tau_{Prandtl} = \rho\ell_m^2\left(\frac{d\bar{u}}{dy}\right)^2$ | Estimate of mixing length and gradient of time-averaged velocity |
| Turbulent Kinetic Energy Method (TKE) | $\tau_{TKE} = C_1\left[0.5\rho(\overline{u'^2}+\overline{v'^2}+\overline{w'^2})\right]$<br>$\tau_{TKE,w} = C_2\rho\overline{w'^2}$ | 3D velocity measurements and instantaneous velocity fluctuations |
| Isovels | $\tau_{Isovel} = \rho g S\frac{\int_o^L dA}{\delta p_b}$ | $p_b$, S, H |
| FST-Hemispheres | $\tau_{fst} = (fst)x^{2.85}$ (hemispheres 1-12)<br>$\tau_{fst} = 7.32(fst)x - 6.60$ (hemispheres 13-24) | Hemisphere set |

[1] $\tau_{avg,bank}$ is average boundary shear stress; $\gamma$ is specific weight of water; $R_h$ is hydraulic radius; H is water depth; S is water surface slope; $\Theta$ is bank slope; u is water velocity; u* is shear velocity; $z_1$ is the elevation from the bed; $z_0$ is the roughness height; $\tau_{uv}$ is a component of Reynolds stress; $\rho$ is water density; u', v', and w' are velocity fluctuation in the streamwise, horizontal, and vertical direction; $\tau_{Prantl}$ is turbulent shear stress; $l_m$ is the mixing length; $\tau_{TKE}$ and $\tau_{TKE,w}$ are shear stress from turbulent kinetic energy; $C_1$ (0.19-0.21) and $C_2$ (0.90) are proportionality constants; $\tau_{Isovel}$ is the shear stress calculated from isovels; $\delta p_b$ is the incremental length of wetted perimeter; $\tau_{fst}$ is shear stress measured with fst-hemispheres; and, fst is fst-hemisphere density.

Assuming the flow is uniform ($H_1$=$H_2$) and the hydrostatic forces ($F_1$ and $F_2$) are equal, only the fluid weight ($W=\gamma Al$) and shear stress acting on the wetted perimeter (P) interact with

the control volume, reducing the equation to the following form after rearrangement (Munson et al., 1998):

$$\tau_{avg} = \frac{W \sin\theta}{Pl} = \frac{\gamma A l \sin\theta}{Pl} \quad [2.4]$$

where A is the area of the cross-section and γ is the specific weight of water.

The equation can be further simplified: sinθ is represented by bottom slope (S) and A/P is defined as the hydraulic radius ($R_h$). This simplification results in the commonly used average boundary shear stress equation (Munson et al., 1998):

$$\tau_{avg} = \gamma R_h S \quad [2.5]$$

For wide channels (width/depth>20), the walls do not influence the central velocity, and water depth, H, is substituted for $R_h$ (Chow, 1959):

$$\tau_{avg} = \gamma H S \quad [2.6]$$

Maximum boundary shear stress occurs at the deepest point and becomes zero just above the water's edge (Equations 2.5 and 2.6; Raudkivi, 1998).

Shear stress is not uniformly distributed around the wetted perimeter (Gray and Sotir, 1996; Graf, 1984). For trapezoidal channels, the maximum for the bed occurs at its center line, and the maximum for the banks occurs along the lower third of the bank (Gray and Sotir, 1996; Raudkivi, 1998). For trapezoidal channels, maximum shear stress for the bottom is typically equal to γHS. For the sides, maximum shear stress is roughly equal to 0.75γHS (Graf, 1984; Julien, 1995; Raudkivi, 1998).

For flow in a trapezoidal channel, wall shear (shear stress at a point on the bank) can be derived and results in a similar solution, beginning with a force balance for a control volume on

the sloping boundary at an angle of Θ. The weight of the fluid equals the shear stress acting on that portion of the bank, resulting in the following equation (Graf, 1984):

$$\tau_{avg,bank}\sqrt{dx^2+dy^2} = \gamma HSdx \qquad [2.7]$$

The following expression results after solving for shear stress (Graf, 1984):

$$\tau_{avg,bank} = \frac{\gamma HSdx}{\sqrt{dx^2+dy^2}} = \gamma HS\cos\Theta \qquad [2.8]$$

*2.2.2 Wall Shear Stress*

For wall-bound flows, viscosity affects velocity near a smooth boundary (Kundu, 1990). In turbulent shear flow, the shear stress at any point from the solid boundary is a combination of shear stress caused by molecular viscosity and shear stress caused by turbulent eddies (Chang, 2002). A turbulent boundary layer bound by a smooth wall follows the law of the wall near the boundary and a logarithmic law away from the boundary. When roughness elements protrude into the viscous sublayer, viscous effects near the boundary become negligible. Velocity distributions for this rough case follow an alternate logarithmic law (Kundu, 1990).

**Law of the Wall for Smooth Boundaries:** The law of the wall describes flow in the inner layer of the turbulent boundary layer. Velocity profiles near a smooth wall depend on water density (ρ), wall shear stress ($\tau_{LOW}$), kinematic viscosity ($\nu$), and distance from the boundary (y). The law of the wall relates nondimensional groups, U/u* and yu*/$\nu$ by a universal function of the following form (Kundu, 1990):

$$\frac{U}{u^*} = f\left(\frac{yu^*}{\nu}\right) = f\left(y_+\right) \qquad [2.9]$$

Shear velocity (u*) can be related to wall shear stress through the following dimensionless relationship (Kundu, 1990):

$$u* = \sqrt{\frac{\tau}{\rho}} \qquad [2.10]$$

where $\tau$ is shear stress.

For fully developed flow in an open channel bounded by a smooth boundary, viscosity influences are present near the wall. Three sublayers define flow near a smooth wall and define the regions of the inner turbulent boundary layer. The sublayer adjacent to the wall is known as the viscous sublayer and is characterized by dominant viscous forces and a linear velocity distribution. Boundary shear stress is defined by the following (Kundu, 1990):

$$\tau_{LOW} = \mu \frac{dU}{dy} \qquad [2.11]$$

The characteristics of this layer are valid when $y_+$ is less than or equal to 5, where $y_+$ is defined below (Kundu, 1990):

$$y_+ = \frac{yu_*}{v} \qquad [2.12]$$

Further from the smooth boundary a logarithmic relationship describes the velocity distribution (valid for $30<y_+<300$; Equation 2.13; Kundu, 1990):

$$U = \frac{u*}{k} \ln y + const. \qquad [2.13]$$

where k is the von Karman constant (0.41). Between the viscous sublayer and logarithmic layer ($5<y_+<30$), a buffer region exists where neither viscous or Reynolds stress are negligible (Kundu, 1990).

**Logarithmic Law for Rough Boundaries:** For hydrodynamically rough surfaces (e.g. gravel, vegetation) roughness elements protrude into the viscous sublayer, such that viscosity has negligible effects on the velocity profile. The velocity profile results from integrating the

general logarithmic equation (Equation 2.13) assuming U is zero within the roughness layer. The following equation (Equation 2.14) describes flow for rough boundaries:

$$\frac{u}{u*} = \frac{1}{k} \ln \frac{z}{z_0} \qquad [2.14]$$

where u is the point velocity, z is the distance from wall, and $z_0$ is the roughness height corresponding to u=0.

The law of the wall and logarithmic relationships have been utilized in studies to determine boundary shear stress. If an estimate of roughness can be made, u* can be estimated by a point or average velocity measurement. From this single velocity measurement, $\tau_{LOW}$ is estimated. If an estimate of roughness is not appropriate, boundary shear stress can be determined by fitting a least squares line fit to the following equation (Wilcock, 1996). Equation 2.14 can be rewritten in the following form:

$$\ln(z) = \frac{uk}{u*} + \ln(z_0) \qquad [2.15]$$

Equation 2.15 is an equation for a straight line for ln(z) vs. u. The shear velocity can be determined from the slope and roughness. Because shear velocity is related to shear stress (Equation 2.10), $\tau_{LOW}$ can be determined (Haritonidis, 1989; Dade et al., 2001). This procedure can be completed without an estimate of channel roughness, but accurate velocity measurements are important (Haritonidis, 1989). Wilcock (1996) utilized the law of the wall in a field study of bed shear stress. Three techniques were used to estimate shear velocity (u*) of the logarithmic equation: (1) shear velocity was estimated based on single observations of u and an estimate of $z_0$ (Equation 2.9); (2) shear velocity was estimated based on a least squares lined fitted to ln(z) vs. u; and, (3) shear velocity was estimated based on the depth-averaged velocity.

Complex flow fields where the velocity profile is not logarithmic may cause this technique to be invalid (Biron, 2004). In a flume study testing the effects of two different vegetation forms on flow, Wilson et al. (2003) showed the flow within a simulated flexible plant layer did not follow a logarithmic velocity profile, suggesting the law of the wall may not be

appropriate to measure bed shear stress for vegetated regions. In a field study comparing local shear stress estimated by the law of the wall and measured using Preston-static tubes, Hoover and Ackerman (2004) found that the law of the wall underestimated shear stress over boulders. For shear stress estimates, shear stress was estimated based on the Preston-static tube technique and based on the law of the wall for the portion of the profile directly above the boulders (2-7 mm). When law of the wall estimates were compared to the Preston-static tube estimates, a positive relationship was found for the log-normal profiles (p=0.03) but not for the wedge shaped (p=0.85) or transitional profiles (p=0.81). When near bed distortion was present (transitional and wedge shaped profiles) the law of the wall underestimated shear stress as compared to the Preston technique by an average of 61%. The law of the wall was limited due to the small thickness of the logarithmic layer. Most velocimeters in field settings are incapable of taking measurements within the layer.

To record shear stress profiles, Martin et al. (2000) used Digital Particle Image Velocimetry (DPIV) to quantify velocity interactions within the boundary layer. Bed shear stresses were calculated in a flume (406 cm length; 35.6 cm height) study for two situations: without sediment (flat bed), and with bed sediment (gravely-sand). For the sediment case, the fine sediment eroded and the large particles formed a stable layer. Bed shear stress was also calculated by the law of the wall (Equation 2.14), resulting in values of 0.37 Pa and 0.28 Pa for setups with and without sediment, respectively. The results indicated the law of the wall is more appropriate for determining bed shear stress channels devoid of sediment (flat-bed channels).

*2.2.3 Reynolds Stresses*

The combination of the Navier-Stokes equations, continuity equations, and rules of time-average computations results in a system of stress-tensor equations: the Reynolds equations. Reynolds stresses due to turbulent velocity components result as the following:

$$\begin{pmatrix} \sigma'_x & \tau'_{xy} & \tau'_{xz} \\ \tau'_{xy} & \sigma'_y & \tau'_{yz} \\ \tau'_{xz} & \tau'_{yz} & \sigma'_z \end{pmatrix} = -\rho \begin{pmatrix} \overline{u'^2} & \overline{u'v'} & \overline{u'w'} \\ \overline{u'v'} & \overline{v'^2} & \overline{v'w'} \\ \overline{u'w'} & \overline{v'w'} & \overline{w'^2} \end{pmatrix} \qquad [2.16]$$

where the second subscript denotes the direction of the stress and the first subscript denotes the perpendicular direction (Schlichting and Gersten, 2000). The diagonal components of the symmetric tensor are the normal stresses, and the off-diagonal components are shear stresses (i.e. Reynolds stresses; Kundu, 1990).

In turbulent shear flow, the shear stress at any point from the solid boundary is a combination of shear stress caused by molecular viscosity and shear stress caused by turbulent eddies (Chang, 2002; Munson et al., 1998). From a force balance on a fluid element , local shear stress can be determined by the following equation (Sabersky et al., 1999; Martin et al., 2000):

$$\tau = \mu \frac{\partial u}{\partial y} - \rho \overline{u' v'} \qquad [2.17]$$

where τ is local shear stress, μ is the dynamic viscosity of water, v is the velocity perpendicular to flow, and an apostrophe denotes the fluctuation from the average.

The first term in the equation represents laminar flow, while the second term represents turbulent flow. Because turbulent flow dominates at all points except very close to the boundary, the laminar part of the equation can be dropped and the total local shear stress can be approximated by the following equation (Chang, 2002; Martin et al., 2000):

$$\tau_{uv} \cong -\rho \overline{u' v'} \qquad [2.18]$$

Equation 2.18 gives the local Reynolds shear stress, $\tau_{uv}$, in a 2D turbulent flow (Vanoni, 1975) and ignores the viscous and logarithmic sublayers found with smooth boundaries (Kundu, 1990). Density is included to account for the momentum transfer of the fluid (Munson et al., 1998). Reynolds stresses can also be considered as "the rate of mean momentum transfer by turbulent fluctuations" (Kundu, 1990). The value $\overline{u'v'}$ is expected to be non-zero and negative due to coupling of negative and positive values: a negative u' is coupled with a positive v', and a negative v' is coupled with a positive u'. The coupling indicates a correlation between downstream and transverse fluctuations of velocity at a position (Schlichting and Gersten, 2000), indicating that velocity in the streamwise and vertical directions need to be measured simultaneously.

*2.2.4 Prandtl's Mixing Length Theory*

Boussinesq, Prandtl and von Karman developed semi-empirical theories (first-order closure models) to relate the Reynolds stresses to the mean velocity. Little progress has been made with these theories because the relationships are flow-specific. Boussinesq used eddy viscosity ($\nu_e$) and a velocity gradient to represent the turbulent stresses (Equation 2.19):

$$-\overline{u'v'} = \nu_e \frac{dU}{dy} \qquad [2.19]$$

where U is the depth-averaged flow velocity in the streamwise direction and *y* is the vertical direction. Eddy viscosity depends on the flow conditions; no method to estimate eddy viscosity from turbulent parameters exists, making it difficult to apply (Kundu, 1990). Prandtl used mixing length ($l_m$) with a velocity gradient to represent turbulent stresses where:

$$\nu_e \sim u' l_m \qquad [2.20]$$

Because little is known about $l_m$ and $l_m$ depends on the flow conditions, little progress has been made to estimate turbulent stresses based on the mixing length theory.

Momentum transfer between the slow, near wall flows to the higher velocity flows away from the wall provided the basis for Prandtl's mixing length theory. The momentum exchange among flows of different velocities causes turbulent eddies. The distance that the fluid travels in the transverse direction is known as the mixing length ($l_m$). According to the mixing length theory, the magnitude of the fluctuating velocity component in the principle flow direction (u') is equal to the mixing length times the velocity gradient (du/dy), and the transverse fluctuating velocity component (v') is proportional to the magnitude of the fluctuating component in the principle flow direction (Crowe et al., 2001) Turbulent shear stress was defined by the following equation (Munson et al., 2002):

$$\tau_{\Pr andtl} = \rho \ell_m^2 \left( \frac{d\bar{u}}{dy} \right)^2 \quad [2.21]$$

where $\tau_{Prandtl}$ is the turbulent shear stress and $l_m$ is the mixing length.

Assumptions regarding the mixing length are necessary because $l_m$ is not constant throughout the flow field. As the distance to the boundary increases, the turbulence is dependent on the distance (Munson et al., 2002).

*2.2.5 Turbulent Kinetic Energy Method (TKE)*

Patterns of turbulent kinetic energy can be related to bed shear stress through a proportionality constant (Daniels and Rhoads, 2004). The method requires measurements of velocity fluctuations to determine the turbulent kinetic energy (TKE). Bed shear stress, historically in ocean environments, is determined by a linear relationship with TKE (Equation 2.22; Kim et al., 2000). Biron et al. (2004) applied the technique in an experimental open channel flow to determine bed shear stress over a plexiglas bed, a sand bed, and flow with deflectors. Bed shear stress was defined by the following formula:

$$\tau_{TKE} = C_1 \left[ 0.5 \rho (\overline{u'^2} + \overline{v'^2} + \overline{w'^2}) \right] \quad [2.22]$$

where $C_1$ is the proportionality constant (0.19-0.21; Daniels and Rhoads, 2004; Biron, 2004), ρ is the fluid density, and (u, v, w) are the three dimensional velocity components. Daniels and Rhoads (2004) selected the TKE method to estimate near bed shear stresses because the TKE method was shown to be consistent and accounted for three-dimensional flows.

The Biron et al. (2004) study used a simplified version of Equation 2.22 that only incorporated the vertical velocity fluctuations to decrease the noise errors:

$$\tau_{TKE,w} = C_2 \rho \overline{w'^2} \quad [2.23]$$

where $C_2$ is an proportionality constant (0.9).

*2.2.6 Isovels*

Kean and Smith (2004) adapted a model developed by Houjou et al. (1990) that calculates velocity and shear stress fields using ray-isovel turbulence closure to include drag effects of vegetated banks. This model expanded ray-isovel approach developed by Leighly (1932). Isovels are lines of constant velocity, and rays, perpendicular to the isovels, range from the channel boundary to the water surface. The water surface defines the point of zero shear stress, while the area between two rays at the boundary represents shear stress on the bank (Kean and Smith, 2004; Griffin et al., 2005). The boundary shear stress can be expressed by the following relationship (Kean and Smith, 2004):

$$\tau_{Isovel} = \rho g S \frac{\int_o^L dA}{\delta p} \qquad [2.24]$$

where L is the total length of the ray and $\delta_P$ is the incremental length of wetted perimeter.

*2.2.7 FST-hemispheres*

To create a simple method to measure flow properties *in situ*, Statzner and Muller (1989) developed Fliesswasserstammtisch (FST)-hemispheres to measure hydraulic characteristics of boundary flow in the field. The set consisted of 24 hemispheres of identical size (radius of 3.9 cm) and surface texture with altering densities. When placed on the stream bed, the movement of the heaviest hemisphere can be related to boundary shear stress. Several practical drawbacks occur with the use of FST-hemispheres: (1) the spheres are relatively large (3.9 cm); (2) the hemispheres must sit on a horizontal plane; and, (3) hemisphere placement disturbs the flow. While there are disadvantages with the technique, the FST-hemispheres provide a field method to investigate near boundary flows that is less labor-intensive than alternative hydraulic measurements (e.g. velocity, depth, slope; Statzner and Muller, 1989).

**2.3 Velocity Measurements**

Shear stress estimation methods based on near wall velocity profiles or measurements (law of the wall, Reynolds stresses, Prandtl's mixing law, TKE, isovels) use advances in water velocity instrumentation for more precise calculations. Constant temperature anemometry offers a direct method for measuring wall shear stress; measurements for a flush mounted probe are

taken at the wall. Acoustic Doppler velocimetry, particle image velocimetry, mechanical devices (miniature propeller), and Pitot tubes are devices used to measure velocity.

*2.3.1 Constant Temperature Anemometry (CTA)*

By sensing changes in heat transfer from small, electrically heated elements, thermal anemometers measure rapid changes in velocity. A constant temperature anemometer maintains the element at a constant temperature as the fluid passes over the element, cooling the element. The change in velocity from the corresponding change in current is displayed as a voltage measurement. The small sensor size (<1 mm) allows the anemometers to be used in turbulent flow without obstructing the flow. Thermal anemometers also respond to changes in temperature, pressure, and fluid composition, so the device can become less accurate in highly turbulent, nonisotropic, or reversing flows (TSI, Shoreview, MN). Frequent calibrations are necessary (Thompson and Wilson, 2004).

For water systems, non-cylindrical film sensors are suggested where contamination cannot be avoided; the hot-film sensors are more rugged than wire sensors (TSI, Shoreview, MN; Fingerson and Freymuth, 1996). Flush mounted sensors can measure wall shear stress (TSI, Shoreview, MN; Fingerson and Freymuth, 1996; Figure 2.1). The non-cylindrical sensors minimize problems of self-generated turbulence due to sensor shape. The sensors do not cause cavitation problems in high speed flows, and the sensor configuration minimizes contaminant problems. Sensor calibration can be difficult (Fingerson and Freymuth, 1996).

**Figure 2.1. Miniature constant temperature anemometer probe being inserted into the model streambank (Dantec MiniCTA flush mounted hot-film probe 55R46).**

Bruun (1996) outlined the problems related to water flow when using hot-film anemometers: contamination, temperature sensitivity, and the presence of ions in the liquid. To prevent electrolysis of hot-wire probes, an impervious, protective quartz coating is used. Failure may occur when the quartz coating cracks. Bubble formation in early hot-film studies lead to calibration shifts but this can be prevented by reducing the temperature difference between the film and liquid to about 20$^{o}$C. Also, the water should be allowed to stand before sensor use; temperature drift and probe contamination alter the calibration. The use of a large storage tank in a test facility or the application of temperature correction to the liquid reduces the temperature drift problem. Frequent probe calibrations are a practical solution for temperature drift. Hot-film probes drift from calibration due to sensor contamination and build-up of algae and minerals. Deionized water can be used in the flume to minimize contamination. The use of deionized water also helps reduce problems caused by ions in the water (Bruun, 1995, 1996).

Thompson and Wilson (2004) conducted a study to evaluate the accuracy of a widely used calibration procedure (Robinson, 1989; Samways et al., 1994; Lekakis, 1996) for a constant temperature anemometer and a flush-mounted hot-film sensor in a low-turbulence environment. The calibration occurred in pipe flow where the sensor mounting accuracy was important. The study analyzed ten flow rates where the average boundary shear stress ranged from 0.56 Pa to 6.79 Pa, the water temperature ranged from 27.1$^{o}$C to 27.9$^{o}$C, and the average anemometer voltage ranged from 4.04 V to 6.59 V. The sensor was maintained at a constant temperature of 67$^{o}$C. More observations during calibration led to better accuracy and less uncertainty. Relative calibration accuracy was 15% for bed shear stress.

The hot-film anemometers are fragile and handling should be minimized. In several studies, researchers (Robinson and Cook, 1998; Thompson et al., 2004) mounted the sensor to a fixed board. The board, rather than the sensor, was then moved. In the Thompson et al. (2004) study, idealized vegetation was mounted from above the flume floor. The shapes were moved and did not touch the flume floor to minimize probe handling. While CTA systems are easily applicable in laboratory studies, the fragility of the probes limits their use in the field.

Robinson (1989) used a constant temperature anemometer to examine the forces that cause the formation, growth, and movement of a headcut. Hydraulic stress and pressure transmitted to an overfall boundary were measured for three drop heights, four flow rates, up to 11 backwater levels, and up to 23 probe positions by a hot-film anemometer. The flume (0.91 m

wide, overfall heights of 76.2, 50.8, and 25.4 cm) study positioned the probe at 7.62-cm intervals along the vertical wall and basin floor. The hot-film anemometer results indicated a nonlinear relationship between time-averaged shear stress and voltage.

*2.3.2 Pitot Tube*

Fluid velocity can be measured by Pitot tubes which determine flow velocity based on pressure difference. A Pitot tube has two pressure taps, one at the upstream end and one a few tube diameters from the upstream end. The upstream pressure tap measures stagnation pressure, while the second pressure tap measures static pressure. Through the use of the Bernoulli equation, velocity can be determined by the piezometric head at the pressure taps. A Pitot-static contains a second, coaxial tube that measures static pressure from the side of the Pitot tube (Crow et al., 2001).

Pitot tubes have been used to determine mean velocity profiles, and measurements had significant error. If Pitot tubes are not aligned in the mean flow direction, angular sensitivity of the device becomes important (Haritonidis, 1989). Ackerman and Hoover (2001) used a Preston-static tube to measure shear stress; a Preston-static tube was described as a wall-mounted Pitot-static tube. Ackerman et al. (1994) proposed a Preston-static tube that provides a simple, convenient, and accurate method to measure wall shear stress. When comparing the Preston-static tube to the use of the conventional wall tap in a lab study, the dimensionless percent difference was approximately 1.6%. The results indicated that the Preston-static tube provided a simple, convenient, and accurate method to measure wall shear stress.

Following the development of a Preston-static tube (surface mounted Pitot-static tube; Ackerman et al., 1994), Ackerman and Hoover (2001) calibrated the Preston-static tube in a lab situation and implemented it in the field. The instrument was limited in areas of turbulent flow where varying flow directions and water depths made it difficult to orient the instrument. Average shear stress was determined by the product of the water depth and slope; local shear stress accounted for 4-10% of the average shear stress due to form drag from bed forms, indicating the distribution and magnitude of local shear stress is variable. The results suggested further study was needed to determine the effects of spatial distributions and local influences such as, pressure gradients, substrate shape, and spacing on local shear stresses (Ackerman and Hoover, 2001).

*2.3.3 Acoustic Doppler Velocimetry (ADV)*

Acoustic Doppler velocimeters (ADV) measure three-dimensional and time-averaged velocities (Figure 2.2). The technology can be utilized to estimate shear stress based on the law of the wall, Reynolds stresses, or TKE approaches. For an ADV, simultaneous measurements of instantaneous three-dimensional flow components are recorded at high sampling rates (0.1-50 Hz for 16 MHz MicroADV; Sontek, 1999). No calibration is required, and the sensors have low noise levels. Limitations of the device are large sample volumes (0.09 $cm^3$ for Sontek 16 MHz MicroADV; Sontek, 1999) and the poor resolution of turbulence eddies (Voulgaris and Trowbridge, 1998). Control volumes are typically measured at a distance ranging from 0.05 to 0.1 m from the probe (Nortek, 2005, and Sontek, 1999) making measurements close to a boundary difficult (Voulgaris and Trowbridge, 1998).

**Figure 2.2. Sontek 16 MHz Side-looking MicroADV (acoustic Doppler velocimeter).**

Erroneous data-biasing mean velocity values and turbulent characteristics may result from ADV measurements due to obstructions near the sampling volume, excessive aeration of flows, Doppler noise, velocity shear, or proximity to the surface, making data filtering necessary (McBride et al., 2007; Wilcox and Wohl, 2007; MacVicar et al., 2007). Several techniques have been adopted to filter ADV data. When using a Sontek Flowtracker ADV in a field study, Wilcox and Wohl (2007) used a multi-step approach that removed measurements with signal to noise ratio (SNR) values <10 db and >35 db. Instantaneous velocities more than three standard deviations away from the SNR mean were discarded; when more than half of the instantaneous values were removed, the time series was discarded and not used in further analysis. Lastly, any remaining time series data with a dimensionless root mean square velocity value greater than five or a standard deviation of the SNRs equal to zero were removed. In a flume study with a Nortek

Vectrino ADV, McBride et al. (2007) removed instantaneous velocity values if the signal correlation was less than 0.7 or if the SNR values were less than 15. When 15% of the instantaneous values were discarded from a time series, the time series was removed from further analysis.

### *2.3.4 Particle Image Velocimetry (PIV)*

Particle image velocimetry (PIV) gives the visualization of a two-dimensional streamline pattern in unsteady flows and a quantification of a velocity field over a plane (Lourenco et al., 1989; Martin et al., 2000). For PIV, a plane parallel to the dominant flow direction is created with tracer particles that should be nearly neutrally buoyant and efficient in scattering light. Seeding the flow with particles is necessary; particle motion is used to estimate the kinematics of the local fluid. Particle movement is recorded through multiple exposure photographs. Velocity is obtained from the particle movement and time between positions. Lasers commonly illuminate the particles due to high recording rates (Grant, 1997).

### *2.3.5 Mechanical Devices*

Mechanical devices can measure point velocities by relating revolutions in a time interval to velocity. In a turbine meter, flowing fluid spins a propeller wheel. The angular speed or number of pulses is then related to flow rate. The accuracy of turbine meters depends on the wheel bearings and longevity (Mattingly, 1996). The performance of these meters is limited in high and low flows, and moving parts are subjective to failure (Julien, 1995). Mechanical impeller current meters are inexpensive, but the moving parts are fragile and require frequent maintenance and calibration (Clifford and French, 1993). A miniature propeller is a mechanical velocity-measurement device that can be used in smaller spaces than traditional devices. A miniature propeller manufactured by Armfield (H33-1, H33-2, and H33-3 velocity probes) consists of a sensing head attached to a stainless steel stem (Figure 2.3). The 5-bladed propeller (11.6-mm diameter) runs on jeweled bearings and rotates within a protective cage. The propeller can rotate freely and responds to low velocities. Both horizontal and vertical velocities can be recorded with the use of two probes (Armfield).

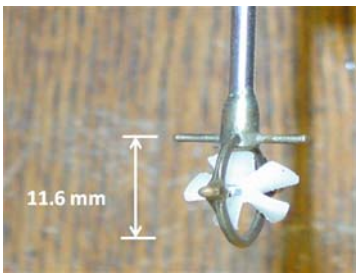


**Figure 2.3 Armfield miniature propeller H33-1 straight, low speed probe (11.6-mm diameter blade).**

## 2.4 Vegetation Influences on Near Bank Flows

Extending Rouse's (1965) classification of flow resistance to vegetated flows results in the addition of terms accounting for vegetation characteristics. Rouse (1965) originally classified drag into surface friction, form resistance, wave resistance, and local acceleration resistance. Since the logarithmic velocity profile does not exist for vegetated flows, the resistance is likely in the form of vegetation drag rather than bed shear (Yen, 2002).

Yen (2002) defined a dimensionless symbolic function, describing the flow over a wide channel in vegetated flows (Equation 2.29):

$$Resistance = F(R, Fr, S_w, S_{bed}, K, L_v, J, D, M) \quad [2.25]$$

where $R$ is the Reynolds number, $Fr$ is the Froude number, $S_w$ is the water surface slope, $S_{bed}$ is the channel bed slope, $K$ is the relative roughness, $L_v$ is the nondimensional vegetation parameter from representative geometry, $J$ is the vegetation flexibility, $D$ is the vegetation relative submergence, and $M$ is the density distribution of vegetation on channel bed. In terms of this study, the parameters R, F, $S_{bed}$, and K will remain constant among the four streambanks. The vegetation parameters D and M will vary among models, providing insight in establishing a functional relationship (Yen, 2002).

The resistance of riparian vegetation reduces velocity and creates a sharp gradient into the main channel flow. The length of velocity penetration is of particular importance for defining mass transport across the interface. In submerged vegetation, the mixing layer is dominated by the downstream progression of vortices responsible for momentum transport; the progressing vortices move high momentum fluid within the canopy (White and Nepf, 2007).

These vortices give the streamwise velocity profile a strong periodic signature and are the main component of Reynolds turbulent stresses (White and Nepf, 2008).

White and Nepf (2007) examined flow structure in a flume channel where one third of the channel was filled with an emergent cylinder array. An inflection point was created in the mean streamwise velocity due to the difference in drag between the main channel and vegetated channel. This instability led to regular periodic vortices at the edge of the array. The presence of these coherent structures likely increases the lateral mass transport between the main channel and the vegetated channel. The shear layer was defined by two distinct length scales: the inner-layer thickness set by the array resistance and the outer-layer thickness set by the water depth and bottom friction.

Yang et al. (2007) examined the effects of floodplain vegetation (grass, shrubs, and trees) on flow structure. With vegetated floodplains, flow resistance increased, resulting in an increase in main stream velocity and a decrease in the floodplain velocity that varied with vegetation type. The resistance difference between the main channel and floodplain also altered the lateral gradient in streamwise velocity, resulting in an increase in shear stress between the main channel and vegetated channel. Turbulent intensities (a statistic that defines velocity deviation from the mean velocity) increased with the addition of vegetation. The streamwise fluctuating velocity showed a periodic and stochastic nature, indicating the presence of coherent vortices progressing downstream.

McBride et al. (2007) examined near-bank turbulence effects caused by forested floodplain vegetation. Forested and non-forested floodplain conditions were compared in a fixed-bed, Froude-scaled model of a northeastern Vermont stream. The non-forested channel consisted of only synthetic grass carpeting on the model floodplain. Wooden dowels were added to the forested model floodplain in addition to the synthetic grass carpeting. An ADV measured three-dimensional velocities to characterize velocity distribution and near-bank turbulence. The streamwise velocities in the near bank region were greater for the non-forested (grass) condition; the resistance provided by the forested vegetation decreased the streamwise velocities, as compared to the non-forested condition. Forested turbulent kinetic energy in the near-bank flow was roughly double the non-forested condition. The higher near-bank turbulence of the forested condition indicated higher erosion potential that might explain the width difference between forested and non-forested streams.

Thorne and Furbish (1995) recognized vegetated roughness on streambanks influences near-bank flow, and possibly affects the patterns of bend migration. Their study examined the influence of coarse vegetated bank roughness on a curved riverbend (Ocklawaha Creek near Tallahassee, FL) by studying near-bank velocity and secondary currents. The meandering, sand-bedded creek had dense bank vegetation composed of cypress and water oak. Velocity and water surface measurements were initially obtained with natural vegetation; then, vegetation was removed (mainly roots) and replaced with a smooth wall. The near-bank flow field changed significantly along the outer bank as a result of the roughness removal. Secondary velocity currents in the center of the channel increased by 19% after the creation of the smooth wall, while magnitudes of near-bed velocities increased by 18 and 107% after the creation of the smooth wall. Vegetation removal also resulted in a 155% increase in near-bank velocities (within 1 m of the bank) and an 85% increase in velocities at the bank surface. Without roughness elements, near-bank velocities were high along the entire channel length, while high velocities were directed toward the channel center line when vegetation was present. With the displacement of high velocities away from the near-bank area, vegetation subdued lateral migration relative to movement associated with a smooth wall (Thorne and Furbish, 1995).

### 2.5 Laboratory Studies of Shear Stress

Physical modeling has both advantages and disadvantages; it allows for a controlled environment where formative processes can be observed, but scaling difficulty leads to simplifying of reality. Simplification increases as spatial and temporal scales increase. While laboratory studies have varying levels of effectiveness, physical models have been used successfully to examine confluence morphology, fluvial sediment transport, bar deposition and migration, channel change, channel pattern, and aggradation. Vegetation influences bank and floodplain strength, but physical modeling including vegetation has been limited (Peakall et al., 1996). Examination of shear stress in flumes has been considered, both with and without vegetation influences.

Petit (1989) examined shear stress partitioning that divides shear stress into that due to form roughness and that due to particle roughness (grain or particle shear stress). In the study, flume tests evaluated methods of calculating grain shear stress and bedform shear stress for a flat bed and a bed with riffles and pools. For the flat bed portion, granite pebbles ($D_{50}$=19.6 mm) were attached to the bottom of the flume (6-m long; 0.5-m wide), not allowing movement. For

the moveable bed portion, the same pebbles were added to the flume and allowed to create riffles and pools. Bed shear stress was calculated by the depth-water slope and law of the wall approaches. Grain shear stress was determined by several methods: based on differences in roughness coefficients in Manning's formula (Richards, 1982); based on the roughness factor (Laursen, 1958); and, based on the Meyer-Peter and Muller approach (Singhal et al., 1980) where the slope was divided into that to overcome particle and bedform resistance. When comparing flat bed results, the law of the wall produced higher shear stress values than the depth-water slope methods (r=0.974). Grain shear stress was compared to total shear stress for the flat bed portion; for all three methods the grain shear stress to total shear stress ratio was very close to one, indicating low bed shear stress for the flat bed experiments. The Laursen (1958) method resulted in grain shear stress values that were the closest to the total shear stress values, indicating it was a good method to estimate grain shear stress. When bedforms were introduced, the grain shear stress was less than the total shear stress. The Laursen (1958) and Singhal et al. (1989) methods resulted in a grain shear stress to total shear stress ratio of 0.40 and 0.22, respectively. The results indicated that bedform roughness accounts for a significant portion of the bed shear stress, supporting the belief that using the slope-water depth approximation (total shear stress in this study) for shear stress may over estimate shear stress estimates in areas with roughness elements.

Thompson et al. (2004) further examined the theory of shear stress partitioning where total shear stress is divided into a portion acting on the soil particles and a portion acting on roughness elements (e.g. vegetation, rocks, microtopography, river bedforms). The goal of the study was to quantify shear stress partitioning for idealized vegetated (nonsubmerged elements) by developing instrumentation for directly measuring particle shear and vegetation shear. The study focused only on vegetation roughness. A constant-temperature thermal anemometer with a flush-mounted sensor was used to measure boundary shear stress. A flume (7.32-m long; 0.38-m wide; 0.38-m deep) was designed and constructed for spatial shear stress measurement collection. A single sensor (flush-mounted probe) was mounted in a movable section of the flume floor, allowing easy movement of the sensor. The flume floor was covered with a layer of 1-mm diameter sand. Simulated vegetation elements were mounted from the top of the channel and were within 3 mm of the channel, making the elements close to the channel bed without touching it. Shapes constructed from PVC represented vegetation (cylinders, rectangular prisms,

trapezoidal prisms). Two cylinder diameters, 0.95 cm and 2.54 cm were used. Rectangle width and thickness were 2.54 and 0.95 cm, respectively. Trapezoidal prisms were oriented both with the small base at the bottom and with the small base at the top; the bases were 0.95 cm and 4.13 cm. All elements had a height of 7.6 cm. Three densities were examined: 1, 4, and 9 elements per 0.145 $m^2$. Two flow rates were evaluated (0.0045 $m^3/s$ and 0.0105 $m^3/s$), resulting in 16 test scenarios. The sensor was calibrated prior, twice during, and following data collection. For each test scenario, particle shear was determined at each location by the hot-film anemometer. Drag force was then measured for each test scenario by a load cell connected to a low-friction linear slide. Drag force caused movement in the linear slide; vegetal shear was calculated by dividing the total measured drag force by the area of the test array. Total shear stress was calculated by summing particle and vegetal shear stress, so that the ratio of particle shear to total shear could be computed. Flow accelerated around the cylinders, resulting in areas of higher shear. This acceleration was present at high vegetation densities, but the particle shear decreased with increasing density. Particle shear stress ranged from 0.73 to 2.27 Pa and vegetation shear ranged from 0.16 to 7.94 Pa. The ratio of particle shear to total shear ranged from 18 to 39%, indicating that the partial coverage reduced the particle shear stress. Future work was suggested to examine a range of test scenarios so the simulated vegetation could be related to natural vegetation (Thompson et al., 2004).

Keller and Wilkinson (2004) recognized direct measurement of BSS in open channel flows is difficult due to the velocity gradient close to the wall; the velocity gradient occurs in a thin layer adjacent to the surface. The authors developed and utilized bed shear stress probes based on constant temperature anemometry theory. The study utilized boundary shear stress measurements at 27 locations in a flume over a range of 0.1 to 8 $N/m^2$. Shear stress probes were constructed with a 25 μm thick insulation coating, and a PVC portable mount. The design allowed the probes to fit tightly though a hole in the wall with an O-ring providing a watertight seal. Probe calibration was conducted before use in the flume to determine the relationship between shear stress and voltage output. Calibration was conducted in fully developed pipe flow at known shear stresses, while temperature was monitored with a thermocouple. Uncertainties that affected the accuracy of shear stress measurements were generated by the following sources: (1) pressure transducer used to determine pressure gradients (uncertainty: ±0.5%), (2) flow rate measurements (uncertainty: ±0.5 to 1%), (3) curve fitting (uncertainty: <6%),( 4) probe

alignment (uncertainty: ±5%), (5) temperature correction (uncertainty: ±7.5%), and (6) sampling error (uncertainty: ±0.6%). Total probe uncertainty was ±12%. After probe development, construction, and calibration, 25 shear stress probes were mounted over a bedform in a flume resulting in a confidence of ± 15%.

To record shear stress profiles, Martin et al. (2000) used DPIV to quantify velocity interactions within the boundary layer. Bed shear stresses were calculated in a flume (406.4 cm length; 35.56 cm height) study for two situations: without sediment (flat bed), and with sediment. Two-thousand captures were taken for both setups, and velocity within the boundary layer, up to 40 mm from the bed, was calculated. Noise from the measurements were filtered, and boundary shear stress was then determined through extrapolation of the Reynolds stresses (Equation 2.17) to the bed. For the setup devoid of sediment, flow depth was 12.5 cm and velocity was measured within 1 mm of the bed; calculations estimated a bed shear stress of 0.345 Pa. After a gravely-sand ($1.190<D_{50}<1.99$ mm) was added to the channel, bed shear stress was measured as 1.34 Pa. Bed shear stress was also calculated by the law of the wall (Equation 2.14), resulting in values of 0.374 Pa and 0.28 Pa for setups with and without sediment, respectively. The results indicated the law of the wall is more appropriate for determining bed shear stress in channels devoid of sediment (flat-bed channels).

Biron et al. (2004) compared bed shear stress estimates from the log profile (law of the wall), drag, Reynolds stresses, and turbulent kinetic energy approaches. The study was conducted in a recirculating laboratory flume (0.6-m wide and 4-m long) with a bed slope and flow depth for all runs of 0.0005 and 0.095 m, respectively; the use of a plexiglas channel reduced the width to 0.04 m. Two sets of experiments were performed to compare the methods. Bed shear stress measurements were examined over a fixed, plexiglas bed and over a mobile bed of uniform sand ($D_{50}$=1 mm). Velocity profiles with eight measurements (five in bottom 20% of flow) were measured, resulting in five fixed bed and nine mobile bed runs. Velocity was measured using an ADV (1 min at 25 Hz). Bed shear stress was calculated by the following methods: log profile (law of the wall), drag ($\tau=C_dU^2$), Reynolds stresses (point and extrapolation), and turbulent kinetic energy (TKE; 3D and vertical). The log profile method utilized a regression of velocity against ln(z) in the bottom 20% of the velocity profile; extrapolation of Reynolds stresses also required a velocity profile. The TKE method was applied using the velocity in three directions and also using only the vertical direction. The remaining

methods used point measurements near the bed at roughly 0.0062 m and 0.0079 m away from the bed for the fixed bed and mobile bed conditions, respectively. Reynolds stresses (Equation 2.17) were also used to calculate the drag coefficient ($C_d$). When comparing the methods for the plexiglas condition, bed shear stress was calculated as 0.110, 0.076, 0.068, 0.055, 0.050, and 0.051 Pa for the log law, TKE, extrapolated Reynolds stress, drag, point Reynolds, and vertical TKE approaches, respectively. For the mobile bed conditions, bed shear stress was 0.427, 0.076, 0.111, 0.073, 0.070, 0.056 Pa log law, TKE, extrapolated Reynolds stress, drag, point Reynolds, and vertical TKE approaches, respectively. The log profile resulted in the largest bed shear stress value for both bed types, while all other methods gave comparable results. This result suggested estimation from near bed turbulence is a better option. The study recommended the use of the extrapolated Reynolds stresses when profiles are available.

After comparing the methods, the study examined the spatial distribution of bed shear stress around deflectors. One 0.05-m long deflector was attached to each wall, constricting the flow. Velocity measurements 0.0064 m from the bed were collected with increasing measurement density around the deflectors. Shear stress was estimated by the drag, Reynolds stresses, and TKE approaches, but instrument limitations of the downward-looking ADV restricted where measurements could be taken close to the deflectors. In the complex flow field (with deflectors) the Reynolds stress approach was not appropriate. Negative values of shear stress resulted and were hard to interpret. The TKE method avoided the problem because it was not affected by local streamline variations and was suggested for use in a complex flow field. The study also addressed the issue of where to take point measurements. Point velocity measurements are generally accepted to be taken at the point closest to the bed above the roughness, but placement needs clarification. The study indicated that the maximum value of shear stress for the Reynolds and TKE methods were found at a non-dimensional height of 0.1 above the bed, suggesting future studies to position velocity instruments at 10% of the flow depth. Continued research for instrument placement is needed to test the height for many conditions (e.g. instrument types, flow rates, bed roughness; Biron et al., 2004).

Ackerman et al. (1994) proposed a Preston-static tube that provides a simple, convenient, and accurate method to measure wall shear stress. The study described the development and use of the Preston-static tubes. Two Preston tube instruments were constructed: a conventional Preston tube and a Preston-static tube. The Preston-static tube included a 900 beveled-tip

syringe needle fixed to a side-bored syringe to measure total and static pressure, respectively. Two sizes of conventional Preston tubes were constructed: 20 and 26 gauge. The Preston-static tubes were tested in a clear PVC pipe (diameter=1.54 cm; 1.8-m from entrance). Pressure taps were present in the wall of the pipe at 0.8 m and 1.8 m from the entrance. The study conducted tests to determine if differences were present from the two gauges of Preston tubes and if differences were present between measurements at the upper and lower walls. The Preston tubes were then calibrated. Secondly, the Preston tubes were located on the upper wall only to determine differences between the wall pressure tap and static tube. An analysis of covariance determined no significant differences existed between measurements made with Preston tubes and Preston-static tubes ($\alpha$=0.05). There were also no differences between the gauges or between the upper and lower walls. When comparing the Preston-static tube to the use of the conventional wall tap, the dimensionless percent difference was approximately 1.6%. This difference resulted in shear stress values clustered to the equality line, indicating the Preston-static tube produced similar results to traditional methods. Scatter was attributed small diameters of the pressure taps that were easily clogged and surface aberrations at the location of the static tubes. Even with scatter present, there was no systematic difference in wall shear stress estimates, and the scatter attributed to the Preston-static tube was not greater than with the conventional methods. The results indicated that the Preston-static tube provided a simple, convenient, and accurate method to measure wall shear stress.

Thornton et al. (2000) also studied the effects of vegetation on shear stress, but studied shear stress at the main channel-floodplain interface. The purpose of the study was to develop an empirical equation to estimate shear stress at the interface as a function of easily measured field parameters, including vegetation density. A flume study (1.22-m wide; 18-m long) was conducted where a model channel was fabricated within the flume composed of a 0.46-m wide channel and a 0.76-m floodplain. Four floodplain vegetation densities were simulated, ranging from none, low (0.025-0.039 $m^{-1}$), middle (0.049-0.056 $m^{-1}$), and high (0.070-0.082 $m^{-1}$). Simulated vegetation was composed of single stemmed, semirigid, multibranched elements (height=10.7 and 30 cm) covered with flexible greenery. Vegetation density was calculated based on the horizontal point frame method outlined by Dudley (1997). Two flow depths (0.30 m and 0.46 m) were tested for each vegetation condition, resulting in eight tests. Velocities were measured by an ADV (30 s at 5 Hz) at eight sites along three cross sections at 20%, 60%, and

80% of the flow depth. Flow velocity and depth in the main channel and floodplain, percent blockage, average bed shear stress, and apparent shear stress (at every measurement location) were determined. Apparent shear stress was determined by velocity fluctuations according to the Reynolds stresses technique. The results indicated the apparent shear stress was greatest at the main channel-floodplain interface; the apparent shear stress at the interface increased with increasing vegetation density. A multivariate, nonlinear regression analysis was preformed incorporating average velocity and flow depth in both the floodplain and main channel. Projected frontal area of the vegetation, cross-sectional area, and distance down from the water surface in the floodplain were also used. An empirical equation was proposed (Equation 2.26) describing the relationship to estimate apparent shear stress at the main channel floodplain interface ($\tau_{mc/fp}$):

$$\tau_{mc/fp} = 0.1025\tau_{bed}\left(\frac{V_{fp}}{V_{mc}}\right)^{-3.4148}\left(\frac{D_{fp}}{D_{mc}}\right)^{2}(1-B) \qquad [2.26]$$

where B is the flow blockage by vegetation (%), $\tau_{bed}$ is the total bed shear stress (Pa), $V_{fp}$ is the average velocity of floodplain (m/s), $V_{mc}$ is the average velocity of main channel (m/s), $D_{fp}$ is the depth of flow in floodplain (m), and $D_{mc}$ is the depth of flow in main channel (m).

Wilson et al. (2003) examined the issues of biomechanical scaling from natural vegetation and studied the influence of flexible vegetation on turbulence structure. Specifically, turbulence characteristics were examined for a flexible rod of constant height and for a flexible rod with attached frond foliage. A 1/10 geometric scaling of kelp (*Laminaria hyperborean*) and the Froude law were used to scale the natural situation incorporating geometric (length and area), kinematic (velocity), and dynamic (force, bending stiffness, and flexural rigidity) relationships in the scaling. Seven kelp samples (58 force deflection tests) were tested for bending stiffness, resulting in a mean value of 9.2 N/m. Twenty-two flexible rods were constructed from a liquid plastic with a bending stiffness of 45.1 N/m; the manufactured rods had a greater bending stiffness, indicating the difficulty of reproducing natural elements. The rods represented grass or reed vegetation, while the added foliage represented common macrophytes. Flexural rigidity of the model rods was evaluated based on the force, deflection, and beam length, resulting in a range of 6.8 to 11.3 $N/m^2$ for the scaled rigidity. The drag force-velocity relationship was

measured in a flume (0.5-m wide; 10-m long) with a force transducer and minipropeller. The turbulence experiments were carried out in the flume with plant stem height/water depth ratios ranging from 1.5 to 3.4 in a 7-m long section. An ADV measured velocity and turbulent characteristics at a frequency of 25 Hz with a 240 s sampling period.

The simulated plants were attached to the flume floor a plant density of 22.4 $m^{-1}$. Velocity profiles indicated flow within the plant layer was reduced and did not follow a logarithmic velocity profile. Within the plant layer with fronds attached, the mean velocity was less than half that observed in the simple rod layer. A higher turbulence was also detected in the simple rod layer, indicating the fronds shifted the peak Reynolds stresses above the flow canopy; the frond layer inhibited momentum exchange between the frond layer and the overlying surface flow. Because the fronds were shown to significantly increase the momentum adsorbing area, plants with fronds may provide more protection than reed or grass plants in restorative efforts.

White and Nepf (2008) developed a model to predict the two-layer structure of shear stress with riparian vegetation. The study examined the distribution of velocity and shear stress in a flume study that incorporated emergent boundary vegetation. Emergent wooden dowels (6.5-mm diameter) covered 40 cm of the flume bottom (1.2 m wide, 13 m long), creating a vegetation channel and a main channel. The void fraction of the vegetation ranged from 0.02 to 0.10. Shallow flow conditions were satisfied and velocity measurements were made using LDV. Two distinct regions of a shear layer were identified: a region of high shear across the vegetation-main channel interface, and the region outside the vegetation into the main channel. The shear dropped rapidly into the vegetation and gradually into the main channel. The maximum shear stress corresponded to the inflection point of the hyperbolic tangent velocity profile. Coherent vortex structures exchanging momentum between channel and vegetation were apparent in the shear layer and were identified as the greatest contributor to turbulent shear stress. The vortices had a strong periodic signature and the vortice width corresponded with the width of the outer layer. The study was successful in predicting the velocity distribution by dividing the flow into four zones: 1) the uniform region within the vegetation layer; 2) the inner layer at the interface; 3) the outer boundary layer in the main channel; and, 4) the region of uniform flow in the main channel. The model used the mean velocity within the vegetation, the constant velocity in the main channel, drag coefficient, and mean projected area per unit volume as inputs and captured the two layer structure of the velocity profile. The shear stress

distribution also predicted the high shear stress in the inner region and the transition into the main channel flow. The model addressed and predicted the sharp decline of Reynolds stresses into the vegetation and the peak shear stress at the vegetation interface.

### 2.6 Field Studies of Shear Stress

Petit (1990) extended an earlier flume study (Petit, 1989) to two rivers, Rulles and Rouge Eau. The Rulles river was a meandering riffle-pool channel, characterized by a pebbley bedload ($D_{50}$~20 mm, based on Petit, 1989). The Rouge Eau was characterized by a sandy bed with ripples reaching up to 1 cm and continuous bedload transport. Continuing the idea of shear stress partitioning, Petit (1990) recognized that particle (or grain) shear stress was responsible for sediment transport. Total shear stress was evaluated based on the slope-water depth and law of the wall approximations. Thirty-seven cross-sections at five sites and seven cross-sections at three sites were used for the Rulles and Rouge Eau, respectively. Velocities profiles (5-cm increments) were measured at 1.5, 3.0, and 5.0 cm from the bed using an OTT velocimeter. Grain shear stress was estimated based on Manning's n (Richards, 1982), Laursen (Laursen, 1958), and Meyer-Peter and Muller (Singhal et al., 1980) methods. When comparing the slope-water depth and law of the wall methods to determine total shear stress, the law of the wall method resulted in lower shear stresses than the slope-water depth method. Grain to total shear stress ratios ranged from 0.02 to 0.46 for the Laursen and Meyer-Peter and Muller methods. Greater ratios were present in the Rulle riffle locations with values ranging from 0.33 to 0.46 for the Laursen method (0.15-0.21 for Meyer-Peter and Muller); ratios in pools in the Rulles river ranged from 0.06 to 0.29 for the Laursen method (0.03-0.12 for Meyer-Peter and Muller). The sandy Rouge Eau river resulted in lower ratios ranging from 0.02-0.12 due to the lack of bedform roughness. The ratios were less than 50% indicating that the values were underestimated and appeared too low to account for the movement of the bed material.

Wilcock (1996) estimated local boundary shear stress in the Trinity River in California using the logarithmic relation (Equation 2.14). The gravel bed river had a median particle size ($D_{50}$) between 22 and 44 mm; straight reaches were selected to ensure grain roughness was dominant. Basic Price AA current meters were used to measure velocity and flow depth with a 40-60 s observation time. Three techniques were used to estimate shear velocity (u*) of the logarithmic equation: (1) based on single observations of u and an estimate of $z_0$ (Equation 2.14); (2) based on a least squares fit of ln(z) vs. u; and, (3) based on the depth-averaged velocity. The

study evaluated the precision of the methods for estimating shear velocity under identical conditions. Estimates derived using single u observations were quick, but the shear stress estimates were less precise than the multiple observation technique; standard error was two to three times lower for estimates using multiple velocity observations than for single measurements. Estimates based on depth-averaged velocity were most precise, but the technique is limited to wide, shallow flow in straight channels with simple roughness. The linear fit technique was the least precise method, but an independent value of bed roughness was not needed. This technique was also limited to measurements in the log layer that may be small in flows with large roughness. The study suggested that the depth-averaged velocity technique may apply to conditions of large roughness where Equation 2.14 is not valid (Wilcock, 1996).

Biron et al. (1998) examined the law of the wall for estimating average bed shear stress. The study evaluated the uncertainty that arises from the law of the wall due to flow depth and elevation of lowest measurement above the bed. Three-dimensional velocity was measured using a Sontek field ADV (2 min at 25 Hz) at three field locations with varying bed sediment, resulting in three vertical velocity profiles: (1) a profile of 20 average velocity measurements was taken beginning 0.0015 m above the bed ($D_{50}$=0.39 mm, H=0.225 m); (2) a profile of 16 average velocity measurements was taken beginning 0.0053 m above the bed ($D_{50}$=1.93 mm, H=0.150 m); and, (3) a profile of 21 average velocity measurements was taken beginning 0.0029 m above the bed ($D_{50}$=21 mm.41, H=0.150 m). For all locations, baseflow and an inactive bed dominated. After the velocity profiles were complete, the results were analyzed according to the law of the wall, regressing time-averaged downstream velocity against the natural log of the elevation. The three velocity profiles were subsampled in two forms: the effect of using the full profile was compared to using the near-bed portion of the profile. The effect of varying the minimum height of velocity measurement was also assessed.

The first velocity profile revealed a fully developed boundary layer with a log portion in the bottom 20% of the flow due to the smooth bed surface. The second velocity profile showed a logarithmic shape and the presence of a depth-limited boundary layer. The third velocity profile was complex where the bed roughness was large, indicating slow moving flow in the roughness elements and a location of local bottom shear higher from the bed. At the first two locations, shear stress estimates increased with percentage elevation and reached a maximum at 20% of the flow depth measured from the bed, the depth corresponding to the height of the logarithmic

layer. Shear stress declined when including a greater portion of the flow (above 20%) in the analysis. At the third site, shear stress increased with distance from the bed until reaching 16% of the flow depth, the point corresponding to the shear layer height. Shear stress increased rapidly from 16 to 35% of the flow depth. The conflicting results were attributed to the bed roughness: deviation from the log profile was expected in the presence of roughness that reduces near bed velocities. At the first two sites, shear stress was higher when computed using the lower portion of the flow due to the steep velocity gradient. At the third location, shear stress increased as the minimum elevation increased; values were 30 times larger when the minimum height was at 12% of the flow (18 mm for this case). The results revealed issues to consider when utilizing the law of the wall; the inclusion of near bed points of velocity is critical. Using the full flow depth rather than 20% of the flow results in an underestimation of shear stress in uniform flow; measuring heights affect the evaluated shear stress (Biron et al., 1998).

Following the development of a Preston-static tube (surface mounted Pitot-static tube; Ackerman et al., 1994), Ackerman and Hoover (2001) calibrated the Preston-static tube in a lab situation and implemented it in the field to determine whether the Preston-static tube was appropriate to measure shear stress in streams. A Preston-static tube (inner diameter=0.56 mm, tap diameter=0.50 mm, inner/outer diameter=1.65) was constructed from a $90^{o}$ beveled tip syringe and tip syringe needles. After calibration, the Preston-static tube was used to measure shear stress and velocity gradient in the Tropy River in Prince George, British Columbia. The reach had a smooth, gravel bottom (0.5-5 cm), and the shear stress measured by the regression method and Preston-static tube was consistent with that found in the lab calibration. Measurements of local shear stress were taken at three locations along the lower Tropy River with varying water depth, width, slope, discharge, average velocity, and bed material. Local shear stresses ranged from 0.1 to 3.8 Pa, with average local shear stress values of 0.8, 0.14, and 2.0 Pa. The Preston-static tube was successful in measuring wall shear stress (shear stress at was within 1/3 of the shear stress measured in the flume at a comparable velocity), but the instrument was limited by the ability to measure pressure difference determined by the dynamic pressure of the flow. The instrument was limited in areas of turbulent flow where varying flow directions and water depths made it difficult to orient the instrument. Average shear stress was determined by the product of the water depth and slope; local shear stress accounted for 4-10% of the average shear stress due to form drag from bed forms, indicating the distribution and magnitude

of local shear stress was variable. The results suggested further study was needed to determine the effects of spatial distributions and local influences, such as pressure gradients, substrate shape, and spacing on local shear stresses (Ackerman and Hoover, 2001).

Moody and Smith (2004) made 3D velocity measurements near a sloping streambank to quantify Reynolds stresses. Measurements were made along the left streambank (opposite a cutbank) of the Powder River in southeastern Montana during snowmelt. The stream had an annual mean discharge of 12.7 $m^3/s$, sand and gravel bed, and an average slope of 0.0015. During the three days of measurement (May 1996), the stream had quasi-steady flow with a peak discharge of 71 $m^3/s$. ADV measurements (1000 s at 25 Hz) were taken along six locations (0.5-m spacing; 0.05 m vertical increments). All normal stresses decreased near the bank and ranged from -6.5 to -0.4 Pa. Boundary shear stress was estimated by extrapolating the stresses to the bed, giving values ranging from 0.61 to 1.2 Pa. Suggestions for improvement of the turbulence measurements included: (1) determining the streamwise direction before beginning measurements; (2) increasing the number of samples; (3) reducing the sampling time; (4) determining the location of the channel bottom before taking measurements; and, (5) making measurements at times of low wind velocity.

Daniels and Rhoads (2004) examined how the TKE related to patterns of mean fluid motion, channel shape, and patterns of bed shear stress within a meander bend with a large woody debris (LWD) obstruction. A headwater agricultural stream, Madden Creek, in East Central Illinois was used for the study. A complex LWD obstruction extended across the channel downstream of the bend apex and was composed of a trunk and exposed tree roots. The stream fits into the criteria stated by Anderson et al. (2004) for vegetation influencing the flow; the drainage area and stream width were 42 $km^2$ and 9 m, respectively. A bimodal distribution of sand and gravel made up the bed. An ADV was used for 3D velocity measurements (60 s at 25 Hz) at five cross sections at the bend entrance (4), near the bend apex (5- 6), immediately upstream of the LWD obstruction (7), and downstream of the obstruction (8). Bed shear stress was calculated based on the TKE method (Equation 2.22) where $C_1$ had a value of 0.21. At cross-sections 4 and 6, TKE was roughly uniform across the channel. Approaching the LWD (cross-section 7), TKE increased towards the outer bank; the maximum value of TKE was immediately upstream of the obstacle. Downstream of the obstruction, large TKE values were along the inner bank, resulting from flow directing off the debris. Bed shear stress followed as

similar trend. For cross-sections 4-6, near bed shear stresses were greatest near the outer bank but were not adjacent to the bank. As flow approached the obstruction (cross-section 7), maximum values of near bed shear stress increased and maximum near bed shear stress values were directed toward the center of the channel. Downstream of the obstruction, high near bed shear stress values were measured near the inner bank as flow was directed past the LWD. The shifts in high near bed shear stresses were consistent with bed scour and widening patterns. The redistribution of TKE across the obstruction from the outer to the inner bank was attributed to directing the mean flow around the debris and to the redistribution of secondary flows. The results suggested that LWD may be used to redirect areas of high shear stresses, but additional research is needed to understand the full impact on bank stability.

Hoover and Ackerman (2004) studied bed shear stress over boulders as it related to stream organisms, recognizing that near wall eddies, wall shear stress, and boundary layer phenomena affect stream organisms. The study examined velocity distributions and local wall shear stress on the upper surfaces of torrential stream boulders and characterized the channel hydraulics. A 20-m study reach on a tributary of the Torpy River near Prince George, British Columbia, Canada was selected (maximum discharge during study = 0.43 $m^3/s$). The study reach was a single thread, straight channel with an average bed slope of 3.2%. The bed consisted of boulders, cobbles, and coarse gravel. Thirty natural boulders (diameter=22-36 cm) were selected, cleaned, identified with a number, deployed in the stream at 1-m offset intervals, and evaluated after 10 d. The stones were evaluated for larval mayfly density, and five stones (S07, S31, S25, S23, and S10) with the highest densities ($>10^{-2}$ larval mayfly/$m^2$ during the day and >150 larval mayfly/$m^2$ during the night) were chosen for further investigation. Three natural boulders (N01, N02, and N03) were also selected for further study that had similar larval mayfly density as the experimental stones. The stream environment was characterized by a point gage to measure water surface and bed topography, and a Preston-static tube to measure shear stress and velocity. Dye was injected upstream of the Preston-static tube to ensure proper orientation of the instrument. Shear stress was determined by Preston's (1954) relationship

Velocity profiles showed a variety of patterns often deviating from the log-normal profile. When the leading edge of the boulders was inclined (S07, S31, S23, and N03), flow was constricted and near bed velocities were greater than mid-stream and surface velocities. With wedge-shaped profiles, the maximum velocity was located 1-10 mm above the boulder and then

decreased in a logarithmic manner toward the surface. A logarithmic profile existed for two boulders (S07 and N01) and developed because there was sufficient distance along the stone surface for the boundary layer to form. For shear stress estimates, shear stress was estimated based on the Preston-static tube technique and based on the law of the wall for the portion of the profile directly above the boulders (2-7 mm). When law of the wall estimates were compared to the Preston-static tube estimates, a positive relationship was found for the log-normal profiles ($p=0.03$) but not for the wedge shaped ($p=0.85$) or transitional profiles ($p=0.81$). When near bed distortion was present (transitional and wedge shaped profiles) the law of the wall underestimated shear stress as compared to the Preston technique by an average of 61%. The law of the wall was limited due to the small thickness of the logarithmic layer. Most velocimeters in field settings are incapable of taking measurements in the layer. Shear velocity ranged between 3.4% and 14.2% of the mean velocity. Near bed velocities were higher in wedge-shaped and transitional velocity profiles ($p<0.001$), and there was no significant difference in near bed velocities between wedge-shaped and transitional profiles ($p=0.71$)

**2.7 Modeling shear stress in vegetated channels**

Conceptual models of channel development (e.g. Schumm et al., 1984; Booth, 1990; Hupp and Simon, 1991; McBride et al., 2008) can explain channel adjustment following disturbance (McBride et al., 2008). McBride et al. (2008) proposed a conceptual model to explain channel adjustment in response to the introduction of forested riparian vegetation. The model describes the multiphase adjustment of channel incision and widening with four steps. The first stage begins as an equilibrium nonforested channel with low turbulence, no LWD input, and high floodplain inundation. In stage two, reforestation begins. The introduction of small woody plants increases floodplain resistance, generating a large velocity differential between the vegetation channel and the main channel. The generation of turbulence by the riparian vegetation results in channel incision. In the third stage, incision slows and the channel widens, establishing mature forest riparian vegetation. Shade provided by the forest vegetation prevents the establishment of grass, likely weakening and widening the streambanks. LWD is present as the banks fail and the forest vegetation ages. In the final model stage, the channel reaches a new equilibrium that has the ability to move the discharge and sediment with the new riparian resistance. The near-bank turbulence decreases compared to stage two and three due to the added channel complexity and widening.

While conceptual models provide guidance on channel development, quantitative models are needed to verify conceptual models. Kean and Smith (2004) adapted a model developed by Houjou et al. (1990) that calculates velocity and shear stress fields using ray-isovel turbulence closure to include the drag effects of vegetated banks. This model expanded ray-isovel approach developed by Leighly (1932). Isovels are lines of constant velocity, and rays, perpendicular to the isovels, range from the channel boundary to the water surface. The area between two rays at the boundary represents shear stress on the boundary (Kean and Smith, 2004; Wobus et al, 2008). The model has been applied to flume studies (Kean and Smith, 2004) and geomorphically stable natural channels (Griffin et al., 2005; Kean and Smith, 2005), with an additional erosion component (Wobus et al., 2008), with small-scale topographic features on the channel boundary (Kean and Smith, 2006a and 2006b), and with a simulated cobbled floodplain (Kean et al., 2009).

Kean and Smith (2004) applied the flow model to examine the impacts of varying vegetation density and channel geometry on velocity and boundary shear stress distributions. The study concluded that two parameters were important to determine near boundary velocity and shear stress distributions in channels with streambank and floodplain vegetation: vegetation drag and boundary friction. The model results indicated that sparse vegetation BSS and velocity distributions were similar to condition with no vegetation. In channels with dense rigid bank vegetation, drag on the vegetation was more important than the stress on the banks, dominating the stress distribution.

Kean and Smith (2005) used the Kean and Smith (2004) model to produce theoretical rating curves for two reaches on a stable channel near USGS gaging stations. The model calculated drag on the boundary features, vegetation stems, and boundary friction. The theoretical curves were in good agreement to direct measurements of stage-discharge at the USGS gaging stations. The calculation of both vegetation drag and lateral boundary friction were necessary to accurately calculate discharge on the narrow wooded channel.

Griffin et al. (2005) applied the Kean and Smith (2004) model to an ephemeral stream in the semi-arid southwest USA. Boundary shear stress distributions were examined by calculating form drag on woody plant stems. The model included the effects of vegetation on the boundary shear stress, velocity, and turbulence fields. Field data were collected from the Rio Puerco (average sinuosity=1.48; trapezoidal shape, average width to depth ratio=9.3). Cross-sections

were surveyed at 49 sites, and vegetation data were collected at each site. Channel banks were densely vegetated by shrub willows and tamarisks. For model input, stem type, size, density, and stem distribution were collected. Stems were counted within six 1.5-m quadrats to provide information about the shrub distribution. The average stem diameter and spacing were 0.01 m and 0.20 m, respectively. Flow records were collected from a gaging station near Bernardo, NW, providing gage heights and discharge estimates for the modeled time period. Shear stress was calculated by an isovel technique that iterated lines of constant velocity. Model sensitivity analysis was performed, examining surface roughness and bank vegetation. Model results calculated perimeter-averaged boundary shear stress within 1% of the value calculated based on $R_h$ and S. Bank friction reduced maximum boundary shear stress at the middle of the channel, but the percent reduction was dependent on flow depth and channel shape. The greatest reduction occurred in channels with smaller width to depth ratios (~8.2). Maximum boundary shear stress was reduced by as much as 20% with bank roughness. The reduction increased to 40% for bankfull flows with dense bank shrubs.

A derivation of the ray-isovel model for steady, streamwise uniform flow with lateral boundaries and vegetation roughness is provided below.

### *2.7.1 Ray-isovel technique for channels with lateral boundaries and vegetation roughness (Kean and Smith 2004)*

For a vegetated channel with lateral boundaries and vegetation roughness, the momentum equation balances the gravitational stress with the deviatoric stresses and the vegetation drag force per unit volume. The momentum equation can be defined by the following equation (for steady, streamwise uniform flow):

$$0 = \rho g S + \frac{\partial \tau_{yx}}{\partial y} + \frac{\partial \tau_{zx}}{\partial z} - F_{stems} \qquad [2.27]$$

where ρ is the water density, g is the acceleration due to gravity, S is the water surface slope, $\tau_{yx}$ is the yx component of the deviatoric stress tensor, $\tau_{zx}$ is the zx component of the deviatoric stress tensor, and $F_{stems}$ is the drag force per unit volume due to the stems (Kean and Smith, 2004).

For uniform flow, the downstream weight of water must be balanced by the friction along the wetted perimeter. This restraint provides the definition of average boundary shear stress for all channel geometries without vegetation:

$$\overline{\tau_b} = \rho g S \frac{A}{p_b} \qquad [2.28]$$

where A is the cross-sectional area, and $p_b$ is the wetter perimeter (Kean and Smith, 2004).

If a new coordinate system is defined, a similar balance exists along a portion of the wetted perimeter for a fractional area of the cross-section. The new coordinate systems is formed by isovels (lines of constant velocity) and rays (lines perpendicular to the isovels). An example of possible ray-isovel distribution for the experimental set-up of this study is provided in Figure 2.4. Rays define the streamwise surface of zero shear and the direction along which mixing occurs. The BSS of a fractional area along the cross section (dA) can be defined as the downstream weight of water between two rays divided by the $\delta p_b$ that separates them (Figure 2.4; Equation 2.29; Kean and Smith, 2004).

$$\tau_b = \rho g S \frac{\int_0^L dA}{\delta p_b} \qquad [2.29]$$

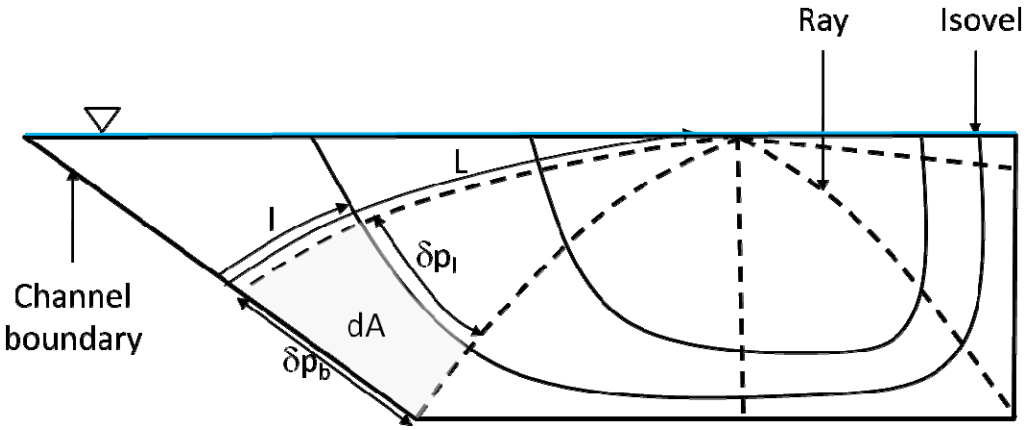


**Figure 2.4. Distribution of ray-isovel grid with incremental area (dA) and incremental wetted perimeter length ($\delta p_b$) highlighted. L is the ray length, l is the length of the ray from the boundary, and $dp_l$ is the isovel length between two rays.**

The ray-isovel coordinate system also simplifies defining the kinematic eddy viscosity because rays define the direction of mixing. Kinematic eddy viscosity that varies in lateral and vertical directions in flow near lateral boundaries is reduced to one-dimensional variation along the ray length:

$$\tau_{lx} = K_b \frac{\partial u}{\partial l} \qquad [2.30]$$

where $K_b$ is the kinematic eddy viscosity in unvegetated areas. $K_b$ depends on the distance from the boundary (l; Figure 2.4), the shear velocity (u*), $\tau_{lx}$ and $\tau_b$ and is expressed by the following equation.

$$K_b = ku^* l \frac{\tau_{lx}}{\tau_b} \qquad [2.31]$$

where k is the Von Karman constant. $K_b$ increases until reaching the channel scale eddy viscosity ($K_o$):

$$K_o = ku^* \frac{H}{\beta} \quad [2.32]$$

where β is a constant (Kean and Smith, 2004).

In the vegetated portions of the channel, the boundary shear stress is reduced due to the drag on the plants and can be calculated by the following equation (Kean and Smith, 2004):

$$\tau_b = \frac{\int_0^L (\rho g S - F_{stems}) dA}{\delta p_b} \quad [2.33]$$

where $F_{stems}$ is the drag force per unit volume due to the stems:

$$F_{stems} = \frac{1}{2} \rho C_D \alpha u_{ref}^2 \quad [2.34]$$

where $C_D$ is the drag coefficient of a single stem (1.2 for high Reynolds numbers), $u_{ref}$ is the reference velocity, and α is the cross-sectional area of the stems oriented perpendicular to the flow direction per unit volume. Alpha can be defined by the following equation:

$$\alpha = nD_s = \frac{D_s}{\lambda^2} \quad [2.35]$$

where n is the number of stems per unit area, $D_s$ is the average stem diameter, and λ is the average stem spacing (Kean and Smith, 2004).

Changes in channel turbulence due to the addition of vegetation assume that the energy removed by flow through the stems produces turbulent energy. Eddy viscosity for vegetated regions ($K_t$) is defined by the following equation:

$$K_t = \frac{1}{8} C_t^{-2} C_D D_S u \quad [2.36]$$

where $C_t$ is the change in local velocity in the stems divided by the mean local velocity and depends on the shape of the streamwise velocity profile (Kean and Smith, 2004).

In a rough channel with vegetated streambanks, turbulence production occurs from a combination of vegetation and wall effects. Overall eddy viscosity ($K_{eddy}$) can then be defined by a weighted average of $K_t$ and $K_b$.

$$K_{eddy} = \frac{1}{1+\left(\lambda / l^2\right)} K_b + \frac{1}{1+\left(\lambda / l^2\right)} K_t \qquad [2.37]$$

By defining kinematic eddy viscosity and $F_{stems}$, the momentum equation can be defined by the following equation:

$$0 = \rho g S + \frac{\partial}{\partial y}\left(\rho K_{eddy} \frac{\partial u}{\partial y}\right) + \frac{\partial}{\partial z}\left(\rho K_{eddy} \frac{\partial u}{\partial z}\right) - \frac{1}{2}\rho C_D \alpha u^2 \qquad [2.38]$$

Equation 2.37 allows turbulence closure for vegetated channels. The model solves the momentum equation and the equations for $\tau_b$, $\tau_{lx}$, and $K_{eddy}$ alternatively until the solution converges. The model must start with a guess of boundary shear stress and inner velocity (Kean and Smith 2004).

## 2.8 Summary

Total applied shear stress on the channel boundary is commonly calculated based on flow depth and slope (Chang, 2002), but this method can cause major errors in soil detachment calculations when resistance is substantial (Abrahams and Parsons, 1991). Shear stress has also been related to channel stability (Temple, 1980, 1983, and 1985) and is important for the design of stable channels where the applied shear stress cannot exceed the critical shear for motion by fluvial erosion (Chang, 2002). While bed shear stress has been examined in flume and field studies, little research has been conducted on streambank erosion, especially for hydraulically rough streambanks (ASCE, 1998b). Previous studies have considered the effects of vegetation on streambank soil erodibility and critical shear stress, but the effects of riparian vegetation on channel hydraulics need to be considered to fully understand the impact of vegetation on streambank erosion (Wynn and Mostaghimi, 2006b).

This study examined the effects of vegetation on boundary shear stress to develop a better understanding of streambank erosion due to fluvial entrainment. This research sought answers to the following questions:

1. How does vegetation type affect boundary shear stress estimates along the streambank?
2. How does boundary shear stress vary spatially along the bank face?
3. How do velocity profiles perpendicular to the streambank vary among vegetation type and along the bank face?
4. Can a method be developed to easily measure boundary shear stress *in situ*?
5. Which theory/instrument combination provides boundary shear stress estimates similar to hot-film anemometer estimates?
6. How do boundary shear stress model results (Kean and Smith 2004) compare to direct measurements of boundary shear stress?

# Chapter 3 Design of the Streambank Flume Model and Data Collection

## 3.1 Introduction

A second order stream, Tom's Creek (watershed area = 20.7 $km^2$) in Blacksburg, Virginia, USA, was modeled within a research flume (1-m wide; 6-m long; 40-cm deep). Three distinct vegetation types exist in close proximity along the channel: trees, shrubs, and grass. An experimental reach was identified within each vegetation type, resulting in three prototype reaches. The reaches exhibited the following characteristics to minimize variability: (1) relatively straight to decrease secondary flow effects; (2) grouped to ensure similar watershed characteristics (Hession et al., 2003); (3) minimal tributary input for constant discharge among reaches; and, (4) at least four bankfull widths in length. Each reach consisted of a riffle and pool so the bedforms were similar among the reaches. The main difference among the research reaches were vegetation density and type. The tree, shrub and grass reaches were dominated by rhododendron, briars and tall fescue grass, respectively. While rhododendron is a shrub, the rhododendrons along the reach were particularly large shrubs (woody stem diameters ranged from 3 cm to 13 cm). Therefore, the streambank dominated by rhododendron was selected as the forest bank and will be referred to as the tree bank throughout this study.

## 3.2 Initial Field Measurements of the Prototype Stream

Channel geometry, grain size, and vegetation parameters were measured to characterize Tom's Creek. Reach lengths were 26 m, 15 m, and 21 m for the tree, shrub and grass reaches, respectively. Discharge for the prototype stream was calculated based on the field data for use in dimensional analysis. Vegetation densities were measured for each vegetation type. Median values of channel geometry information are presented in Table 3.1.

**Table 3.1. Median values for channel geometry values for the forest, shrub, and grass experimental reach.**

| | Forest | Shrub | Grass |
|---|---|---|---|
| **Cross-sectional area ($m^2$)** | 12.2 | 4.8 | 5.7 |
| **Width (m)** | 12.5 | 8.3 | 6.0 |
| **Mean depth (m)** | 1.0 | 0.6 | 0.9 |
| **Max depth (m)** | 1.3 | 1.0 | 1.5 |
| **Wetted perimeter (m)** | 13.2 | 9.2 | 7.7 |
| **Hydraulic radius (m)** | 0.9 | 0.6 | 0.7 |
| **Width-depth ratio** | 12.8 | 13.3 | 6.6 |

*3.2.1 Bank Slope*

A detailed survey of each experimental field reach was conducted with a total station, resulting in five cross-sections for the tree reach and eight cross-sections for the shrub and grassed reaches. A summary of the total station cross-section data is available in Appendix A. Fewer tree cross-sections were measured due to dense leaf cover. Average bank slope and length were calculated by the least squares estimate of the combined survey data for each reach (Table 3.2).

For each stream cross-section, the top of bank point was set as distance zero. Cross-section data were then combined for each vegetation type, and bank slope was determined by a least squares estimate. The least squares estimate of the combined cross-section data for the tree reach resulted in a bank slope and bank length of 0.33 m/m and 4.5 m, respectively ($R^2$=0.71; Table 3.2). For the shrub reach, cross-section 4 was not representative of the overall reach and skewed the data ($R^2$=0.35). The cross-section was removed from the analysis, resulting in a bank slope and bank length of 0.71 m/m and 1.36 m, respectively ($R^2$=0.50; Table 3.2). For the grass reach, cross-section 7 was not representative of the overall reach and skewed the data ($R^2$=0.51). The cross-section was removed from the analysis, resulting in a bank slope and bank length of 1.10 and 1.8 m, respectively ($R^2$=0.59; Table 3.2).

**Table 3.2. Bank slope, length, and angle calculated for the prototype stream based on surveyed cross-sections and a regression analysis ($R^2$ is presented); bank angle defined as the angle between the streambank and the horizontal. .**

| Stream Reach | Bank Slope (m/m) | Bank Angle ($^o$) | Bank Length (m) | $R^2$ |
|---|---|---|---|---|
| Tree | 0.33 | 18 | 4.50 | 0.71 |
| Shrub | 0.71 | 35 | 1.36 | 0.50 |
| Grass | 1.10 | 47 | 1.80 | 0.59 |

*3.2.2 Longitudinal Slope*

Longitudinal slope was calculated based on bed slope along the thalweg from top of riffle to top of riffle for each experimental reach (Appendix A). The least squares estimate of the bed slope was 0.48%, 0.06%, and 0.46% for the tree, shrub, and grass reach, respectively. The bed slope calculated for the shrub reach was less than the tree and grass reaches. This section is upstream of a bridge and may have been altered during bridge construction (Figure 3.1). A slope of 0.5% was used in the flume study.

**Figure 3.1. Bridge downstream of shrub reach cross-section.**

*3.2.3 Vegetation Characteristics*

**Tree:** Woody vegetation along the tree reach was quantified in seven 1.5-$m^2$ quadrats. Stems were counted adjacent to the bank and diameters were recorded. Stems were also counted and diameters were recorded at breast height (DBH). Based on the data from the quadrats, there was an average stem density of 10.1 stems/$m^2$ adjacent to the bank (Table 3.3). The average

stem diameter was 9.4 cm. On average the stems split twice (Table 3.4) and the average stem DBH was 3.2 cm.

**Table 3.3. Tree vegetation characteristics of stems adjacent to the streambank, indicating stem count, stem density, stem diameter, total stem area, and vegetation density measured for each 1.48-$m^2$ quadrat of the tree experimental reach at Tom's Creek.**

| Quadrat | Stem Count | Stem Density | Stem Diameter | | | Total stem area | Vegetation Density |
|---|---|---|---|---|---|---|---|
| | | | min | max | average | | |
| | (number) | (stems/$m^2$) | (cm) | (cm) | (cm) | ($m^2$) | ($m^2/m^2$) |
| 1 | 14 | 9.42 | 2.54 | 46.48 | 11.41 | 0.28 | 0.1858 |
| 2 | 21 | 14.13 | 3.05 | 16.00 | 8.45 | 0.14 | 0.0930 |
| 3 | 10 | 6.73 | 4.06 | 16.00 | 8.08 | 0.06 | 0.0403 |
| 4 | 30 | 20.18 | 2.03 | 22.86 | 5.94 | 0.11 | 0.0773 |
| 5 | 11 | 7.40 | 3.30 | 7.37 | 4.78 | 0.02 | 0.0143 |
| 6 | 11 | 7.40 | 2.03 | 30.73 | 12.63 | 0.23 | 0.1555 |
| 7 | 8 | 5.38 | 4.32 | 52.32 | 14.48 | 0.25 | 0.1708 |
| **Average** | | **10.1** | | | **9.4** | | **0.105** |

**Table 3.4. Tree vegetation characteristics of stems measured at breast height (BH), indicating stem count, the number of splits of the trees at BH, stem diameters at BH.**

| Quadrat | Stem Count | Number of splits to BH | | | Stem diameter at BH | | |
|---|---|---|---|---|---|---|---|
| | | min | max | average | min | max | average |
| | | (number) | (number) | (number) | (cm) | (cm) | (cm) |
| 1 | 26 | 0 | 5 | 2.00 | 0.51 | 29.97 | 4.76 |
| 2 | 36 | 0 | 4 | 0.51 | 0.51 | 14.73 | 3.50 |
| 3 | 22 | 0 | 6 | 2.20 | 0.51 | 8.64 | 2.83 |
| 4 | 59 | 0 | 6 | 1.97 | 0.51 | 11.43 | 2.25 |
| 5 | 26 | 0 | 5 | 2.36 | 0.51 | 3.81 | 1.86 |
| 6 | 31 | 0 | 9 | 2.82 | 0.51 | 24.13 | 3.57 |
| 7 | 28 | 0 | 7 | 2.57 | 0.76 | 34.54 | 5.19 |
| **Average** | | | | **2.06** | | | **3.42** |

Tree placement along the bank face was also surveyed. The location of each tree was surveyed and the circumference at the base of the tree was recorded (Figure 3.2). A combination of the survey and DBH data was used to determine vegetation placement and size. Placement was determined using the field survey, and stem diameter was determined using a combination of DBH and circumference measurement data.

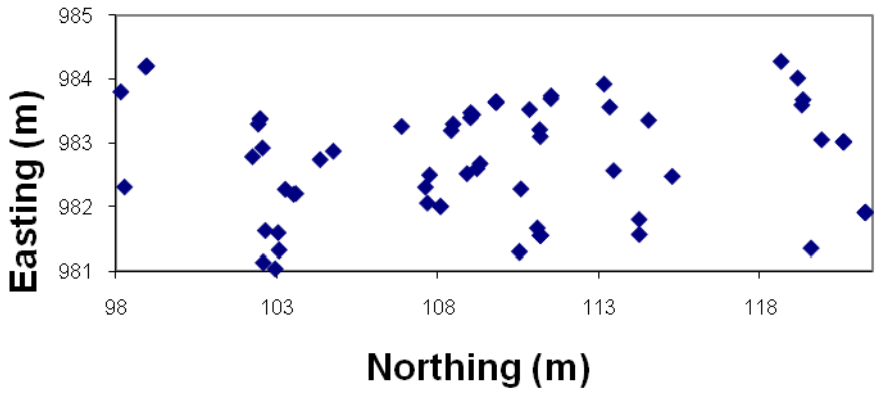


**Figure 3.2. Tree placement along the tree streambank; the easting and northing are relative to the site where the northing is the downstream distance and the easting is perpendicular to the downstream distance.**

**Shrub:** To quantify the shrub vegetation, stems were counted in a 324 $cm^2$ ring; the stems were counted three times to minimize variability. Three random stems were selected from each ring to characterize the diameter of the vegetation. On average, the shrub density was 324 stems/$m^2$ with an average diameter of 0.57 cm (Table 3.5; Appendix A). By observation, the shrubs evenly covered the bank and were relatively uniform in diameter. The average stem length of five clipped samples was 91.4 cm.

**Table 3.5. Shrub stem count and average diameter for six randomly placed 324-$cm^2$ rings along the shrub experimental reach at Tom's Creek.**

| Location | Average Stem Count (number) | Average Diameter (cm) | Vegetation Density ($m^2/m^2$) | Stem Density (stems/$m^2$) |
|---|---|---|---|---|
| **1** | 13 | NA | NA | 401 |
| **2** | 9 | 0.34 | 0.0010 | 278 |
| **3** | 7 | 0.76 | 0.0024 | 216 |
| **4** | 13 | 0.85 | 0.0026 | 401 |
| **5** | 13 | 0.47 | 0.0014 | 401 |
| **6** | 8 | 0.42 | 0.0013 | 247 |
| **Average** | **10.5** | **0.57** | **0.0018** | **324** |

**Grass:** To quantify the grass vegetation, stems were counted in a 324 $cm^2$ ring at five locations; the stems were cut and counted three times to minimize variability. The cut samples were collected and analyzed. On average, the grass stem density was 1039 stems/$m^2$ (Table 3.6; Appendix A). By observation, the grass evenly covered the top of the bank, but the bottom half

of the bank was bare due to mass wasting. The bank material deposited at the toe of the bank after mass wasting contained similar grass type and densities. A leaf area meter (Model 3100 Area Meter, LI-Cor, Inc., Lincoln, NE) was used to determine surface area of the cut vegetation. Stem length, total surface area, leaf number, leaf surface area, and leaf length were recorded (

Table 3.7). Only completely intact leaves were used in analysis because many of the samples dried and lost surface area.

**Table 3.6. Average stem count and density for the grass reach of Tom's Creek.**

| Location | Average Stem Count (number) | Stem Density (stems/m$^2$) |
|---|---|---|
| 1 | 31 | 967 |
| 2 | 29 | 895 |
| 3 | 36 | 1111 |
| 4 | 48 | 1489 |
| 5 | 24 | 733 |
| **Average** | **34** | **1039** |

**Table 3.7. Average total surface area of grass plants and individual leaves (n=20).**

| Plant | | Leaves | | |
|---|---|---|---|---|
| Length (cm) | Surface Area (cm$^2$) | Leaves (number) | Surface Area (cm$^2$) | Length (cm) |
| 41.2 | 50.6 | 11.8 | 6.0 | 17.7 |

*3.2.4 Particle Size*

Particle size was determined for both the bed and the bank for each experimental reach to determine grain roughness.

**Streambed:** A Wolman pebble count was conducted to determine bed roughness in both the riffle and the pool of the experimental reaches (Wolman, 1954). One hundred random pebbles were sampled and measured using a gravelometer. The distribution collected in each reach is presented in Appendix A (Table A.13). The 84$^{th}$ percentile ($D_{84}$) and the median particle size ($D_{50}$) were recorded to characterize the bed roughness of each reach (Table 3.8). The median particle size ranged from 6.6 to 86 mm, indicating Tom's Creek is a gravel bed stream.

**Table 3.8. Median particle size ($D_{50}$) and $D_{84}$ from both the riffle and the pool of each study site collected from Wolman (1954) pebble counts.**

| Bed $D_{50}$ | | | | |
|---|---|---|---|---|
| **Reach** | **Riffle** | | **Pool** | |
| | **Size range (mm)** | **Wentworth range (in)** | **Size range (mm)** | **Wentworth range (in)** |
| **Grass** | 16-32 | 0.63-1.26 | 4-8 | 0.157-0.31 |
| **Shrub** | 32-64 | 1.26-2.5 | 16-32 | 0.63-1.26 |
| **Tree** | 32-64 | 1.26-2.5 | 8-16 | 0.31-0.63 |
| **Bed $D_{84}$** | | | | |
| **Reach** | **Riffle** | | **Pool** | |
| | **Size range (mm)** | **Wentworth range (in)** | **Size range (mm)** | **Wentworth range (in)** |
| **Grass** | 32-64 | 1.26-2.5 | 16-32 | 0.63-1.26 |
| **Shrub** | 64-256 | 2.5-10.1 | 32-64 | 1.26-2.5 |
| **Tree** | 64-256 | 2.5-10.1 | 32-64 | 1.26-2.5 |

**Streambank:** Six soils samples (three upper and three lower) were collected from the banks at each experimental stream reach. The upper soil samples were combined, and lower soil samples were combined for each experimental reach, resulting in two bank soil samples for each experimental reach. Particle size analysis was conducted for each composite sample (ASTM, 2002a, 2002b, 2002c), resulting in the percent sand, silt, and clay for each sample (Table 3.9; Appendix A). For each experimental reach, both upper and lower, the $D_{50}$ was in the sand fraction. Bed grain roughness for the prototype stream was estimated as 2 mm.

**Table 3.9. Sand, silt, and clay percentages of composite soil samples collected at each experimental reach.**

| | **Tree** | | **Shrub** | | **Grass** | |
|---|---|---|---|---|---|---|
| | **Lower** | **Upper** | **Lower** | **Upper** | **Lower** | **Upper** |
| **Sand (%)** | 59 | 58 | 62 | 56 | 69 | 67 |
| **Silt (%)** | 31 | 34 | 26 | 30 | 24 | 24 |
| **Clay (%)** | 10 | 8 | 13 | 14 | 7 | 8 |

*3.2.5 Discharge Calculations for the Prototype Stream*

Flow data were not available for the Toms Creek. Depth-averaged velocity and discharge were estimated based on flow calculations. The Manning's equation was used to estimate flow for the gravel bed stream.

Manning's n values were determined based on several methods outlined by Chow (1959), Hicks and Mason (1998), and Arcement and Schneider. Reach characteristics assumed vegetation growth similar to the time of the survey, late fall. The average n for each

experimental reach was used for further analysis. A Manning's n value of 0.078, 0.053, and 0.044 were used for the tree, shrub, and grass experimental stream reaches, respectively (Table 3.10).

**Table 3.10. Manning's n values estimated by methods outlined in Chow, 1959; Hicks and Mason 1998; and Arcement and Schneider.**

| | Manning's n values | | |
|---|---|---|---|
| **Reference** | **Tree** | **Shrub** | **Grass** |
| **Chow, 1959** | 0.065 | 0.0415 | 0.0315 |
| | 0.08 | 0.035 | 0.035 |
| | 0.15 | 0.045 | 0.04 |
| | | 0.08 | |
| **Hicks and Mason, 1998** | 0.0365 | 0.042 | 0.0275 |
| | 0.035 | 0.05 | 0.031 |
| | | | 0.038 |
| | | | 0.06 |
| | | | 0.0815 |
| **Arcement and Schneider** | 0.1065 | 0.069 | 0.049 |
| **Average** | **0.078** | **0.053** | **0.044** |

Discharge and depth-averaged velocity were determined using the Manning'sequation (Equations 3.1 and 3.2). Hydraulic radii ($R_h$) and cross-sectional areas (A) were determined from the averages of the cross-section survey data (Appendix A). Slope of the energy grade line was approximated by the bed slope from top of riffle to top of riffle for each experimental reach. The depth-averaged velocities were calculated as 0.39 m/s, 0.16 m/s, and 0.39 m/s for the tree, shrub, and grass experimental reach, respectively (Table 3.11).

$$U = \frac{1.49}{n} R_h^{\frac{2}{3}} S^{\frac{1}{2}} \quad [3.1]$$

$$Q = AU \quad [3.2]$$

where, U is the depth-averaged velocity (m/s), n is Manning's n, $R_h$ is the hydraulic radius (m), S is the slope of the energy grade line (m/m), Q is the flow discharge ($m^3/s$), and A is the cross-sectional area ($m^2$).

**Table 3.11. Parameters used in Manning's equation discharge (Q) calculations: hydraulic radius ($R_h$), bed slope (S), cross-sectional area (A), Manning's n, and depth-averaged velocity (U).**

| | Tree | Shrub | Grass |
|---|---|---|---|
| **$R_h$ (m)** | 0.96 | 0.51 | 0.71 |
| **S (m/m)** | 0.00480 | 0.00063 | 0.00460 |
| **A ($m^2$)** | 12.21 | 4.46 | 6.02 |
| **Manning's n** | 0.078 | 0.053 | 0.044 |
| **U (m/s)** | 0.39 | 0.16 | 0.39 |
| **Q ($m^3$/s)** | 4.80 | 0.73 | 2.34 |

### 3.3 Dimensional Analysis

To determine the shape and size of the scaled streams, dimensional analysis was performed using the Buckingham Pi Theorem (Appendix B). Ten significant variables were identified: hydraulic radius ($R_h$), vegetation density ($V_{den}$), dynamic viscosity ($\mu$), water density ($\rho_w$), bed slope ($S_{bed}$), bank slope ($S_{bank}$), depth-averaged velocity (U), acceleration due to gravity (g), bank grain roughness, and bed grain roughness. Vegetation density was defined as the area of the bank covered by vegetation, while stem density was defined as the number of stems per area. The analysis ignored vegetation flexibility, but flexibility was represented in a relative manner. A gradient in increasing flexibility existed among the tree, shrub, and grass vegetation. Surface tension effects were ignored, and infiltration was assumed negligible. Water was used in the flume model; the analysis assumed the same fluid for the prototype and the model (Peakall et al., 1996; Fathi-Maghadam and Kouwen, 1997; Munson et al., 2002).

The analysis resulted in seven Pi terms ($V_{den}$, $S_{bed}$, $S_{bank}$, Fr, $R_{bank}$, $R_{bed}$, and Re). The Reynolds (Re) number was indicated as a Pi term but was removed, resulting in six Pi terms (Equation 3.3 and 3.4); flow through vegetation was considered in the turbulent zone and independent of Re (Peakall et al., 1996; Fathi-Maghadam and Kouwen, 1997). The model was based on Froude similarity, while verifying the Reynolds number remained large (>500; Peakall et al., 1996).

$$\text{Dependent Pi Term} = \Theta(\lambda_p, S_{bed}, S_{bank}, Fr, R_{bank}, R_{bed}) \quad [3.3]$$

$$Fr = \frac{gR_h}{U^2} \quad [3.4]$$

$$R_{bank} = k_{s,bank}/R_h \quad [3.5]$$

$$R_{bed} = k_{s,bed}/R_h \quad [3.6]$$

where, $\lambda_p$ is the vegetation density ($m^2/m^2$), $S_{bed}$ is the bed slope (m/m), $S_{bank}$ is the bank slope (m/m), Fr is the Froude number, $R_{bank}$ is the relative bank grain roughness, $R_{bed}$ is the relative bed grain roughness, $k_{s,bank}$ is the bank grain roughness (mm), $R_h$ is the hydraulic radius (m), $k_{s,bed}$ is the bed grain roughness (mm), g is the acceleration due to gravity ($m/s^2$), and U is the depth-averaged velocity (m/s).

## 3.4 Scaling the Flume Model

Originally, each prototype stream reach was to be scaled separately. After examining the survey and field data, it became apparent that many of the variables in addition to vegetation characteristics identified as significant by the dimensional analysis (e.g. hydraulic radius, bank slope, depth-averaged velocity) were different among the reaches. Vegetation has been shown to impact stream width (Hey and Thorne, 1986; Hession et al., 2003), showing different levels of erosion for varying vegetation types and densities (Hey and Thorne, 1986; Davies-Colley, 1997; Trimble, 1997b; Hession et al., 2003). To isolate for vegetation impacts, channel characteristics (e.g. bank slope, hydraulic radius, grain roughness, and discharge) remained constant among all model streambanks. Vegetation characteristics provided the only difference among the constructed streambanks.

### *3.4.1 Flume Model Channel Characteristics*

The shrub reach was chosen for scaling because the bank slope allowed for the largest measureable streambank surface area and for a greater water depth for measurements in the flume. First, channel geometry was determined through geometric scaling (McBride et al., 2007). Assuming a trapezoidal channel and maintaining the bank slope for the shrub reach, depth and top width were geometrically scaled. This technique resulted in a hydraulic radius scale appropriately between the model and prototype. A 1:2 scaling allowed for the largest streambank while maintaining a width of two times the water depth adjacent to the streambank (Figure 3.3). The longitudinal bed slope remained constant as field observations (0.5%) and was used in all flume runs. A frequency distribution was developed for particles collected from the Wolman pebble counts, resulting in a $D_{50}$ of 20 mm; the $D_{50}$ for the constructed stream bed was

10 mm. Mean particle size of the streambank for the prototype reaches were consistently 2 mm; bank roughness maintained a $D_{50}$ of 1 mm in the constructed stream (Figure 3.3).

Stream discharge as calculated by Manning's equation varied among the three prototype reaches for bankfull flow. In the flume, discharge remained constant among the treatments to isolate vegetation effects. The maximum discharge available for the flume (0.042 $m^3/s$) was used. Froude similitude was checked with the corresponding flume discharge for subcritical flow (Fr<1), and Reynolds number was calculated to ensure turbulent flow (Re>500).

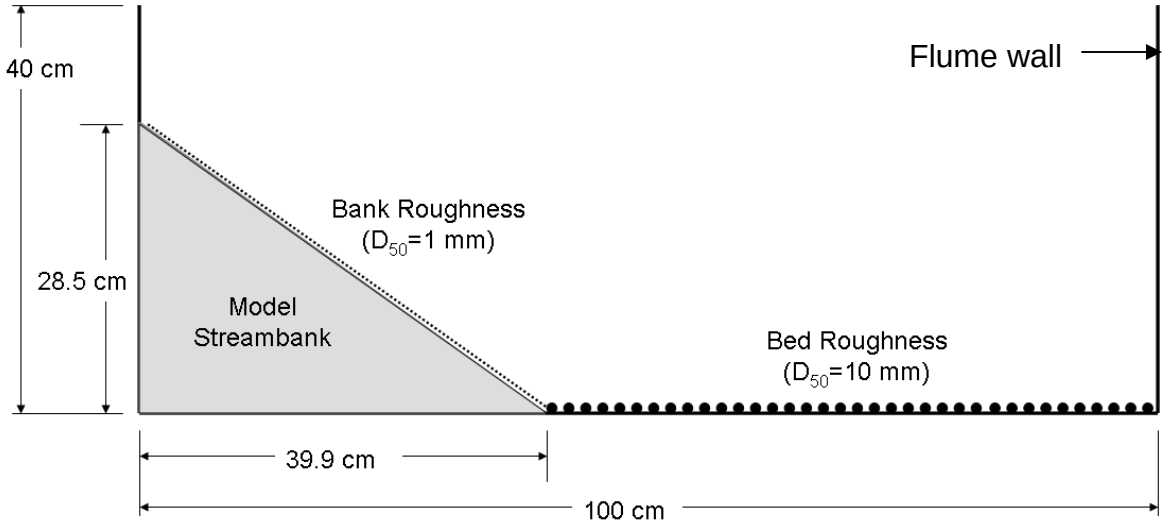


**Figure 3.3. Dimensions for constructed flume streambank without vegetation; bank dimensions, bed roughness, bank roughness, and bed slope remained constant among all vegetation types.**

*3.4.2 Flume Model Vegetation Characteristics*

Vegetation size and density were scaled (1:2) from the measurements of the prototype stream. While vegetation placement was set by the field survey for the tree bank, spacing was determined randomly for the shrub and grass reaches.

**Tree:** The trees were simulated by placing wooden dowels in locations identified during the field survey, resulting in nine trees. Model tree stem diameters ranged from 1.5 cm to 6.4 cm.

**Shrub:** Shrubs were simulated using wooden dowels with a stem diameter and density of 0.3 cm and 1296 stems/$m^2$, respectively. The specified dowel density was achieved using a

0.15 $m^2$ template applied end to end down the entire research streambank (18 templates total). A random number generator was used to specify the dowel location within each template. Dowels were oriented vertically and secured with flexible adhesive, allowing movement at the attachment point.

**Grass:** Scaling the average grass stem density (1039 stems/$m^2$) for the prototype stream resulted in a model stem density of 4156 stems/$m^2$. The streambank area (2.94 $m^2$) resulted in 12,219 stems for the grass model streambank. Grass length was based on the average length of cut stems and was modeled at a length of 20.5 cm. Average width of the grass was one half of the observed field value (1.2 cm), resulting in a model grass with of 0.6 cm.

## 3.5 Flume model construction

The flume model was constructed using a frame to provide the correct streambank geometry (Figure 3.4). Vegetation roughness was created by constructing interchangeable roughness panels with the four vegetation treatments: bare, tree, shrub, and grass (Figure 3.5-Figure 3.8).

### *3.5.1 Construction of Streambank Geometry*

The streambank geometry was constructed using masonry board (0.64 cm thick). The bank was hinged at the base so a hot-film anemometer (CTA) could be mounted behind the bank. The bank was 5.5 m long and was preceded by a constructed flow straightener (1.27 cm PVC pipe). The bank was 50 cm in length and rested at a 35$^o$ angle with the horizontal. The streambank was built in four sections longitudinally (three 1.52-m sections and one 0.91-m section; Figure 3.4). The stem densities and diameters were constructed to the specifications in the previous sections.

**Figure 3.4. Streambank geometry constructed of masonry board hinged at the bank toe to provide sensor access for the hot-film probe.**

*3.5.2 Construction of Roughness Panels*

Each roughness treatment (bare, shrub, grass, and trees) was constructed using a removable panel. Four panels were constructed for each vegetation type. Three panel dimensions were 1.52 m by 0.5 m, and the fourth panel dimensions were 0.91 m by 0.5 m. The stem densities and diameters were constructed to the specifications in the previous sections.

**Bare:** The bare bank was constructed to simulate a bank with only grain roughness. The grain roughness was simulated by sand paper glued to the bank panels (Figure 3.5).

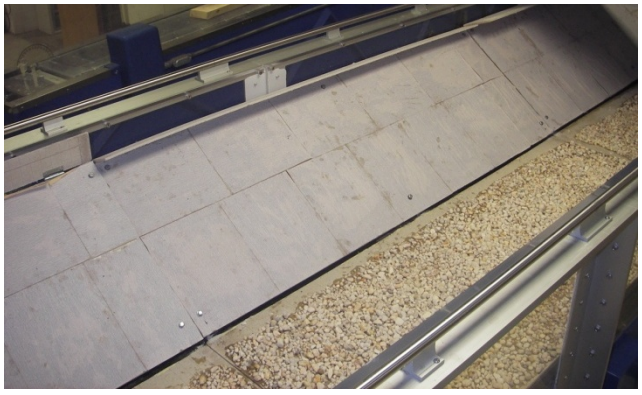

**Figure 3.5. Bare bank panel.**

**Tree:** The tree bank was constructed using dowel rods in addition to the bank roughness (Figure 3.6).

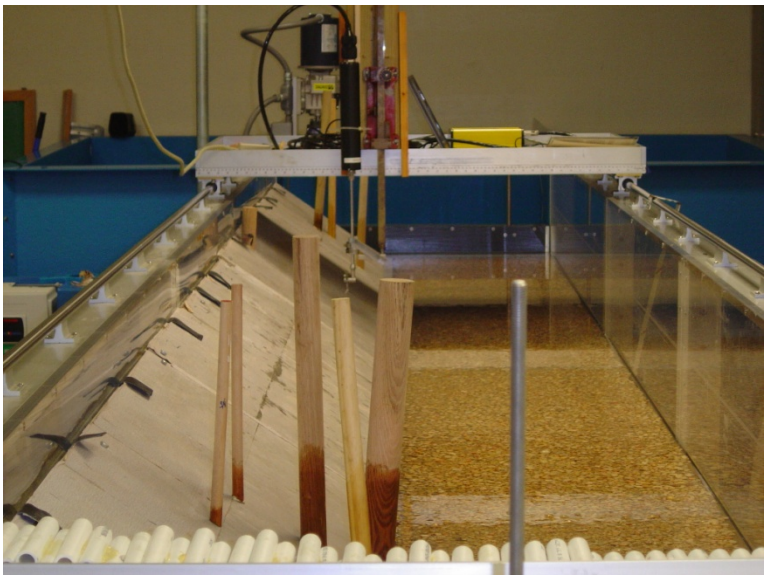

**Figure 3.6. Tree bank panel.**

**Shrub:** The shrub bank was constructed using dowel rods in addition to the bank roughness (Figure 3.7).

**Figure 3.7. Shrub bank panel.**

**Grass:** The grass panel was constructed like the bare panel with the simulated grain roughness. Then, grass was added using strips of rafia woven into a mat using a latch and hook technique (Figure 3.8).

**Figure 3.8. Grass bank panel.**

## 3.6 Data Collection: ADV, Miniature Propeller and Hot-film Anemometer

Velocity fields were measured using both a Sontek MicroADV and miniature propeller. Direct measurements of shear stress were made using a flush-mount hot-film anemometer. Measurements were made 3.3 m downstream from the flow straightener at five points along four cross-sections (Figure 3.9). Measurements were recorded after the flow was determined steady and uniform: water depth was measured throughout the test section and velocity measurements began when the water depth remained constant. Discharge, calculated with a Venturi meter within the flume piping system remained constant among all vegetation types (0.042 $m^3/s$). Bed slope and the tailgate height remained constant at 0.5% and 15 cm, respectively, for all tests. Flow depth remained constant at 20.4 cm. The following sections describe the measurement procedure for each instrument.

### *3.6.1 Acoustic Doppler Velocimeter (ADV)*

A Sontek 16 MHz Side-looking MicroADV was utilized to provide 3D velocity profiles (1 min sample time; 25 Hz). The probe was mounted parallel to the flume wall and the orientation was checked by measuring the distance from the transmitters to the bank. Probe orientation was further verified by analyzing continuity through the test section. The average percent of total flow unaccounted for was 0.46%, 0.18%, 0.27%, 0.09% for the bare, tree, shrub, and grass bank, respectively, confirming proper probe alignment. Velocity profiles were measured at four locations along five cross-sections. The five cross-sections were located at 5-

cm intervals along the bank (Figure 3.9a). The velocity profiles were measured at 0.5-cm intervals perpendicular to the boundary (Figure 3.9b).

Erroneous data which bias mean velocity values and turbulent characteristics may result from ADV measurements due to obstructions near the sampling volume, excessive flow aeration, Doppler noise, velocity shear, or proximity to the surface, making data filtering necessary (MacVicar et al., 2007; McBride et al., 2007; Wilcox and Wohl, 2007). Instantaneous velocity values with an average signal correlation value less than 70% or an average signal to noise ratio less than 15 were removed (Wahl, 2000; McBride et al., 2007). When 15% of the instantaneous values were discarded from a time series, the time series was removed from further analysis (McBride et al., 2007). Time series were only removed for the grass treatment as grass waving often interfered with measurements. Five complete profiles (A4, B4, C4, D4, and E4) as well as some points close to the streambank were discarded for the grass treatment because a large percentage of the values were deleted from the time series. To measure velocity within the shrub treatment, individual dowels were removed so there was sufficient space for the ADV probe. The dowels were replaced for subsequent measurements.

### *3.6.2 Miniature Propeller*

An Armfield miniature propeller (H33-1 straight, low speed probe) was utilized to provide time-averaged velocity profiles in the streamwise direction. Velocity profiles (30 s sample time; 0.5-cm increments) were measured in the same locations as the ADV measurements (Figure 3.9). To measure velocity within the shrub treatment, individual dowels were removed so there was sufficient space for the ADV probe. The dowels were replaced for subsequent measurements.

### *3.6.3 Hot-film Anemometer:*

A Dantec MiniCTA (CTA) system with a flush mounted hot-film probe (55R46) measured shear stress at the streambank wall. For this study, measurements made by the hot-film anemometer were considered representative of the actual boundary shear stress. The sensor was mounted from behind the streambank flush with the bank wall (Figure 3.10). The hot-film sensor measured voltage at 20 locations along the bank (Locations 3-6 along five cross-sections; Figure 3.9).

The Dantec MiniCTA hot-film probe calibration was completed in a calibration pipe following the design of Thompson (Thompson, 2001; Thompson and Wilson, 2004; Figure 3.11). Five manometers located at 0.46-m intervals were constructed into a 5.1-cm diameter, 3.7-m long PVC pipe. The piezometric gradient, water temperature, and sensor voltage were measured for 10-12 flow rates. Shear stress was calculated based on the following equation for fully developed, turbulent, pipe flow (Thompson, 2001; Thompson and Wilson, 2004):

$$\tau = \rho g R_h S_p \qquad [3.7]$$

where $\tau$ is the average boundary shear stress (Pa) , $\rho$ is water density (kg/m$^3$), g is the acceleration due to gravity (m/s$^2$), $R_h$ is the hydraulic radius (m), and $S_p$ is the piezometric gradient (m/m). Shear stresses ranged from 0.6 Pa to 10 Pa. Data were fit to the following equation (Garcia et al., 1998; Robinson, 1989; Thompson, 2001):

$$V^* = \frac{V^2}{\Delta T} = A\tau^B + C \qquad [3.8]$$

where V is the time-averaged CTA voltage (V); $\tau$ is the average boundary shear stress (Pa); $\Delta$T is the operating temperature of the sensor minus the water temperature (°C); V* is the squared voltage normalized by the temperature difference; and A, B, and C are fitted calibration parameters. To ensure no drift occurred during measurement, the hot-film probe was calibrated at least twice per bank; Appendix C presents the calibration curves used in the analysis.

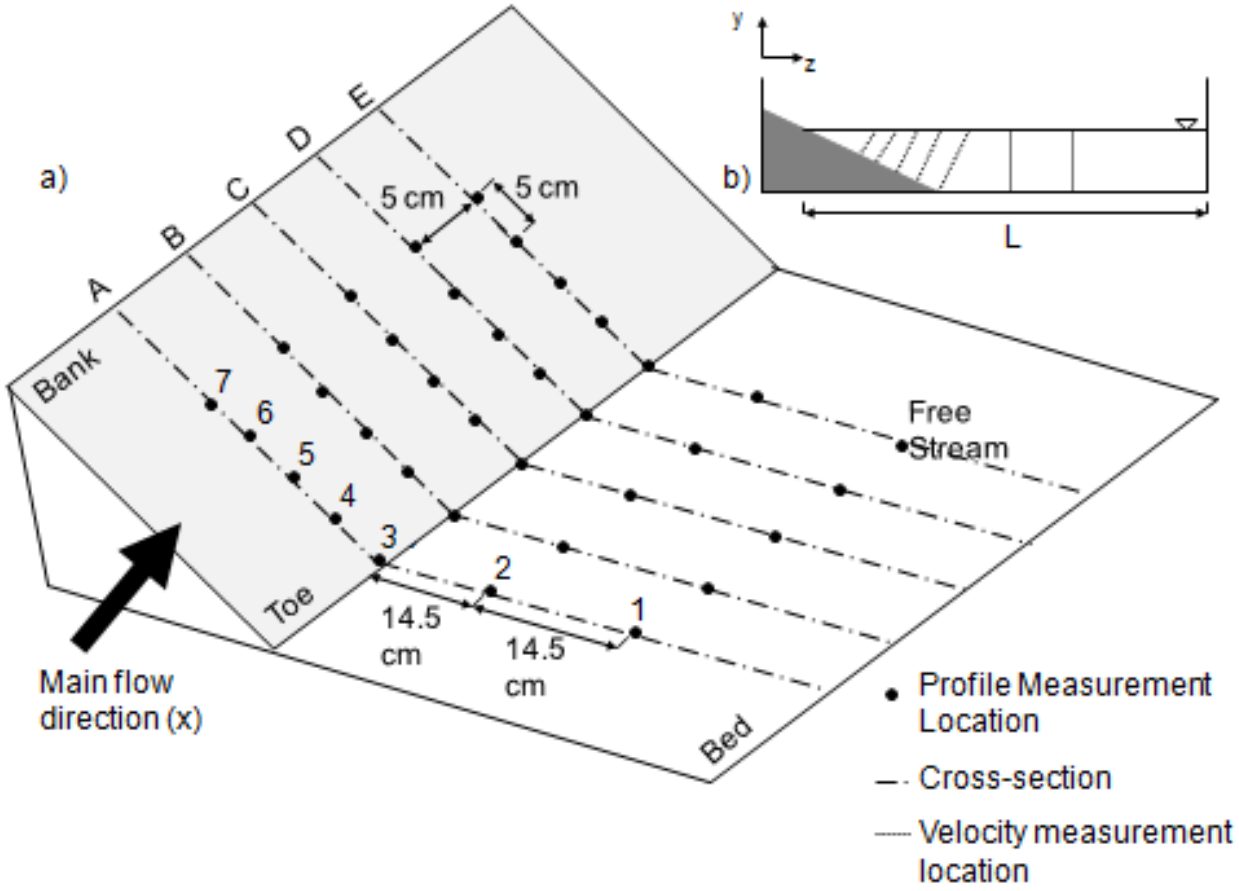


**Figure 3.9. a) Five cross sections of sample locations for the velocity profiles and hot-film sensor measurements along the boundary and b) description of velocity profile perpendicular to the channel boundary.**

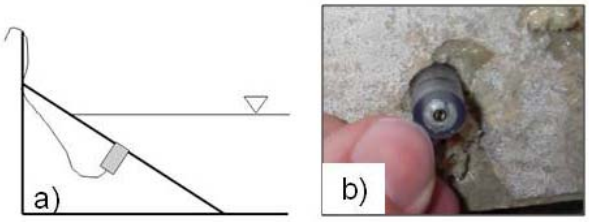


**Figure 3.10. a) Hot-film anemometer placement behind the streambank, and b) mounting hot-film anemometer into streambank.**

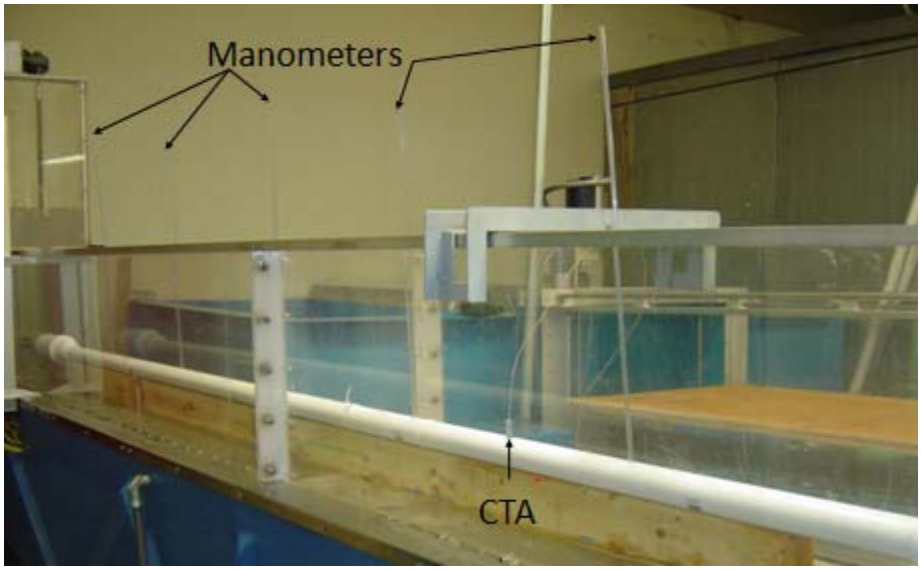


**Figure 3.11. Hot-film anemometer (CTA) calibration pipe with five manometers.**

# Chapter 4 Vegetation impacts on near bank flow

## 4.1 Introduction

While considerable research has been conducted on the role of vegetation in reducing streambank failures (Abernethy and Rutherfurd, 2001; Simon and Collison, 2002; Simon et al., 2006; Pollen, 2007), less is known about the influence of vegetation on flow turbulence and boundary shear stress, particularly for the case of a vegetated, sloping bank, a stream form commonly created during any instream construction. The effects of vegetation on flow have been explored for submerged vegetation (Ghisalberti and Nepf, 2002; Jarvela, 2002; Ghisalberti and Nepf, 2006; Liu et al., 2008; Nepf and Ghisalberti, 2008) and emergent vegetation (Nepf, 1999; Nepf and Vivoni, 2000; Jarvela, 2002; Thompson et al. 2004, Liu et al., 2008) when placed on the channel bed. This analysis was extended to examine the effects of vegetation on turbulence structure with vegetation on the floodplain (Thornton et al., 2000; McBride et al., 2007; Yang et al., 2007) and as streamside vegetation (White and Nepf, 2007); however, the effects of vegetation on sloping streambanks have not been analyzed. The present study examined turbulence characteristics and velocity structure caused by streambank vegetation and discussed it in the context of fluvial erosion.

### *4.1.1 Goals and Objectives*

The overall study goal was to evaluate how three-dimensional velocity structure and turbulence characteristics vary with different streambank vegetation types. Specifically, the research addressed the following questions:

1. How does the addition of streambank vegetation alter the three-dimensional velocity compared to a bare streambank?
2. How does the addition of stiff vegetation (trees and shrubs) and flexible vegetation (grass) impact turbulence characteristics near the streambank compared to a bare streambank?
3. How can the different vegetation types potentially influence fluvial erosion of the streambank?

To address these questions, velocity profiles, turbulent intensities, average turbulent kinetic energy (TKE), and Reynolds stresses were evaluated.

## 4.2 Methods

A second order prototype stream (Tom's Creek in Blacksburg, Virginia, USA), with individual reaches dominated by each vegetation treatment was modeled in a research flume using a fixed-bed Froude-scale modeling technique. One model streambank of the prototype stream was constructed for each vegetation type and compared to a bare control (only grain roughness). Velocity profiles perpendicular to the flume model boundary were measured using a three-dimensional acoustic Doppler velocimeter as explained in Ch. 3.

### *4.2.1 Analytical Methods*

To characterize flow turbulence, turbulence intensities, average TKE estimates, and Reynolds stresses were evaluated at each velocity measurement location (bare, n=515; tree, n=515; shrub, n=515, and grass, n=335). Turbulent intensities were analyzed in the streamwise ($u$), lateral ($v$), and vertical ($w$) directions by calculating the root mean square (RMS) of the fluctuating velocities for each direction (Wilcox and Wohl, 2007):

$$RMS_u = \sqrt{\overline{u'^2}} \quad [4.1]$$

$$RMS_v = \sqrt{\overline{v'^2}} \quad [4.2]$$

$$RMS_w = \sqrt{\overline{w'^2}} \quad [4.3]$$

This analysis required separating the instantaneous velocity fluctuation ($u'$, $v'$, and $w'$) from the mean velocity ($\overline{u}$, $\overline{v}$, and $\overline{w}$) for each velocity component ($u = \overline{u} + u'$, $v = \overline{v} + v'$, and $w = \overline{w} + w'$). Turbulent kinetic energy (*TKE*) was also evaluated to represent the average three-dimensional turbulence intensity using the following relationship (Kim et al., 2000; Biron et al., 2004; Pope et al., 2006; Wilcox and Wohl, 2007; McBride et al., 2007):

$$TKE = \rho 0.5(\overline{u'^2} + \overline{v'^2} + \overline{w'^2}) \quad [4.4]$$

where $\rho$ is water density and the overbar denotes a mean.

Calculation of Reynolds stresses required velocity fluctuation values in the streamwise, vertical, and lateral directions (Biron et al., 2004; McBride et al., 2007). Three components of Reynolds stresses, $\tau_{uv}$, $\tau_{uw}$, and $\tau_{vw}$, were calculated as defined by the following equations (Schlichting and Gersten, 2000):

$$\tau_{uv} = -\rho\overline{u'v'} \quad [4.5]$$

$$\tau_{uw} = -\rho\overline{u'w'} \quad [4.6]$$

$$\tau_{vw} = -\rho\overline{v'w'} \quad [4.7]$$

## 4.3 Results and Discussion

The addition of vegetation to the streambank increased the free stream streamwise velocities up to 33% and altered secondary flow. The vegetation resistance reduced streamwise velocity near the streambank and created a sharp velocity gradient into the main channel, indicating areas of higher shear stress. Qualitative evidence of turbulence structure was observed in the vegetated channels. For the grass treatment, progressive waving of the vegetation (*monami*; Nepf and Ghisalberti, 2008) was observed, indicating the downstream movement of coherent structures. A downstream-progressing vibration of the dowels was also observed in the shrub channel, also suggesting turbulence structure. The following sections address each study objective individually.

### *4.3.1 Vegetation impacts on three-dimensional velocity*

When evaluated graphically, there were few visible differences in the distribution of streamwise velocities among the five cross sections; therefore, the average of the five cross-sections for each vegetation type is presented. The velocity profile closest to the flume side wall (location 1; 30 cm from the flume wall) was used to illustrate the effect of the vegetation on the main channel velocity. This profile was removed from further quantitative analyses due to the possibility of side-wall effects from the flume wall. The presence of vegetation on the streambank increased the depth-averaged free stream velocity (location 1) in the streamwise direction by 33% (Figure 4.1). Depth-averaged velocity for the bare, tree, shrub, and grass channels at location 1 were 40 cm/s, 42 cm/s, 50 cm/s, and 53 cm/s, respectively. These findings

are consistent with Yang et al. (2007), who reported an increase in main channel velocity when idealized vegetation was added to the floodplain. Figure 4.1 illustrates the distribution of the spatially (five cross-sections) and temporally averaged streamwise velocity normalized by the shear velocity ($u^* = \sqrt{gHS}$, where $g$ is the acceleration due to gravity, $H$ is water depth, and $S$ is water slope). Differences in water depth were not detected among vegetation types, so a constant measurement of 20.4 cm was used. Because the flow was uniform, the flume slope (0.5%) was used as $S$. The vertical axis ($y$) was normalized by $H$, and the lateral distance (z) was normalized by the flume width ($L$). While the depth-averaged free stream streamwise velocity was greater in the vegetated channels as compared to the bare channel, higher streamwise velocities occurred close to the boundary of the bare bank. Near the streambank ($z/L<0.6$), the streamwise velocity decreased compared to the bare channel by 9%, 43%, and 66% for the tree, shrub, and grass bank, respectively. The difference in downstream velocity distribution between the bare and vegetated channels altered the lateral velocity gradient and lateral transport of streamwise momentum (Yang et al., 2007). The lines of constant velocity for the vegetated conditions are more vertical than the bare condition, suggesting momentum exchange in the lateral direction. The lateral velocity gradients were also steepest for the shrub and grass channels at the main channel/vegetation channel interface. Even with a few isolated roughness elements, streamwise velocities near the tree streambank decreased along the bank; the isolated elements provided resistance to the flow and enhanced momentum transport between the main channel and the streambank. The grass channel had an area of low velocity near the boundary that was spatially larger than a similar area for the shrub condition (Figure 4.1). Because the grass was flexible and movement was not as limited as with the more rigid shrubs, the grass (stem length=20.5 cm) interacted with a greater portion of the flow and shifted the area of high velocity gradient further into the main channel. Thorne and Furbish (1995) found that near bank velocities were high along the entire channel length when bank vegetation was replaced with a smooth wall, while high velocities were directed toward the channel center line when natural vegetation was present. With the high velocity displacement from the near bank area, vegetation will suppress lateral channel migration relative to movement associated with a smooth wall (Thorne and Furbish, 1995). Because the higher streamwise velocities were moved away from the bank, a steep velocity gradient was present in the vegetated conditions, indicating areas of high shear stress (Figure 4.1).

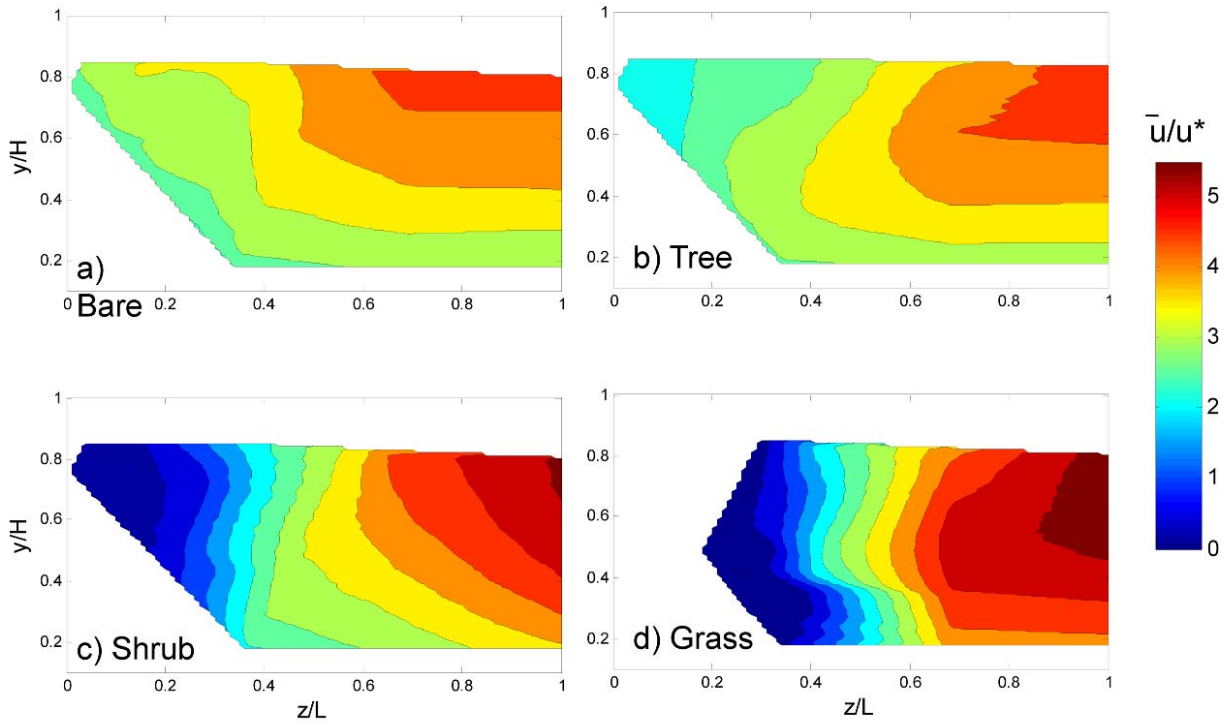


**Figure 4.1. Distribution of temporally and spatially (five cross-sections) averaged nondimensional streamwise velocity ( ū/u*) for the (a) bare, (b) tree, (c) shrub, and (d) grass vegetation treatments; the white space on the grass figure indicates the data points for two profiles on the upper bank removed in filtering.**

Secondary flow (i.e. velocity in the lateral and vertical directions) was analyzed for each vegetation condition. The bare condition showed little variation in lateral and vertical velocity. The lateral velocity in close proximity to the bare bank ($z/L$<0.5) remained fairly uniform at 2.5% of the streamwise velocity. This lateral velocity near the bank increased with the addition of streambank vegetation, representing up to 10% of the streamwise velocity. The vertical velocity in close proximity to the bare bank ($z/L$<0.5) remained fairly constant (1.3% of the streamwise velocity). This vertical velocity increased with the addition of streambank vegetation, representing up to 3.8% of the streamwise velocity. The variation in secondary flow between the bare and vegetated channels indicated a non-streamwise structure to the flow (e.g. eddies, lateral vortices) existed in the vegetated channels: the addition of the rigid and flexible vegetation increased secondary flow.

Evidence of secondary flow was also analyzed in the y-z plane. Velocity vectors of the secondary flow ($\sqrt{\overline{v}^2 + \overline{w}^2}$) were plotted for each vegetation type (Figure 4.2). Only profiles 3-7

were analyzed to ensure there were no side-wall effects from the vertical flume wall. Only the results from cross-section C are presented because the plots were similar among the five cross-sections. The addition of vegetation to the streambank altered momentum transfer, as compared to a bare trapezoidal channel. The secondary flow of the bare channel suggested the presence of two circulating cells within this region close to the sloping bank. The velocity vectors (Figure 4.2) suggest one clockwise cell ($z/L>0.2$) and one counterclockwise cell ($z/L<0.2$) with the size scaling to the water depth, supporting previous research in trapezoidal channels (Tominaga et al., 1989; Knight et al., 2007). Due to the 5-cm spacing between the profiles, secondary flow structure in the vegetation was not distinct, but some observations could be made. Figure 4.2b suggests the presence of a large clockwise cell along the tree streambank. For sparsely vegetated channels where the average spacing between vegetation elements is greater than the water depth (tree treatment in this study), eddies scale to the water depth (Nepf, 1999). When comparing the secondary velocity vectors of the bare (Figure 4.2a) and tree (Figure 4.2b) streambanks, the middle set of arrows ($z/L\sim0.15$) indicates an increase in lateral velocity and momentum transfer. The high secondary velocity is near the bed for the tree treatment, while the high secondary velocity is near the surface for the bare treatment. This difference suggests higher velocity flows and more momentum transfer to the toe of the slope when trees are added to a bare bank. This observation is further supported by the curved velocity contours in Figure 4.1b, which indicate a decrease in streamwise velocity near the water surface, likely due to the presence of secondary currents (Ead et al., 2000). The secondary flow for the shrub condition illustrates mixing from the main, fast moving channel into the slow moving vegetated area at the main channel/vegetation interface. This mixing is important when considering the movement of sediment-bound pollutants and dissolved oxygen into vegetated areas. This mixing between the main channel and the shrub bank occurred approximately 5 cm into the vegetation (roughly three rows of shrubs), and this length was controlled by the vegetation spacing. Because the spacing of the shrub dowels was less than the water depth, eddies within the vegetation scaled to the stem diameter, as evidenced by the lower lateral velocities for the upper three profiles (Nepf, 1999). In flows with emergent vegetation along the boundary, White and Nepf (2007) observed a shear layer composed of two layers. The vegetation resistance influences the length over which momentum exchange occurs within the vegetation. The shear layer at the interface between the vegetation and the main flow resembles a boundary layer in which water depth and bottom

friction influence the shear layer length outside the vegetation (White and Nepf, 2007). Less lateral mixing was evident in the grass channel, likely due to the folding of the vegetation. Evidence of the shape of the secondary flow was not apparent in the vector plots along the y-z plane. This result could be due to the large spacing (5 cm) between velocity profiles or due to the plane examined (y-z). The vortex shedding occurred due to the vegetation and due to the sloping streambank. If another plane was examined, the secondary structure may be more evident, but the measurement spacing used in this analysis did not support such an analysis.

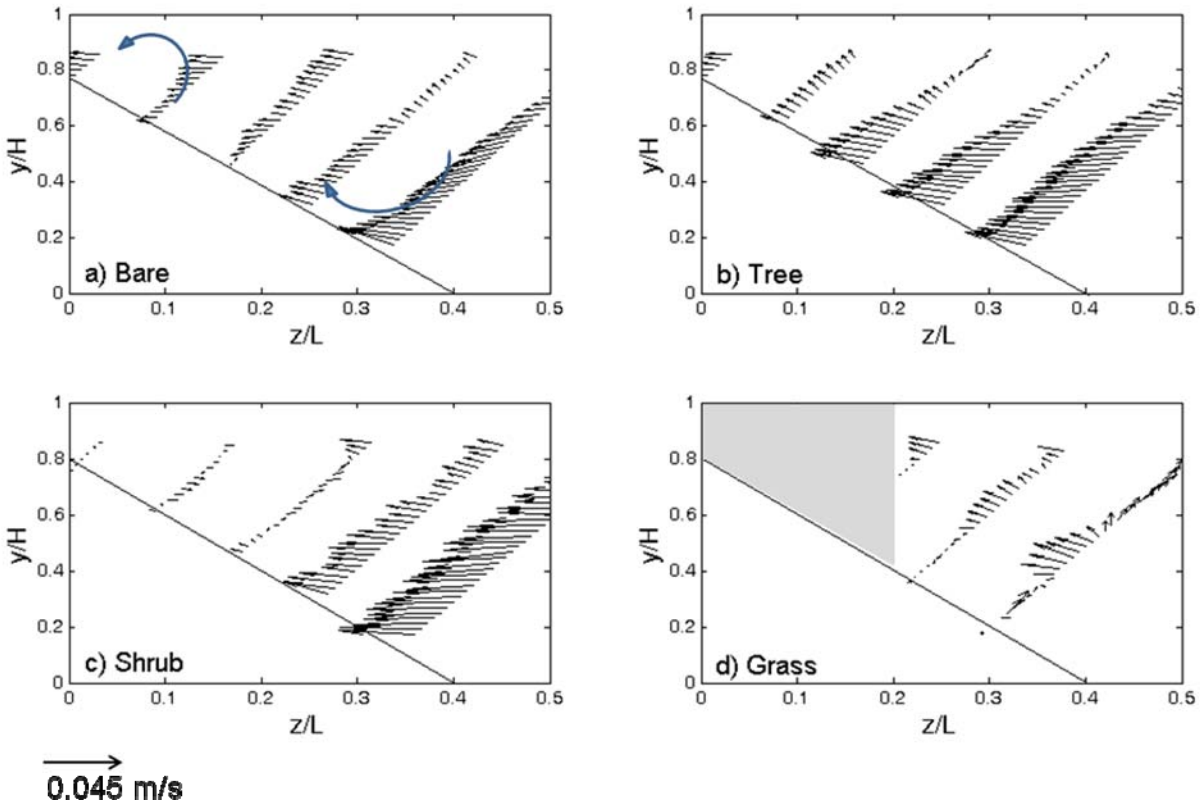


**Figure 4.2. Vector field diagrams of the lateral and vertical velocity ($\sqrt{\overline{v}^2 + \overline{w}^2}$) for profiles 3-7 along cross-section C for each vegetation type: (a) bare, (b) tree, (c) shrub, and (d) grass. The highlighted portion of the grass figure represents the data removed in data filtering. Arrows indicate proposed counter-rotating cells (6a).**

To examine the contributions of secondary circulation and turbulent mixing to the transverse momentum exchange, the spatially averaged transverse shear stress ($\langle \tau_{xy} \rangle$) was examined using the following equation (van Prooijen et al., 2005; White and Nepf, 2008):

$$\left\langle \tau_{xy} \right\rangle = -\rho\left\langle \overline{u'v'} \right\rangle - \rho\left\langle \left(\overline{U} - \left\langle \overline{U} \right\rangle\right)\left(\overline{V} - \left\langle \overline{V} \right\rangle\right) \right\rangle \quad [4.8]$$

where brackets denote spatial averaging. The depth-averaged transverse shear stress is composed of two terms: a Reynolds stress (first term) and a stress due to secondary circulation (second term; White and Nepf, 2008). Locations 2-7 for each cross-section and vegetation type were examined; location 1 was excluded due to possible secondary flow effects caused by the flume wall. Excluding location 7 (high on the bank) for the bare streambank, both stresses had the same order of magnitude for each location (0.2 N/m$^2$, 0.3 N/m$^2$, 0.2 N/m$^2$, 0.1 N/m$^2$, and 0.1 N/m$^2$ for location 2, 3, 4, 5, and 6, respectively). For all profiles on the tree bank, the stress due to secondary circulation (0.01-0.08 N/m$^2$) was at least an order of magnitude less than the Reynolds stress (0.1-0.4 N/m$^2$). This result supports findings by White and Nepf (2008) that indicated stress due to secondary circulations was at least an order of magnitude less than the Reynolds stress in flows with emergent vegetation along a boundary. The bank profiles (locations 3-7) of the shrub and grass channels showed a similar pattern. For the shrub bank profiles near the bank toe (locations 3 and 4), the secondary circulation stress (0.1-0.2 N/m$^2$) was an order of magnitude less than the Reynolds stress (1.4-1.5 N/m$^2$). The difference between the two stresses and the magnitudes of the stresses decreased with distance into the shrubs. At location 5, the shrub Reynolds stresses (0.4-0.5 N/m$^2$) were larger than the shrub secondary stresses (0.1-0.2 N/m$^2$). Deep in the vegetation both shrub stresses were similar with values less than 0.1 N/m$^2$ at location 6 and values less than 0.02 N/m$^2$ at location 7. The secondary circulation stress of the grass bank profiles (rows 3-5) were up to an order of magnitude less than the Reynolds stress, but the data were less reliable due to missing data from filtering. Reynolds stresses dominated along the boundary of vegetated streambanks. This result indicates that the secondary circulation term may be ignored when calculating the transverse shear stress along vegetated streambanks, supporting findings by White and Nepf (2008).

Within the main channel, the vegetation did not appear to affect the distribution of $\tau_{xy}$. The vertical profiles on the bed of the shrub and grass conditions (location 2) did not support the findings of White and Nepf (2008). The shrub Reynolds stresses (0.1-0.2 N/m$^2$) were on the same order of magnitude as the secondary circulation stresses (0.3 N/m$^2$). The grass Reynolds stresses (0.4 N/m$^2$) were generally on the same order of magnitude as the grass secondary

circulation stresses (0.04-0.3 N/m$^2$). These results suggest secondary circulation may significantly contribute to the depth-averaged transverse shear stress in the main channel of vegetated flows.

*4.3.2 Effects of vegetation on turbulence characteristics*

Evidence of turbulence structure was observed visually in the shrub and grass channels. Progressive waving of the grass was observed. The downstream migration of vortices generates progressive waving of the grass vegetation (Ghisalberti and Nepf, 2006; Nepf and Ghisalberti, 2008). Because the vortices move faster than the mean velocity, areas of plant deflection that progress downstream indicate the presence of such coherent structures within the flow (Ghisalberti and Nepf, 2002; Nepf and Ghisalberti, 2008). This coherent waving enhances momentum transport compared to a bare channel (Nepf and Ghisalberti, 2008). A downstream-progression vibration of the dowels was also observed in the shrub channel, suggesting coherent turbulence structure (perhaps due to the presence of ejections and sweeps). Analysis of turbulence intensities, TKE, and Reynolds stresses confirmed the visual observation of coherent structures, as explained in the following sections.

**Turbulence Intensities:** Turbulent intensities were calculated for each velocity component ($RMS_u$, $RMS_v$, and $RMS_w$) to show how the velocities varied from the mean (Wilcox and Wohl, 2007). Turbulence intensity profiles ($RMS_u$, $RMS_v$), measured perpendicular to the boundary are presented in Figures 4.3 and 4.4. The top of the profiles indicate the free water surface, and the shorter profiles were measured near the top of the bank. When considering profile locations with respect to the streambank vegetation, profile 3 was outside the vegetation and profile 4 was partially within the vegetation. The interface between the vegetation and the main channel was located at a perpendicular distance of 7 cm for profile 4. Profiles 5, 6, and 7 were measured entirely within the vegetation. The horizontal error bars indicate the standard deviation calculated among the five cross-sections.

Streamwise turbulence intensity profiles (Figure 4.3) for the bare and tree treatments remained constant at all locations. The bare $RMS_u$ values for every location were evenly distributed along all locations with a median value of 0.03 m/s, suggesting no coherent structures. At location 3, the tree condition showed a slight increase in $RMS_u$ near the free surface. This increase was expected because there was a slight increase in the free stream

velocity for the bank with trees, and turbulence intensity increased with increasing velocity. The vertical $RMS_u$ profile (location 3) for the shrub condition was greater in magnitude than all other vegetation conditions (maximum shrub $RMS_u$=0.05 m/s). At the same location, the grass profile had a sharp gradient at a perpendicular distance of 5 cm (roughly the height of the folded, submerged grass), increasing to a value of 0.04 m/s. The small magnitude of the grass $RMS_u$ compared to the shrub vegetation can be partially attributed to the reduced momentum exchange efficiency in the presence of *monami* (Nepf and Ghisalberti, 2008) and to the higher grass vegetation density (shrub stem density=1296 stems/$m^2$; grass stem density=4150 stems/$m^2$). The variation of the grass $RMS_u$ values at the vegetation/main channel interface also support the presence of progressing coherent structures. At location 4, the boundary between the vegetation and the main channel occurred at a distance of 7 cm perpendicular to the streambank. The increase of $RMS_u$ through this distance for the shrub and grass vegetation indicates mixing within the vegetation (max shrub $RMS_u$=0.05 m/s; max grass $RMS_u$=0.03 m/s). At location 5, the shrub treatment followed a similar trend as the grass, but the shrub $RMS_u$ increased to 0.02 m/s. This increase occurred within 5 cm of the main channel where mixing occurred (as seen in Figure 4.3). All measurements for locations 6 and 7 were made within vegetation for the shrub and tree channels. At these locations (6-7), average velocity and turbulence fluctuations decreased within the vegetation, with reduced the turbulence intensities for the vegetation treatments as compared to the bare condition. The grass data for locations 6 and 7 were removed in filtering.

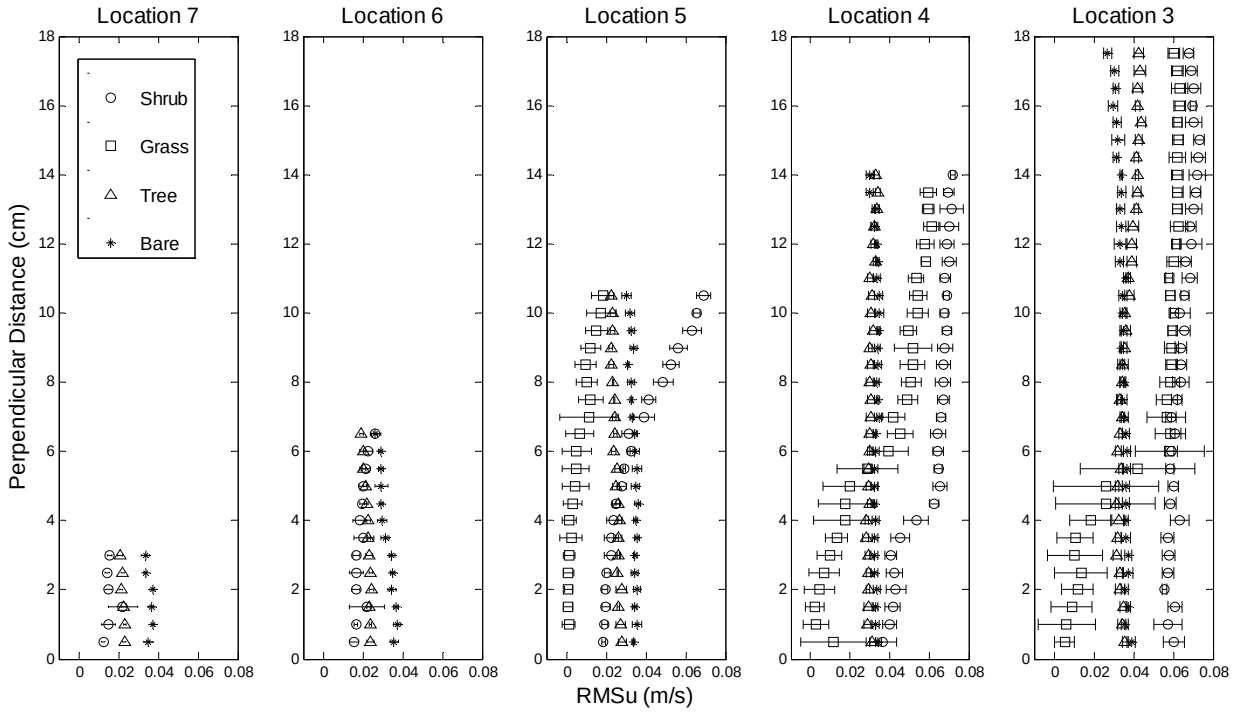


**Figure 4.3. Streamwise turbulence intensity ($RMS_u$) profiles measured perpendicular to the sloping bank for each bank profile location (3, 4, 5, 6, and 7) and vegetation type (bare, tree, shrub, and grass). Error bars denote the standard deviation of five cross-section replications, except for the grass condition where some data were removed in filtering. Location 3 was measured at the bank toe in the main channel, location 4 was measured partially in the vegetation, and locations 5-7 were measured fully within the vegetation.**

The trends and magnitudes of the $RMS_v$ and $RMS_w$ profiles were similar. As a result, only the $RMS_v$ profiles are presented graphically (Figure 4.4). The distributions of the three components were similar, but the magnitudes of $RMS_v$ and $RMS_w$ were less than the $RMS_u$ magnitudes for all vegetation types (p-values<0.001). The median $RMS_v$ and $RMS_w$ values for the bare condition were 37% lower than $RMS_u$. Compared to $RMS_u$, the median $RMS_v$ was 24%, 33%, and 54% lower for the trees, shrub, and grass conditions, respectively. Compared to $RMS_u$, the median $RMS_w$ was 30%, 24%, and 30% lower for the trees, shrub, and grass conditions, respectively. This percent decrease is comparable to the 33% decrease that Liu et al. (2008) reported between $RMS_u$ and $RMS_w$ in submerged rigid vegetation.

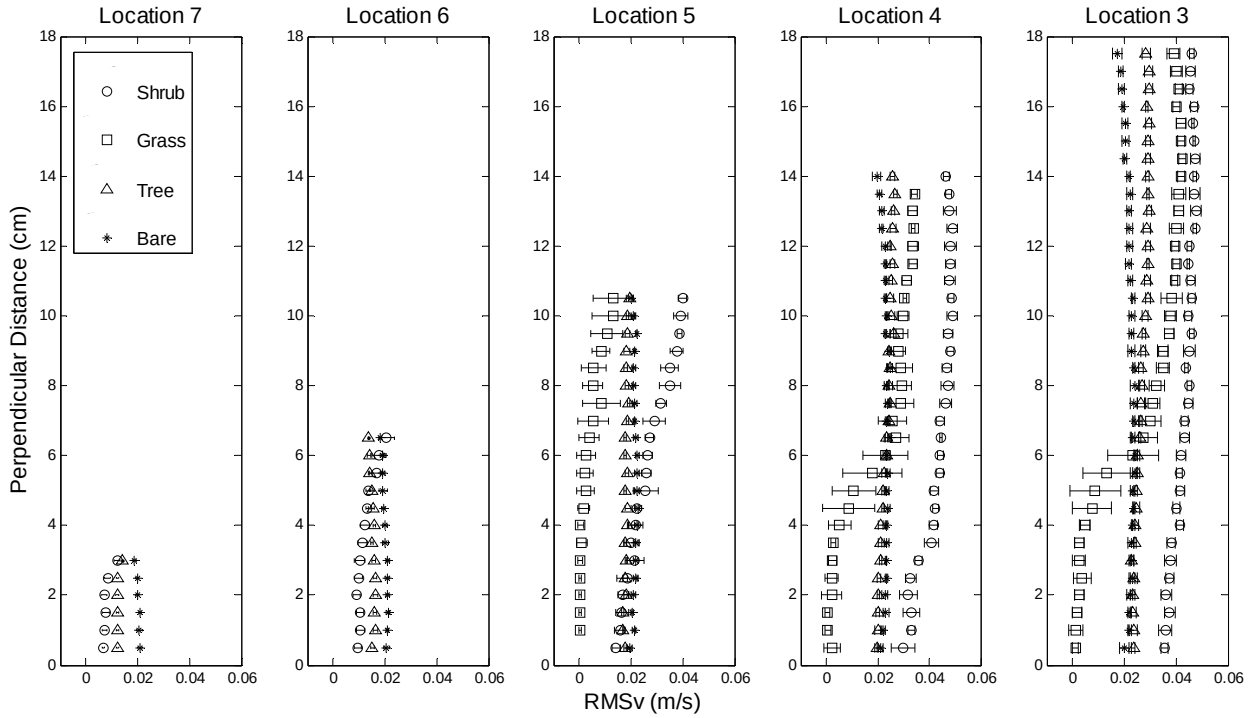


**Figure 4.4. Lateral turbulence intensity ($RMS_v$) profiles measured perpendicular to the sloping bank for each bank profile location (3, 4, 5, 6, and 7) and vegetation type (bare, tree, shrub, and grass). Error bars denote the standard deviation of five cross-section replications, except for the grass condition where some data were removed in filtering. Location 3 was measured at the bank toe in the main channel, location 4 was measured partially in the vegetation, and locations 5-7 were measured fully within the vegetation.**

While the RMS values can be considered a measure of the violence of the turbulence fluctuations, the RMS divided by the mean velocity represents the relative intensity of turbulence. The relative turbulence intensities ( $RMS_u / \bar{u}$ , $RMS_v / \bar{v}$, and $RMS_w / \bar{w}$) were calculated in the same locations as the RMS values for each vegetation type. For the downstream direction ( $RMS_u / \bar{u}$ ), the grass and shrub conditions had greater relative turbulence intensities as compared to the bare and tree streambanks, likely due to coherent structures. For the bare and tree conditions, $RMS_u$ represented roughly 10% of the mean downstream velocity for all locations and means were not significantly different ($\alpha$=0.05). Shrub means were significantly different than the bare and tree $RMS_u$ values. At the vegetation/main channel interface, the shrub $RMS_u$ represented 20-30% of the mean downstream velocity. This percentage increased with depth into the vegetation, reaching up to 120% of the mean velocity at location 7. In the mixing zone for the grass channel (within a perpendicular distance of 5 cm at

location 3), there was great variation in $RMS_u$. The grass $RMS_u$ represented 60-200% of the downstream velocity, further supporting the progression of vortices downstream. There was much more variability for the v and w components. At locations 3, 4, and 5, $RMS_v / \bar{v}$ and $RMS_w / \bar{w}$ generally increased with distance from the streambank boundary for all four streambanks. The values of $RMS_v / \bar{v}$ (>0.5 for all locations) and $RMS_w / \bar{w}$ (generally >1) were an order of magnitude greater than the $RMS_u / \bar{u}$ values.

**Turbulent Kinetic Energy (TKE):** The cross-sectional distribution of TKE represents the competition between the reduced velocity and increased turbulence generated by the addition of streambank vegetation (Nepf, 1999). The TKE estimates for the bare condition were uniform along a cross-section as compared to the vegetation treatments (median bare TKE=1.1 N/m$^2$). The small range in bare TKE values (0.4 N/m$^2$-1.8 N/m$^2$) had peak TKE productions at the channel boundary near the bed and the top of the bank. The bed peak TKE was likely influenced by the turbulence originating from the rough bed while the peak at the water surface was influenced by secondary currents near the surface. The tree TKE values (0.4 N/m$^2$-2.3 N/m$^2$) increased with flow depth, but there was an area of low TKE values along the top of the bank not present in the bare condition. While the maximum TKE shrub values (approximately 5 N/m$^2$) were shifted away from the streambank, the shrub treatment had an area of high TKE near the streambank toe. The mass and momentum exchanged between main channel and vegetation streambank contributed to mixing and high TKE along this vegetation/main channel interface. Turbulence was dampened within the first three rows of shrubs. The grass treatment also moved maximum TKE estimates (approximately 4 N/m$^2$) away from the streambank boundary, and TKE values were lower near the streambank boundary for the grass treatment. The grass folded along the bank, dampening the turbulence characteristics at the bank toe.

**Reynolds Stresses:** Reynolds stresses, stresses due to the turbulent fluctuations that represent momentum exchange (Robert, 2003), were analyzed in three planes: $\tau_{uv}$, $\tau_{uw}$, and $\tau_{vw}$ (Figure 4.5, Figure 4.6, and Figure 4.7). The Reynolds stress, $\tau_{vw}$, had the lowest magnitude compared to the other stresses. While $\tau_{uw}$ contributed to positive stresses for the shrub and grass treatments, $\tau_{uv}$ had the greatest magnitude among the stressors for the vegetation treatments, suggesting lateral momentum exchange between the vegetation channel and main channel. $\tau_{uw}$ was an important component for the bare and tree channel; the bare channel had the greatest $\tau_{uw}$

estimates at most locations (Figure 4.6). With respect to Reynolds stresses, the tree treatment mimicked a bare channel rather than the vegetated channels, indicating less lateral momentum exchange than in the vegetated channels.

Bare $\tau_{uv}$ profiles were vertical and constant among locations (median bare $\tau_{uv}$=0.2 N/m$^2$; Figure 4.5). Tree $\tau_{uv}$ profiles were the most similar to the bare condition (median tree $\tau_{uv}$ =0.2 N/m$^2$), only deviating at location 3 where it increased slightly compared to the bare bank. The sparse tree coverage induced turbulence that was captured only in that profile. The deviation was likely in the mixing zone caused by momentum exchange created by the dowels. Shrub $\tau_{uv}$ estimates were nearly vertical at location 3 and were greater than all other treatments (maximum of 1.8 N/m$^2$), indicating greater lateral momentum exchange at the vegetation/main channel interface than the other vegetation types and greater lateral momentum exchange than the bare channel. The base of profile 3 was located at the bank toe in the main channel adjacent to the bank vegetation. The shrub values were greatest for this profile because of vortex shedding from the rigid vegetation in this mixing zone. At location 3 near the bank, the grass $\tau_{uv}$ values were similar to the bare and tree results, but increased away from the boundary reaching a maximum value of 1.2 N/m$^2$. The grass folded near the boundary mimicking a smooth boundary, but coherent structures induced waving. Compared to rigid vegetation, the flexible grass was less efficient in momentum transfer due to the presence of *monami* (Nepf and Ghisalberti, 2008), as indicated in the lower shear stress. At location 4, the shrub treatment had the highest $\tau_{uv}$ values, reaching 1.8 N/m$^2$. The shrub profile (location 4) was vertical and similar to the bare and tree treatments near the bank (<4 cm). The interface of the dowels with the main channel occurred at a perpendicular distance of roughly 7 cm. Mixing of the fast moving main channel into the vegetated channel induced momentum exchange within the first 5 cm of shrub vegetation. In this mixing zone, the shrub profile has a sharp increase as the profile moves from the streambank toe, through the vegetation, and into the main channel. The maximum $\tau_{uv}$ value for the shrub condition occurred outside the vegetation in the shear layer. The grass profile (location 4) followed a similar trend as the shrub profile but reached a smaller maximum value (0.9 N/m$^2$). The rigid shrub vegetation produced large rapidly rotating vortices about a vertical axis because the vortex continually contacts the formation geometry (stem diameter). In comparison, the waving of the grass caused the vortices to lose coherence (Nepf and Ghisalberti, 2008). Due to this difference in flexibility, the shrub vegetation produced higher shear stresses than the grass

vegetation at the vegetation/main channel interface. Profiles 5, 6, and 7 were measured completely within the vegetation. The streamwise velocity decreased in this area (<25 cm/s for shrubs and <15 cm/s for grass), as well as the $\tau_{uv}$ estimates for the shrub and grass condition. The increase of the shrub $\tau_{uv}$ estimates at location 6 corresponds with the mixing zone 5 cm into the vegetation. Thornton et al. (2000) also reported that shear stress was greatest at the interface between the main channel and the vegetated channel. Within the vegetation (location 6, 7, and 8) all vegetation types reduced $\tau_{uv}$ compared to the bare control (Figure 4.5). The lateral momentum transfer toward the streambank of the densely vegetated channels may form a wider channel to balance the applied and critical shear stress. The small standard deviations of the bare and tree treatment (locations 3 and 4) support the idea of large scale coherent structures, while the greater variation in the shrub and grass treatment supports the progression of smaller scale structures.

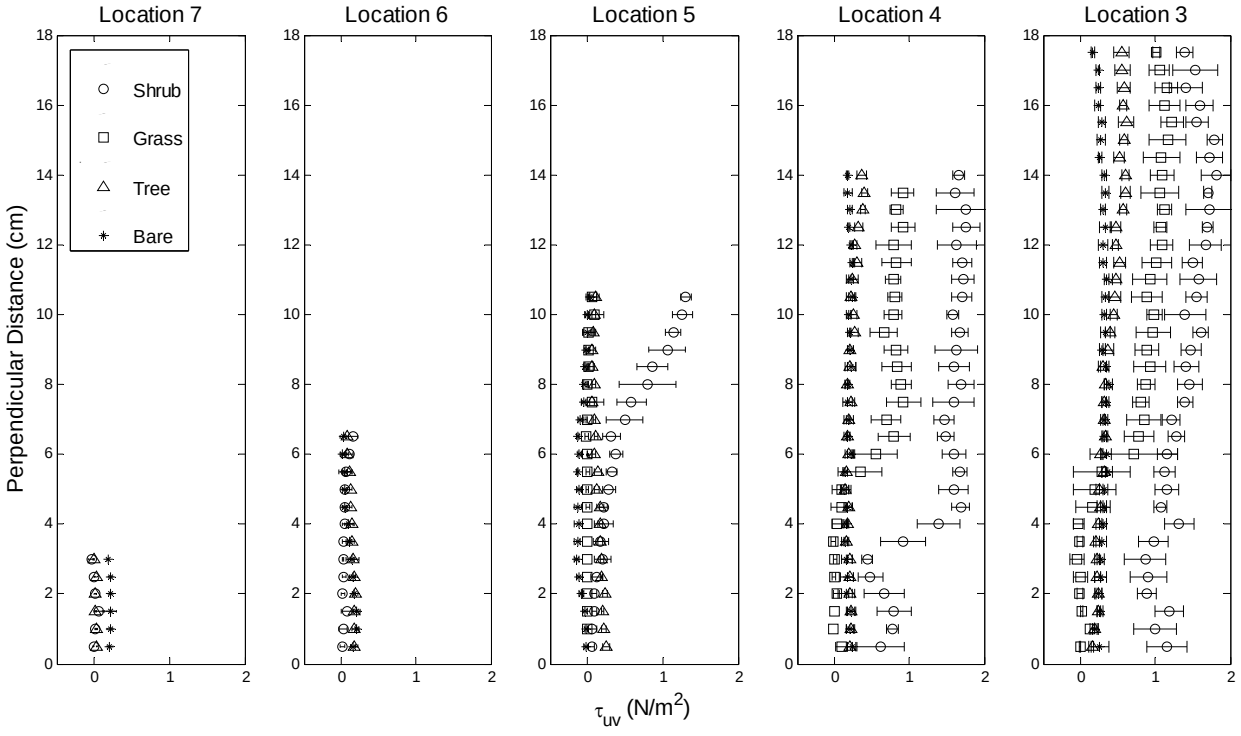


**Figure 4.5. Reynolds stress ($\tau_{uv}$) profiles measured perpendicular to the sloping bank for each bank profile location (3, 4, 5, 6, and 7) and vegetation type (bare, tree, shrub, and grass). Error bars denote the standard deviation of five cross-section replications except for the grass condition where some data were removed in filtering. Location 3 was measured at the bank toe in the main channel, location 4 was measured partially in the vegetation, and locations 5-7 were measured fully within the vegetation.**

$\tau_{uv}$ was the main stress tensor for all vegetation types (shrub, tree, and grass), likely caused by velocity fluctuations created by downstream progressing vortices rotating around a vertical axis (White and Nepf, 2007). A major stress tensor for the bare condition was $\tau_{uw}$, indicating turbulence and momentum transfer occurred due to the channel boundary. These findings are consistent with Tritico and Hotchkiss (2005) who reported that the maximum $\tau_{uw}$ occurred at the boundary for unobstructed turbulent flow with no trend in $\tau_{uv}$. Excluding location 3 for all vegetation treatments and location 4 for the shrub treatment, the bare $\tau_{uw}$ values were greater than all the vegetation treatments (median=0.2 N/m$^2$; Figure 4.6). These results indicate a difference in momentum exchange between the bare channel and the vegetated channels. The lateral momentum exchange between the main channel and vegetated channel dominated in the vegetated conditions, while the vertical momentum exchange was important for the bare channel.

The least significant Reynolds stress tensor was $\tau_{vw}$. Profiles for all vegetation types and locations were roughly vertical, centering around 0 N/m$^2$ (Figure 4.7). There was an increase in $\tau_{vw}$ at the boundary where the sloping bank met the rough bed. All the treatments had increased $\tau_{vw}$ at the boundary, but the $\tau_{vw}$ for the shrub condition increased more than the other treatments, indicating an area of strong, three-dimensional turbulence at the interface of the bank toe for dense, semi-rigid streambank vegetation. This area of turbulence may lead to fluvial erosion of the bank toe, moving to a vertical bank observed in natural channels.

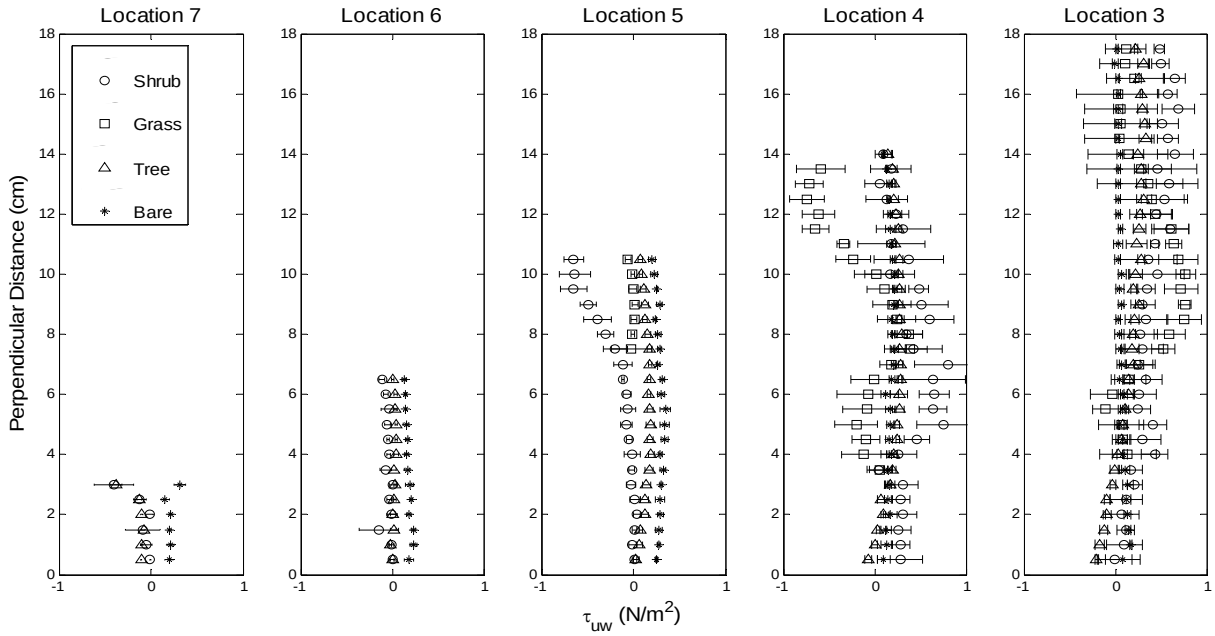


**Figure 4.6. Reynolds stress ($\tau_{uw}$) profiles measured perpendicular to the sloping bank for each bank profile location (3, 4, 5, 6, and 7) and vegetation type (bare, tree, shrub, and grass). Error bars denote the standard deviation of five cross-section replications except for the grass condition where some data were removed in filtering. Location 3 was measured at the bank toe in the main channel, location 4 was measured partially in the vegetation, and locations 5-7 were measured fully within the vegetation.**

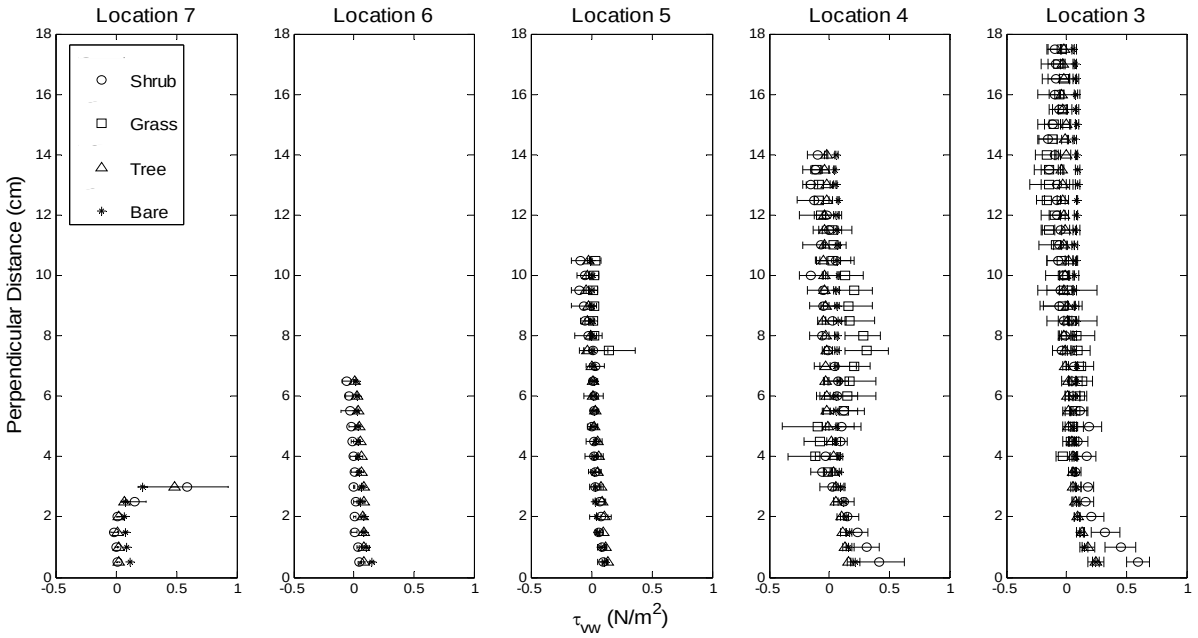


**Figure 4.7. Reynolds stress ($\tau_{vw}$) profiles measured perpendicular to the sloping bank for each bank profile location (3, 4, 5, 6, and 7) and vegetation type (bare, tree, shrub, and grass). Error bars denote the standard deviation of five cross-section replications except for the grass condition where some data were removed in filtering. Location 3 was measured at the bank toe in the main channel, location 4 was measured partially in the vegetation, and locations 5-7 were measured fully within the vegetation.**

*4.3.3 Impacts of vegetation on streambank fluvial erosion*

Fluctuating forces in turbulent flow are likely responsible for fluvial erosion (Lavelle and Mofjeld, 1987; Chang, 2002; Diplas, 2008). Turbulence characteristics and Reynolds stresses measured at the streambank boundary provide insight into the impact of streambank vegetation on fluvial erosion. The excess shear stress equation, which relates the streambank erosion rate to the difference between the applied grain shear stress and the soil critical shear stress, predicts the erosion rate of fine grain soils due to stream channel scour (Osman and Thorne, 1988; Hanson and Simon, 2001). The applied shear stress can be related to TKE and Reynolds stresses (Biron et al., 2004; Daniels and Rhoads, 2004; Pope et al., 2006). TKE estimates and Reynolds stresses ($\tau_{uv}$) adjacent to the streambank were analyzed for the bare, tree, and shrub treatment. The velocity record measured 0.5 cm from the streambank for each profile along the bank was used in this analysis (n=25). The grass treatment was removed from this analysis because the data close to the streambank boundary were removed in filtering.

The distribution of TKE and Reynolds stresses adjacent to the bank face (Figure 4.8) indicates a relatively uniform distribution across the bare bank. The shrub and tree TKE and Reynolds stresses increased with water depth and with decreasing distance to the bank toe. The shrub condition had the lowest median shear stress value but the range in stresses was large (0.1-3.6 $N/m^2$). The shrub treatment had an area of high Reynolds stresses and TKE near the streambank toe. Mass and momentum exchange between the main channel and the vegetated area contributed to mixing and high Reynolds stresses along this interface. This area of high shear stress may encourage fluvial erosion, moving the bank to a more vertical orientation. The greater turbulence near the bank toe will also discourage sedimentation.

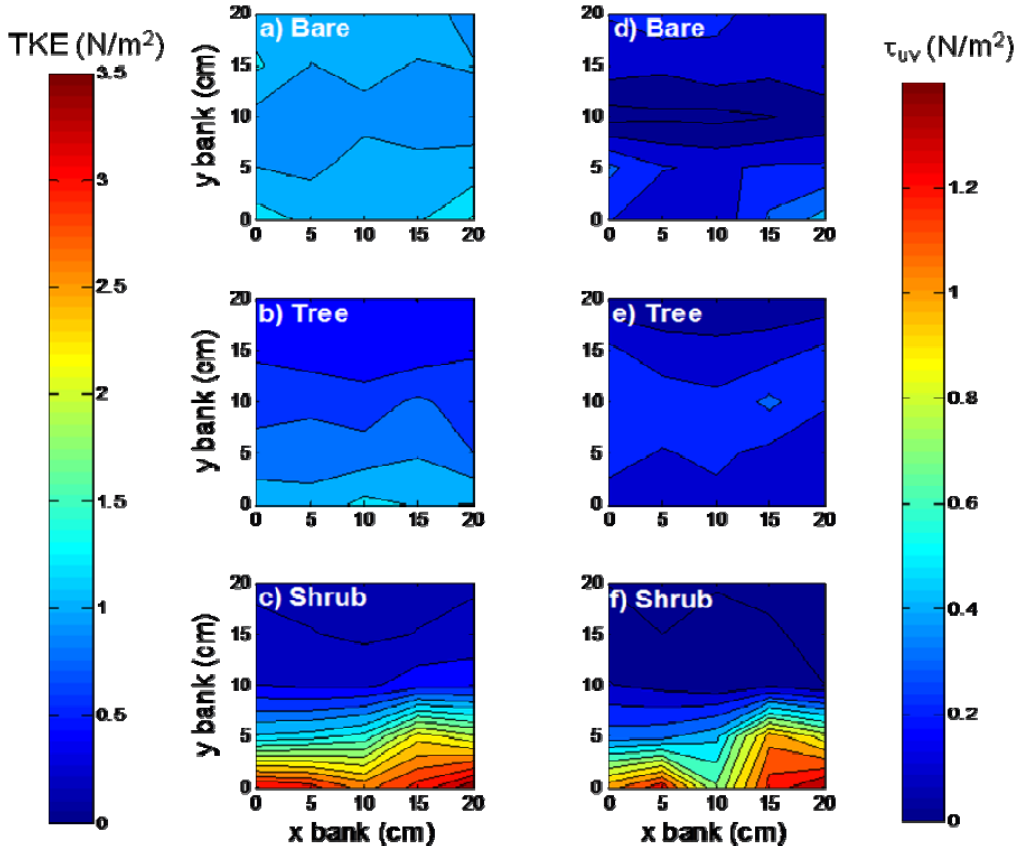


**Figure 4.8. Distribution of *TKE* ($N/m^2$; a, b, and c) and Reynolds stresses ($\tau_{uv}$, $N/m^2$; d, e, and f) measured adjacent to the streambank (0.5-cm distance from bank) for the bare, tree, and shrub vegetation treatments (n=25).**

Although grass data adjacent to the streambank were removed in filtering, general trends caused by the influence of grass on fluvial erosion were observed. The grass treatment moved high Reynolds stresses and TKE away from the streambank. The grass may provide greater protection than the shrubs against fluvial erosion because the grass folds, protecting the bank. The waving grass also reduced the momentum exchange efficiency, as compared to the rigid vegetation (Nepf and Ghisalberti, 2008). Fluvial erosion is less likely to occur along the grass streambank because the stresses are reduced, and the turbulence reduction will likely promote sedimentation. Because there is less turbulence, the energy of narrower channels can be maintained, supporting findings that grass channels are narrower than forested channels (Zimmerman et al., 1967; Clifton, 1989; Sweeney, 1992; Davies-Colley, 1997; Trimble, 1997b; Bott et al., 2006; McBride et al., 2008).

### 4.4 Conclusions

A flume study was conducted analyzing the turbulent flow structure and velocity profiles on a sloping streambank for four streambank vegetation conditions: no vegetation, tree, shrub, and grass. The following statements summarize the major research findings:

1. The addition of vegetation on a sloping streambank increased the streamwise free stream velocity as compared to a bare streambank. Velocity in the downstream direction decreased in the area close to the streambank boundary for all vegetation treatments, but the reduction in velocity did not result in a reduction in overall shear stress for all vegetation types.
2. Isolated roughness elements (trees) impacted the flow near the streambank, as compared to a bare streambank. However, compared to the other vegetation treatments (shrubs and grass), the sparse rigid elements produced a velocity and shear stress distribution more similar to the bare streambank than the vegetated streambanks. Tree turbulence intensity profiles and Reynolds stress profiles measured perpendicular to the boundary were similar to those measured with bare banks, supporting previous findings that the planting of sparse vegetation may not promote sediment accumulation (Nepf, 1999).
3. The maximum turbulence intensities ($RMS_u$, $RMS_v$, and $RMS_w$) for the shrub and grass treatments occurred in the mixing zone of the main and vegetated channel areas. The turbulence intensities within the vegetation were low and increased into the main

channel. The gradient of the downstream turbulence intensity indicated that the extent of mixing into the vegetated zone was approximately 5 cm.

4. The lateral Reynolds stresses ($\tau_{uv}$) were the largest Reynolds stress tensor for the shrub and grass treatments, indicating vortex shedding in the lateral plane with a vertical rotation axis. The vertical Reynolds stress was a significant component for the bare condition, showing turbulence was generated at the rough bed.
5. Fluctuating forces in turbulent flow are likely responsible for fluvial erosion (Lavelle and Mofjeld, 1987; Chang, 2002; Diplas, 2008). The turbulence caused by the upright shrub treatment increased TKE and Reynolds stresses near the streambank, particularly at the streambank toe. This area is susceptible to fluvial erosion and the presence of dense, semi-rigid vegetation may encourage the formation of a wider channel with a vertical streambank.

This research was intended to improve our understanding of the role of riparian vegetation in stream morphology by evaluating the effects of vegetation on boundary shear stress, providing insight to the type and density of vegetation required for streambank stability. These results will also aide in quantifying sediment inputs from streambanks and in providing quantitative information for stream restoration design and watershed management planning.

# Chapter 5 Determining field methods to measure boundary shear stress along hydraulically rough streambanks

## 5.1 Introduction

Shear stress on the channel boundary is commonly calculated based on flow depth and slope (Chang, 2002), but this method can cause major errors in soil detachment calculations when flow resistance (e.g. vegetation) is substantial (Thompson et al., 2004). A key component of erosion models is the determination of BSS. While methods exist to determine BSS (e.g. law of the wall, Reynolds stresses, turbulent kinetic energy, FST-hemispheres, Prandtl's mixing length theory, and average boundary shear stress), those models do not consider the impact of vegetation; therefore, research is needed to quantify the influence of riparian vegetation on BSS so the effects of stream restoration can be assessed at the watershed scale.

### *5.1.1 Objectives*

The overall goal of this research was to determine a method for measuring BSS in the field along hydraulically rough streambanks, suggesting both an instrument and theory for estimation. Four roughness treatments were studied: no vegetation (bare), trees, shrubs, and grass.

## 5.2 Boundary shear stress (BSS)

A better prediction of the local applied boundary shear stress is necessary to quantify and predict the erosion of vegetated streambanks (ASCE, 1998). Turbulent fluctuations of shear stress higher than the average shear stress may be responsible for erosion (Lavelle and Mofjeld, 1987; Chang, 2002) and must be considered when estimating BSS. Several theories exist to quantify shear stress (e.g. law of the wall, Reynolds stresses, turbulent kinetic energy, Prandtl's mixing length theory, isovels, and FST-hemispheres), and these methods require different types of field measurements and instruments. Methods used in this experiment are summarized in Table 5.1 and are explained in Chapter 2.

**Table 5.1. Review of methods to estimates boundary shear stress, including field measurement requirements for each method**

| Method | Equation | Measurement Requirements |
|---|---|---|
| Average Boundary Shear Stress | $\tau_{avg} = \gamma R_h S$<br>$\tau_{avg} = \gamma H S$ (wide stream)<br>$\tau_{avg,bank} = \gamma H S \cos\Theta$ (sloping bank) | Estimates of $R_h$, S, H, and/or $\Theta$ |
| Law of the Wall | $\frac{u}{u*} = \frac{1}{k}\ln\frac{z_1}{z_0}$ | 1D velocity profiles near boundary (<0.2 flow depth) or depth-averaged velocity and an estimate of roughness ($z_0$) |
| Reynolds Stresses | $\tau_{uv} \cong -\rho\overline{u'v'}$<br>$\tau_{uw} \cong -\rho\overline{u'w'}$<br>$\tau_{vw} \cong -\rho\overline{v'w'}$ | 3D velocity measurements and instantaneous velocity fluctuations |
| Turbulent Kinetic Energy Method (TKE) | $\tau_{TKE} = C_1\left[0.5\rho(\overline{u'^2} + \overline{v'^2} + \overline{w'^2})\right]$<br>$\tau_{TKE,w} = C_2\rho\overline{w'^2}$ | 3D velocity measurements and instantaneous velocity fluctuations |

[1] $\tau_{avg}$ is the average boundary shear stress; $\tau_{avg,bank}$ is average boundary shear stress along a sloping bank; $\gamma$ is specific weight of water; $R_h$ is hydraulic radius; H is water depth; S is water surface slope; $\Theta$ is bank slope; u is water velocity; u* is shear velocity; $z_1$ is the elevation from the bed; $z_0$ is the roughness height; $\tau_{uv}$ is a component of Reynolds stress; $\rho$ is water density; u', v', and w' are velocity fluctuation in the streamwise, horizontal, and vertical direction; $\tau_{TKE}$ and $\tau_{TKE,w}$ are shear stress from turbulent kinetic energy; $C_1$ (0.19-0.21) and $C_2$ (0.90) are proportionality constants.

### 5.3 Methods

A second order prototype stream (Tom's Creek in Blacksburg, Virginia, USA), with individual reaches dominated by each vegetation treatment was modeled in a research flume using a fixed-bed Froude-scale modeling technique. One model streambank of the prototype stream was constructed for each vegetation type and compared to a bare control (only grain roughness). Velocity profiles perpendicular to the flume model boundary were measured using a three-dimensional acoustic Doppler velocimeter and a miniature propeller as explained in Ch. 3. Direct measurements of shear stress were made using a flush-mount constant temperature hot-film anemometer (Ch. 3) at locations 3-6 (Figure 3.9).

*5.3.1 Data Analysis*

Several methods of calculating BSS were evaluated (Table 5.1): the law of the wall (LOW; $\tau_{LOW,ADV}$, $\tau_{LOW,ADV,20\%}$, $\tau_{LOW,MP}$, and $\tau_{LOW,MP,\ 20\%}$), Reynolds stresses ($\tau_{uv}$, $\tau_{uw}$, $\tau_{vw}$, $\tau_{uv,extrap}$, $\tau_{uw,extrap}$, and $\tau_{vw,extrap}$), and TKE ($\tau_{TKE}$ and $\tau_{TKE,w}$). Because it is typically used in channel design, the average boundary shear stress was also calculated (Table 5.1).

The law of the wall was evaluated following the procedures outlined in Wilcock (1996), using the time-averaged MicroADV (ADV) and miniature propeller (MP) velocity measurements. Shear velocity (u*) was calculated from the slope of the least squares fit of ln(z) vs. u. Shear stress was then estimated by the following relationship:

$$u^* = \sqrt{\frac{\tau}{\rho}} \qquad [5.1]$$

where $\tau$ is the local shear stress (Wilcock, 1996; Robert, 2003). LOW estimates were made using the entire velocity profile ($\tau_{LOW,ADV}$ and $\tau_{LOW,MP}$) and only the points close to the bank (bottom 20% of profile; $\tau_{LOW,ADV,20\%}$ and $\tau_{LOW,MP,\ 20\%}$; Wilcock, 1996; Biron et al., 2004). Analysis of the Reynolds stresses and the TKE method required separating the instantaneous velocity fluctuation (u', v', and w') from the mean velocity ($\bar{u}$, $\bar{v}$, and $\bar{w}$) for each velocity component ($u = \bar{u} + u'$, $v = \bar{v} + v'$, and $w = \bar{w} + w'$). The three components of the Reynolds stresses ($\tau_{uv}$, $\tau_{uw}$, and $\tau_{vw}$) were calculated (Table 5.1). Reynolds estimates were calculated adjacent to the streambank (distance = 0.5 cm from the bank; $\tau_{uv}$, $\tau_{uw}$, and $\tau_{vw}$) and by extrapolating the Reynolds stress profiles to the stream bank boundary ($\tau_{uv,extrap}$, $\tau_{uw,extrap}$, and $\tau_{vw,extrap}$; Biron, 2004). TKE estimates of BSS were calculated adjacent to the bank (distance = 0.5 cm; $\tau_{TKE}$, and $\tau_{TKE,w}$; Table 5.1). A perpendicular distance of 0.5 cm from the bank was considered adjacent to the bank. This distance was the minimum distance at which the ADV could provide reliable data. Only the miniature propeller data were examined for the grass treatment because much of the near-bank ADV data were removed in filtering.

*5.3.2 Statistical Analysis*

Results from the combinations of experimental theories (LOW, Reynolds, and TKE) and instruments (ADV and MP) were compared to the hot-film anemometer measurements (Appendix D). To determine the most accurate combination of estimation method and instrumentation, sum of squares (SS) were evaluated (Equation 5.1); each vegetation type was examined separately.

$$\sum \left(s_i - \hat{s}_i\right)^2 = e_i \qquad [5.2]$$

where $s_i$ is the measured values of BSS, $\hat{s}_i$ is the estimated values of BSS at the same location on the streambank, and $e_i$ is the sum of squares. The technique resulting in the lowest $e_i$ indicates the best technique to estimate BSS for that particular vegetation treatment.

A chi-squared comparison was used to determine groups of appropriate tests for each bank vegetation type. The following equation was used to calculate the $\chi^2$ statistic.

$$\chi^2 = \frac{\sum \left(y_i - y_{oi}\right)^2}{y_i} \qquad [5.3]$$

where $y_i$ is the measured value of shear stress (as measured with the CTA), measurement and $y_{oi}$ is the observed value of shear stress (as calculated by the estimation techniques) at the same location on the streambank. Each bank was analyzed separately (degrees of freedom = 19) and as a combination of bare, tree, and shrub (degrees of freedom = 38) at an $\alpha$ value of 0.05.

**5.4 Results**

Average boundary shear stress was calculated as 6.4 Pa when using the hydraulic radius ($R_h$ = 13 cm). When using the water depth (20.4 cm), average boundary shear stress was calculated as 10.0 Pa. After accounting for the sloping bank (35.5$^o$) the average boundary shear stress was calculated as 5.2 Pa and 8.1 Pa using the hydraulic radius and water depth, respectively. For each vegetation type, estimates of average boundary shear stress were the worst estimates of shear stress (SS > 400). The average boundary shear stress estimates were typically an order of magnitude greater than the CTA measurements and the other estimation

techniques. The following sections examine CTA BSS measurements and the following shear stress estimation techniques: Reynolds stresses ($\tau_{uv}$, $\tau_{uw}$, $\tau_{vw}$, $\tau_{uv,extrap}$, $\tau_{uw,extrap}$, and $\tau_{vw,extrap}$), TKE estimates ($\tau_{TKE}$ and $\tau_{TKE,w}$), and LOW estimates ($\tau_{LOW,ADV}$, $\tau_{LOW,ADV,20\%}$, $\tau_{LOW,MP}$, and $\tau_{LOW,MP,\ 20\%}$).

*5.4.1 Hot-film Anemometer Shear Stress Measurements*

By sensing changes in heat transfer from small, electrically heated elements, the anemometer (CTA) measured rapid changes in velocity that were related to shear stress with a calibration pipe, following the design of Thompson (Thompson, 2001; Thompson and Wilson, 2004). CTA measurements of BSS showed differences in BSS among vegetation types. The median boundary shear stress measurements were 0.57 Pa, 0.42 Pa, 0.23 Pa, and 1.56 Pa for the bare, tree, shrub, and grass streambanks, respectively (n = 20; Figure 5.1). The addition of vegetation altered the variance of the data; the standard deviations for the bare, tree, shrub, and grass bank were 0.15 Pa, 0.24 Pa, 0.05 Pa, and 0.46 Pa, respectively.

Comparing BSS medians using the Mann-Whitney U-test, the tree and shrub CTA measurements were not statistically different, but both vegetation treatments (tree and shrub) were different from the bare CTA measurements (p-values <0.005). The grass treatment was statistically greater than all of the other treatments (bare, tree, and shrub; p-value<0.001; Figure 5.1). Thompson and Wilson (2004) determined that the relative calibration accuracy of a constant temperature anemometer was 15%. The spread of the data were greater than 15% of the median value, indicating that BSS differences were not due to error of the CTA probe.

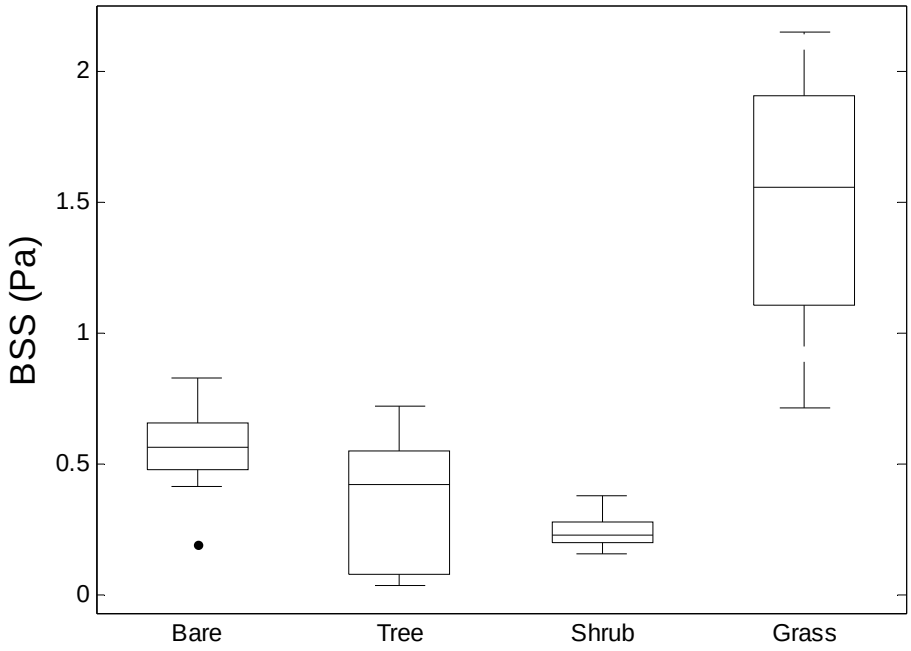


**Figure 5.1. Distribution of measurements of boundary shear stress measurements using a flush mount hot-film anemometer at four points along five cross-sections (n=20) for each vegetation treatment (bare, tree, shrub, and grass).**

The average boundary shear stress equation indicates that shear stress increases linearly with water depth (Table 5.1). To examine the changes in CTA shear stress with depth, the distribution of the CTA shear stresses were analyzed by row and by contour plots (Figure 5.2 and Figure 5.3). The CTA BSS increased consistently with water depth for the shrub bank only. The median CTA measurement at the bank toe was 0.29 Pa and decreased with decreasing water depth (0.23 Pa, 0.21 Pa, and 0.18 Pa, respectively). The bare BSS values were consistently greater than the shrub and tree bank; the median bare BSS values were 0.63 Pa, 0.66 Pa, 0.49 Pa, and 0.59 Pa for locations 3-6, respectively. While locations 4 and 6 of the tree bank were similar to the bare bank, locations 3 and 5 tree BSS values were less than the bare condition. The median tree BSS values were 0.14 Pa, 0.49 Pa, 0.07 Pa, and 0.57 Pa, for locations 3-6, respectively. The tree bank provided some protection as compared to the bare bank, but not as much protection as the dense, shrub bank. The median grass CTA shear stress values were higher than all other treatments for all rows and increased with decreasing water depth: 0.82, 1.49 Pa, 1.75 Pa, 1.93 Pa, respectively (Figure 5.3).

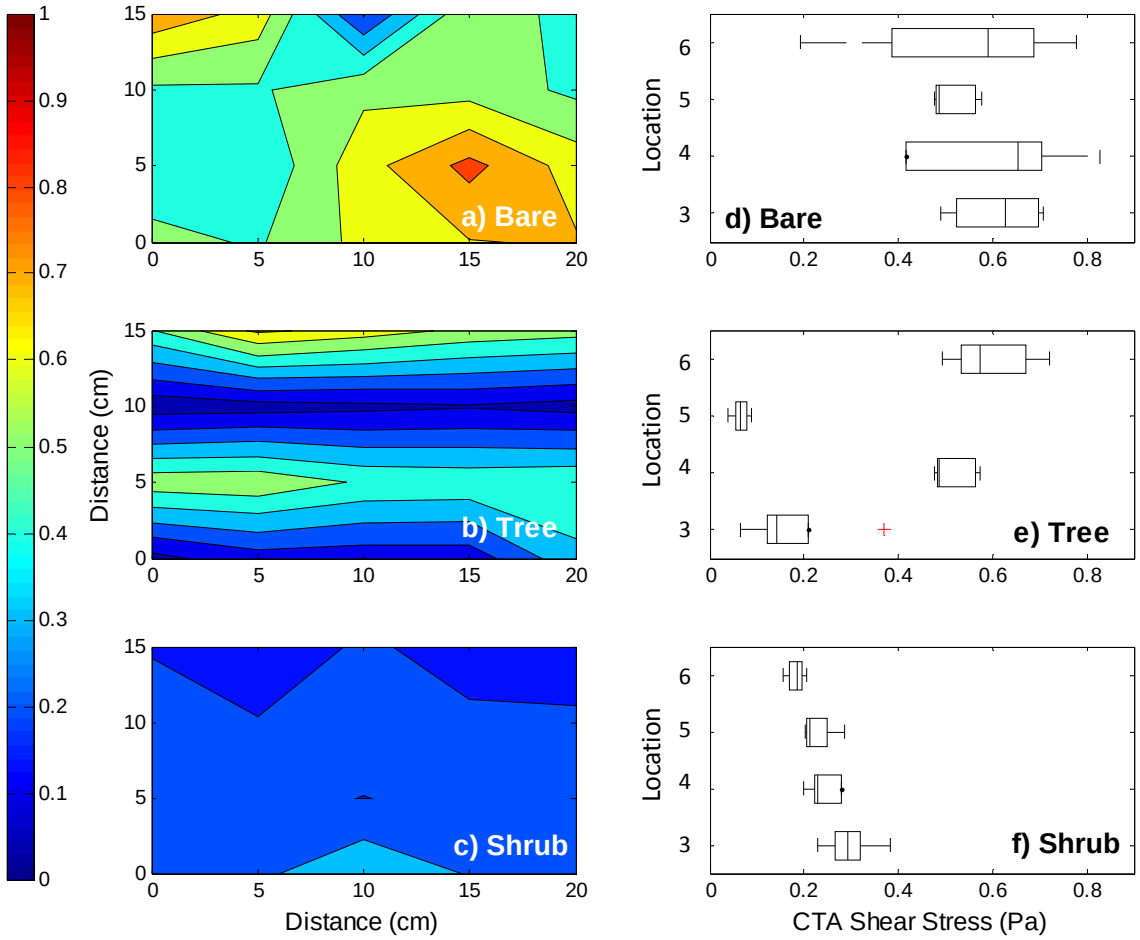


**Figure 5.2. Distribution of CTA boundary shear stresses (Pa) for three bank types: bare (a and d), tree (b and e), and shrub (c and f). Contour plots show the distribution along the bank (a, b, and c) and the boxplots show the distribution by rows (d, e, and f).**

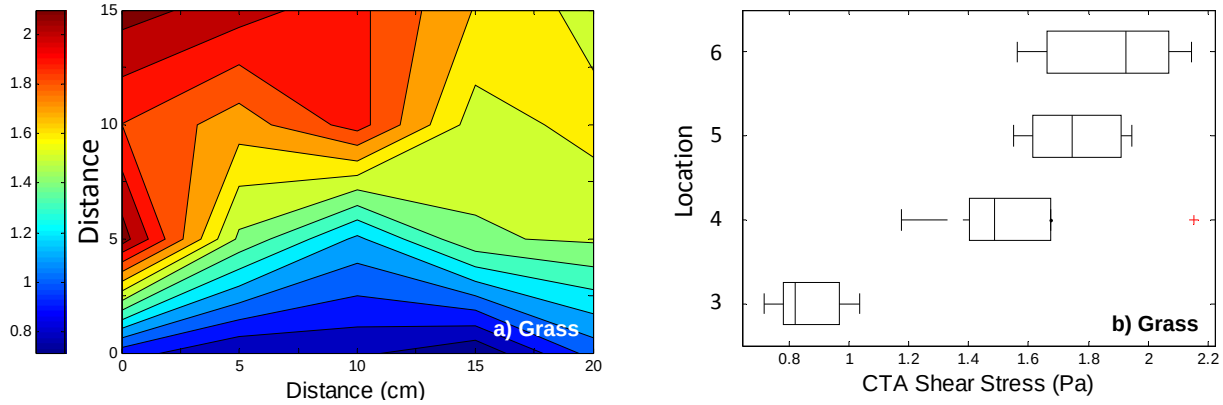


**Figure 5.3. Distribution of CTA boundary shear stresses (Pa) for the grass bank. The contour plots shows the distribution along the bank (a) and the boxplot shows the distribution by rows (b).**

Lui et al. (2008) reported the presence of a velocity spike near the bed directly behind dowels, likely caused by a junction vortex that formed at the dowel base. The velocity spike was also present in the free stream region between dowels and increased with increasing bed roughness. Since the BSS was measured at the streambank boundary using the CTA, velocity spikes behind dowels and in the free stream may result in higher BSS values. Figure 5.4 indicates the location of CTA measurements along the shrub streambank in reference to dowel location. Yellow marks indicate locations where CTA measurements of shear stress were greater than the bank median. None of the high CTA measurements were made directly behind a dowel, but locations A3, B3, C5, and E4 were measured adjacent to a dowel. All measurements made adjacent to a dowel were not higher than the median (e.g. B4). Locations A4, C3, and D4 were located in the free stream between dowels and exhibited high shear stress. All measurements made in the free stream were not greater than the median (e.g. E3). The presence of the velocity spike was not evident with the CTA measurements, and was not apparent with the measured velocity profiles (Figure 5.13). The velocity profiles were not measured close enough to the boundary (0.5 cm) to observe the spike. Also, the high density of the shrub vegetation may have contributed to the lack of the observed velocity spike. A similar analysis was not performed for the tree streambank because no dowels were present within the test section.


**Figure 5.4. Location of hot-film anemometer measurements of boundary shear stress in reference to the shrub dowel location for 5 cross-sections (A-E). Locations where BSS was greater than the bank median are highlighted with yellow symbols.**

**Discrepancy in Grass Hot-film Anemometer Shear Stress Measurements:** The high grass CTA shear stress values were unexpected. The TKE and Reynolds results (Ch. 4) indicated that the grass decreased the lateral momentum exchange as compared to the shrub condition. The TKE and Reynolds stresses near the grass bank toe were also less than the shrub bank (Ch. 4). These previous results indicated that the grass CTA BSS would be less than the shrub bank, but the grass CTA BSS values were greater than all other treatments. Unfortunately, the ADV data adjacent to the bank face (0.5 cm) were removed in filtering, so Reynolds stresses and TKE cannot be examined adjacent to the bank boundary. To confirm these findings, several checks were conducted.

First, the calibration curves were verified and grass calibration was repeated (Appendix C). Then, the probe specifications were verified to ensure the probe was within its range. Within the grass vegetation near the streambank, the downstream velocity was < 5 cm/s (as measured by the MP), but probe specifications do not report a minimum velocity value (Dantec, 2009). In correspondence with a Dantec representative, the range of the hot-film anemometer was confirmed appropriate for this flow. The grass may have interfered with the MP, resulting in

measured velocities lower than actual velocities, or the boundary layer was too small to be measured by the MP and ADV.

There was a difference in bank roughness compared for the grass bank as compared to the bare, tree, and shrub banks that may have contributed turbulence production. The grass was attached using a latch and hook technique. The grass was attached to a gridded canvas using small knots. Two grass blades extended from each knot. The grass mat was then attached to the masonry board panel, over the simulated grain roughness (sand paper; Figure 5.5). The bare, tree, and shrub streambanks did not have the extra roughness from the latch-hook canvas. The latch-hook canvas was significantly larger than the grain roughness present in the sandpaper and may produce greater turbulence at the streambank boundary with additional separation and attachment. This increased turbulence may have resulted in the high grass BSS measurements.

Lui et al (2008) reported a velocity spike at the boundary in flow through dowels. This spike increased with increasing bed roughness. The velocity profiles along the grass bank did not indicate a velocity spike, likely not observed with coarse incremental distance of the velocity profiles. Much of the ADV data close to the grass streambank were removed in filtering and the MP was unreliable in the dense grass cover. The waving grass interfered with the MP measurements. In this study, velocity was measured at a minimum distance of 0.5 cm and at 0.5-cm increments. In the Lui et al. (2008) study, velocity measurements were made at a minimum distance of 0.5 mm from the boundary. The velocity spike may have been present for the grass vegetation, increasing the BSS but not observed in the velocity profiles.

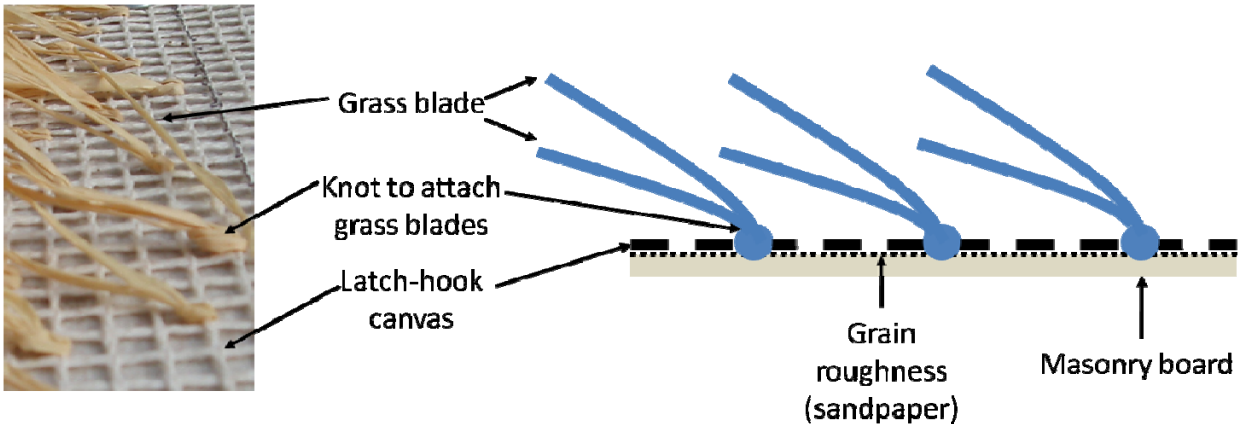


**Figure 5.5. Additional boundary roughness provided by the latch-hook canvas used for grass blade attachment.**

An examination of the location of high BSS along the grass bank revealed that the grass bank had high BSS values at the upstream end of the test-section near the top of the bank (locations A4, A5, A6, B5, B6, C5, C6, and D6; Figure 5.6). These locations were identified as high because the CTA measurements were greater than the bank median. No relationship between grass stem location and CTA measurement location was observed. There was a seam between vegetation panels located roughly 20 cm upstream of the test section (Figure 5.7). The seam was sealed with silicone caulk, smoothed along the bank, and cured for 24 hours before data collection. For the velocity profile measurements, the caulked seal provided a smooth barrier between the vegetation panels. The CTA provided greater difficulty in data collection because the CTA mounted from behind the bank. The streambanks were hinged at the bank toe to allow access behind the bank. Before each CTA measurement, the streambank section was raised to position the CTA, breaking the caulk seal. To keep a similar seal as used with the profile measurements, the caulk seal was put in place and allowed to cure for 24 hours. The seam was then cut with a razor to allow bank movement, but also to provide a seal. Due to the density of the grass, it was hard to observe the seal during testing to make sure that the banks remained in place. Before and after each CTA measurement, the banks were checked for appropriate positioning, but it is possible that the bank lifted slightly during measurements. This separation may have increased turbulence at the top of the streambank and the upstream end of the test section.

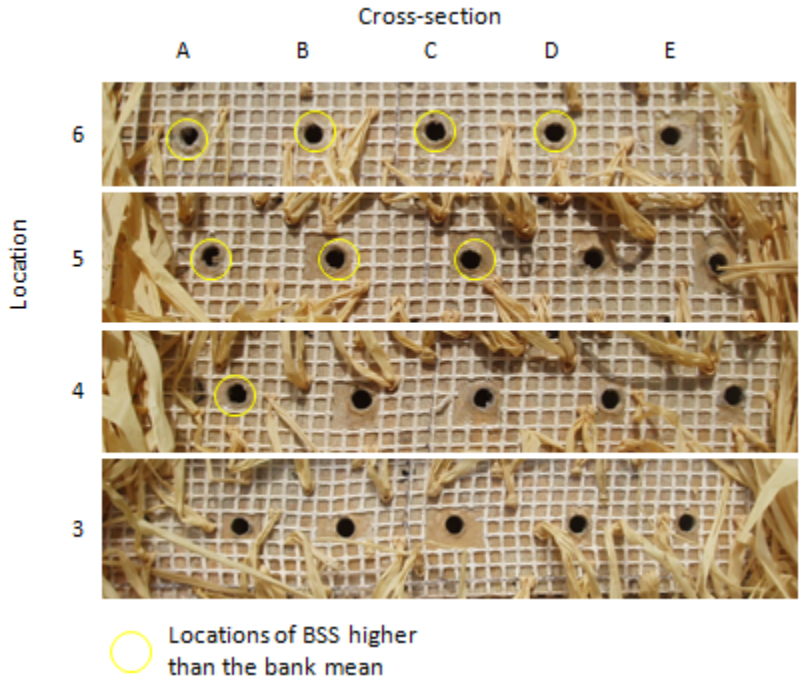


**Figure 5.6. Location of hot-film anemometer measurements of boundary shear stress in reference to the grass attachment points for 5 cross-sections (A-E). Locations where BSS was greater than the bank median are highlighted with yellow circles.**


**Figure 5.7. Seam between vegetation panels upstream of the test section on the bare bank.**

A momentum balance was completed for the grass channel to examine the reliability of the high BSS measurements. It was assumed that the pressure gradient due to the free surface balances with the total array drag and the boundary drag:

$$gHS = \frac{1}{2} C_D \frac{A_b}{A_r} U^2 H + \frac{\tau}{\rho} \quad [5.4]$$

where g is the acceleration due to gravity, H is the water depth, S is the water surface slope, $C_D$ is the drag coefficient, $A_b$ is the projected plant area, $A_r$ is the total flow area per unit length, U is average velocity within the vegetation, $\tau$ is boundary shear stress, and $\rho$ is water density (Wilson, 2007) . Vegetative drag ($C_D$') is expressed by the following equation:

$$C_D^{'} = \lambda C_D \quad [5.5]$$

where $\lambda$ is the ratio of $A_b$ to $A_r$. Combining Equation 5.2 and 5.3 results in the following equation:

$$gHS = \frac{1}{2} C_D^{'} U^2 H + \frac{\tau}{\rho} \quad [5.6]$$

The MP data was used to calculate velocity within the vegetation (0.12 m/s) because much of the grass ADV data were removed in filtering. Velocity was measured at more points within the vegetation using the MP. Water surface slope was not measured for the flume and was approximated using the bed slope (0.005). The minimum (0.71 Pa), median (1.56), and maximum (2.14 Pa) CTA measurements of BSS represented $\tau$. These values were used to calculate a range for the vegetative drag coefficient (0.53-0.63).

Wilson (2007) combined vegetation drag data as a function of Reynolds number for five studies with submerged flexible vegetation (Kouwen et al., 1969; Chen, 1976; Graf and Chhun, 1976; Wu, et al., 1999; Carollo et al., 2002). The calculated $C_D$' values were within the reported range (0.2 to 1) for the Reynolds number of this study (~100,000). This result may support that the grass BSS values were on the correct order of magnitude.

*5.4.2 Reynolds Shear Stress Estimates*

The three components of the Reynolds stresses ($\tau_{uv}$, $\tau_{uw}$, and $\tau_{vw}$) were analyzed adjacent to the streambank. A distance of 0.5 cm, the shortest distance for the ADV to function, is referred to as adjacent to the streambank. The grass Reynolds stresses were removed from the analysis due the amount of data removed through data filtering; only five data points adjacent to the bank remained after filtering. Median $\tau_{uv}$ values were 0.17 Pa, 0.19 Pa, and 0.23 Pa for the bare, tree, and shrub bank, respectively. Median $\tau_{uw}$ values were 0.19 Pa, 0.03 Pa, and -0.03 Pa for the bare, tree, and shrub bank, respectively. Median $\tau_{vw}$ values were 0.17 Pa, 0.14 Pa, and 0.17 Pa for the bare, tree, and shrub bank, respectively (Figure 5.8). For the bare bank, $\tau_{uv}$ and $\tau_{uw}$ were the same order of magnitude. For both the tree and shrub channels, $\tau_{uv}$ was an order of magnitude greater than $\tau_{uw}$, indicating that the boundary has less influence on momentum transfer for vegetated streambanks. Reynolds shear stress components were also calculated by extrapolating the shear stresses along the profile to the streambank. The extrapolated distributions are show in Figure 5.8.

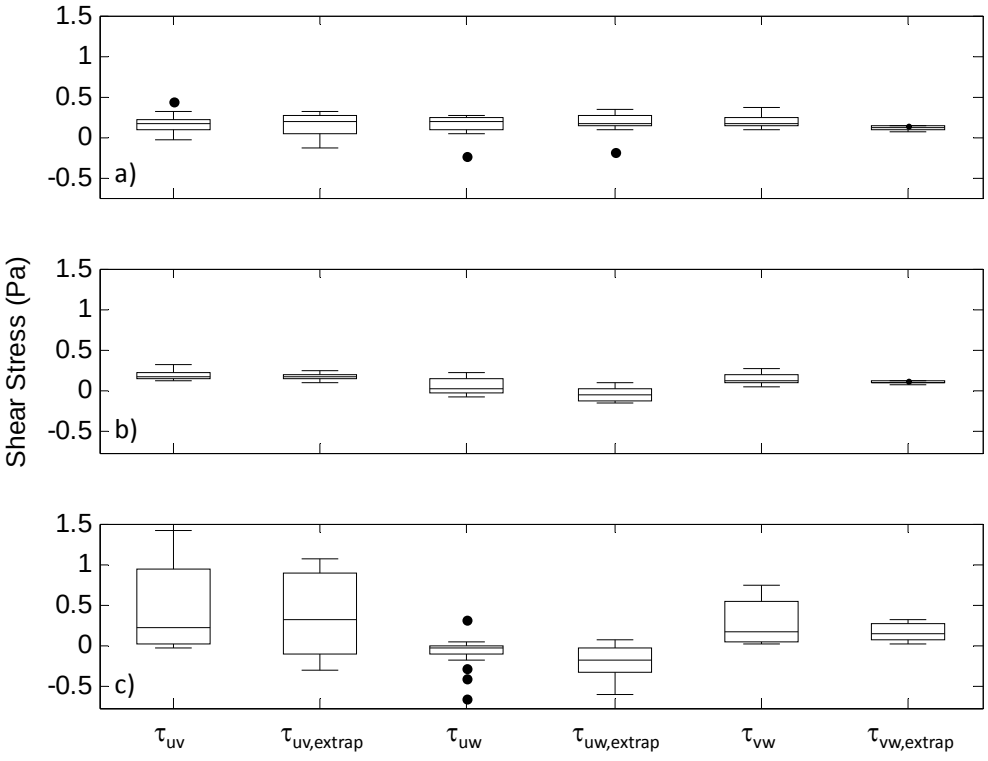


**Figure 5.8. Reynolds shear stress estimates (Pa; $\tau_{uv}$, $\tau_{uv,extrap}$, $\tau_{uw}$, $\tau_{uw,extrap}$, $\tau_{vw}$, $\tau_{vw,extrap}$) for four points along five cross-sections (n=20) for the vegetation treatments: a) bare, b) tree, and c) shrub.**

*5.4.4 TKE Shear Stress Estimates*

Adjacent to the streambank, median $\tau_{TKE}$ estimates were 0.20 Pa, 0.16 Pa, and 0.17 Pa for the bare, tree, and shrub bank, respectively. $\tau_{TKE,w}$ estimates were roughly two times greater than the $\tau_{TKE}$ estimates. Median $\tau_{TKE,w}$ estimates were 0.39 Pa, 0.34 Pa, and 0.54 Pa for the bare, tree, and shrub bank, respectively (Figure 5.9).

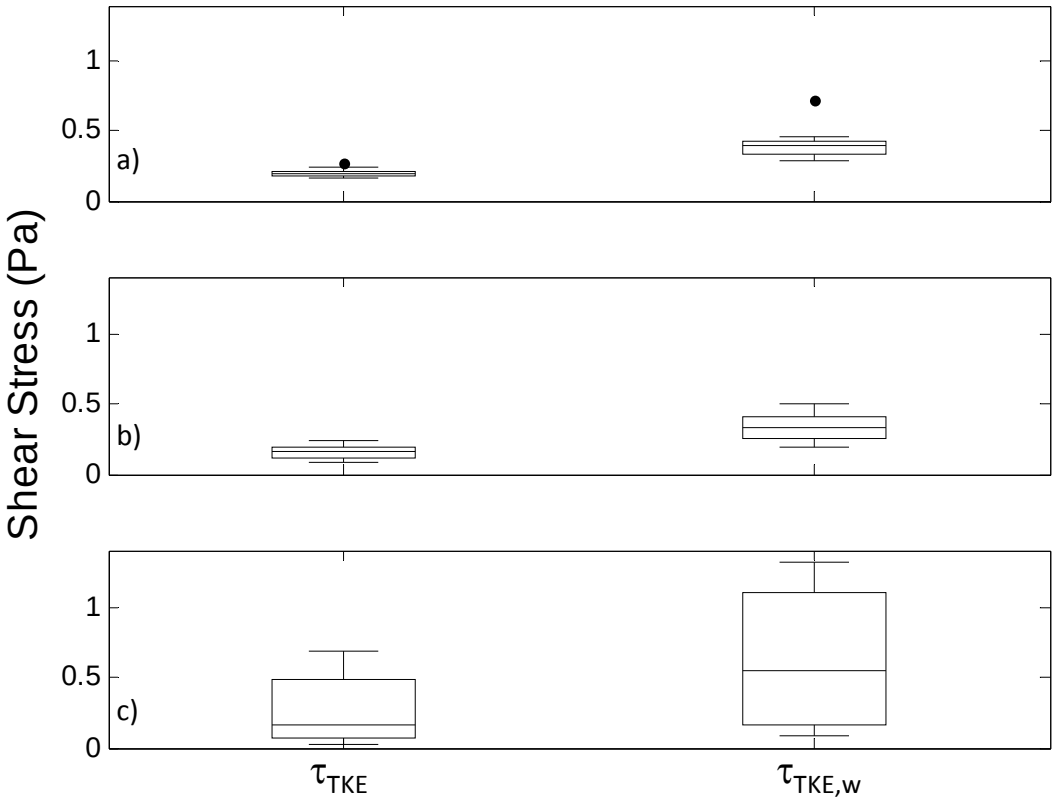


**Figure 5.9. Distribution of turbulent kinetic energy (TKE) estimates of boundary shear stress ($\tau_{TKE}$ and $\tau_{TKE,w}$) for four points along five cross-sections (n=20) for the vegetation treatments: a) bare, b) tree, and c) shrub.**

*5.4.5 Law of the Wall (LOW) Shear Stress Estimates*

LOW shear stresses were estimated using velocity profiles measured with an ADV and a miniature propeller (MP). The values were calculated using the entire measured velocity profile ($\tau_{LOW,ADV}$ and $\tau_{LOW,MP}$) and the portion of the profile closest to the bank (a distance < 20% of profile depth; $\tau_{LOW,ADV,20\%}$ and $\tau_{LOW,MP,20\%}$). There are no estimates of $\tau_{LOW,ADV}$ or $\tau_{LOW,ADV,20\%}$ for the grass treatment because the necessary data were removed in filtering.

The median LOW estimates for the bare treatment were 0.23 Pa, 0.12 Pa, 0.30 Pa, and 0.086 Pa for $\tau_{LOW,ADV}$, $\tau_{LOW,ADV,20\%}$, $\tau_{LOW,MP}$, and $\tau_{LOW,MP,20\%}$, respectively. The median LOW estimates for the tree treatment were 0.02 Pa, 0.05 Pa, 0.04 Pa, and 0.04 Pa for $\tau_{LOW,ADV}$, $\tau_{LOW,ADV,20\%}$, $\tau_{LOW,MP}$, and $\tau_{LOW,MP,20\%}$, respectively. The dense vegetation (shrub and grass) increased the range of shear stress estimates, indicating deviation from the logarithmic profile. The median LOW estimates for the shrub treatment were 0.24 Pa, 0.01 Pa, 0.35 Pa, and 0.24 Pa for $\tau_{LOW,ADV}$, $\tau_{LOW,ADV,20\%}$, $\tau_{LOW,MP}$, and $\tau_{LOW,MP,20\%}$, respectively. Maximum shrub $\tau_{LOW,MP}$ was an order of magnitude greater than the median value (5.9 Pa), and the maximum shrub $\tau_{LOW,MP,20\%}$ value (18.86 Pa) was two orders of magnitude greater than the median value. Grass $\tau_{LOW,MP}$ and $\tau_{LOW,MP,20\%}$ also had greater ranges of BSS with maximum BSS values of 5.9 Pa and 25.5 Pa, respectively. The median LOW BSS values for the grass treatment were 0.87 Pa and 3.91 Pa for $\tau_{LOW,MP}$, and $\tau_{LOW,MP,20\%}$, respectively (Figure 5.10).

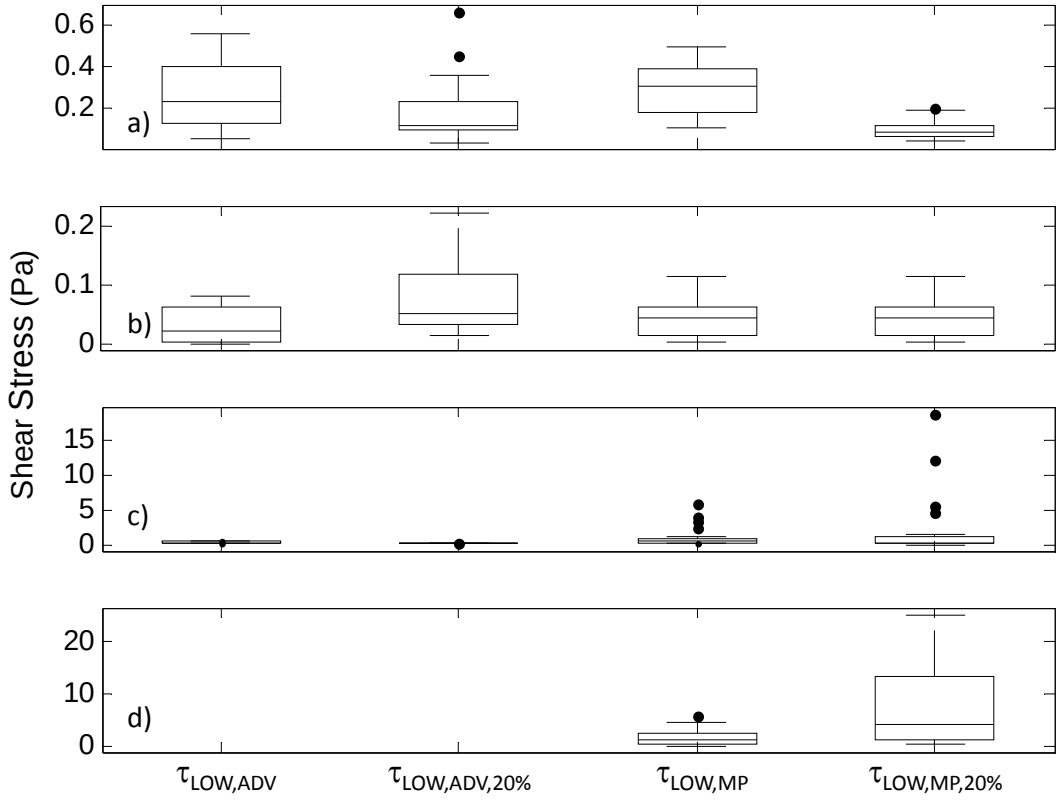


**Figure 5.10. Distribution of law of the wall (LOW) estimates of boundary shear stress ($\tau_{LOW,ADV}$, $\tau_{LOW,ADV,20\%}$, $\tau_{LOW,MP}$, and $\tau_{LOW,MP,20\%}$) for four points along five cross-sections (n=20) for each vegetation treatment: a) bare, b) tree, c) shrub, and d) grass; grass $\tau_{LOW,ADV}$ and $\tau_{LOW,ADV,20\%}$ were eliminated due to data filtering.**

Velocity measurements were less reliable within the vegetation. Interference with the ADV resulted in data removal through filtering. The miniature propeller intermittently reported unusually high velocity measurements when the propeller was stationary within the vegetation, overestimating average velocity. For the LOW method to be valid, the time-averaged streamwise velocity profiles must follow a logarithmic shape (Wilcock, 1996; Biron et al., 2004). The spatially averaged (across five cross-sections) ADV and MP velocity profiles are presented for each vegetation type (Figure 5.11-Figure 5.14). The bare profile roughly followed a logarithmic shape (Figure 5.11), and the addition of each vegetation treatment altered the shape from a logarithmic profile. The tree profiles roughly followed the logarithmic shape (Figure 5.12) due to the sparse dowel placement. At the shrub bank toe (location 3; Figure 5.13), the ADV velocity profile also roughly followed a logarithmic shape, suggesting that the LOW method can be used in non-vegetated portions of a vegetated channel. The ADV captured the logarithmic shape better than the MP. Within the dense shrub vegetation (locations 4-6), the velocity profile deviated from the logarithmic shape. The grass profiles differed from the logarithmic shape at all locations (Figure 5.14).

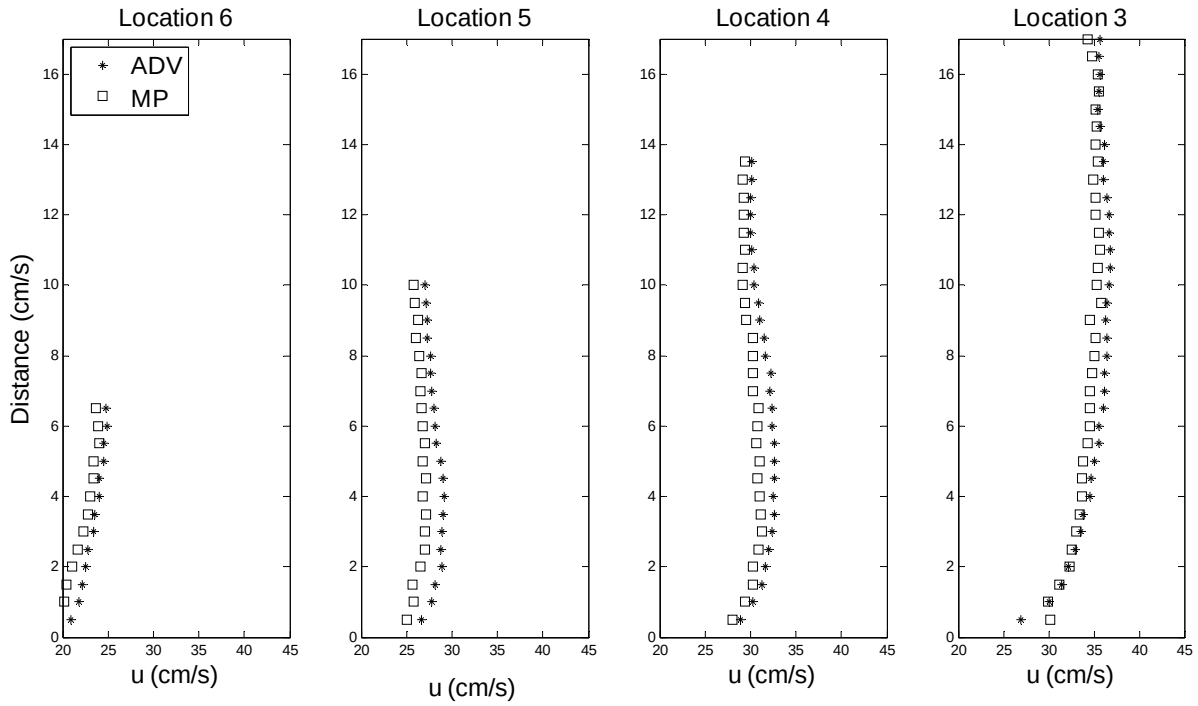


**Figure 5.11. Time-averaged streamwise velocity profiles (cm/s) measured with the acoustic Doppler velocimeter (ADV) and miniature propeller (MP) along the bare streambank spatially averaged among five cross-sections at location 3-6. Location 3 is measured at the bank toe and locations 3-6 are measured every 5-cm up the bank.**

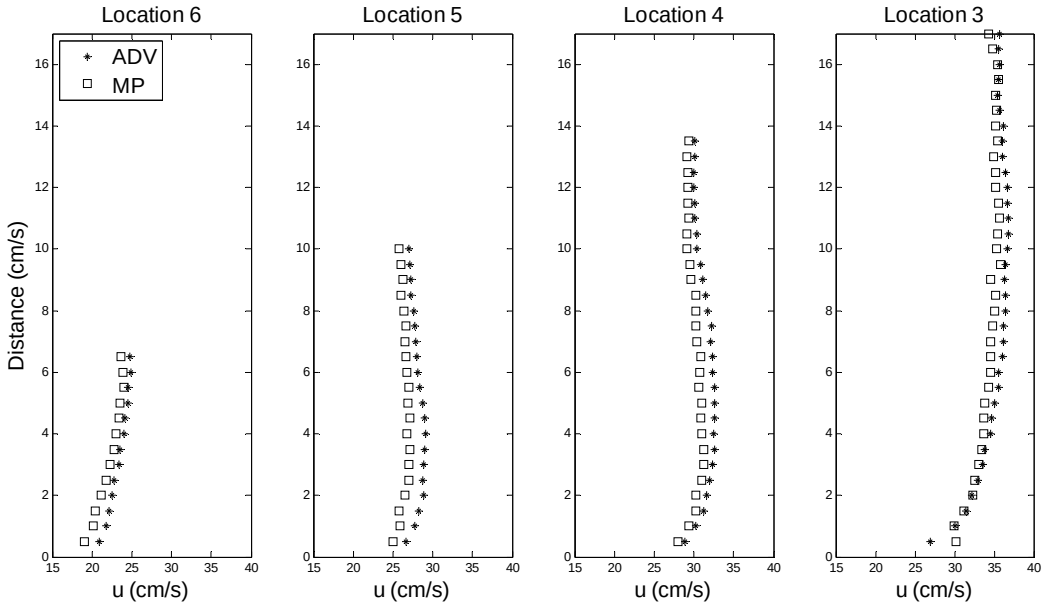


**Figure 5.12. Time-averaged streamwise velocity profiles (cm/s) measured with the acoustic Doppler velocimeter (ADV) and miniature propeller (MP) along the tree streambank spatially averaged among five cross-sections at location 3-6. Location 3 is measured at the bank toe in the main channel, location 4 is measured partially in the vegetation, and locations 5-6 are measured fully within the vegetation.**

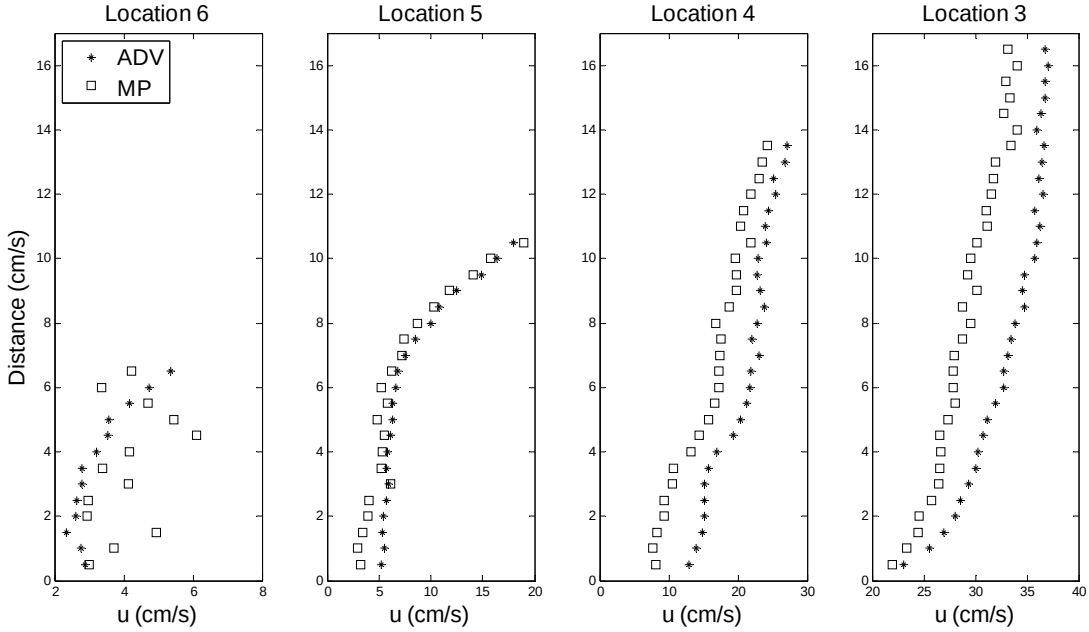


**Figure 5.13. Time-averaged streamwise velocity profiles (cm/s) measured with the acoustic Doppler velocimeter (ADV) and miniature propeller (MP) along the shrub streambank spatially averaged among five cross-sections at location 3-6. Location 3 is measured at the bank toe in the main channel, location 4 is measured partially in the vegetation, and locations 5-6 are measured fully within the vegetation.**

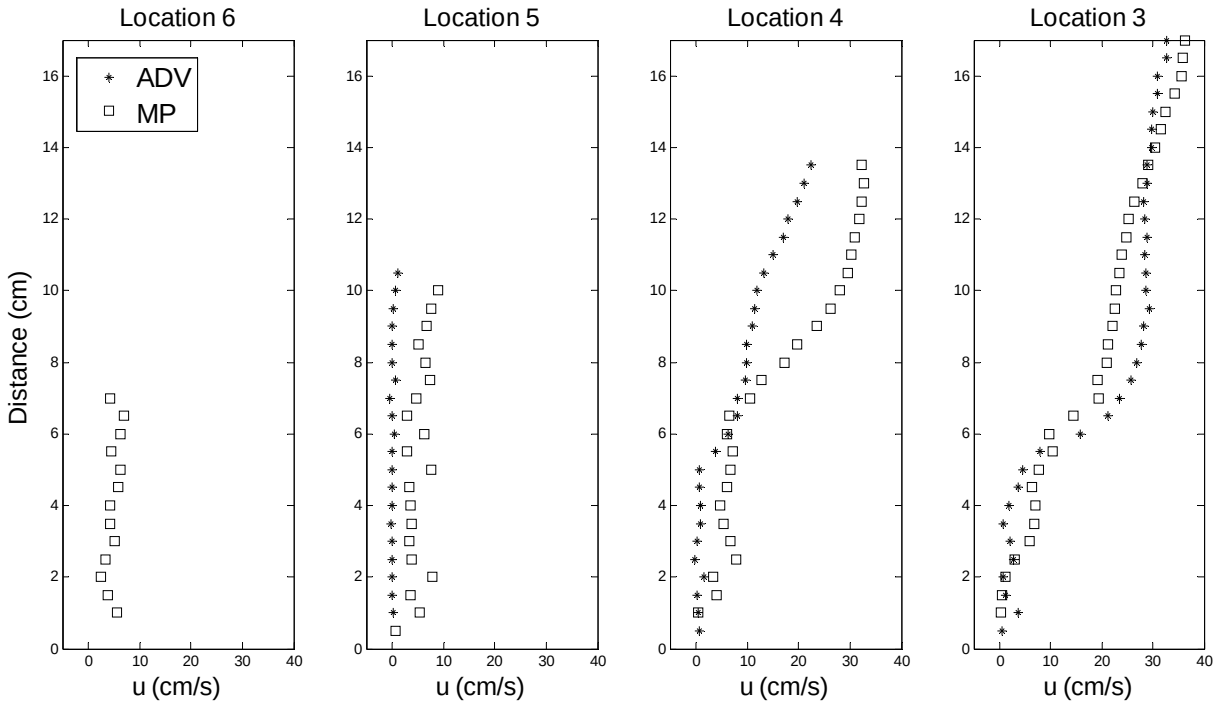


**Figure 5.14. Time-averaged streamwise velocity profiles (cm/s) measured with the acoustic Doppler velocimeter (ADV) and miniature propeller (MP) along the grass streambank spatially averaged among five cross-sections at location 3-6. Location 3 is measured at the bank toe in the main channel, location 4 is measured partially in the vegetation, and locations 5-6 are measured fully within the vegetation.**

## 5.5 Discussion

The research objective was to determine a field method to estimate boundary shear stress. The following sections compare the estimation techniques to the CTA measurements using ordinary least squares and chi-squared comparisons.

### *5.5.1 Comparison of Direct Shear Stress Measurements to Shear Stress Estimates*

This ordinary least squares analysis allowed the comparison of the CTA measurements to the BSS estimates at each location on the bank; each vegetation treatment was analyzed separately for this analysis. To determine the best estimation technique to approximate BSS, the sum of squares (SS) were examined. The minimum SS indicated the best estimation technique for each bank (and is highlighted in Table 5.2).

The estimates of shear stress based on the flow depth and slope ($\tau_{avg,Rh}$, $\tau_{avg,bank,Rh}$, $\tau_{avg,H}$, and $\tau_{avg,bank,H}$) were 11-44 times larger than the measurements of BSS. The sums of squares (Table 5.2) for these estimates were up to five orders of magnitude greater than the estimate of

best fit, indicating these estimation techniques are not appropriate for calculating BSS along a sloping streambank of a vegetated channel.

$\tau_{TKE,w}$ had the minimum SS for the bare bank, indicating that the technique is best for banks without large roughness elements and that bed roughness is important for bare channels. $\tau_{LOW,ADV}$, and $\tau_{TLOW,MP}$ also had low SS for the bare bank. Because of the lack of large roughness elements, the bare velocity profiles had a better fit to the log law than the other bank types (Figure 5.11-Figure 5.14); the LOW technique can be used where the log profile occurs and may be appropriate along sloping banks with no large roughness elements.

For the tree bank, $\tau_{TKE,w}$ and $\tau_{uv}$ represented BSS well (Table 5.2) as the estimates had the lowest SS. The estimation techniques with the next lowest SS were turbulence characteristics ($\tau_{TKE}$ and $\tau_{uv,extrap}$) and not LOW estimates. Unlike the bare bank, the best fit methods were all turbulence characteristics. This result indicated secondary flow dominated BSS for the tree bank.

The minimum SS for the shrub bank corresponded with the $\tau_{vw,extrap}$ estimation technique. The SS also indicate the LOW estimates ($\tau_{LOW,ADV}$ and $\tau_{LOW,ADV,20\%}$) were good approximations of BSS. At the bank toe (location 3; Figure 5.13) of the shrub channel, the profile roughly followed the logarithmic shape because the profile was in the main channel outside of the vegetation, but the shape was only present for the ADV measurements. The LOW technique may be used in non-vegetated portions of a vegetated channel if the velocity profile follows a logarithmic shape. Within the shrub vegetation (locations 4-6), the profiles varied significantly from the logarithmic shape, suggesting that the LOW should not be used within dense vegetation.

**Table 5.2. Sum of squares for boundary shear stress (BSS) of each estimation technique; minimum sum of squares highlighted.**

| Estimation Techniques | Sum of Squares for BSS | | |
|---|---|---|---|
| | **Bare** | **Tree** | **Shrub** |
| $\tau_{avg,Rh}$ | 672.15 | 726.16 | 749.67 |
| $\tau_{avg,bank,Rh}$ | 426.45 | 469.81 | 488.55 |
| $\tau_{avg,H}$ | 1830.35 | 1918.39 | 1957.15 |
| $\tau_{avg,bank,H}$ | 1181.72 | 1252.79 | 1283.95 |
| $\tau_{LOW,ADV}$ | 2.49 | 3.04 | 0.32 |
| $\tau_{LOW,ADV,20\%}$ | 3.38 | 2.80 | 0.76 |
| $\tau_{LOW,MP}$ | 2.05 | 2.83 | 62.06 |
| $\tau_{LOW,MP,20\%}$ | 4.90 | 2.83 | 537.88 |
| $\tau_{uv}$ | 3.91 | 1.70 | 5.44 |
| $\tau_{uw}$ | 4.28 | 2.96 | 2.61 |
| $\tau_{vw}$ | 3.25 | 2.10 | 1.04 |
| $\tau_{uv,extrap}$ | 4.19 | 1.73 | 5.06 |
| $\tau_{uw,extrap}$ | 3.64 | 4.08 | 4.20 |
| $\tau_{vw,extrap}$ | 4.55 | 2.27 | 0.24 |
| $\tau_{TKE}$ | 2.99 | 1.99 | 0.79 |
| $\tau_{TKE,w}$ | 0.93 | 1.70 | 6.99 |

Each bank was examined using a chi-squared comparison to minimize error and determine which estimation techniques were similar to the CTA values. Each bank was analyzed separately ($\chi^2_{0.95,19}$) and as a combination of bare, tree, and shrub data ($\chi^2_{0.95,38}$). Only the miniature propeller data were examined for the grass treatment because ADV estimates were removed in filtering.

**Bare:** The twelve estimation techniques based on velocity measurements presented in Table 5.2 ($\tau_{LOW,ADV}$, $\tau_{LOW,ADV,20\%}$, $\tau_{LOW,MP}$, $\tau_{LOW,MP,20\%}$, $\tau_{uv}$, $\tau_{uw}$, $\tau_{vw}$, $\tau_{uv,extrap}$, $\tau_{uw,extrap}$, $\tau_{vw,extrap}$, $\tau_{TKE}$, and $\tau_{TKE,w}$) were statistically similar to the CTA measurements for the bare bank ($\alpha = 0.05$; Table 5.3). An extrapolated $\tau_{TKE}$ and $\tau_{TKE,w}$ were calculated and will be referred to as $\tau_{TKE,extrap}$ and $\tau_{TKE,w,extrap.}$ These values were not significantly different from the CTA measurements, suggesting that there are multiple methods for determining boundary shear stress on a sloping bank with no large roughness elements. The bare velocity profiles roughly followed the logarithmic shape at all locations (Figure 5.11), suggesting the LOW as well as turbulence techniques can be used along sloping boundaries with no large roughness.

**Tree:** All of the LOW estimates were statistically similar to the CTA estimates, likely due to the sparse placement of the roughness elements. The sparse vegetation did alter the logarithmic profile but not to the degree of the grass and shrub treatments. Reynolds stresses ($\tau_{uv}$, $\tau_{uw}$, $\tau_{vw}$, $\tau_{uv,extrap}$, $\tau_{vw,extrap}$), as well as TKE estimates ($\tau_{TKE}$ and $\tau_{TKE,extrap}$), were good BSS estimates ($\alpha = 0.05$; Table 5.3).

**Shrub:** At a 95% confidence interval, LOW estimates ($\tau_{LOW,ADV}$ and $\tau_{LOW,ADV,20\%}$) were good approximations of BSS. At the bank toe (location 3; Figure 5.13) of the shrub channel, the profile roughly followed the logarithmic shape because the profile was in the main channel outside of the vegetation. The LOW technique may be used in non-vegetated portions of a vegetated channel if the velocity profile follows a logarithmic shape. Within the shrub vegetation (locations 4-6), the profiles varied significantly from the logarithmic shape, suggesting that the LOW should not be used within dense vegetation. Estimation techniques based on turbulence characteristics determined similar to the CTA measurements included $\tau_{vw}$, $\tau_{vw,extrap}$, $\tau_{TKE}$, and $\tau_{TKE,extrap}$ ($\alpha$=0.05). $\tau_{TKE}$ may represent shear stress well because TKE represents overall average turbulence, suggesting that velocity fluctuations in all directions (u, v, and w) are important when estimating BSS. $\tau_{vw}$ may be a good estimate of shear stress because the stress uses velocity fluctuations in the lateral and vertical direction. Turbulence was generated from the vegetation as well as the rough, sloping bank, indicating that the coupling of velocity fluctuations from u and v are important.

**Combined Banks:** Table 5.3 indicates the BSS estimates determined similar to the CTA estimates at a 95% confidence interval for all vegetation treatments combined (bare, tree, and shrub). LOW estimates ($\tau_{LOW,ADV}$ and $\tau_{LOW,ADV,20\%}$) appeared to be good approximations of BSS; however, because the velocity profiles were not logarithmic within the dense vegetation, the LOW technique should be not used within densely vegetated areas. The technique should only be used when the logarithmic velocity profile requirement is met (Wilcock, 1996; Biron et al., 2004). $\tau_{LOW,MP}$ and $\tau_{LOW,MP,20\%}$ were not good approximations of BSS at any confidence level, suggesting the velocity instrument is important when calculating BSS by the LOW. The ADV captured the logarithmic shape better than the MP in this experiment (Figure 5.6-5.9), likely due to the difference in sampling frequency. The ADV (25 Hz) measured velocity at a higher frequency than the MP (1 Hz). The 95% confidence interval also included the following BSS estimates: $\tau_{vw}$ $\tau_{uw}$, $\tau_{TKE}$, $\tau_{TKE,extrap}$, and $\tau_{vw,extrap}$. The grass data were examined using the

LOW technique. The grass $\tau_{LOW,MP}$ and $\tau_{LOW,MP,20\%}$ were not equal to the CTA estimates at an 80% confidence interval.

**Table 5.3. Boundary shear stress (BSS) estimates determined statistically similar to the constant temperature anemometer (CTA) measurements of BSS for the bare, tree, shrub, and combined streambanks; methods determined statistically similar to the CTA measurements are marked with an X for the 90% and 95% confidence intervals (CI).**

| Vegetation | CI | $\tau_{LOW,ADV}$ | $\tau_{LOW,ADV,20\%}$ | $\tau_{LOW,MP}$ | $\tau_{LOW,MP,20\%}$ | $\tau_{uv}$ | $\tau_{uw}$ | $\tau_{vw}$ | $\tau_{uv,extrap}$ | $\tau_{uw,extrap}$ | $\tau_{vw,extrap}$ | $\tau_{TKE}$ | $\tau_{TKE,w}$ | $\tau_{TKE,extrap}$ | $\tau_{TKE,w,extrap}$ |
|---|---|---|---|---|---|---|---|---|---|---|---|---|---|---|---|
| Bare | 95 | X | X | X | X | X | X | X | X | X | X | X | X | X | X |
| Tree | 95 | X | X | X | X | X | X | X | X | | X | X | | X | |
| Shrub | 95 | X | X | | | | | X | | | X | X | | X | |
| Bare, tree, and shrub | 95 | X | X | | | | X | X | | | X | X | | X | |

**Table 5.4. Boundary shear stress (BSS) estimates determined statistically similar to the constant temperature anemometer (CTA) measurements of BSS for the bare, tree, shrub, and combined streambanks as analyzed at varying distances from the streambank; methods determined statistically similar to the CTA measurements are marked with an X for the 80, 90, and 95% confidence intervals (CI).**

| Vegetation | CI | $\tau_{uv,2cm}$ | $\tau_{uw,2cm}$ | $\tau_{vw,2cm}$ | $\tau_{uv,4cm}$ | $\tau_{uw,4cm}$ | $\tau_{vw,4cm}$ | $\tau_{TKE,2cm}$ | $\tau_{TKE,4cm}$ |
|---|---|---|---|---|---|---|---|---|---|
| Bare | 95 | X | X | X | X | X | X | X | X |
| Tree | 95 | X | | X | X | | X | | |
| Shrub | 95 | | | X | | | X | X | X |
| Bare, tree, and shrub | 95 | | | X | | | X | | |

In the field, it is more difficult to measure velocity in a precise location adjacent to the streambank. To determine if it is important to measure velocity adjacent to the streambank to get a good estimate of BSS, Reynolds stresses and $\tau_{TKE}$ were calculated at a distance of 10% (~2 cm; ($\tau_{uv,2cm}$, $\tau_{uw,2cm}$, $\tau_{vw,2cm}$, and $\tau_{TKE,2cm}$) and 20% (~4 cm; ($\tau_{uv,4cm}$, $\tau_{uw,4cm}$, $\tau_{vw,4cm}$, and $\tau_{TKE,4cm}$) of the flow depth away from the streambank. For the bare bank, all estimates were statistically similar to the CTA measurements ($\alpha$=0.05) at 10% and 20% of the flow depth. $\tau_{vw}$ and $\tau_{uv}$ did not vary with distance from the tree bank when measured within a distance of 20% of the flow depth ($\alpha$=0.05). For the shrub channel, $\tau_{vw}$, $\tau_{TKE}$, and $\tau_{TKE,w}$ were a good estimates of BSS at a distance of 10% and 20% of the flow depth ($\alpha$ = 0.05). For the combined (bare, tree, and shrub) data, $\tau_{vw}$ was a good estimate of BSS at a distance of 10% and 20% of the flow depth ($\alpha$ = 0.05). These results indicate that for the turbulence estimates of shear stress, it may not be important to measure velocity adjacent to the streambank to get a good representation of BSS, simplifying probe placement in the field.

### 5.6 Conclusions

The small range of CTA shear stress measurements (0.02–2.14 Pa) suggests one estimate of shear stress can be used for an entire bank. If the grass CTA estimates were removed, the range in CTA shear stresses was less than 1 Pa (0.04-0.83 Pa). In reality, bank vegetation is not composed of a monoculture. Typically banks are composed of a mixture of herbaceous and woody vegetation. This composition may be best represented by a combination of the shrub, grass, tree banks in this study. Considering bank roughness is typical along natural streambanks, the LOW technique is not an appropriate estimate of boundary shear stress because velocity profiles within dense vegetation did not follow the assumed logarithmic shape. Shear stress should then be estimated by a turbulence characteristic, supporting previous findings by Biron et al. (2004) that recommended estimation of bed shear stress from near bed turbulence in complex flowfields. For each vegetation treatment separately and the combination of treatments, $\tau_{vw}$, $\tau_{TKE}$, $\tau_{vw,extrap}$, and $\tau_{TKE,extrap}$ shear stress estimates were statistically similar to the CTA measurements ($\alpha$ = 0.05). While $\tau_{uv,extrap}$ and $\tau_{TKE,extrap}$ are valid methods, the values are difficult to calculate because an entire profile of $\tau_{vw}$ and $\tau_{TKE}$ estimates are required. For $\tau_{vw}$ estimates, velocity fluctuations in the vertical and lateral direction are necessary. For $\tau_{TKE}$, turbulent fluctuations in the downstream, vertical, and lateral direction are necessary. The ADV probes

available may dictate the estimate technique used. Also $\tau_{vw}$ did not vary with distance from the streambank when measured within a distance of 20% of the water depth from the streambank (~4 cm). This result suggests that velocity measurements could be made further from the streambank than the $\tau_{TKE}$ estimates, simplifying field data collection.

*5.6.1 Recommendations for a Field Measurement Technique*

The following statements provide recommended methods for measuring boundary shear stress in the field along vegetated streambanks:

1. The small spatial ranges of CTA shear stress measurements for each vegetation type (bare: 0.19-0.83 Pa, tree: 0.04-0.72 Pa shrub: 0.16-0.38, and grass: 0.71-2.15) suggest one estimate of shear stress can be used for an entire bank. The median boundary shear stress measurements were 0.57 Pa, 0.39 Pa, 0.23 Pa, and 0.92, Pa for the bare, tree, shrub, and grass streambanks, respectively.
2. The LOW technique is not an appropriate method to calculate boundary shear stress within dense streambank vegetation because the profiles measured perpendicular to the boundary for the vegetated conditions did not follow a logarithmic shape.
3. The large roughness elements present in vegetated channels create secondary flow, so turbulent characteristics were more appropriate to estimate shear stress. $\tau_{vw}$ and $\tau_{TKE}$ were both good measures for shear stress for every vegetated condition.
4. A propeller-type velocimeter should be not used to calculated $\tau_{vw}$ and $\tau_{TKE}$ because velocity fluctuations cannot be calculated and velocity cannot be measured simultaneously in multiple directions for a single control volume.
5. An ADV can be used to calculate $\tau_{vw}$ and $\tau_{TKE}$, but several precautions need to be considered: Data need to be filtered to ensure erroneous data which bias mean velocity values and turbulent characteristics are removed. In the field, a longer sample time than used in this study (1 min) should be employed to ensure the entire turbulence structure is represented in the time series. High sample frequencies are desirable (> 20 Hz) to capture the turbulent series.
6. $\tau_{vw}$ did not vary with distance from the streambank when the measurements were close to the streambank (< 20% of the flow depth). Velocity should be measured within this distance to the bank. $\tau_{TKE,w}$ should be measured adjacent to the streambank (a distance <

5% of the flow depth) to represent BSS. $\tau_{TKE}$ varied with distance from the streambank for the tree condition and when examining the combination of treatments. Measuring further from the streambank may result in estimating shear stress in the shear layer. In this mixing layer, turbulence measures would likely over estimate boundary shear stress.

This research supports previous research indicating average boundary shear stress is not an appropriate measure of shear stress for vegetated channels when large roughness is significant (Thompson et al., 2004). For each vegetation type, estimates of average boundary shear stress overestimated BSS by up to an order of magnitude. These suggestions for field measurement of boundary shear stress need to be tested in the field.

# Chapter 6 Application of a boundary shear stress model along vegetated streambanks

## 6.1 Introduction

Vegetation type plays a key role in channel morphology (Hey and Thorne, 1986; Hession, 2001; Bennett and Simon, 2004). Several researchers have noted that streams were 2-2.5 times wider with forested riparian buffers than with grass buffers (Zimmerman et al., 1967; Clifton, 1989; Sweeney, 1992; Davies-Colley, 1997; Trimble, 1997a; Bott et al., 2006; McBride et al., 2008). Alternatively, others have shown that forested streams are narrower than streams with herbaceous buffers (Hey and Thorne 1986; Gregory and Gurnell, 1988). Hession (2001) hypothesized these conflicting findings on the effects of vegetation on channel form are the result of site-specific differences in watershed characteristics, such as vegetation density and type, soils, flow regimes, slopes, geology, stream size, and disturbance history. Vegetation also provides flow complexity, provided desirable habitat features for aquatic organisms (Crowder and Diplas, 2002). Velocity gradients are important for drift-feeding fish (Fausch and White, 1981; Fausch, 1984, Hughes and Dill, 1990; and Hayes and Jowett, 1994; Hayes et al., 2007). Vegetation creates velocity gradients at the vegetation/main channel interface that may be important areas for fish feeding. Ultimately, further studies are necessary to evaluate the impact of vegetation type on stream morphology for effective stream and river management (Mosley, 1981; Gregory and Gurnell, 1988; Heede and Rinne, 1990; Thorne, 1990; Abernethy and Rutherfurd, 1998; ASCE, 1998a; Horwitz et al., 2000; Lyons et al., 2000; Hession, 2001; Simon and Collison, 2001). While conceptual models (Allmendinger et al., 2005; McBride et al., 2008) provide a context for the width differences, quantitative explanations are necessary.

### *6.1.1 Objectives*

This study analyzed the effects of differing vegetation types on boundary shear stress, a parameter used to estimate channel erosion rates. The Kean and Smith (2004) model and the application of the ray-isovel method to measured velocity flow fields (Leighly, 1932; Kean and Smith, 2004; Kean et al., 2009) were used to examine boundary shear stress for three streambank vegetation conditions: bare, tree, and shrub.

## 6.2 Model Description: Kean and Smith (2004) model

Kean and Smith (2004) adapted a model developed by Houjou et al. (1990) that calculates velocity and shear stress fields using ray-isovel turbulence closure to include the drag effects of vegetated banks. Isovels are lines of constant velocity and rays, perpendicular to the isovels that range from the channel boundary to the water surface. The water surface defines the point of zero shear stress (Houjou et al., 1990; Kean and Smith, 2004; Griffin et al., 2005; Wobus et al., 2008). The area between two rays at the channel boundary represents shear stress on the bank (Kean and Smith, 2004; Wobus et al, 2008). The model has been applied to flume studies (Kean and Smith, 2004), applied to geomorphically stable natural channels (Griffin et al., 2005; Kean and Smith, 2005), combined with an additional erosion component (Wobus et al., 2008), and combined with small-scale topographic features on the channel boundary (Kean and Smith, 2006a and 2006b). The portion of the model regarding boundary shear stress in vegetated channels is summarized below. A complete derivation of the ray-isovel technique with lateral boundaries and vegetation roughness is provided in Ch. 2.

Equation 6.1 defines the momentum equation for steady, stream-wise, uniform flow in a channel with vegetated banks and balances the gravitational stress (first term) and the deviatoric stress components (second and third terms) with the drag per unit volume (fourth term; Kean and Smith, 2004).

$$0 = \rho g S + \frac{\partial}{\partial y}\left(\rho K_{eddy}\frac{\partial u}{\partial y}\right) + \frac{\partial}{\partial z}\left(\rho K_{eddy}\frac{\partial u}{\partial z}\right) - \frac{1}{2}\rho C_D \alpha u^2 \qquad [6.1]$$

where ρ is the water density, g is the acceleration due to gravity, S is the water slope, K is the kinematic eddy viscosity, u is the velocity in the downstream direction, y is the cross-stream direction, and z is the vertical direction.

In the portions of the channel with no vegetation roughness, the boundary shear stress ($\tau_b$) can be calculated as the area between two rays responsible for producing shear stress on the boundary. This stress is defined by the following equation (Kean and Smith, 2004):

$$\tau_b = \rho g S \frac{\int_0^L dA}{\delta p_b} \quad [6.2]$$

where L is the length of the ray, A is the fractional area responsible for producing shear, and $\delta p_b$ is the incremental length of the wetted perimeter.

In the vegetated portions of the channel, the boundary shear stress is reduced due to the drag on the plants and can be calculated by the following equation (Kean and Smith, 2004):

$$\tau_b = \frac{\int_0^L (\rho g S - F_{stems}) dA}{\delta p_b} \quad [6.3]$$

where F is the drag force per unit volume due to the stems:

$$F_{stems} = \frac{1}{2} \rho C_D \alpha u_{ref}^2 \quad [6.4]$$

where $C_D$ is the drag coefficient of a single stem (1.2 for high Reynolds numbers), $u_{ref}$ is the reference velocity, and $\alpha$ is the cross-sectional area of the stems oriented perpendicular to the flow direction per unit volume. The velocity with stem removal, averaged over the stem volume represents the reference velocity and was approximated using the local mean velocity. The parameter $\alpha$ can be defined by the following equation:

$$\alpha = n D_s = \frac{D_s}{\lambda^2} \quad [6.5]$$

where n is the number of stems per unit area, $D_s$ is the average stem diameter, and $\lambda$ is the average stem spacing (Kean and Smith, 2004).

### 6.3 Methods

A second order prototype stream (Tom's Creek in Blacksburg, Virginia, USA), with individual reaches dominated by each vegetation treatment was modeled in a research flume

using a fixed-bed Froude-scale modeling technique. One model streambank of the prototype stream was constructed for each vegetation type and compared to a bare control (only grain roughness; Ch. 3). A flowchart with the overall methods to analyze BSS and velocity fields is presented in Figure 6.1 and detailed methods are explained in the following sections.

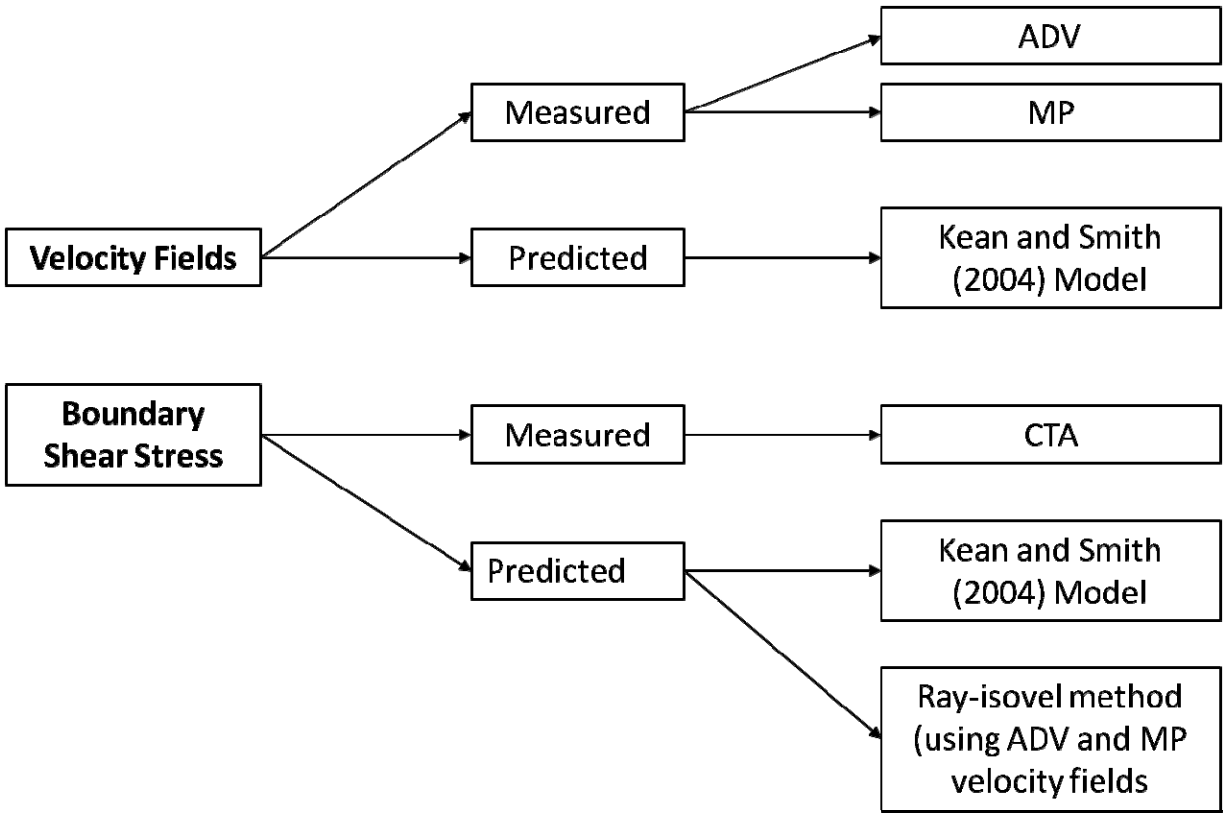


**Figure 6.1. Flow chart explaining how velocity fields and boundary shear stress were measured and predicted using the acoustic Doppler velocimeter (ADV), miniature propeller (MP), constant temperature anemometer, ray-isovel method, and Kean and Smith (2004) model.**

*6.3.1 Velocity Fields*

Velocity profiles perpendicular to the flume model boundary were measured using a three-dimensional acoustic Doppler velocimeter and a miniature propeller at seven locations along five cross-sections (Figure 3.14) as explained in Ch. 3. These measurements resulted in five cross-sectional flow fields for each vegetation type and measurement instrument (ADV and MP). The measured flow fields were then used to calculate BSS by applying the ray-isovel method following the approach of Leighly (1932; outlined in section 6.3.1).

*6.3.2 Measuring Boundary Shear Stress*

Direct measurements of shear stress were measured using a flush-mount hot-film anemometer at five locations (3-7) along five cross-sections (A-E; Ch. 3). Due to limitations of the hot-film probe (e.g. water depth), only four measurements (locations 3-6; Figure 3.14) along each cross-section were used in the analysis.

*6.3.3 Modeling Boundary Shear Stress*

The following sections detail the use of the Kean and Smith (2004) model and the application of ray-isovel method to the measured velocity flow fields. The study also measured velocity fields along a grass bank with flexible bank vegetation with the ADV and MP. Much of the ADV data near the grass bank were removed in filtering. Calculations of BSS using the ray-isovel technique and ADV data were not possible due to the lacking data. The variability of the velocity fields within the grass vegetation when using the MP data resulted in BSS calculations that were not reliable. The Kean and Smith (2004) model determines vegetation drag using the drag coefficient for a single roughness element. The assumptions associated with this method are not applicable to flexible vegetation, so the Kean and Smith (2004) model was not applied to the grass bank.

**Kean and Smith (2004) model:** The Kean and Smith (2004) model uses ray-isovel turbulence closure to numerically solve the momentum equation for steady, uniform flow (Kean and Smith, 2004; Wobus et al. 2008). A compiled computer version of the model provided by Jason Kean with the USGS was utilized in this study. The initially model was applied using the inputs based on the experimental set-up of the flume model Bank and bed roughness were then increased to achieve the same discharge between the predicted model and the flume measurements. The experimental flume set-up is explained in Ch. 3 for the three vegetation types (bare, tree, and shrub), and the basic model requirements (Table 6.1) are summarized here.

Basic inputs required by the model included channel geometry, flow depth, slope, bed roughness (bed $z_o$), bank roughness (bank $z_o$), height above the bank where roughness begins, elevation where vegetation begins, mean stem diameter, and mean stem spacing (Table 6.1). Channel geometry mimicking the flume model with one sloping streambank and one vertical streambank was used (Figure 6.2). Flow depth and slope were set at 0.204 m and 0.5%, respectively, as detailed in the flume experiment. Bed roughness and bank roughness matched the bed roughness (0.01 m) and bank roughness (0.001 m) of the flume model. Because

vegetation and bank roughness in the flume model began at the toe of the sloping bank, two parameters (i.e. the elevation where vegetation begins and height above bank where bank roughness begins) were set at the minimum value (0.01 m).

Mean stem diameter and mean stem spacing were calculated from the flume model for each vegetation type. The bare bank had no vegetation roughness elements, and both parameters were set to zero. Mean stem diameter of the tree dowels was calculated as 0.03 m. The shrub bank vegetation roughness was simulated using as single wooden dowel size. This diameter (0.003 m) was used as the mean stem diameter for the shrub channel. Mean stem spacing ($\lambda$) was calculated using Equation 6.5; $\lambda$ was 0.55 m and 0.03 m for the tree and shrub channel, respectively.

The Kean and Smith (2004) model produced velocity flow fields and BSS distributions for all vegetation types. The predicted velocity flow fields were compared to the flow fields measured by the ADV and MP for each vegetation type. The predicted distribution of BSS was compared to the CTA BSS measurements and the BSS calculated by the application of the ray-isovel method to the measured velocity flow fields.

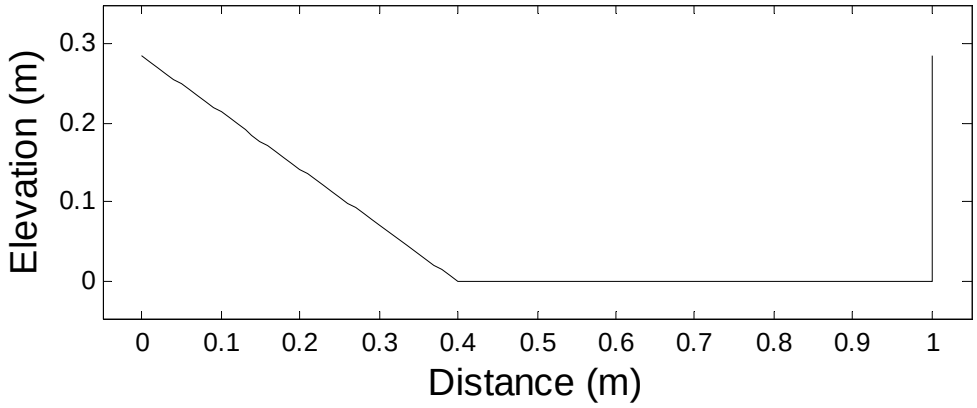


**Figure 6.2. Cross-sectional geometry of flume model used as input for the Kean and Smith (2004) model. The left sloping bank included vegetation roughness.**

**Table 6.1. Input for Kean and Smith (2004) model for three streambanks: bare, tree, and shrub.**

| Model Parameters[1] | Bare | Tree | Shrub |
|---|---|---|---|
| **Stage (m)** | 0.204 | 0.204 | 0.204 |
| **Slope (m)** | 0.005 | 0.005 | 0.005 |
| **Bed $z_o$ (m)** | 0.01 | 0.01 | 0.01 |
| **Bank $z_o$ (m)** | 0.001 | 0.001 | 0.001 |
| **Height above bed where bank $z_o$ begins (m)** | 0.01 | 0.01 | 0.01 |
| **Elevation where vegetation begins (m)** | 0.01 | 0.01 | 0.01 |
| **Mean stem diameter right bank (m)** | 0 | 0 | 0 |
| **Mean stem diameter left bank (m)** | 0 | 0.03 | 0.003 |
| **Mean stem spacing right bank (m)** | 0 | 0 | 0 |
| **Mean stem spacing left bank (m)** | 0 | 0.55 | 0.03 |

[1]Bed $z_o$ is bed roughness and bank $z_o$ is bank roughness

**Ray-isovel method:** The ray-isovel method was also applied using the approach of Leighly (1932) that analyzes BSS between two rays. Between two rays of a vegetated streambank, BSS is equal to the downstream component of the weight of water minus the vegetative drag force, divided by the wetted perimeter length between the two rays (Equation 6.3; Kean and Smith, 2004; Kean et al., 2009; Wobus et al., 2008).

First flow fields were measured using the ADV and MP along five cross-sections for each vegetation type (bare, tree, and shrub). Lines of constant velocity (isovels) was calculated and used to plot the perpendicular rays. Because the bare bank had no vegetation roughness, BSS was calculated using Equation 6.2. For the tree and shrub banks, BSS was calculated using Equation 6.3 that accounts for vegetation drag (Leighly, 1932; Kean et al., 2009; calculations in Appendix E).

BSS was calculated by the ray-isovel method at locations 3-6 (Figure 3.9) along five cross sections for each vegetation type. These locations resulted in averaging over an incremental wetted perimeter length of roughly 5 cm. This length averaged out some of the variability associated with the variations in the measured flow fields.

**Average boundary shear stress:** For comparison, average boundary shear stress was also calculated based on the flow depth (H) and slope (S) by the following equations:

$$\tau_{avg} = \gamma HS \qquad [6.6]$$

where, $\tau_{avg}$ is the average boundary shear stress (Pa), $\gamma$ is the specific weight of water ($kN/m^3$), and H is the flow depth (m). This equation is equivalent to the ray-isovel equation (Equation 6.2) averaged over the entire wetted perimeter.

## 6.4 Results

All estimates and measurements of BSS indicated a difference in BSS among vegetation types, but the degree of vegetation influence differed among estimation techniques. Results of measured and predicted velocity fields and boundary shear stresses are presented in the following sections.

### *6.4.1 Velocity Fields*

There were few visible differences in plots of the streamwise velocity fields among the five cross sections as measured with the ADV and miniature propeller; therefore, the average of the five cross-sections for each vegetation type is presented (Figure 6.3). To examine the differences between the ADV and MP velocity fields, the sum of squares normalized by the number of velocity measurements were evaluated. The error between the ADV and MP velocity measurements was less than 0.4% of the depth-averaged velocity, indicating little difference existed between the velocity measurement devices. Depth-averaged velocity for the bare, tree, and shrub channels at location 1 were 0.40 m/s, 0.42 m/s, and 0.50 m/s, respectively. Near the streambank, the streamwise velocity decreased compared to the bare channel by 9% and 43% for the tree and shrub channel, respectively as compared to the bare channel (Hopkinson and Wynn, In Press).

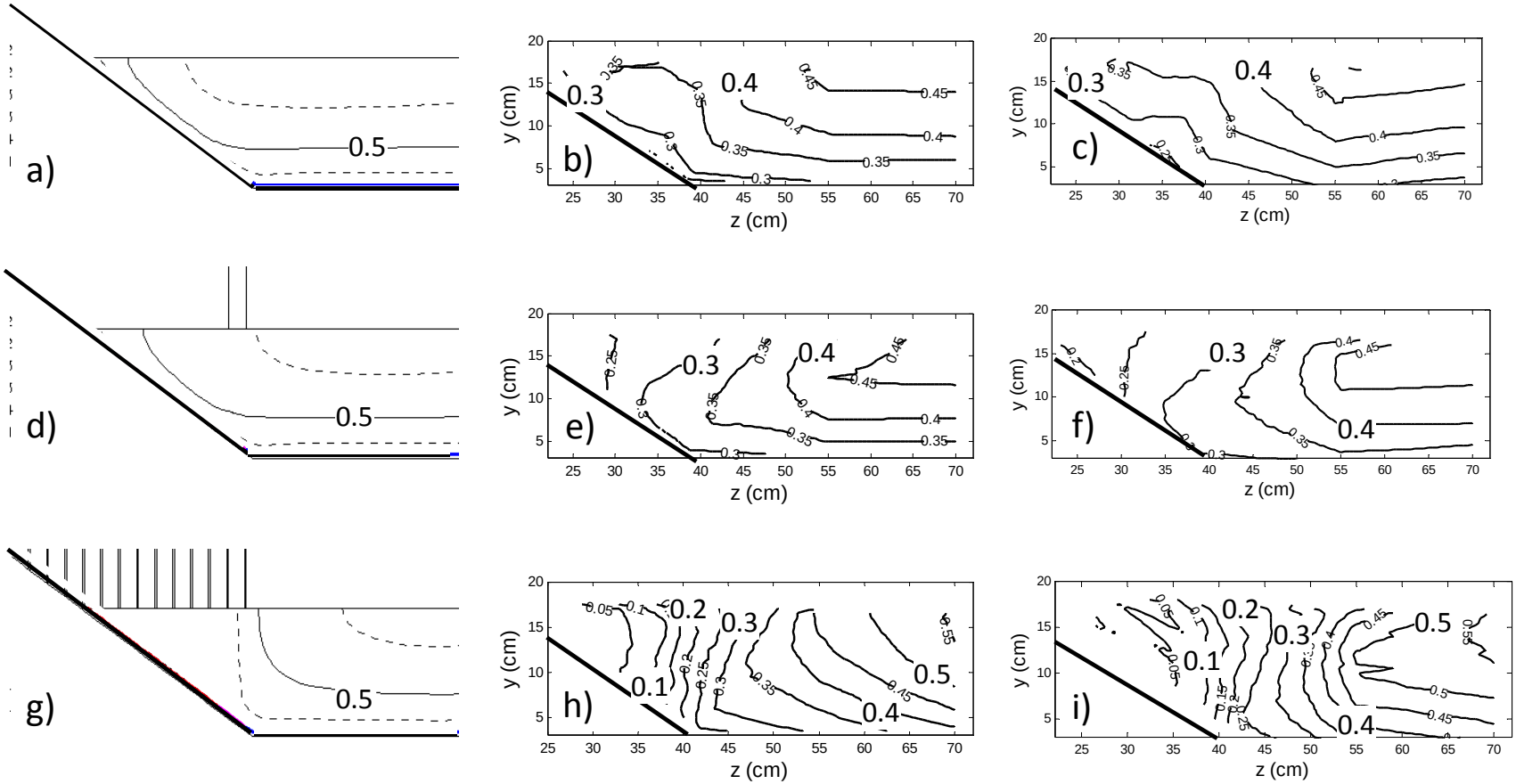


**Figure 6.3. Streamwise velocity (m/s) flow fields as calculated by the Kean and Smith (2004) model (a, d, and g) before calibration, measured with an ADV (b, e, and h), and measured with a miniature propel (c, f, and i) for the three vegetation treatments: bare (a, b, and c), tree (d, e, and f), and shrub (g, h, and i).**

*6.4.2 Boundary Shear Stress*

Average boundary shear stress was calculated as 10.0 Pa (Equation 6.5). This value was three orders of magnitude greater than the CTA measurements of shear stress for all locations and vegetation treatments. This value was used as a baseline for comparison and to normalize the model BSS results.

**CTA Shear Stress Measurements:** The median CTA boundary shear stress measurements were 0.57 Pa, 0.39 Pa, and 0.23 Pa for the bare, tree, and shrub streambanks, respectively (Figure 6.4), suggesting a decrease in BSS with increasing vegetation density. Boundary shear stress can be estimated by turbulence parameters (e.g. Reynolds stress and TKE) and using streamwise time-averaged velocity profiles. Compared to the CTA measurements, these estimation techniques were typically the same order of magnitude for all locations and vegetation types (Ch. 5).

**Ray-isovel method:** BSS was calculated at four points (locations 3-6; Figure 3.9) along five cross sections using the ray-isovel method with the ADV and MP velocity fields. Using the ray-isovel method and the ADV data, the median calculated BSS values were 1.9 Pa, 1.4 Pa, and 1.1 Pa for the bare, tree, and shrub streambank, respectively. Using the ray-isovel method and the MP data, the median calculated BSS values were 2.4 Pa, 1.4 Pa, and 2.1 Pa for the bare, tree, and shrub streambank, respectively (Figure 6.4). BSS calculated using the ADV data indicated a decrease in median BSS with increasing vegetation density. The median BSS using the MP data decreased with the addition of trees, but the shrub BSS values did not decrease.

A pairwise t-test indicated that BSS calculated using the ray-isovel technique was significantly different between the ADV and MP data for both the bare and shrub streambanks ($\alpha$=0.05). For the tree streambank, BSS calculated using the ADV data was statistically similar to BSS calculated using the MP data (p-value=0.22). While the examination of the error between ADV and MP velocity flow fields revealed little variation in velocity distribution, differences in the BSS values indicated differences in measured velocity flow fields between the ADV and MP data for the bare and shrub banks. These slight differences between measurement instruments were observed in the plotted streamwise velocity profiles presented in Ch. 5 (Figures 5.7 and 5.9). The tree streamwise velocity profiles show the best agreement between measurement devices (Figure 5.8).

BSS calculated using the ray-isovel method confirmed that boundary shear stress decreased with the addition of vegetation to the streambank. The shrub vegetation reduced BSS by up to a 74%, while the tree vegetation resulted in less than a 2.8% reduction in boundary shear stress. Thompson et al. (2004) examined shear stress partitioning in rigid, emergent vegetation. With roughness densities of 0.03-0.09 (a density between the tree and shrub treatment in this study), the vegetation decreased the boundary shear stress by 80-90%.

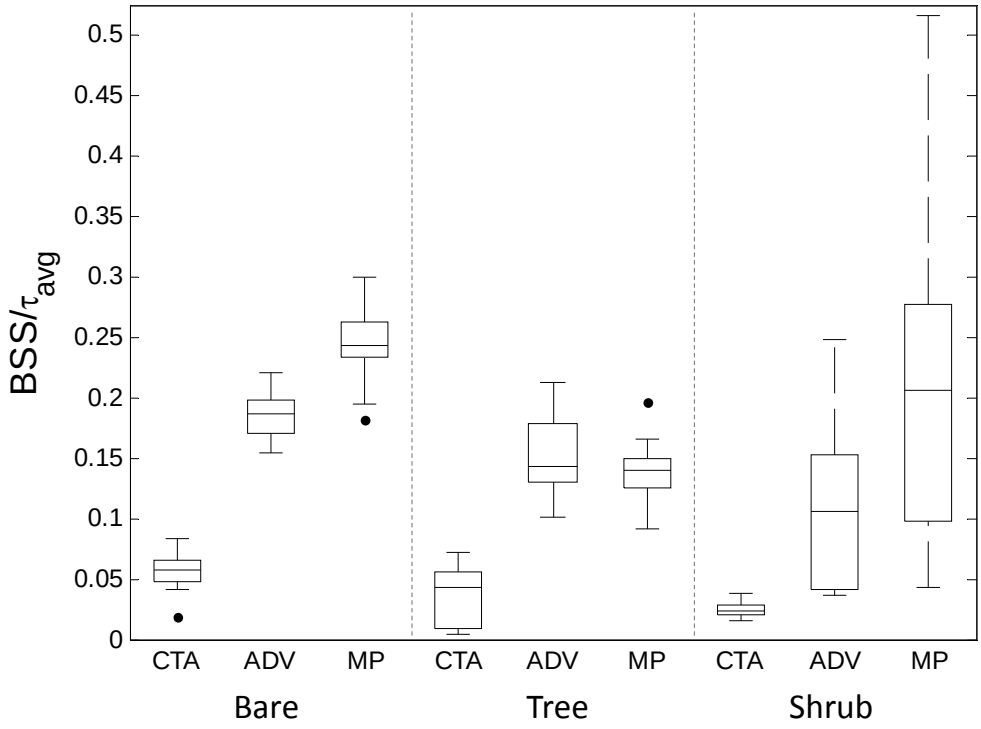


**Figure 6.4. Distribution of boundary shear stress (BSS; Pa) normalized by average boundary shear stress ($\tau_{avg}$=10 Pa) measured by a constant temperature anemometer (CTA) and calculated by the ray-isovel method using acoustic Doppler velocimeter (ADV) and miniature propeller (MP) velocity measurements along a streambank with three vegetation treatments: bare, tree, and shrub (n=20).**

**Kean and Smith (2004) model:** The distribution of BSS normalized by the average BSS ($\tau_{avg}$=10 Pa) along the channel boundary for the bare, tree, and shrub channels as calculated by the Kean and Smith (2004) model is presented in Figure 6.5. The channel is divided into three sections: streambank, streambed, and flume wall (Figure 6.5). The dashed line located at x=0.34 represents the location of the streambank toe. In general, the BSS increased with water depth

and decreased with distance into the vegetation. The bare channel BSS distribution was influenced by turbulence from the sloping bank, the rough bank (1 mm), and the rough bed (10 mm). The boundary shear stress ($\tau_b$) equaled the average BSS ($\tau_{avg}$) along the bed where there were few side-wall effects and the water depth was at the maximum (H=0.204 m). Along the bare streambank, BSS was less than 70% of $\tau_{avg}$ and spiked at the streambank toe ($\tau_b/\tau_{avg}$ =0.7). The tree BSS increased slightly at the streambank toe ($\tau_b/\tau_{avg}$ =0.6) but decreased with distance into the vegetation ($\tau_b/\tau_{avg}$<0.4). The shrub BSS also spiked at the streambank toe ($\tau_b/\tau_{avg}$ >1) and decreased with distance into the vegetation ($\tau_b/\tau_{avg}$ <0.4). The model results followed the general trend of the measured (CTA) and ray-isovel estimated BSS. BSS along the streambank decreased with increasing vegetation density, excluding the area at the streambank toe. The shrub BSS spiked in this area. This area of high shear stress may encourage fluvial erosion, developing a more vertical bank orientation.

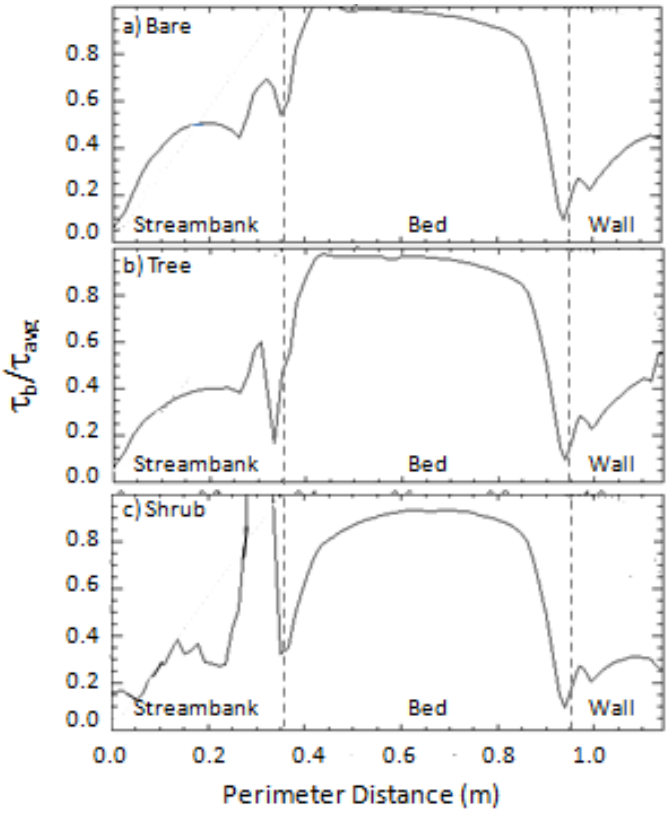


**Figure 6.5. Kean and Smith (2004) model results of BSS ($\tau_b$) normalized by average boundary shear stress ($\tau_{avg}$) as estimated by the flow depth and slope (10 Pa) for three vegetated streambanks: bare, tree, and shrub. The perimeter distance along the channel boundary is divided into the streambank, stream bed, and flume wall.**

The $\tau_b/\tau_{avg}$ spike at the streambank toe was consistent with the distribution of turbulent kinetic energy (TKE; Equation 6.7; Figure 6.6) that represents the overall intensity of the increased turbulence generated by the addition of streambank vegetation (Figure 6.6):

$$TKE = \rho 0.5(\overline{u'^2} + \overline{v'^2} + \overline{w'^2}) \quad [6.7]$$

where $\rho$ is water density (kg/m$^3$), u is the streamwise velocity (m/s), v is the lateral velocity (m/s), and w is the vertical velocity (m/s), apostrophes indicate fluctuations from the mean, and the overbar denotes a mean (Kim and Friedrichs, 2000; Biron et al., 2004; Pope et al., 2006; Wilcox and Wohl, 2007; McBride et al., 2007).

The small range in bare TKE values (0.4 N/m$^2$-1.8 N/m$^2$) included peak TKE productions at the channel boundary near the bed and the top of the bank (Figure 6.6). The bed peak TKE was likely influenced by the turbulence originating from the rough bed while the peak at the water surface was influenced by secondary currents near the surface. The tree TKE values (0.4 N/m$^2$-2.3 N/m$^2$) increased with flow depth, with a slight increase at the streambank toe. While the maximum shrub TKE values (approximately 5 N/m$^2$) were shifted away from the streambank, the shrub treatment had an area of high TKE near the streambank toe (Figure 6.6). The mass and momentum exchanged between main channel and vegetated streambank contributed to mixing and high TKE along this vegetation/main channel interface.

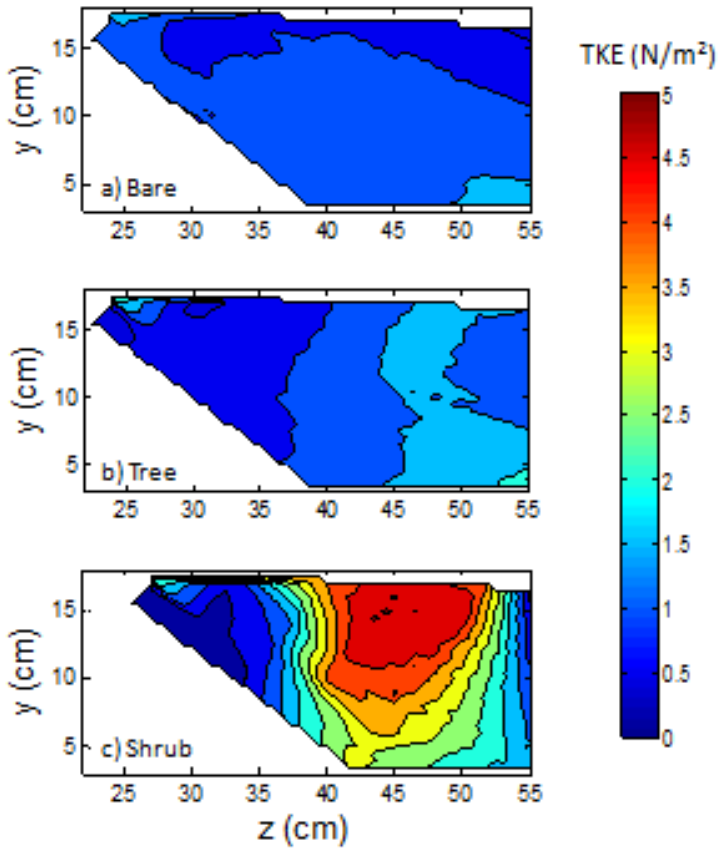


**Figure 6.6. Turbulent kinetic energy (TKE; N/m$^2$) distributions for profiles 2-7 spatially averaged (5 cross-sections) for the (a) bare, (b) tree, and (c) shrub streambanks.**

## 6.5 Discussion

The distribution of the predicted velocity flow fields were similar to the measured velocity flow fields (ADV and MP; error<0.2 cm/s), but the model predicted twice the measured discharge. The modeled and measured BSS distributions indicated that BSS increased with increasing water depth and decreased with increasing vegetation density. The following sections discuss the predicted and measured velocity and BSS.

### *6.5.1 Velocity fields*

The Kean and Smith (2004) model predicted a similar velocity distribution as that measured by both the ADV and MP (Figure 6.3). The predicted isovel shape illustrated several important differences with increasing vegetation density. The predicted bare velocity distribution was typical of the logarithmic shape (Figure 6.3a) of the measured velocity fields (Figure 6.3b and c). Compared to the bare channel, the predicted vegetated velocity distributions

indicated a decrease in downstream velocity near the streambank and an increase in depth-averaged velocity in the main channel. The predicted velocity distributions also illustrated a difference in isovel shape with differing vegetation. The addition of vegetation created vertical isovels near the streambank, most apparent in the shrub channel (Figure 6.3g, h and i), suggesting momentum exchange in the lateral direction. The steep lateral velocity gradient in the vegetated channels, as compared to the bare channel, indicated areas of greater shear stress.

Discharge was calculated with a Venturi meter within the flume piping system for all vegetated treatments (0.042 $m^3/s$). The predicted discharge (0.07-0.08 $m^3/s$) was greater than the measured discharge for all vegetation types. Kean et al. (2009) suggested two causes for the high predicted discharge: (1) more turbulent mixing exists in the flume than is accounted for in the model; and, (2) the boundary roughness is greater than used in the model calculation (Kean et al., 2009).

*6.5.2 Boundary Shear Stress*

To compare model output to measured BSS values, the measured BSS values were added to the bank portion of Figure 6.5 as seen in Figure 6.7. With no adjustment to the model parameters, the model overestimated BSS compared to the CTA measurements up to 1200%. The model overestimated bare BSS (median=0.57 Pa), tree BSS (median=0.43 Pa), and shrub BSS (median=0.23 Pa) by 770%, 830%, and by 1200% respectively. For all vegetation types, the model differed the greatest from the CTA measurements at the toe of the bank (location 3), the area where the most turbulent mixing occurred. The model deviated most from the measured BSS values along the shrub bank, the bank with the most vegetation roughness. These differences were likely due to an inaccurate estimation of boundary roughness or turbulent mixing (Kean et al., 2009). The BSS values calculated by the ray-isovel method using both the ADV and MP data were also added to Figure 6.5 for comparison to the model results (Figure 6.7). The model overestimated BSS by 50-200% when compared BSS calculated by the ray-isovel method using the MP data. The model overestimated BSS by roughly 200% when compared BSS calculated by the ray-isovel method using the ADV data for all vegetation types.

A pairwise t-test indicated the CTA measurements of shear stress were statistically different than BSS calculated by the ray-isovel method for both sets of velocity data (ADV and MP; $\alpha$=0.05; Figure 6.7). Using the ADV data, the ray-isovel method overestimated BSS by 230%, 230%, and 360% for the bare, tree, and shrub streambank, respectively. Using the MP

data, the ray-isovel method overestimated BSS by 330%, 230%, and 800% for the bare, tree, and shrub streambank, respectively. Kean et al. (2009) also reported poor agreement between BSS calculated by velocity fields and BSS measured by a Preston tube. BSS calculated by measured velocity fields in a flume experiment with cobble floodplain overestimated BSS along the bed near a sloping bank. This area of shear stress overestimation was attributed to an area of low velocity. The addition of streambank vegetation increased the presence of secondary flow, especially at the vegetation/main channel interface and may result in distortions in the measured velocity field. Kean and Smith (2009) reported that small variations in velocity result in significant variation in BSS when calculating BSS using the ray-isovel method.

The model indicated a decrease in streambank BSS with increasing vegetation density Figure 6.7. The CTA measurements of shear stress followed this trend (median bare BSS=0.57 Pa, median tree BSS=0.39 Pa, and median shrub BSS=0.23 Pa), although the CTA $\tau_b/\tau_{avg}$ were an order of magnitude less than the model results. BSS calculated with the ray-isovel method using the ADV data also indicated a decrease in streambank BSS with increasing vegetation density (median bare BSS=1.9 Pa, median tree BSS=1.4 Pa, and median shrub BSS=1.1 Pa). BSS calculated with the ray-isovel method using the MP data indicated that tree BSS (median tree BSS=1.4 Pa) was less than BSS along the bare bank (median bare BSS=2.4). The BSS calculated along the shrub bank by the ray-isovel method using the MP data with a median value of 2.1 Pa and did not support this trend. The difference between the ADV and MP estimates of BSS by the ray-isovel method were due to slight variations in the measured velocity flow field (Kean et al., 2009). While the error between the ADV and MP velocity measurements was less than 0.4% of the depth-averaged velocity, slight differences existed in the flow fields. These slight differences were evident in the plotted streamwise time-average velocity profiles (Figures 5.7-5.9).

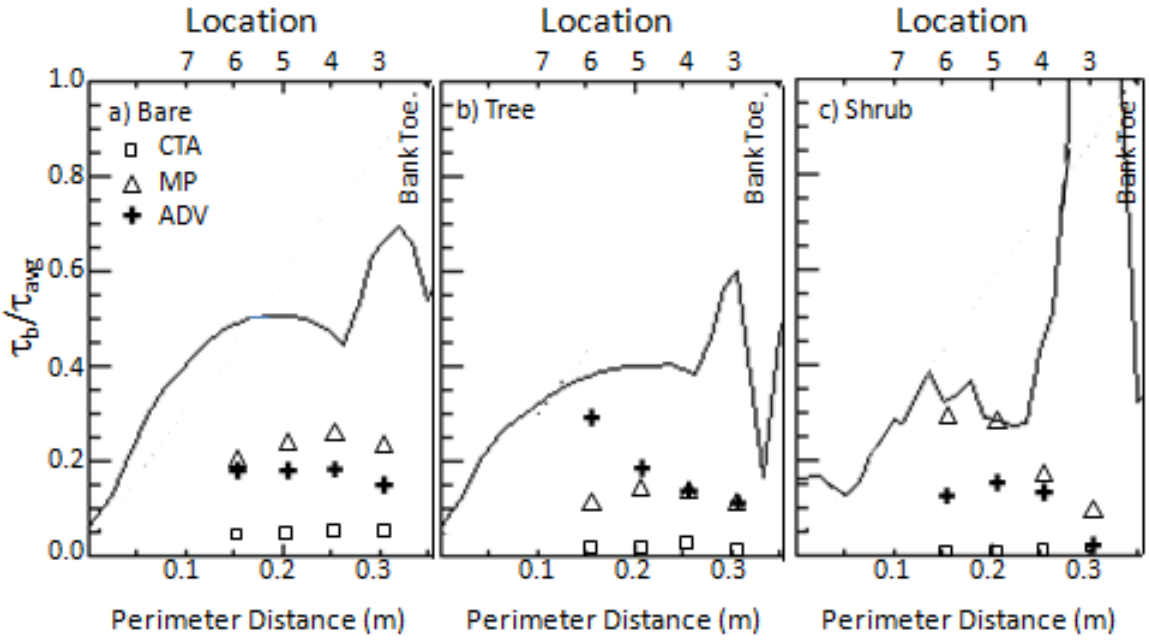


**Figure 6.7. Comparison of measured boundary shear stress (BSS) by the hot-film CTA and calculated BSS with the ray-isovel method using a miniature propeller (MP) and acoustic Doppler velocimeter (ADV) to the Kean and Smith (2004) model results. Location 3 was measured at the bank toe and locations 3-6 were situated every 5-cm up the bank. Location 3 was measured in the main channel, location 4 was measured partially in the vegetation, and locations 5-7 was measured fully within the vegetation.**

Initially, the model was applied using the inputs based on the experimental set-up of the flume model with no adjustment to the model parameters. The predicted discharge (0.07-0.08 $m^3/s$) was two times greater than the measured discharge for all vegetation types. The high predicted discharge could be attributed to greater boundary roughness than was used in the model calculation (Kean et al., 2009). Boundary roughness (bank $z_o$ and bed $z_o$) was increased for all streambank types to decrease the predicted discharge. The vegetation roughness parameters (mean stem diameter and mean stem spacing) were not altered because these parameters could not be changed for the bare condition due to the lack of vegetation.

To match the experimental discharge, bed and bank roughness were increased by 300% for the bare and tree channel. Bed and bank roughness were increased by 200% for the shrub channel. Increasing the bed and bank roughness altered the predicted BSS distribution (Figure

6.8). The increase in bed and bank roughness (bed $z_o$=0.04 and bank $z_o$=0.004 m) did not significantly alter the predicted BSS distribution along the bare streambank. The increase in bank roughness decreased the distribution of predicted BSS for the tree streambank. The entire distribution of $\tau_b/\tau_{avg}$ values along the bank was less than 0.6. The most obvious change in BSS distribution occurred along the densely vegetated shrub streambank. The entire distribution of predicted $\tau_b/\tau_{avg}$ values along the shrub streambank was less than 0.25. The calibrated predicted values overestimated BSS by 550% compared to the measured CTA estimates. Initial overestimation value was 1200% along the shrub bank. Thompson et al. (2004) reported ratios of particle shear ($\tau_b$) to average boundary shear ($\tau_{avg}$) ranging from 0.1 to 0.2 for roughness densities ranging from 0.03 to 0.09, a roughness between the tree and shrub bank of this study.

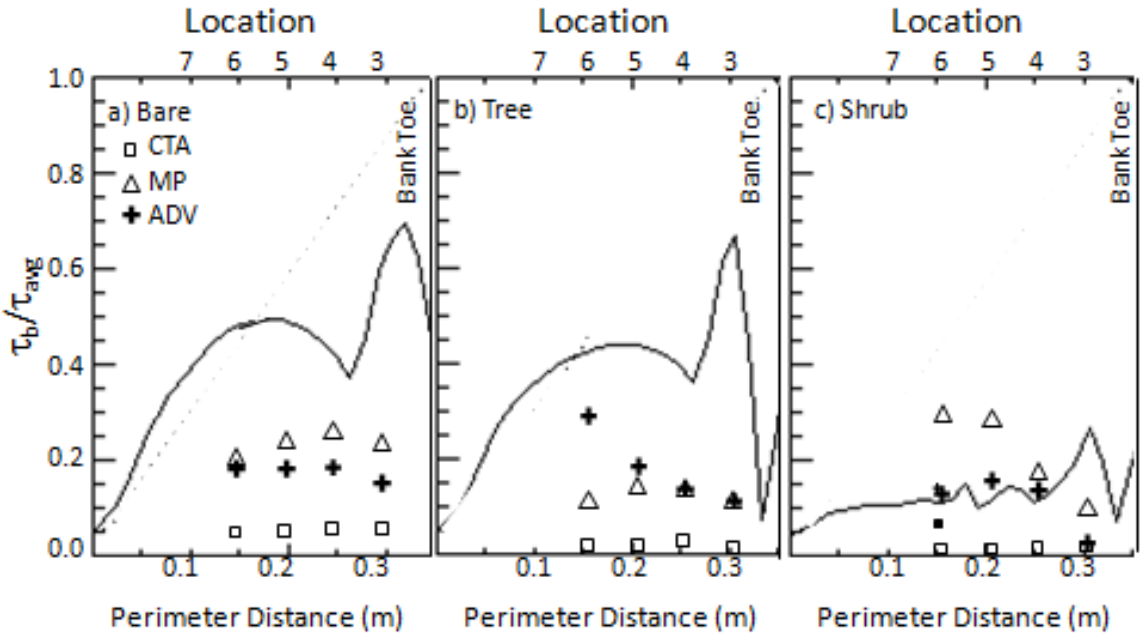


**Figure 6.8. Comparison of measured boundary shear stress (BSS) by the hot-film CTA and calculated BSS with the ray-isovel method using a miniature propeller (MP) and acoustic Doppler velocimeter (ADV) to the calibrated Kean and Smith (2004) model results (with increased bed and bank roughness). Location 3 was situated at the bank toe and locations 3-6 were situated very 5-cm up the bank. Location 3 was measured in the main channel, location 4 was measured partially in the vegetation, and locations 5-7 were measured fully within the vegetation.**

## 6.6 Conclusions

A flume study was conducted analyzing boundary shear stress on a sloping streambank for three streambank vegetation conditions: bare, tree, and shrub. Boundary shear stress was measured using a flush-mount hot-film anemometer (CTA), calculated by applying the ray-isovel method to measured velocity fields, and predicted using the Kean and Smith (2004) model. Velocity fields were measured using an acoustic Doppler velocimeter (ADV) and a miniature propeller (MP).

The Kean and Smith (2004) model predicted velocity fields with a similar distribution as that measured by the ADV and MP, but the magnitudes were different. The predicted velocity distributions also illustrated a difference in isovel shape with varying vegetation density: as vegetation density increased, the isovels became more vertical near the streambank. The uncalibrated predicted discharge (0.07-0.08 $m^3/s$) was two times greater than the discharge measured in the flume, likely due to an inaccurate estimation of boundary roughness or turbulent mixing (Kean et al., 2009). By increasing the bed and bank roughness by 0.03 m and 0.003 m, respectively, for the bare and tree bank, the predicted discharge equaled the measured flume discharge. For the shrub bank, the bed and bank roughness were increased by 0.02 m and 0.002 m, respectively, such that predicted discharge equaled the measured flume discharge.

Compared to the measurements and estimates of BSS, $\tau_{avg}$ (10 Pa; Equation 6.5) over estimated BSS along the streambank by at least an order of magnitude (Figure 6.4). With no adjustment to the model parameters, the model overestimated BSS compared to the CTA measurements by 13 times. For all vegetation types, the model differed the greatest from the CTA measurements at the streambank toe (location 3), the area where the most turbulent mixing occurred. These differences were likely due to due to an inaccurate estimation of boundary roughness or turbulent mixing (Kean et al., 2009) and model assumptions. A pairwise t-test indicated that BSS calculated using the ray-isovel method for both velocity measurement data (ADV and MP) was different than the measured BSS values ($\alpha$=0.05), likely to distortions of the measured velocity flow fields (Kean et al., 2009). The model deviated most from the measured BSS values along the shrub bank, the bank with the most vegetation roughness.

In general, the predicted BSS distribution increased with water depth and decreased with increasing vegetation density. The model results supported findings by Kean and Smith (2004) that vegetation drag dominates in densely vegetated channels. The predicted BSS at the shrub

toe indicated a spike in shear stress consistent with TKE estimates. This area is susceptible to fluvial erosion and the presence of dense, semi-rigid vegetation may encourage the formation of a wider channel with a vertical streambank.

# Chapter 7 Summary and Conclusions

The goal of this study was to determine the role of riparian vegetation in stream retreat by completing the following objectives: (1) evaluating the effects of streambank vegetation on near-bank three-dimensional velocity structure and turbulence characteristics; (2) determining a method for measuring boundary shear stress (BSS) in the field along hydraulically rough streambanks; and, (3) examining the effects of streambank vegetation on BSS using an existing model (i.e. Kean and Smith, 2004). The results will aide in quantifying sediment load from streambanks, providing water quality information for use in watershed management planning. The methods and major research findings for each objective are summarized in the following sections.

## 7.1 Objective 1: Evaluate the effects of streambank vegetation on BSS

The goal of this research was to evaluate how three-dimensional velocity structure and turbulence characteristics vary with three vegetation treatments: tree, shrub, and grass. A second order prototype stream (Tom's Creek in Blacksburg, Virginia, USA), with individual reaches dominated by each vegetation treatment was modeled in a research flume using a fixed-bed Froude-scale modeling technique. One model streambank of the prototype stream was constructed for each vegetation type and compared to a bare control (only grain roughness), resulting in four model streambanks. Velocity profiles perpendicular to the flume model boundary (0.5-cm increments) were measured using a Sontek MicroADV (1 min at 25 Hz). Three-dimensional velocity records, turbulent kinetic energy (TKE), turbulence intensities and Reynolds stresses were analyzed to characterize near-bank flow.

The addition of vegetation on a sloping streambank increased the streamwise free stream velocity as compared to a bare streambank, and velocity in the downstream direction decreased in the area close to the streambank boundary for all vegetation treatments. Compared to the shrubs and grass streambanks, the tree streambank produced a velocity and shear stress distribution more similar to the bare streambank than the vegetated streambanks. Tree turbulence intensity profiles and Reynolds stress profiles were similar to those measured with bare banks, supporting previous findings that the planting of sparse vegetation may not promote sediment accumulation (Nepf, 1999). The maximum turbulence intensities ($RMS_u$, $RMS_v$, and $RMS_w$) for the shrub and grass treatments occurred in the mixing zone of the main and vegetated

channel. The intensities within the vegetation were low and increased into the main channel. The gradient of the downstream turbulence intensity indicated that the extent of mixing into the vegetated zone was approximately 5 cm. The lateral Reynolds stresses ($\tau_{uv}$) were the largest Reynolds stress tensor for the shrub and grass treatments, indicating vortex shedding in the lateral plane with a vertical rotation axis. The vertical Reynolds stress was a significant component for the bare condition, indicating that turbulence was generated at the rough bed. The turbulence caused by the upright shrub treatment increased TKE and Reynolds stresses near the streambank toe, an area susceptible to fluvial erosion. The presence of dense, semi-rigid vegetation may encourage the formation of a wider channel with a vertical streambank.

### 7.2 Objective 2: Determine a method for measuring BSS in the field along hydraulically rough streambanks

The goal of this study was to determine a field method for measuring boundary shear stress (BSS) along hydraulically rough streambanks. This goal was achieved using a flume experiment designed to examine both BSS measurement theory and instruments suitable for field use. A second order prototype stream (Tom's Creek in Blacksburg, VA) with individual reaches dominated by three vegetation types (trees, shrubs, and grass) was modeled using a fixed-bed Froude-scale modeling technique. A model streambank was constructed for each of the three prototype stream sections and compared to one control streambank without vegetation. A Dantec MiniCTA system with a flush-mounted hot-film probe (55R46) measured shear stress at the streambank wall and was considered representative of the actual boundary shear stress. Both theory (law of the wall (LOW), Reynolds stresses, turbulent kinetic energy (TKE), and average boundary shear stress) and instruments (ADV and miniature propeller) were examined to suggest an estimation technique. Several methods of calculating near bank shear stress were evaluated (Table 5.1): the law of the wall ($\tau_{LOW,ADV}$, $\tau_{LOW,ADV,20\%}$, $\tau_{LOW,MP}$, and $\tau_{LOW,MP,\ 20\%}$), Reynolds stresses ($\tau_{uv}$, $\tau_{uw}$, $\tau_{vw}$, $\tau_{uv,extrap}$, $\tau_{uw,extrap}$, and $\tau_{vw,extrap}$), and TKE ($\tau_{TKE}$ and $\tau_{TKE,w}$). Because it is typically used in channel design, average boundary shear stress ($\tau_{avg,Rh}$,$\tau_{avg,bank,Rh}$, $\tau_{avg,H}$, $\tau_{avg,bank,H}$) was also calculated.

The small spatial ranges of CTA shear stress measurements for each vegetation type (bare: 0.19-0.83 Pa, tree: 0.04-0.72 Pa shrub: 0.16-0.38, and grass: 0.71-2.15) suggest one estimate of shear stress can be used for an entire bank. The median boundary shear stress measurements were 0.57 Pa, 0.39 Pa, 0.23 Pa, and 0.92, Pa for the bare, tree, shrub, and grass

streambanks, respectively. The LOW technique was not an appropriate method to calculate boundary shear stress with the dense vegetation of vegetated channels because the velocity profiles did not follow the necessary logarithmic shape. The large roughness present in vegetated channels creates secondary flow, so turbulent characteristics were more appropriate to estimate shear stress. Both $\tau_{vw}$ and $\tau_{TKE}$ were both good shear stress estimates for every vegetated condition. Study results also indicated a propeller-type velocimeter should be not used to calculated $\tau_{vw}$ and $\tau_{TKE}$. Velocity fluctuations cannot be calculated and velocity cannot be measured simultaneously in multiple directions for a single control volume. An ADV can be used to calculate $\tau_{vw}$ and $\tau_{TKE}$, but several precautions need to be considered: (1) Data should be filtered to ensure erroneous data which bias mean velocity values and turbulent characteristics are removed; (2) A longer sample time than used in this study (1 min) should be used in the field to ensure the entire turbulence structure is represented in the time series; and, (3) high sample frequencies are desirable (> 20 Hz). Because $\tau_{vw}$ did not vary with distance from the streambank when the measurements were close to the streambank, velocity should be measured within the lower 20% of the flow depth. $\tau_{TKE}$ should be measured adjacent to the streambank (a distance < 5% of the flow depth) to represent BSS because $\tau_{TKE}$ varied with distance from the streambank for the tree condition and when examining the combination of treatments. Measuring further from the streambank may result in estimating boundary shear stress in the shear layer. In this mixing layer, turbulence measures will likely over-estimate boundary shear stress.

### 7.3 Objective 3: Develop predictive methods for estimating BSS based on measurable vegetative properties

This study analyzed the effects of differing vegetation types on boundary shear stress, a parameter used to estimate channel erosion rates. It utilized the Kean and Smith (2004) model to examine boundary shear stress for three streambank vegetation conditions: bare, tree, and shrub. A second order prototype stream (Tom's Creek in Blacksburg, Virginia, USA), with individual reaches dominated by each vegetation treatment was modeled in a research flume using a fixed-bed Froude-scale modeling technique. One model streambank of the prototype stream was constructed for each vegetation type and compared to a bare control (only grain roughness). Time-averaged streamwise velocity flow fields were measured along five cross-sections using the MicroADV and miniature propeller for each vegetation treatment. Streamwise velocity flow fields were also predicted using the Kean and Smith (2004) model. Direct measurements of

shear stress were measured using a flush-mount constant temperature hot-film anemometer at four locations along five cross-sections. BSS was also calculated using the ray-isovel technique applied to the measured velocity fields (ADV and MP; Leighly, 1932; Kean et al., 2009) and was predicted using the Kean and Smith (2004) model. For comparison, average boundary shear stress was calculated.

The Kean and Smith (2004) model predicted velocity fields with a similar distribution as that measured by the ADV and MP. The predicted velocity distributions also illustrated a difference in isovel shape with varying vegetation density: as vegetation density increased, the isovels became more vertical near the streambank. The uncalibrated predicted discharge (0.07-0.08 $m^3/s$) was two times greater than the discharge measured in the flume, likely due to an inaccurate estimation of boundary roughness or turbulent mixing (Kean et al., 2009). By increasing the bed and bank roughness to 0.04 m and 0.004 m, respectively, for the bare and tree bank, the predicted discharge equaled the measured flume discharge. For the shrub bank, the bed and bank roughness were increased to 0.03 m and 0.003 m, respectively, such that the predicted discharge equaled the measured flume discharge.

Compared to the measurements and estimates of BSS, $\tau_{avg}$ (10 Pa) over estimated BSS along the streambank by at least an order of magnitude. With no adjustment to the model parameters, the model overestimated BSS compared to the CTA measurements up to 1200% with the greatest differences at the streambank toe (location 3). These differences were likely due to due to an inaccurate estimation of boundary roughness or turbulent mixing (Kean et al., 2009). A pairwise t-test indicated that BSS calculated using the ray-isovel method for both velocity measurement methods (ADV and MP) was different than the measured BSS values ($\alpha$=0.05), likely to distortions of the velocity flow field (Kean et al., 2009). In general, the predicted BSS distribution increased with water depth and decreased with increasing vegetation density. The model results supported findings by Kean and Smith (2004) that vegetation drag dominates in densely vegetated channels. The Kean and Smith (2004) model predicted velocity fields in similar distribution to that measured by the ADV and MP. The predicted velocity distributions also illustrated a difference in isovel shape with differing vegetation: isovels became more vertical near the streambank as vegetation density increased.

## 7.4 Implications of the Study

The goal of this research was to improve our understanding of the role of riparian vegetation in streambank retreat by evaluating the effects of vegetation on boundary shear stress. In addition to providing insight to the type and density of vegetation necessary to minimize streambank erosion, these results will also aide in quantifying sediment inputs from streambanks and in providing quantitative information for stream restoration design and watershed management planning. The following contributions have been made to the field:

1. This research tested the configuration of a typical stream restoration: vegetation along a sloping streambank. Although the most common stream restoration technique involves reshaping streambanks to a stable angle and then establishing riparian vegetation on the streambank face and floodplain (Bernhardt et al., 2005, 2007; Bernhardt and Palmer, 2007), the effects of vegetation on near-bank flow and BSS along sloping streambanks have not been analyzed. The present study examined turbulence characteristics and velocity structure caused by streambank vegetation and discussed it in the context of fluvial erosion.
2. The study of turbulence characteristics caused by streambank vegetation may help explain the difference in morphology between grass and forest channels (Zimmerman et al., 1967; Clifton, 1989; Sweeney, 1992; Davies-Colley, 1997; Trimble, 1997; Hession et al., 2003; Anderson et al., 2004; Sweeney et al., 2004; Eaton and Giles, 2008; McBride et al., 2008). The turbulence caused by the upright shrub treatment increased TKE and Reynolds stresses near the streambank, particularly at the streambank toe. This area is susceptible to fluvial erosion and the presence of dense, semi-rigid vegetation may encourage the formation of a wider channel with a vertical streambank.
3. The excess shear stress equation, which relates the streambank erosion rate to the difference between the BSS and the soil critical shear stress, predicts the erosion rate of fine grain soils due to stream channel scour (Osman and Thorne, 1988; Hanson and Simon, 2001). BSS on the channel boundary is commonly calculated based on flow depth and slope (Chang, 2002), but this method can cause major errors in soil detachment calculations when resistance (e.g. vegetation) is substantial (Thompson et al., 2004; Clark and Wynn, 2007). This research suggested a field method to measure boundary shear

stress along vegetated streambanks, illustrating that BSS calculated based on flow depth and slope overestimates BSS.

4. McBride et al. (2008) proposed a conceptual model to explain channel adjustment in response to the introduction of forested riparian vegetation. The model describes the multiphase adjustment of channel incision and widening with four steps: (1) equilibrium nonforested, (2) reforestation and channel incision, (3) channel widening and forest maturation, and (4) forested equilibrium. The study of TKE, turbulence intensities, Reynolds stresses, and boundary shear stress may provide quantitative support this conceptual model of channel evolution (McBride et al., 2008).

### 7.5 Limitations of the Study and Future Research Recommendations

A flume study was conducted to analyze boundary shear stress and velocity distributions in vegetated channels. This research had limitations due to model simplification that may lead to future research:

1. This study was limited to a monoculture of trees, shrubs, and grass along the streambanks. In reality, bank vegetation is not composed of a monoculture. Typically banks are composed of a mixture of forbs, herbaceous, and woody vegetation. This composition may be best represented by a combination of the shrub, grass, tree bank in this study. A combination of vegetation types should be studied to better mimic the natural condition.
2. This study use idealized shapes to represent vegetation. Similar research involving natural plant morphology along sloping streambanks should be considered for future research. Also vegetation at varying ages and seasons should be studied.
3. Sediment load affects streambank erosion. In this experiment, all bed and boundary sediment roughness was fixed, and there was no suspended sediment. This simplification was due to the sensitivity of the hot-film anemometer and the miniature propeller. The interaction between streambank vegetation along a sloping streambank with sediment transport should be considered for future study.
4. This study involved Froude-scale modeling of the natural system. Field-scale testing of the results should be completed, especially for the field method to measure boundary shear stress.

5. The grass bank presented several difficulties with measurements. Much of the ADV data were lost due to filtering. The Kean and Smith (2004) model is not valid for flexible vegetation and should be extended to flexible vegetation.

## Chapter 8 References


Abernethy, B. and I. D. Rutherfurd, 1998. Where along a river's length will vegetation most effectively stabilize stream banks? Geomorphology 23 (1), 55-75.

Abernethy, B., and I. D. Rutherfurd. 2000. Does the weight of riparian trees destabilize riverbanks? *Regulated Rivers Res. Mgmt.* 16: 565-576. DOI: 10.1002/1099-1646(200011/12)16:6<565::AID-RRR585>3.0.CO;2-1.

Abernethy, B., and I. D. Rutherfurd. 2001. The distribution and strength of riparian tree roots in relation to riverbank reinforcement. *Hydrological Processes* 15: 63-79. DOI: 10.1002/hyp.152.

Abrahams, A. D., and A. J. Parsons. 1991. Resistance to overland flow on desert pavement and its implications for sediment transport modeling. *Water Resources Res*. 27(8): 1827-1836.

Ackerman, J. D., and T. M. Hoover. 2001. Measurement of local bed shear stress in streams using a Preston-static tube. *Limnology and Oceanography* 46(8): 2080-2087.

Ackerman, J. D., L. Wong, C. R. Ethier, D. G. Allen, and J. K. Spelt. 1994. Preston-static tubes for measurement of wall shear stress. *J. Fluids Eng.* 116: 645-649.

Allen, P.M., J. Arnold, and E. Jakubowski. 1997. Design and testing of a simple submerged-jet device for field determination of soil erodibility. *Environ. Eng. Geosci.* 3(4): 579-584.

Allmendinger, N.E., J.E. Pizzuto, N. Potter, T.E. Johnson, W.C. Hession, 2005. The influence of riparian vegetation on stream width, Eastern Pennsylvania, USA. Geological Society of America Bulletin B25447.

Anderson, R. J., B. P. Bledsoe, and W. C. Hession. 2004. Width of streams and rivers in response to vegetation, bank material, and other factors. *J. American Water Res. Assoc.* 40(5): 1159-1172.

Arcement, G. J., and V. R. Schneider. Guide for selecting Manning's roughness coefficients for natural channels and flood plains. USGS Water-supply Paper 2339.

Armfield. Hydraulic measurement instruments. Issue 3. Armfield.

ARS. 2003. Helping states slow sediment movement: a high-tech approach to clean water act sediment requirements. *Agric. Res. Magazine* 51(12): 12-14.

ASCE. 1998a. River width adjustment. I: Processes and mechanisms. Journal of Hydraulic Engineering 124 (9), 881-902.

ASCE. 1998b. River width adjustment. II: Modeling. *J. Hydraulic Eng.* 124(9): 903-917.

*ASTM International Standards.* 2002. D421-85: Standard practice for dry preparation of soil samples for particle-size analysis and determination of soil constants. West Conshohocken, PA: ASTM.

*ASTM International Standards.* 2002b. D3977-97 Standard test methods for determining sediment concentration in water samples. West Conshohocken, PA: ASTM.

*ASTM International Standards.* 2002c. D422-63: Standard test method for particle-size analysis of soils. West Conshohocken, PA: ASTM.

Bennett, S.J., and A. Simon. 2004. *Riparian Vegetation and Fluvial Geomorphology.* Washington D.C.: American Geophysical Union.

Bernhardt, E. S., and E. B. Sudduth, M. A. Palmer, J. D. Allan, J. L. Meyer, G. Alexander, J. Follastad-Shah, B. Hassett, R. Jenkinson, R. Lave, J. Rumps, L. Pagano. 2007. Restoring rivers one reach at a time: Results from a survey of U.S. river restoration practitioners. *Restoration Ecology* 15(3): 482-493. DOI:10.1111/j.1365-2427.2006.01718.x.

Bernhardt, E. S., and M. A. Palmer. 2007. Restoring streams in an urbanizing world. *Freshwater Biology* 52: 738-751. DOI: doi:10.1111/j.1365-2427.2006.01718.x.

Bernhardt, E. S., M. A. Palmer, J. D. Allan, G. Alexander, K. Barnas, S. Brooks, J. Carr, S. Clayton, C. Dahm, J. Follstad-Shah, D. Galat, S. Gloss, P. Goodwin, D. Hart., B. Hassett, R. Jenkinson, S. Katz, G. M. Kondolf, P. S. Lake, R. Lave, J. L. Meyer, T. K. O'Donnell, L. Pagano, B. Powell, and E. Sudduth. 2005. Synthesizing U.S. river restoration efforts. *Science* 308: 636-637. DOI: 10.1126/science.1109769

Bicknell, B. R., J. C. Imhoff, J. L. Kittle, Jr., A. S. Donigian, Jr., and R. C. Johanson. 1997. Hydrological Simulation Program – Fortran, User's Manual for Version 11. EPA/600/R-97/080. Washington, D.C.: EPA.

Biron, P. M., C. Robson, M. F. Lapointe, and S. J. Gaskin. 2004. Comparing different methods of bed shear stress estimates in simple and complex flow fields. *Earth Surface Processes Landforms* 29: 1403-1415.

Biron, P. M., S. N. Lane, A. G. Roy, K. F. Bradbrook, and K. Richards. 1998. Sensitivity of bed shear stress estimated by vertical velocity profiles: the problem of sampling resolution. *Earth Surface Processes Landforms* 23: 133-139.

Blaisdell, F. W., L. A. Clayton, and G. G. Hebaus. 1981. Ultimate dimension of local scour. *J. Hydraulic Div. ASACE* 107(HY3): 327-337.

Booth, D.B. 1990. Stream-channel incision following drainage-basin urbanization. *Water Resources Bulletin* 26(3): 407-417.

Bott, T.L., J.D. Newbold, and D.B. Arscott. 2006. Ecosystem metabolism in piedmont streams: Reach geomorphology modulates the influence of riparian vegetation. *Ecosystems* 9: 398-421. DOI: 10.1007/s10021-005-0086-6

Bruun, H. H. 1996. Hot-film anemometry in liquid flows. *Measurement Sci. Tech.* 7: 1301-1312.

Bruun, H. H. 1995. *Hot-wire Anemometry: Principles and Signal Analysis.* New York, N.Y.: Oxford University Press.

Cancienne, R. M., G. A. Fox, and A. Simon. 2008. Influence of seepage undercutting on the stability of root-reinforced streambanks. *Earth Surface Processes and Landforms* 33: 1769-1786. DOI: 10.1002/esp.1657.

Carollo, F.G., V. Ferro, and D. Temini. 2002. Flow velocity measurements in vegetated channels. *ASCE J. Hydraulic Engineering* 128(7): 664-673.

Chang, H. H. 2002. *Fluvial Processes in River Engineering.* Malabar, FL.: Krieger Publishing.

Chen, C.L. 1976. Flow resistance in broad shallow grassed channels. *ASCE J. Hydraulics Division* 102: 307-322.

Chow, V. T. 1959. *Open-channel Hydraulics*. New York, NY: McGraw-Hill Book Company.

Clark, L. A., and T. M. Wynn. 2007. Methods for determining streambank critical shear stress and soil erodibility: Implications for erosion rate predictions. Trans. ASABE 50(1): 95-106.

Clifford, N. J., and J. R. French. 1993. Monitoring and modeling turbulent flow: historical and contemporary perspectives. In *Turbulence: Perspectives on Flow and Sediment Transport*. 1-34. N. J. Clifford, J. R. French, and J. Hardisty, ed. New York, N.Y.: John Wiley and Sons.

Clifton, C.F., 1989. Effects of vegetation and land use on channel morphology. In *Practical Approaches to Riparian Resource Management*. 121-129. Gresswell, R.E., B.A. Barton, and J.L. Kershner, ed. Billings, MT: U.S. Bureau of Land Management.

Crowder, D.W., and P. Diplas. 2002. Vorticity and circulation: Spatial metrics for evaluating flow complexity in stream habitats. *Can. J. Fish Aquat. Sci.* 59:633-645.

Crowe, C. T., D. F. Elger, and J.A. Roberson. 2001. *Engineering Fluid Mechanics.* 7th ed. New York, NY: John Wiley and Sons.

Dade, w. B., A. J. Hogg, and B. P. Boudreau. 2001. Chapter 2: Physics of flow above the sediment water interface. In *The Benthic Boundary Layer: Transport Processes and Biogeochemistry*, 4-43. B. P. Boudreau and B. B. Jorgensen, ed. New York, N.Y.: Oxford University Press.

Daniels, M. D., and B. L. Rhoads. 2004. Spatial pattern of turbulence kinetic energy and shear stress in a meander bend with large woody debris. In *Riparian Vegetation and Fluvial Geomorphology,* 87-97. Bennett, S. J. and A. Simon, ed. Washington, D.C.: AGU.

Davies-Colley, R. 1997. Stream channels are narrower in pasture than in forest. *New Zealand Marine Freshwater Res.* 31: 599-608.

Davies-Colley, R. 2000. Can riparian forest be restored without destabilizing stream channels and discrediting managers?. In: Wigington, P. J. and R. L. Beschta, eds. *Riparian Ecology and Management in Multi-Land Use Watersheds, Proceedings, AWRA 2000 Summer Specialty Conference, August 28-31, Portland, OR.* AWRA: Middleburg, VA. pp. 381-385.

Diplas, P., C.L. Dancey, A.O. Celik, M. Valyrakis, K. Greer, and T. Akar. 2008. The role of impulse on the initiation of particle movement under turbulent flow conditions. *Science* 322: 717-720. DOI: 10.1126/science.1158954

Dudley, S. 1997. Vegetation measurements for estimating flow resistance. Ph.D. dissertation, Colorado State Univ., Fort Collins, CO.

Dunn, I. S. 1959. Tractive resistance of cohesive channels. *J. Soil Mech. Foundations Div*. 85(SM3): 1-24.

Ead, S. A., N. Rajarathnam, C. Katopodis, and F. Ade. 2000. Turbulent open-channel flow in circular corrugated culverts. *J. Hydraulic Eng.* 126(10): 750-757. DOI: 10.1061/(ASCE)0733-9429(2000)126:10(750).

Eaton, B.C., and T.R. Giles, 2008. Assessing the effect of vegetation-related bank strength on channel morphology and stability in gravel-bed streams using numerical models. Earth Surface Processes and Landforms

ESRD. 2004. Outfall analysis based on incipient shear stress method. Environmental and Site Review Division: Department of Public Works and Environmental Services.

Fathi-Maghadam, and N. Kouwen. 1997. Nonrigid, nonsubmerged, vegetative roughness on floodplains. *J. Hydraulic Eng.* 123(1): 51-57.

Fausch, K.D., and R.J. White. 1981. Competition between brook trout (*Salvelinus fontinalis)* and brown trout (*Salmo trutta)* for positions in a Michigan stream. *Can. J. Fish. Aquat. Sci.* 38: 1220-1227.

Fausch, K.D. 1984. Profitable stream positions for salmonids: Relating specific growth rate to net energy gain. *Can. J. Fish. Aquat. Sci.* 62: 441-451.

Fingerson , L. M., and P. Freymuth. 1996. Ch. 3: Thermal anemometers. In *Fluid Mechanics Measurements,* 575-648. R. J. Goldstein, ed. Washington, D.C.: Taylor and Francis.

Foster, G. R., L. D. Meyer, and C. A. Onstad. 1977. An erosion equation derived from basic erosion principles. *Trans. ASAE.* 20(4): 678-682.

Garcia, M. H., D. M. Admiraal, J. Rodriguez, and F. Lopez. 1998. Navigation-induced bed shear stresses: Laboratory measurements, data analysis, and application. Civil Eng. Studies, Hydraul. Eng. Series No. 56.

Ghisalberti, M., and H. M. Nepf. 2002. Mixing layers and coherent structures in vegetated aquatic flows. *J. Geophysical Res.* 107(C2): 3011-3021. DOI: 10.1029/2001JC000871.

Ghisalberti, M., and H. M. Nepf. 2006. The structure of the shear layer in flows over rigid and flexible canopies. *Env. Fluid Mech*. 6:277-301. DOI: 10.1007/s10652-006-0002-4.

Graf, W. H. 1984. *Hydraulics of Sediment Transport.* Chelsea, MI: BookCrafters.

Graf, W.H., and V.H. Chhun. 1976. Manning's roughness for artificial grasses. *ASCE J. Irrigation and Drainage Division* 102: 413-423.

Grant, I. 1997. Particle image velocimetry: a review. *J. Mech. Eng. Sci.* 211(1):55-76.

Gray, D.H. and R.B. Sotir. 1996. *Biotechnical and Soil Bioengineering Slope Stabilization: A Practical Guide for Erosion Control.* New York, NY: John Wiley and Sons.

Gregory, K. J., A. M. Gurnell. 1988. Vegetation and river channel form and process. Viles, H.,ed. *Biogeomorphology*. Basil Blackwell:Oxford. pp. 11-42.

Griffin, E.R., J.W. Kean, K.R. Vincent, J.D. Smith, and J. M. Firedman. 2005. Modeling effects of bank friction and woody bank vegetation on channel flow and boundary shear stress in Rio Puerco, New Mexico. *J. Geophysical Research* 110: F04023.

Grissinger, E. H, 1982. Bank erosion of cohesive materials. In *Gravel-Bed Rivers*, 273-287. Hey, R. D., J. C. Bathurst, and C. R. Thorne, ed. New York, NY: John Wiley and Sons.

Hann, C. T., B. J. Barfield, and J. C. Hayes. 1994. *Design Hydrology and Sedimentology for Small Catchments*. San Diego, CA: Academic Press.

Hanson, G. J. 1990a. Surface erodibility of earthen channels at high stresses part I: open channel testing. *Trans. Agric.* 33(1): 127-131.

Hanson, G. J. 1990b. Surface erodibility of earthen channels at high stresses part II-developing and *in situ* testing device. *Trans. Agric*. 33(1):132-137.

Hanson, G. J., A. Simon, and K. R. Cook. 2002. Non-vertical jet testing of cohesive streambank materials. ASAE Paper No. 022119. Chicago, IL: ASAE.

Hanson, G. J., and A. Simon. 2001. Erodibility of cohesive streambeds in the loess area of the midwestern USA. *Hydrological Processes* 15: 23-38. DOI: 10.1002/hyp.149.

Hanson, G. J., and K. R. Cook. 1997. Development of Excess shear stress parameters for circular jet testing. ASAE Paper No. 972227. Minneapolis, Minn.: ASAE.

Hanson, G. J., K. R. Cook, and A. Simon. 1999. Determining erosion resistance of cohesive materials. In *Proceedings of the ASCE International Water Resources Engineering Conference.* CD-ROM. Seattle, WA: ASCE.

Haritonidis, J.H. 1989. The measurement of wall shear stress. In *Lecture Notes in Engineering: Advances in Fluid Mechanics Measurements*. 229-261. Brebbia, C. A. and S. A. Orszag, ed. New York: NY: Springer-Verlag.

Hayes. J.W., N.F. Hughes, and L.H. Kelly. 2007. Process-based modeling of invertebrate drift transport, net energy intake and reach carrying capacity for drift-feeding salmonids. *Ecological Modelling* 207: 171-188.

Hayes, J.W., and I.G. Jowett. 1994. Microhabitat models of large brown trout in three New Zealand rivers. *N. Am. J. Fish. Management* 14: 710-725.

Heede, B. H. and J. N. Rinne, 1990. Hydrodynamic and fluvial morphologial processes and implication for fisheries management and research. North American Journal of Fisheries Management 10 (3), 249-268.

Hession, W. C. 2001. Riparian forest and urban hydrology influences on stream channel morphology: Implications for restoration. In: D. Phelps and G. Sehlke, (eds). *Proceedings of the World Water and Environmental Resources Congress, May 20-24, 2001, Orlando, FL.* ASCE:Reston, VA.

Hession, W. C., J. E. Pizzuto, T. E. Johnson, R. J. Horwitz. 2003. Influence of bank vegetation on channel morphology in rural and urban watersheds. *Geology* 31(2): 147-150.

Hey, R. D., and C. R. Thorne. 1986. Stable channels with mobile gravel beds. *J. Hydraulic Eng. ASCE* 112(8): 671-689.

Hicks, D. M., and P. D. Mason. 1998. *Roughness Characteristics of New Zealand Rivers.* Christchurch, New Zealand: National Institute of Water and Atmospheric Research.

Hoover, T. M., and J. D. Ackerman. 2004. Near-bed hydrodynamic measurements above boulders in shallow torrential streams: implications for stream biota. *J. Environ. Eng. Sci.* 3: 365-378.

Horwitz, R. J., W. C. Hession, and B. S. Sweeney. 2000. Effects of forested and unforested riparian zones on stream fishes. In: Wigington, P. J. and R. L. Beschta, eds. *Riparian Ecology and Management in Multi-Land Use Watersheds, Proceedings, AWRA 2000 Summer Specialty Conference, August 28-31, Portland, OR.*

Houjou, K., Y. Shimizu, and c. Ishii. 1990. Calculation of boundary shear stress in open channel flow. *J. Hydroscience and Hydraulic Eng.* 8(2): 21-37.

Hughes, N.F., and L.M. Dill. 1990. Position choice by drift-feeding salmonids: Model and test for Arctic grayling (*Thymallus arcticus)*in subarctic streams, interior Alaska. *Can. J. Fish. Aquat. Sci.* 47: 2039-2048.

Hupp, C.R., and A. Simon. 1991. Bank accretion and the development of vegetated depositional surfaces along modified alluvial channels. *Geomorphology* 4(2): 111-124.

Jarvela, J. 2002. Flow resistance of flexible and stiff vegetation: a flume study with natural plants. *J. Hydrology* 44-54. DOI: 10.1016/S0022-1694(02)00193-2.

Julian, J. P., and R. Torres. (2006). Hydraulic erosion of cohesive riverbanks. *Geomorphology* 76: 193-206.

Julien, P.Y. 1995. *Erosion and Sedimentation*. New York, NY: Cambridge University Press.

Kamphuis, J. W., and K. R. Hall. 1983. Cohesive material erosion by unidirectional current. *J. Hydraulic Eng.* 109(1):49-61.

Kean, J.K., and J.D. Smith. 2004. Flow and boundary shear stress in channels with woody bank vegetation. In *Riparian Vegetation and Fluvial Geomorphology,* 237-252. S.J. Bennett and A. Simon, ed. Washington, D.C.: AGU.

Kean, J.W., and J.D. Smith. 2005. Generation and verification of theoretical rating curves in the Whitwater River basin, Kansas. *J. Geophysical Research* 110: F04012.

Kean, J.W., and J.D. Smith. 2006a. Form drag in rivers due to small-scale natural topographic features: 1. Regular sequences. *J. Geophysical Research* 111: F04009.

Kean, J.W., and J.D. Smith. 2006b. Form drag in rivers due to small-scale natural topographic features: 1. Irregular sequences. *J. Geophysical Research* 111: F04010.

Kean, J.W., R.A. Kuhnle, J.D. Smith, C.V. Alonso, and E.J. Langendoen. 2009. Test of a method to calculated near-bank velocity and boundary shear stress. *J. Hydraulic Eng.* 135(7): 588-601.

Keller, R., and S. Wilkinson. 2004. *HMEM 2002.* 1-10.

Kim, S. C., C. T. Friedrichs, J. P. Y. Maa, and L. D. Wright. 2000. Estimating bottom stress in tidal boundary layer from acoustic Doppler velocimetry data. *J. Hydraulic Eng.* 126(6): 399-406.

Knight, D. W., M. Omran, and X. Tang. 2007. Modeling depth-averaged velocity and boundary shear stress in trapezoidal channels with secondary flows. *J. Hydraulic Eng.* 133(1): 39-47. DOI: 10.1061/(ASCE)0733-9429(2007)133:1(39).

Kouwen, N., A.M. Unny, and H.M. Hill. 1969. Flow retardance in vegetated channels. *ASCE J. Irrigation and Drainage Division* 95: 329-343.

Kundu, P. K. 1990. *Fluid Mechanics.* San Diego, CA: Academic Press.

Laursen, E. M. 1958. The total sediment load of streams. *J. Hydrol. Div.* 1530-1565.

Lavelle, J.W., and H.O. Mofjeld. 1987. Do critical stresses for incipient motion and erosion really exist? *J. Hydraulic Eng*.113(3): 370-393.

Lawler, D. M., C. R. Thorne, and J. M. Hooke. 1997. Bank erosion and instability. In *Applied Fluvial Geomorphology for River Engineering and Management*. C. R. Thorne, R. D. Hey, and M. D. Newson, eds. New York, N.Y.: John Wiley and Sons.

Leighly, J.B. 1932. Toward a theory of morphologic significance of turbulence in the flow of water in streams. *Univ. Calif. Publ. Geogr.* 6(1): 1-22.

Lekakis, I. 1996. Calibration and signal interpretation for single and multiple hot-wire hot-film probes. *Measurement Sci. Tech.* 7(10): 1313-1333.

Liu, D., P. Diplas, J. D. Fairbanks, and C. C. Hodges. 2008. An experimental study of flow through rigid vegetation. *J. Geophysical Res.* 113: 1-16. DOI: 10.1029/2008JF001042.

Lourenco, L. M., A. Krothappalli, and C. A. Smith. 1989. Particle Image Velocimetry. In *Lecture Notes in Engineering: Advances in Fluid Mechanics Measurements*. 127-199. Brebbia, C. A. and S. A. Orszag, ed. New York, NY: Springer-Verlag.

Lyons, J., S. W. Trimble, and L. K. Paine, 2000. Grass versus trees: Managing riparian areas to benefit streams of central North America. Water Resources Bulletin 36 (4), 919-930.

MacVicar, B. J., and E. Beaulieu, V. Champagne, and A. G. Roy. 2007. Measuring water velocity in highly turbulent flows: Field tests of an electromagnetic current meter ECM and an acoustic Doppler velocimeter (ADV). *Earth Surface Processes and Landforms* 32: 1412-1432. DOI: 10.1002/esp.1497.

Martin, J.R., L.J. Steinberg, and E.E. Michaelides. 2000. Determination of bed shear stress by Digital Particle Image Velocimetry in turbulent open channel flow. *Water Resources.* 1-9.

Mattingly, G. E. 1996. Chapter 5: Volume flow measurements. In *Fluid Mechanics Measurements*, 301-366. 2nd ed. R. J. Goldstein, ed. Washington, D.C.: Taylor and Francis.

McBride, M., W. C. Hession, D. M. Rizzo, and D. M. Thompson. 2007. The influence of riparian vegetation on near-bank turbulence: A flume experiment. *Earth Surface Processes and Landforms* 32 (13): 2019-2037. DOI: 10.1002/esp.1513.

McBride, M., W.C. Hession, and D.M. Rizzo. 2008. Riparian reforestation and channel change: A case study of two small tributaries to Sleepers River, northeastern Vermont, USA. *Geomorphology* 102: 445-459. DOI: 10.1016/j.geomorph.2008.05.008.

Moody, J. A., and J. D. Smith. 2004. Field measurements of Reynolds stress near a riverbank. Hydraulic Measurements and Experimental Methods Conference 2002. Estes Park, CO: ASCE.

Mosley, M. P., 1981. Semi-determinate hydraulic geometry of river channels, South Island, New Zealand. Earth Surface Processes and Landforms 6,127-137.

Munson, B. R., D. F. Young, and T. H. Okiishi. 2002. *Fundamentals of Fluid Mechanics.* 4th ed. New York, N.Y.: John Wiley and Sons Inc.

Munson, B. R., D. F. Young, and T. H. Okiisi. 1998. *Fundamentals of Fluid Mechanics,* 3rd ed. New York, N.Y.: John Wiley and Sons.

Murgatroyd, A. L. and J. L. Ternan, 1983. The impact of afforestation on stream bank erosion and channel form. Earth Surface Processes and Landforms 8 (4), 357-370.

Nearing, M. A., G. R. Foster, L. J. Lane, and S. C. Finkner. 1989. A process-based soil erosion model for USDA-water erosion prediction project technology. *Trans. ASAE* 32(5): 1587-1593.

Neill, C. R. 1967. Mean-velocity criterion for scour of coarse uniform bed-material. *Proc. International Assoc. Hydraulic Res*. 3: 46-54.

Nepf, H. and M. Ghisalberti. 2008. Flow and transport in channels with submerged vegetation. *Acta Geophysica* 56(3): 753-777. DOI: 10.2478/s11600-008-0017-y.

Nepf, H. M. 1999. Drag, turbulence, and diffusion in flow through emergent vegetation. *Water Resources Res.* 35(2): 479-489.

Nepf, H. M., and E. R. Vivoni. 2000. Flow structure in depth-limited, vegetated flow. *J. Geophysical Research* 105(12): 28547-28557.

Nortek. 2005. The vectrino-a new generation 3D water velocity sensor. Annapolis, MD: Nortek.

Osman, A. M., and C. R. Thorne. 1988. Riverbank stability analysis I: theory. *J. Hydraulic Eng.* 114(2): 134-150.

Owoputi, L. O., and W. J. Stolte. 1995. Soil detachment in the physically based soil erosion process: A review. *Trans. ASAE* 38(4): 1099-1110.

Partheniades, E. 1965. Erosion and deposition of cohesive soils. *J. Hydraulics Division Proceedings of the American Society of Civil Engineers* 91(HY1): 105-139.

Peakall, J., P. Ashworth, and J. Best. 1996. Physical modeling in fluvial geomorphology: Principles, applications, and unresolved issues. In *The Scientific Nature of Geomorphology: Proceedings of the 27th Binghamton Symposium in Geomorphology held 27-29 September,* 221-254. B. L. Rhoads and C. E. Thorne, ed. John Wiley and Sons.

Petit, F. 1989. The evaluation of grain shear stress from experiments in a pebble-bedded flume. *Earth Surface Processes Landforms* 14: 499-508.

Petit, F. 1990. Evaluation of grain shear stresses required to initiate movement of particles in natural rivers. *Earth Surface Processes Landforms* 15: 135-148.

Pollen, N. 2007. Temporal and spatial variability in root reinforcement of streambanks: Accounting for soil shear strength and moisture. *Catena* 69: 197-205. DOI: 10.1016/j.catena.2006.05.004.

Pope, N. D., J. Widdows, and M. D. Brinsley. 2006. Estimation of bed shear stress using the turbulent kinetic energy approach: A comparison of annular flume and field data. Continental Shelf Res. 26: 959-970. DOI: 10.1016/j.csr.2006.02010.

Preston, J. H. 1954. Determination of turbulent skin friction by means of pitot tubes. *J. Royal Aeronautical Soc.* 109-121.

Prosser, I.P., A. O. Hughes, and I. D. Rutherfurd. 2000. Bank erosion of an incised upland channel by subaerial processes: Tasmania, Australia. *Earth Surface Processes Landforms* 25(10):1085-1101.

Raudkivi, A. J. 1998. *Loose Boundary Hydraulics.* Brookfield, Vt.: Balkema Publishers.

Richards, K. 1982. *Rivers, forms and processes in alluvial channels. Methuen,* London

Robert, A. 2003. River Processes: An Introduction to Fluvial Dynamics. New York, NY: Oxford University Press Inc.

Robinson, K. M., and K. R. Cook. 1998. Stress measurement upstream of an overfall. *Trans. ASAE* 41(4): 1019-1024.

Robinson, K.M. 1989. Hydraulic stresses on an overfall boundary. *Trans. ASAE* 32(4): 1269-1274.

Rouse, H. 1965. Critical analysis of open-channel resistance. *J. Hydraulic Div. Am. Soc. Civ. Eng.* 91(HY4): 1-25.

Sabersky, R. H., A. J. Acosta, E. G. Hauptmann, and E. M. Gates. 1999. *Fluid Flow: A First Course in Fluid Mechanics.* Upper Saddle River, N. J.: Prentice Hall.

Samways, A. L., J. Ali, M. F. N., Aldeen, and H. H. Bruun. 1994. The calibration of and measurements with cylindrical hot-film probes in water flows. *Measurement Sci. Tech.* 5(12): 1551-1559.

Schlichting, H., and K. Gersten. 2000. *Boundary-Layer Theory.* 8th ed. Berlin, Germany: Springer-Verlag.

Schumm, S.A., M.D. Harvey, and C.C. Watson. 1984. Incised channels: Morphology, dynamics, and control. Water Resources Publications, Littleton, CO.

Simon, A. and A. Collison. 2001. Scientific basis for streambank stabilization using riparian vegetation. *Proceedings of the 7th Federal Interagency Sedimentation Conference, Reno, NV.* pp. V-47-54.

Simon, A., and A. J. C. Collison 2002. Quantifying the mechanical and hydrologic effects of riparian vegetation on streambank stability. *Earth Surface Processes and Landforms* 27: 527-546. DOI: 10.1002/esp.325.

Simon, A., N. Pollen, and E. Langendoen. 2006. Influence of two woody riparian species on critical conditions for streambank stability: Upper Truckee River, California. *J. American Water Resources Association* 42(1): 99-113. DOI: 10.1111/j.1752-1688.2006.tb03826.x.

Singhal, M. K, J. Mohan, and A. K. Agrawal. 1980. Role of grain shear stress in sediment transport. *Irrig. Power* 37: 105-108.

Smerdon, E. T., and R. P. Beasley. 1961. Critical tractive forces in cohesive soils. *Agric. Eng.* 26-29.

Smith, C., 1992. Riparian afforestation effects on water yields and water quality in pasture catchments. Journal of Environmental Quality 21, 237-245.

Sontek. 1999. The standard in high-resolution velocity measurements. San Diego, CA: Sontek.

Statzner, B., and R. Muller. 1989. Standard hemispheres as indicators of flow characteristics in lotic benthos research. *Freshwater Biol.* 21: 445-459.

Sweeney, B.W., 1992. Streamside forests and the physical, chemical and trophic characteristics of piedmont streams in eastern North America. Water Science and Technology 26 (12), 2653-2673.

Sweeney, B.W., T.L. Bott, J.K. Jackson, L.A. Kaplan, J.D. Newbold, L.J. Stanley, W.C. Hession, and R.J. Horwitz. 2004. Riparian deforestation, stream narrowing, and loss of stream ecosystem services. *Proceedings of the National Academy of Sciences* 101(39): 14132-14137.

Temple, D. M. 1980. Tractive force design of vegetated channels. *Trans. ASAE* 884-890.

Temple, D. M. 1983. Design of grass-lined open channels. *Trans. ASAE* 1064-1069.

Temple, D. M. 1985. Stability of grass-lined channels following mowing. *Trans. ASAE* 28(3): 750-754.

Temple, D. M. 1992. Estimating flood damage to vegetated deep soil spillways. *Applied Eng. Agric.* 8(2): 237-242.

Temple, D. M., and G. J. Hanson. 1994. Headcut development in vegetated earth spillways. *Applied Eng. Agric*. 10(5): 677-682.

Thompson A. M., B. N. Wilson, and H. V. Nguyen. 2001. Effectiveness of erosion control blankets on reducing shear stress acting on soil particles. ASAE Paper No. 701P0007. Honolulu, Hi.: ASAE.

Thompson, A. M. 2001. Shear stress partitioning for vegetation and erosion control blankets. PhD diss. St. Paul, Minn.: University of Minnesota.

Thompson, A. M., and B. M. Wilson. 2004. Calibration accuracy for constant temperature thermal anemometer. *J. Hydraulic Eng.* 833-836.

Thompson, A. M., B. N. Wilson, and B. J. Hansen. 2004. Shear stress partitioning for idealized vegetated surfaces. *Trans. ASAE* 47(3): 701-709.

Thorne, C. R. 1990. Ch. 10: Effects of vegetation on riverbank erosion and stability. In *Vegetation and Erosion.* J. B. Thornes, ed. New York, NY: John Wiley and Sons.

Thorne, C. R. 1982. Processes and mechanisms of river bank erosion. In *Gravel-bed Rivers, 227-259.* Hey, R. D., J. C. Bathurst, and C. R. Thorne, ed. New York, NY: .John Wiley and Sons.

Thorne, S. D., and D. J. Furbish. 1995. Influences of coarse bank roughness on flow within a sharply curved river bend. *Geomorphology* 12: 241-257. DOI: 10.1016/S0022-1694(02)00193-2.

Thornton, C. I., S. R. Abt, C. E. Morris, and J. C. Fischenich. 2000. Calculating shear stress at channel-overbank interfaces in straight channels with vegetated floodplains. *J. Hydraulic Eng.* 126(12): 929-936. DOI: 10.1061/(ASCE)0733-9429(2000)126:12(929).

Tominaga, A., Nezu, I., Ezaki, K., and Nakagawa, H. 1989. Turbulent structure in straight open channel flows. *J. Hydraulic Res.*27(1): 149-173.

Trimble, S.W. 1997a. Contribution of stream channel erosion to sediment yield from an urbanizing watershed. *Science* 278: 1442-1444.

Trimble, S.W., 1997b. Stream channel erosion and change resulting from riparian forests. *Geology* 25(5): 467–469.

Tritico, H. M., and H. Hotchkiss. 2005. Unobstructed and obstructed turbulent flow in gravel bed rivers. *J. Hydraulic Eng.* 131(8): 635-645. DOI: 10.1061/(ASCE)0733-9429(2005)131:8(635).

TSI. *Innovation in Thermal Anemometry: a Complete Family of Thermal Anemometry Systems, Probes and Accessories.* St. Paul, Minn.: TSI Incorporated Laser Diagnostics Division.

USACE. 1993. HEC-6: Scour and Deposition in Rivers and Reservoirs, User's Manual, Version 4.1. Alexandria, VA: Department of the Army, US Army Corps of Engineers, Hydrologic Engineering Center.

USDA-NRCS. 1996. Ch. 16: Streambank and shoreline protection. National Engineering Handbook Series, Part 650. Washington, D.C.: US Government Printing Office.

USEPA. 2002. National Water Quality Inventory: 2000 Report. EPA 841-R-02-001. USEPA: Washington, DC.

van Prooijen, B., J. Battjes, and W. Uijttewall. 2005. Momentum exchange in straight uniform channel flow. *J. Hydraulic Eng.*131(3): 177-185. DOI: 10.1061/(ASCE)0733-9429(2005)131:3(175).

Vanoni, V. A. 1975. *Sedimentation Engineering*. New York, N.Y.: ASCE.

Voulgaris, G., and J. H. Trowbridge. 1998. Evaluation of the acoustic doppler velocimeter (ADV) for turbulence measurements. *J. Atmospheric Oceanic Tech.* 15(1): 272-289.

Wahl, T. 2000. Analyzing ADV data using WinADV. 2000 Joint Conference on Water Resources Engineering and Water Resources Planning and Management. Minneapolis, MN.

Wallbrink, P.J., A.S. Murray, and J.M. Olley. 1998. Determining sources and transit times of suspended sediment in the Murrumbidgee River, New South Wales, Australia, using fallout $^{137}$Cs and $^{210}$Pb. *Water Resources Res.* 34(4): 879-887.

White, B. L., and H. M. Nepf. 2007. Shear instability and coherent structures in shallow flow adjacent to a porous layer. *J. Fluid Mech.* 593: 1-32. DOI:10.1017/S0022112007008415.

White, B. L., and H. M. Nepf. 2008. A vortex-based model of velocity and shear stress in a partially vegetated shallow channel. Water Resources Res. 44: W01412. DOI: 10.1029/2006WR005651.

Wilcock, P.R. 1996. Estimating local bed shear stress from velocity measurements. *Water Resources Res.* 32(11): 3361-3366.

Wilcox, A. C., and E. E. Wohl. 2007. Field measurements of three-dimensional hydraulics in a step-pool channel. *Geomorphology* 83: 215-231. DOI:10.1016/j.geomorph.2006.02.017.

Wilson, C.A.M.E. 2007. Flow resistance models for flexible submerged vegetation. *J. Hydrology* 342: 213-222.

Wilson, C. A. M. E., T. Stoesser, P. D. Bates, and A. B. Pinzen. 2003. Open channel flow through different forms of submerged flexible vegetation. *J. Hydraulic Eng.* 129(11): 847-853.

Wobus, C.M., J.W. Kean, G.E. Tucker, and R.S. Anderson. 2008. Modeling the evolution of channel shape: Balancing computational efficiency with hydraulic fidelity. *J. Geophysical Research* 113: F02004.

Wolman, M.G. 1954. A method of sampling coarse river-bed material. Trans. American Geophysical Union 35: 951-956.

Wu, F.C., H.W. Shen, and Y.J. Chou. 1999. Variation of roughness coefficients for unsubmerged and submerged vegetation. *ASCE J. Hydraulic Engineering* 125(9): 934-942.

Wynn T., and S. Mostaghimi. 2006b. The effects of vegetation and soil type on streambank erosion, southwestern Virginia, USA. *J. American Water Resources Association* 42(1): 69-82.

Wynn, T. M, and S. Mostaghimi. 2006a. Effects of riparian vegetation on stream bank subaerial processes in southwestern Virginia, USA. *Earth Surface Processes and Landforms* 31: 399-413. DOI: 10.1002/esp.1252.

Yang, K., S. Cao., and D. W. Knight. 2007. Flow patterns in compound channels with vegetated floodplains. *J. Hydraulic Eng.* 133(2): 148-159. DOI: 10.1061/(ASCE)0733-9429(2007)133:2(148).

Yen, B. C. 2002. Open channel flow resistance. *J. Hydraulic Eng.* 128(1): 20-39.

Zimmerman, R.C., Goodlett, J.C., Comer, G.H., 1967. The influence of vegetation on channel form of small streams. Symposium on River Morphology. International Association of Scientific Hydrology, Bern, Switzerland, pp. 255–27

# Appendix A: Field Data from Tom's Creek

## A.1 Tree cross-sections

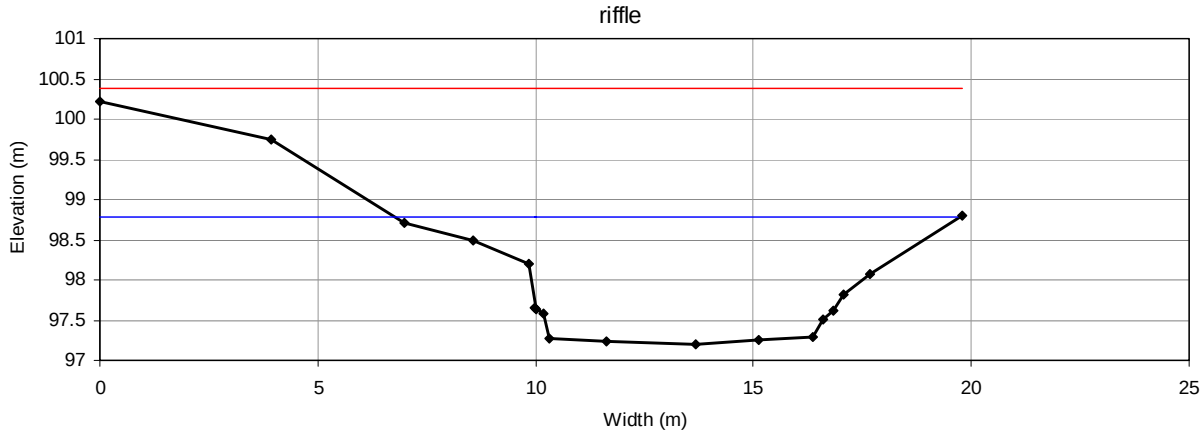


**Figure A.1. Tree cross section 1; right bank used for analysis. Red line is the flood prone width; blue line indicates top of bank/bankfull.**

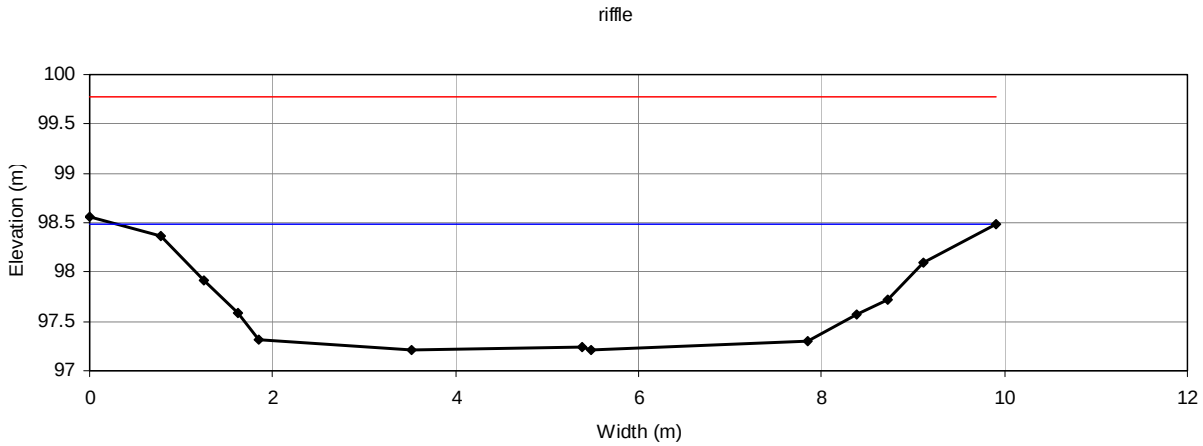


**Figure A.2. Tree cross section 2: right bank used for analysis. Red line is the flood prone width; blue line indicates top of bank/bankfull.**

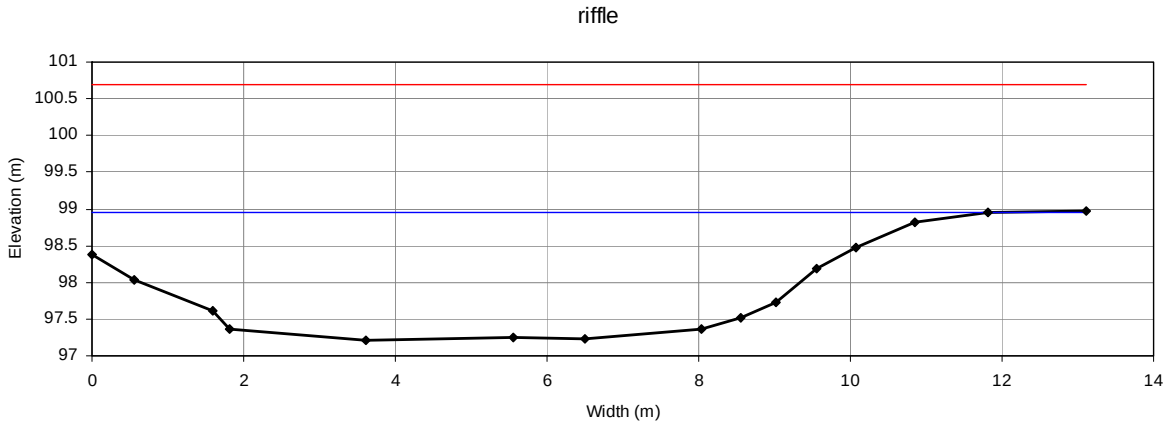


**Figure A.3. Tree cross section 3; right bank used for analysis. Red line is the flood prone width; blue line indicates top of bank/bankfull.**

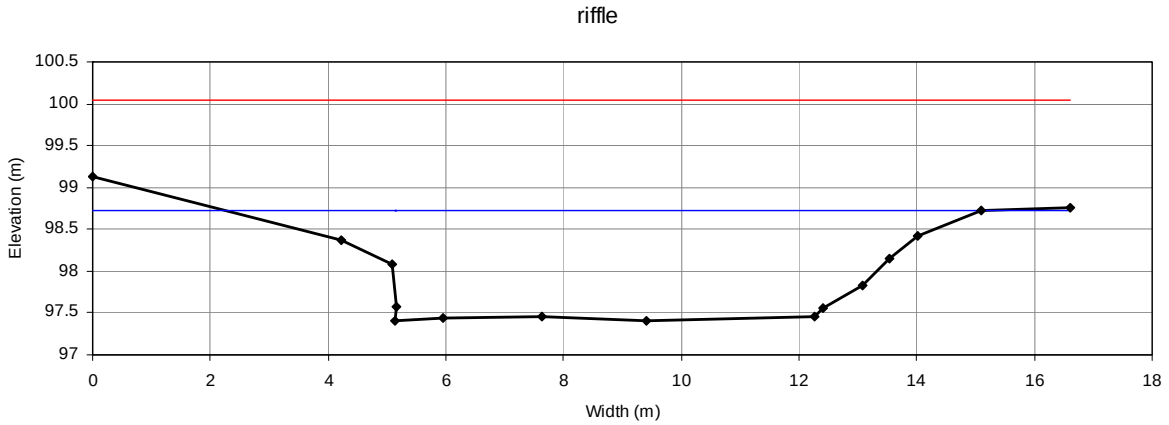


**Figure A.4. Tree cross section 4; right bank used for analysis. Red line is the flood prone width; blue line indicates top of bank/bankfull.**

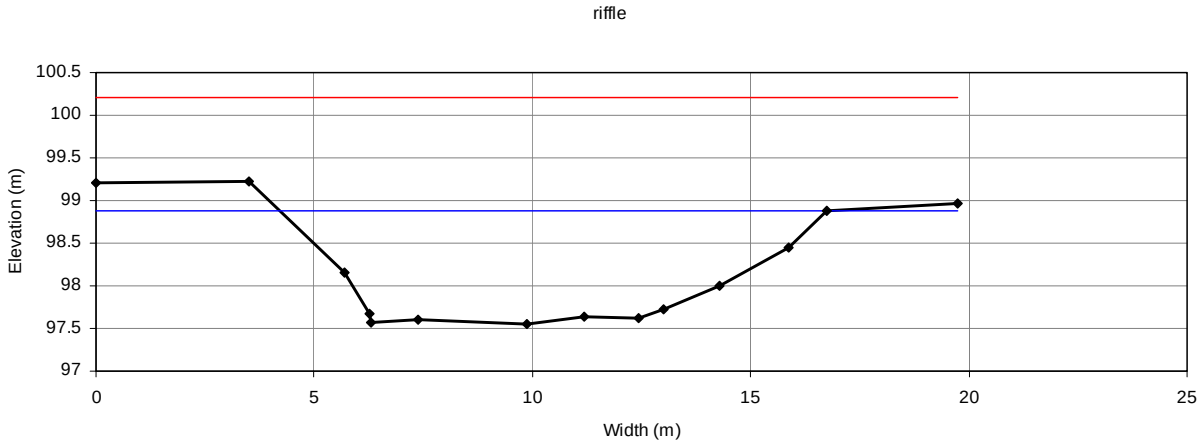


**Figure A.5. Tree cross section 5; right bank used for analysis. Red line is the flood prone width; blue line indicates top of bank/bankfull.**

## A.2 Shrub cross-sections

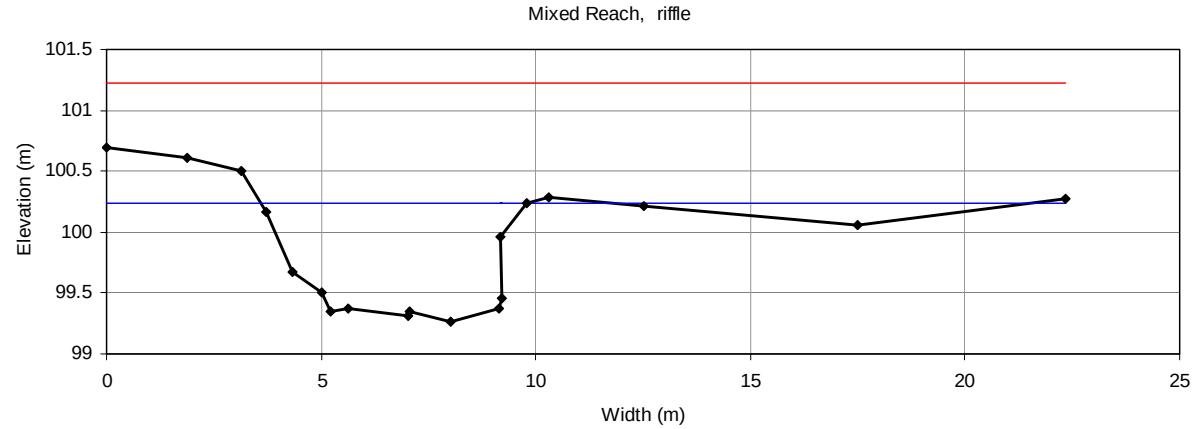


**Figure A.6. Shrub cross section 1; Left bank used for analysis. Red line is the flood prone width; blue line indicates top of bank/bankfull.**

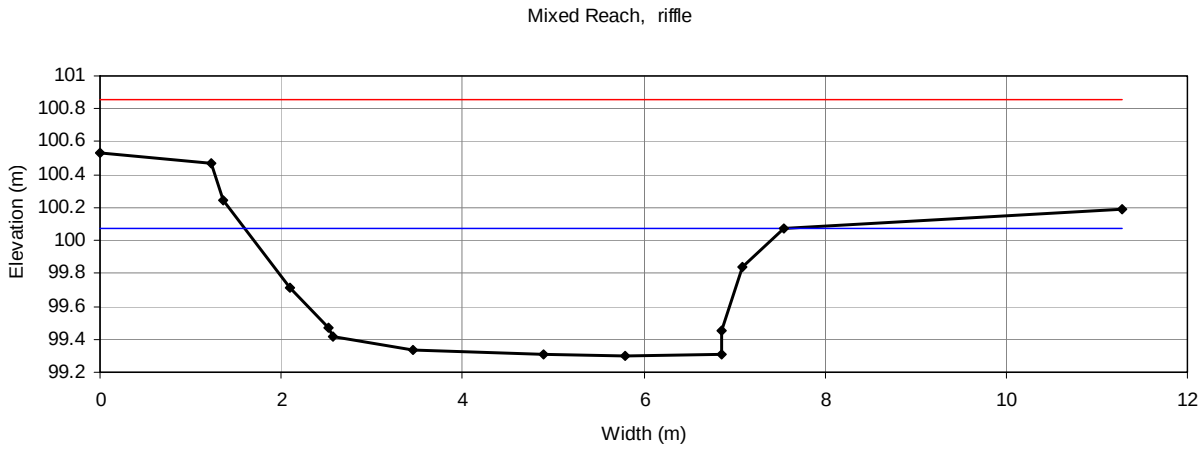


**Figure A.7. Shrub cross section 2: Left bank used for analysis. Red line is the flood prone width; blue line indicates top of bank/bankfull.**

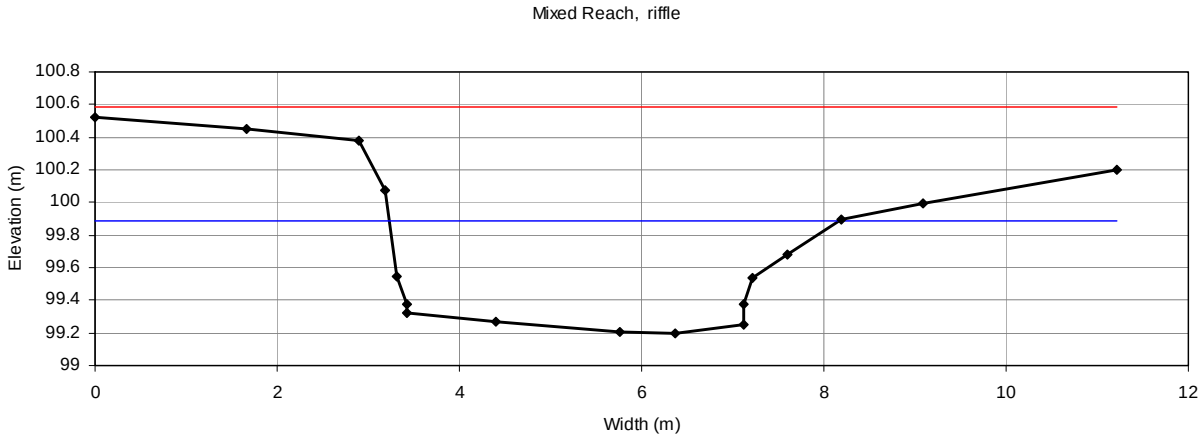


**Figure A.8. Shrub cross section 3; Left bank used for analysis. Red line is the flood prone width; blue line indicates top of bank/bankfull.**

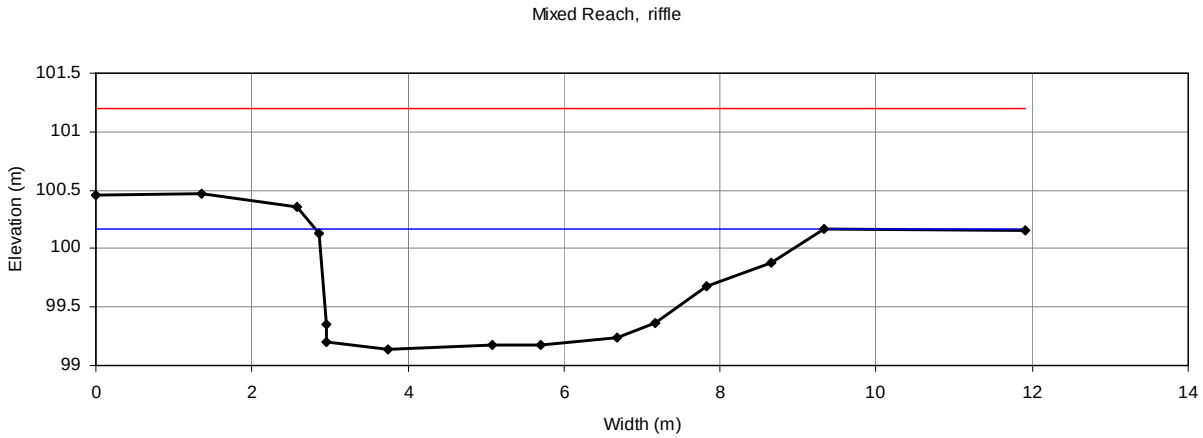


**Figure A.9. Shrub cross section 4; Left bank used for analysis. Red line is the flood prone width; blue line indicates top of bank/bankfull.**

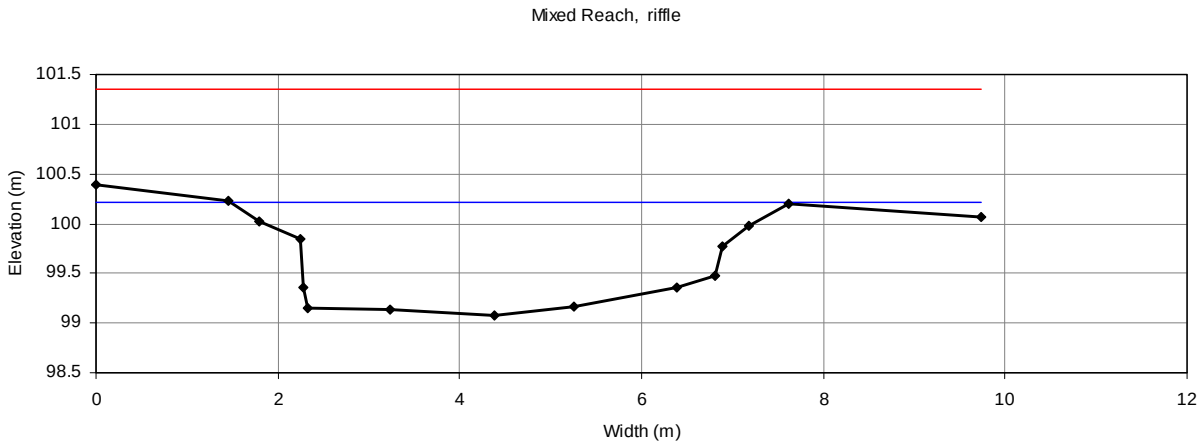


**Figure A.10. Shrub cross section 5; Left bank used for analysis. Red line is the flood prone width; blue line indicates top of bank/bankfull.**

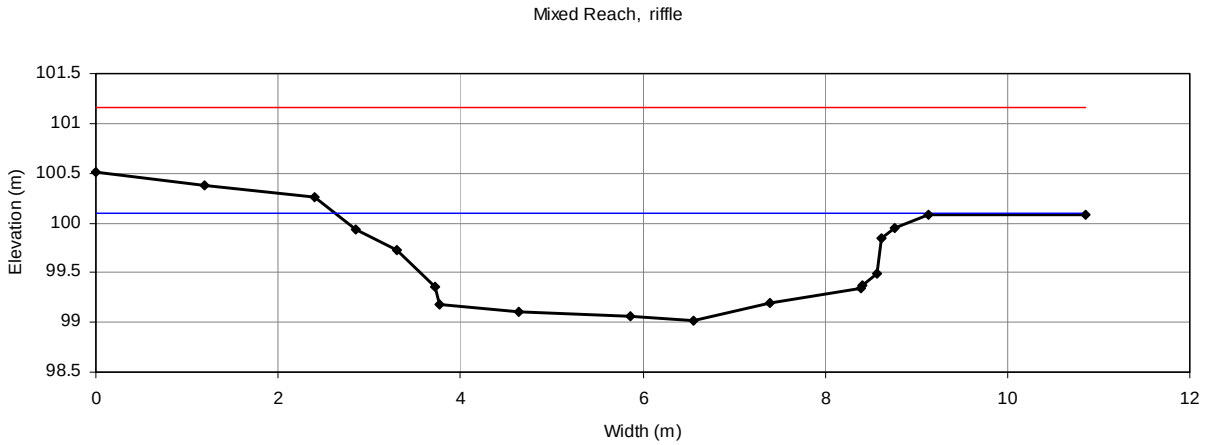


**Figure A.11. Shrub cross section 6; Left bank used for analysis. Red line is the flood prone width; blue line indicates top of bank/bankfull.**

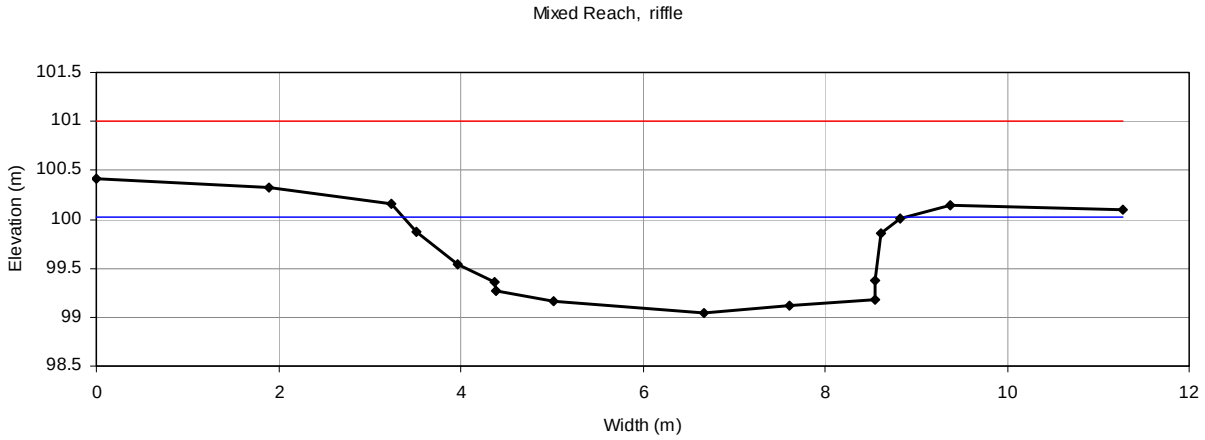


**Figure A.12. Shrub cross section 7; Left bank used for analysis. Red line is the flood prone width; blue line indicates top of bank/bankfull.**

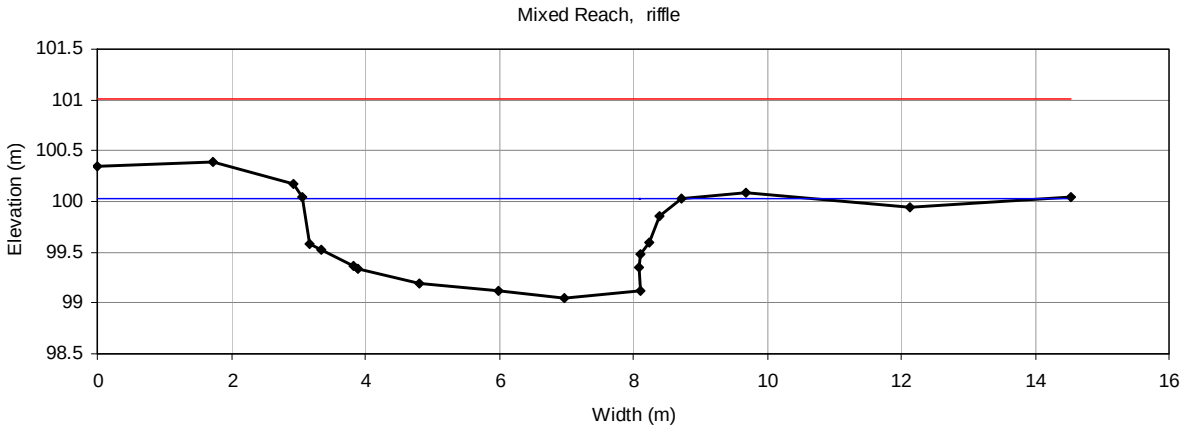


**Figure A.13. Shrub cross section 8; Left bank used for analysis. Red line is the flood prone width; blue line indicates top of bank/bankfull.**

## A.3 Grass cross-sections

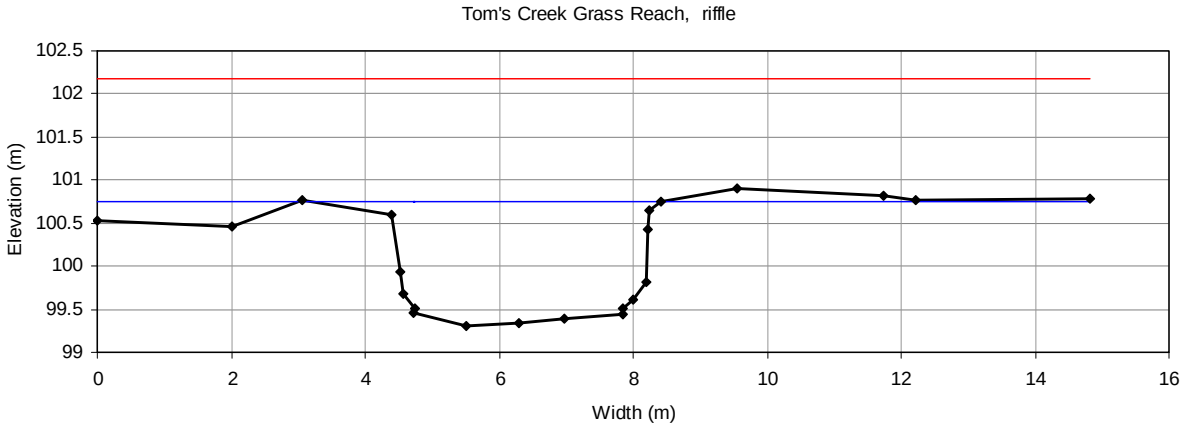


**Figure A.14. Grass cross section 1; Right bank used for analysis. Red line is the flood prone width; blue line indicates top of bank/bankfull.**

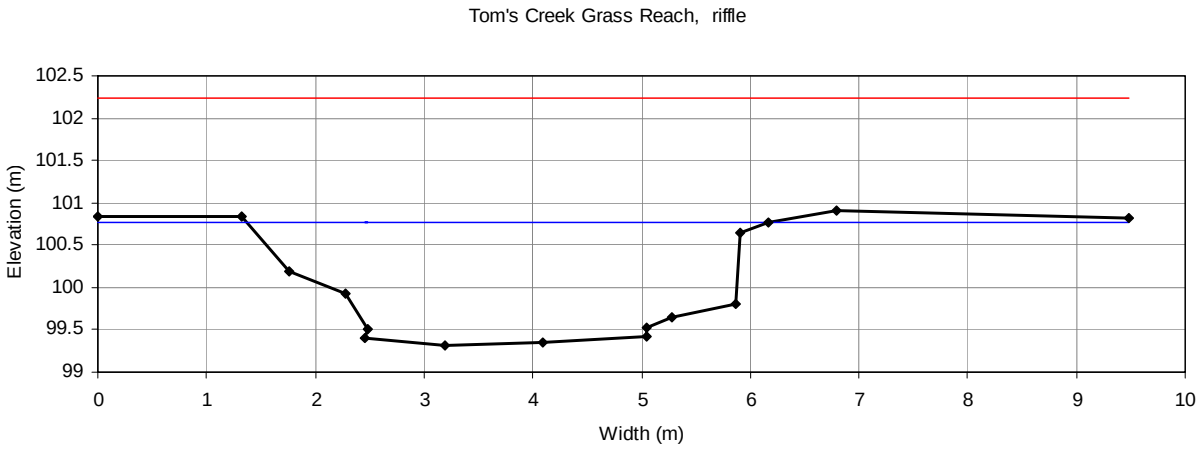


**Figure A.15. Grass cross section 2; Right bank used for analysis. Red line is the flood prone width; blue line indicates top of bank/bankfull.**

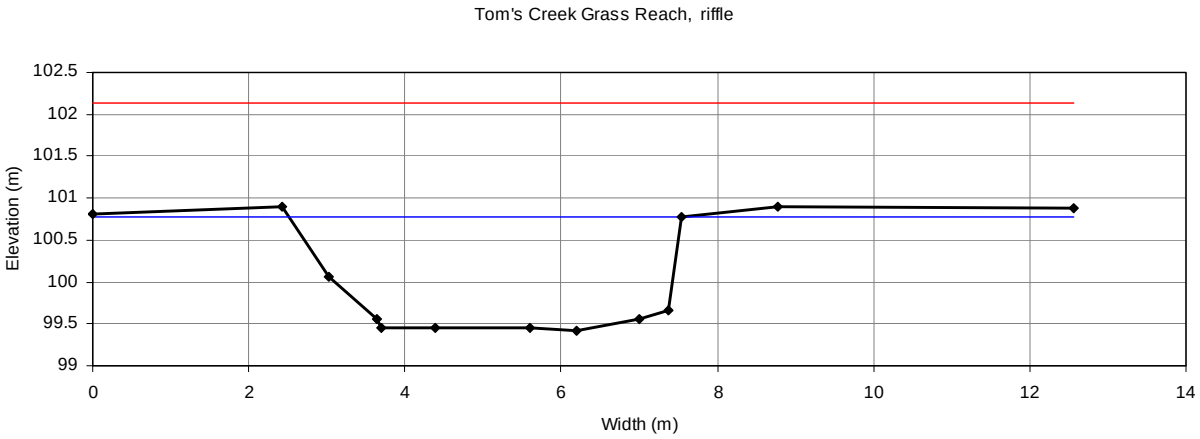


**Figure A.16. Grass cross section 3; Right bank used for analysis. Red line is the flood prone width; blue line indicates top of bank/bankfull.**

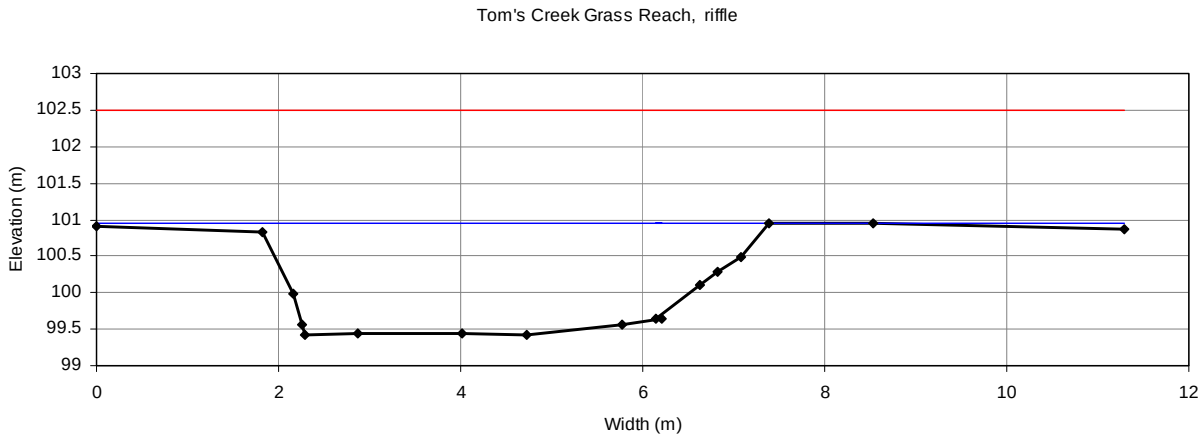


**Figure A.17. Grass cross section 4; Right bank used for analysis. Red line is the flood prone width; blue line indicates top of bank/bankfull.**

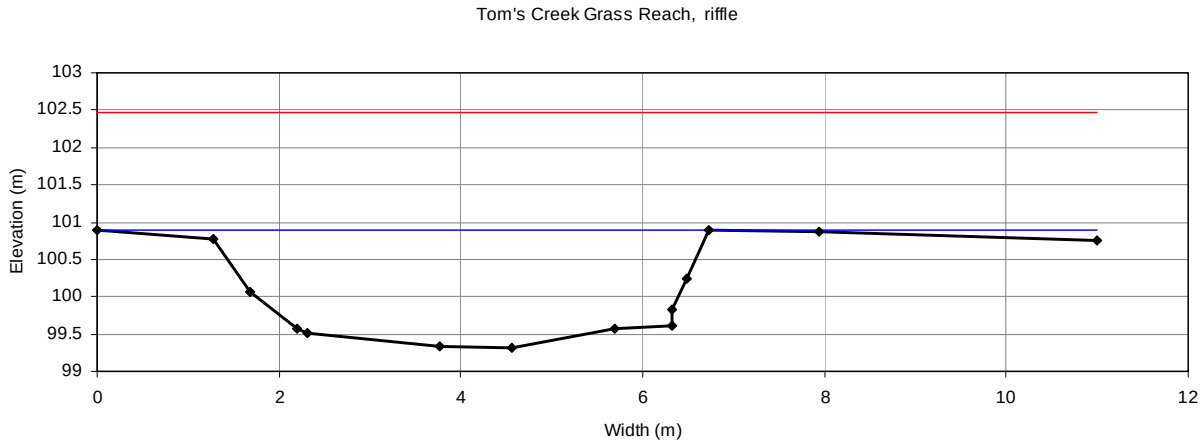


**Figure A.18. Grass cross section 5; Right bank used for analysis. Red line is the flood prone width; blue line indicates top of bank/bankfull.**

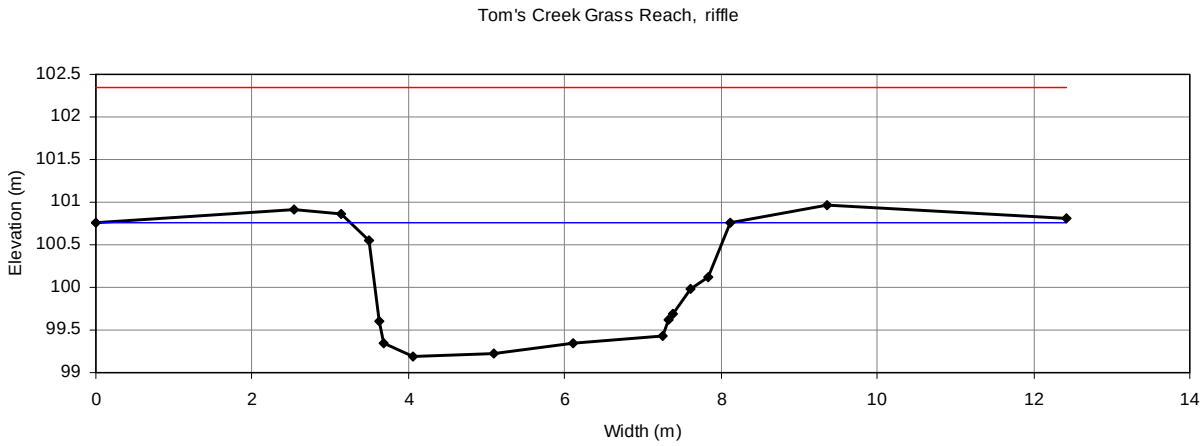


**Figure A.19. Grass cross section 6; Right bank used for analysis. Red line is the flood prone width; blue line indicates top of bank/bankfull.**

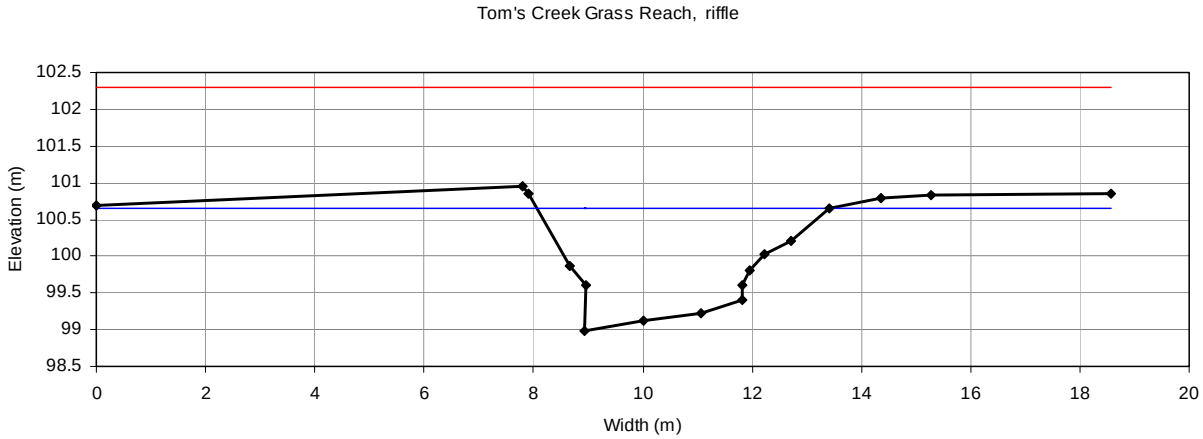


**Figure A.20. Grass cross section 7; Right bank used for analysis. Red line is the flood prone width; blue line indicates top of bank/bankfull.**

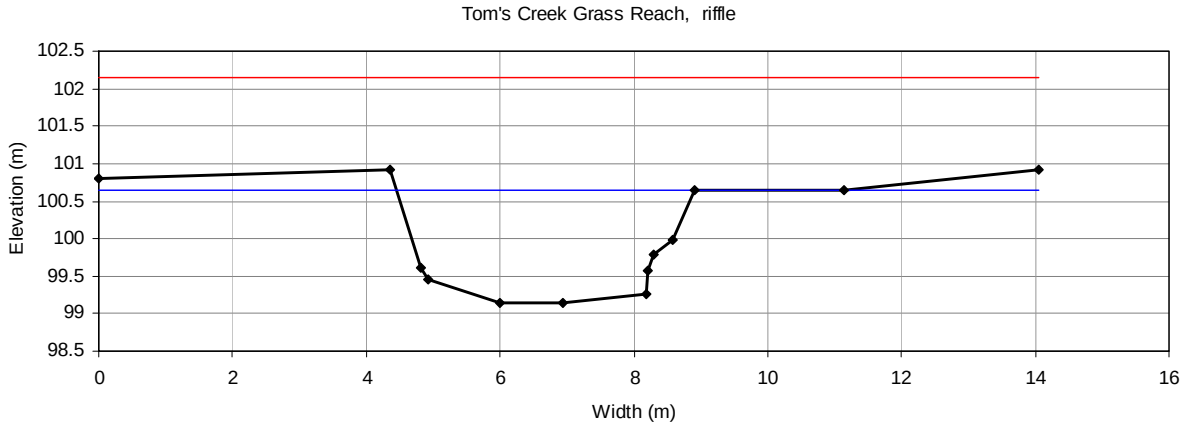


**Figure A.21. Grass cross section 8; Right bank used for analysis. Red line is the flood prone width; blue line indicates top of bank/bankfull**

## A.4 Longitudinal slope

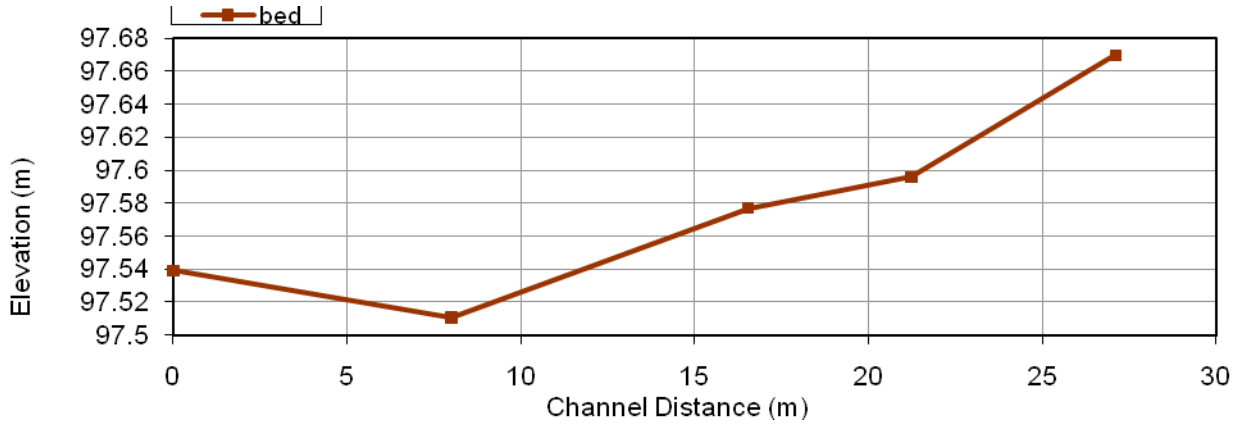


**Figure A.22. Longitudinal survey for tree channel; longitudinal slope was 0.48%.**

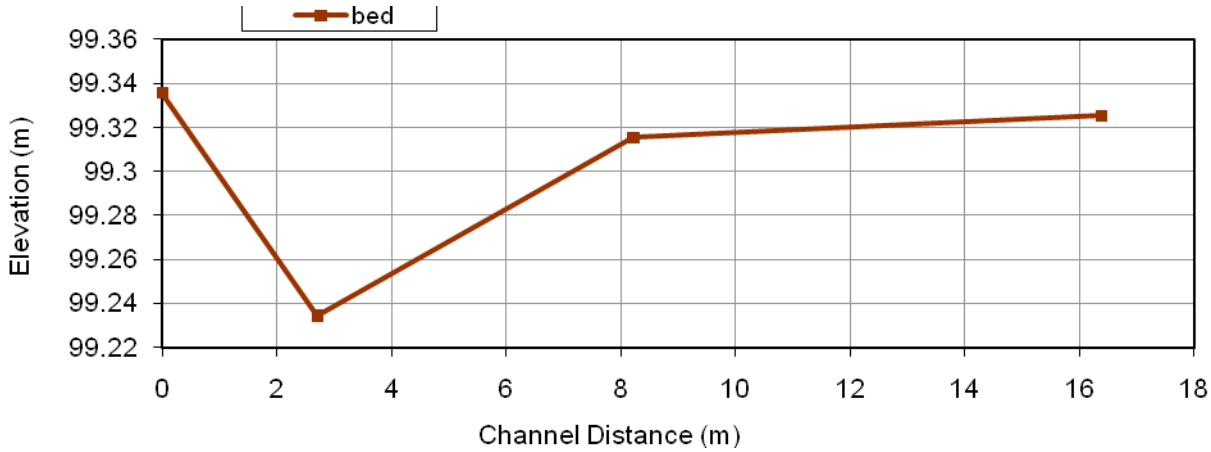


**Figure A. 23. Longitudinal survey for shrub channel; longitudinal slope was 0.06%.**

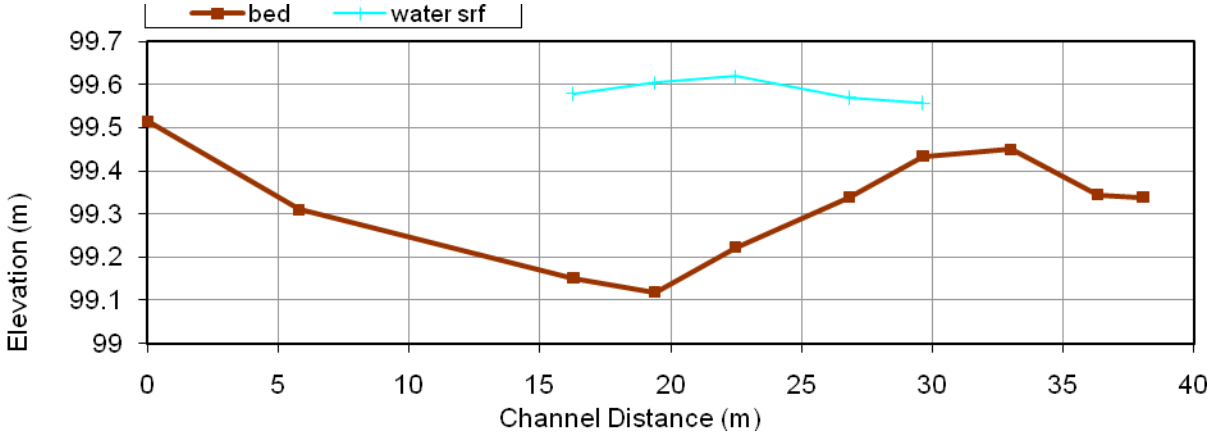


**Figure A.24. Longitudinal survey for grass channel; longitudinal slope was 0.46%.**

## A.5 Particle size analysis

**Table A.1. Tree lower hydrometer readings.**

| Time | Readings R | Blank Hydrometer | Temp C |
|---|---|---|---|
| 30 sec | 54 | 14 | 65.3 |
| 1 min | 49 | 14 | 65.3 |
| 3 min | 43 | 14 | 66.2 |
| 10 min | 36 | 14 | 66.8 |
| 30 min | 31 | 14 | 66.6 |
| 60 min | 26 | 13 | 66.6 |
| 90 min | 24 | 14 | 65.9 |
| 120 min | 23 | 14 | 62.8 |
| 300 min | 22 | 15 | 59.8 |
| 1440 min | 18 | 15 | 62.4 |

**Table A.2. Tree lower sieve weights; total oven dry weight was 97.15 g.**

| Sieve Weights (g) | |
|---|---|
| 10 | 0 |
| 20 | 0.74 |
| 40 | 1.48 |
| 60 | 7.31 |
| 140 | 23.34 |
| 200 | 23.07 |
| pan | 8.39 |

**Table A.3. Tree upper hydrometer readings.**

| Time | Readings R | Blank Hydrometer | Temp C |
|---|---|---|---|
| 30 sec | 50 | 12 | 64.5 |
| 1 min | 42 | 12 | 64.5 |
| 3 min | 37 | 12 | 64.5 |
| 10 min | 31 | 12 | 64.5 |
| 30 min | 24 | 12 | 64.8 |
| 60 min | 21 | 12 | 64.8 |
| 90 min | 20 | 12 | 62.8 |
| 120 min | 20 | 12 | 59 |
| 300 min | 18 | 13 | 59.1 |
| 1440 min | 13 | 11 | 70 |

**Table A.4. Tree upper sieve weights; total oven dry weight was 89.27 g.**

| Sieve Weights (g) | |
|---|---|
| 10 | 0 |
| 20 | 0.75 |
| 40 | 1.97 |
| 60 | 10.88 |
| 140 | 21.27 |
| 200 | 18.27 |
| pan | 6.47 |

**Table A.5. Shrub lower hydrometer readings.**

| Time | Readings R | Blank Hydrometer | Temp C |
|---|---|---|---|
| 30 sec | 52 | 14 | 66.8 |
| 1 min | 49 | 14 | 66.8 |
| 3 min | 44 | 14 | 66.8 |
| 10 min | 38 | 14 | 66.7 |
| 30 min | 33 | 13 | 66.6 |
| 60 min | 29 | 14 | 66.7 |
| 90 min | 27 | 14 | 65.3 |
| 120 min | 26 | 14 | 61 |
| 300 min | 24 | 15 | 59.6 |
| 1440 min | 19 | 15 | 58.8 |

**Table A.6. Shrub lower sieve weights; total oven dry weight was 98.8 g.**

| Sieve Weights (g) | |
|---|---|
| 10 | 0 |
| 20 | 1.04 |
| 40 | 1.76 |
| 60 | 8.6 |
| 140 | 22 |
| 200 | 20.54 |
| pan | 13.35 |

**Table A.7. Shrub upper hydrometer readings.**

| Time | Readings R | Blank Hydrometer | Temp C |
|---|---|---|---|
| 30 sec | 51 | 12 | 62.4 |
| 1 min | 48 | 12 | 62.4 |
| 3 min | 44 | 12 | 61.5 |
| 10 min | 38 | 12 | 60.8 |
| 30 min | 33 | 12 | 59.1 |
| 60 min | 30 | 13 | 58.4 |
| 90 min | 27 | 13 | 57.8 |
| 120 min | 26 | 13 | 58.4 |
| 300 min | 22 | 13 | 60.8 |
| 1440 min | 16 | 12 | 67.2 |

**Table A.8. Shrub upper sieve weights; total oven dry weight was 86.22 g.**

| Sieve Weights (g) | |
|---|---|
| 10 | 0 |
| 20 | 1.28 |
| 40 | 1.76 |
| 60 | 9.06 |
| 140 | 17.75 |
| 200 | 15.76 |
| pan | 5.09 |

**Table A.9. Grass lower hydrometer readings.**

| Time | Readings R | Blank Hydrometer | Temp C |
|---|---|---|---|
| 30 sec | 45 | 14 | 66.8 |
| 1 min | 41 | 14 | 66.8 |
| 3 min | 35 | 13 | 66.8 |
| 10 min | 30 | 13 | 66.8 |
| 30 min | 26 | 14 | 66.7 |
| 60 min | 23 | 14 | 65.3 |
| 90 min | 22 | 14 | 61 |
| 120 min | 21 | 15 | 59.4 |
| 300 min | 19 | 15 | 63.5 |
| 1440 min | 15 | 15 | 64.8 |

**Table A.10. Grass lower sieve weights; total oven dry weight was 99.7 g.**

| Sieve Weights (g) | |
|---|---|
| 10 | 0 |
| 20 | 1.01 |
| 40 | 3.82 |
| 60 | 20.09 |
| 140 | 24.54 |
| 200 | 19.28 |
| pan | 11.11 |

**Table A.11. Grass upper hydrometer readings.**

| Time | Readings R | Blank Hydrometer | Temp C |
|---|---|---|---|
| 30 sec | 42 | 13 | 59.5 |
| 1 min | 41 | 13 | 59.5 |
| 3 min | 36 | 13 | 58.8 |
| 10 min | 32 | 13 | 58.6 |
| 30 min | 27 | 13 | 58.5 |
| 60 min | 24 | 13 | 58.2 |
| 90 min | 22 | 13 | 58.4 |
| 120 min | 22 | 13 | 58.5 |
| 300 min | 19 | 13 | 64 |
| 1440 min | 15 | 13 | 65.5 |

**Table A.12. Grass upper sieve weights; total oven dry weight was 83.38 g.**

| Sieve Weights (g) | |
|---|---|
| 10 | 0 |
| 20 | 1.07 |
| 40 | 1.94 |
| 60 | 11.28 |
| 140 | 21.22 |
| 200 | 15.98 |
| pan | 5.72 |

## A.6 Pebble count

**Table A.13. Description of Wolman (1954) pebble count for tree, shrub, and grass channel.**

| Particle Size (mm) | Particle Count | | | | | |
|---|---|---|---|---|---|---|
| | Tree | | Shrub | | Grass | |
| | Riffle | Pool | Riffle | Pool | Riffle | Pool |
| 1 - 2 | 1 | 26 | 0 | 14 | 1 | 35 |
| 2 - 4 | 1 | 3 | 1 | 13 | 2 | 4 |
| 4 - 6 | 1 | 3 | 0 | 5 | 6 | 8 |
| 6 - 8 | 2 | 4 | 2 | 3 | 8 | 9 |
| 8 - 11 | 5 | 12 | 4 | 8 | 8 | 4 |
| 11 - 16 | 5 | 12 | 3 | 5 | 19 | 10 |
| 16 - 22 | 13 | 17 | 14 | 5 | 20 | 7 |
| 22 - 32 | 15 | 6 | 4 | 7 | 13 | 11 |
| 32 - 45 | 21 | 4 | 18 | 14 | 9 | 4 |
| 45 - 64 | 18 | 2 | 18 | 13 | 8 | 5 |
| 64 - 90 | 10 | 9 | 23 | 11 | 6 | 1 |
| 90 - 128 | 6 | 1 | 11 | 3 | 0 | 1 |
| 128 - 180 | 1 | 1 | 2 | 0 | 0 | 1 |
| 180 - 256 | 1 | 0 | 0 | 0 | 0 | 0 |

## A.7 Vegetation characteristics

**Table A.14. Three stem counts of shrub stems along six locations of the shrub streambank within a 20.3-cm diameter circle.**

| Ring | Stem Count | | |
|---|---|---|---|
| | 1 | 2 | 3 |
| 1 | 13 | 13 | 13 |
| 2 | 9 | 9 | 9 |
| 3 | 7 | 7 | 7 |
| 4 | 13 | 13 | 13 |
| 5 | 13 | 13 | 13 |
| 6 | 8 | 8 | 8 |

**Table A.15. Measured diameter of three collected shrub samples from locations 2-6 along the shrub streambank.**

| Location | Diameter (cm) | | |
|---|---|---|---|
| | 1 | 2 | 3 |
| 2 | 0.51 | 0.25 | 0.25 |
| 3 | 0.89 | 1.02 | 0.38 |
| 4 | 0.64 | 1.14 | 0.76 |
| 5 | 0.25 | 0.64 | 0.51 |
| 6 | 0.51 | 0.25 | 0.51 |

**Table A.16. Three stem counts of grass stems along five locations of the grass streambank within a 20.3-cm diameter circle. Stems were cut and counted in each location. Stems were not cut in location 1.**

| Location | Cut count | Stem Count | | |
|---|---|---|---|---|
| | | 1 | 2 | 3 |
| 1 | NA | 30 | 32 | 32 |
| 2 | 22 | 30 | 33 | 31 |
| 3 | 36 | 38 | 36 | 34 |
| 4 | 47 | 48 | 51 | 47 |
| 5 | 25 | 22 | 24 | 24 |

**Table A.17. Stem count and cut count of grass stems at three mass wasted locations along the grass streambank.**

| Mass Waste | | Stem Count | | |
|---|---|---|---|---|
| Location | Cut count | 1 | 2 | 3 |
| 1 | 188 | too high to count stems | | |
| 2 | 41 | 47 | 51 | 47 |
| 3 | 56 | 55 | 55 | 59 |

**Table A.18. Stem length (cm) and surface area ($cm^2$) of grass stems collected from the grass streambank.**

| Grass ID | Length (cm) | Surface Area ($cm^2$) |
|---|---|---|
| 1 | 49 | 47.8 |
| 2 | 56 | 97.54 |
| 3 | 37 | 37.59 |
| 4 | 84 | 75.39 |
| 5 | 30 | 61.57 |
| 6 | 38 | 59.4 |
| 7 | 29 | 34.9 |
| 8 | 73 | 83.74 |
| 9 | 24 | 26.45 |
| 10 | 30 | 18.79 |
| 11 | 17 | 40.26 |
| 12 | 61 | 123.69 |
| 13 | 20 | 13.46 |
| 14 | 16 | 14.13 |
| 15 | 26 | 38.01 |
| 16 | 11 | 17.68 |
| 17 | 30 | 31.87 |
| 18 | 65 | 75.68 |
| 19 | 47 | 32.83 |
| 20 | 81 | 80.64 |

# Appendix B: Dimensionless Analysis-Flow with a Free Surface (Buckingham Pi Theorem)

## Important Variables

$R_h$=hydraulic radius (L)
$V_{den}$=vegetation density ($L^2/L^2$)
$\mu$=dynamic viscosity ($FL^{-2}T$)
$\rho$=water density ($FL^{-4}T^2$)
$S_{bed}$=bed slope (L/L)
$S_{bank}$=bank slope (L/L)
U=depth-averaged velocity ($LT^{-1}$)
g=acceleration due to gravity ($LT^{-2}$)
$k_{s,bank}$=bank grain roughness, $D_{84}$ (L)
$k_{s,bed}$=bed grain roughness, $D_{84}$ (L)

Analysis ignores vegetation flexibility
Ignores surface tension effects
Assume same fluid between prototype and model
Vegetation roughness quantified by density (% coverage on bank)

**Seven Pi terms** (10-3)

**Repeating Variables:** $\rho$, $R_h$, U

## Form Pi terms

$V_{den}$, $S_{bed}$, and $S_{bank}$ are already dimensionless
$\mu$ results in Reynolds number ($II_4=\rho R_h U/\mu$=Re)
g results in Froude number ($II_5=U/\sqrt{(gR_h)}$ =Fr)
$k_{s,bank}$ results in $II_6=k_{s,bank}/R_h$
$k_{s,bed}$ results in $II_7=k_{s,bed}/R_h$

## Final form and assumptions

Dependent Pi Term=$\Theta(V_{den}, S_{bed}, S_{bank}, Re, Fr, k_{s,bank}/R_h, k_{s,bed}/R_h)$

- Drop Reynolds number; Reynolds numbers are large so viscous forces are small in comparison to the forces due to gravity and inertia. Base the model on Froude similarity. Make sure the Reynolds number is large (>500) but does not need to equal that of the prototype.

Dependent Pi Term = $\Theta(V_{den}, S_{bed}, S_{bank}, Fr, k_{s,bank}/R_h, k_{s,bed}/R_h)$

# Appendix C: CTA Calibration Curves

Calibration curves used for CTA measurements:

**090209_Calibration 2**
General model Power2:
f(x) = a*x^b+c
Coefficients (with 95% confidence bounds):
a = 0.3085 (0.0877, 0.5293)
b = 0.3108 (0.153, 0.4687)
c = 0.4683 (0.2384, 0.6982)
Goodness of fit:
SSE: 0.02501
R-square: 0.9601
Adjusted R-square: 0.9586
RMSE: 0.02193

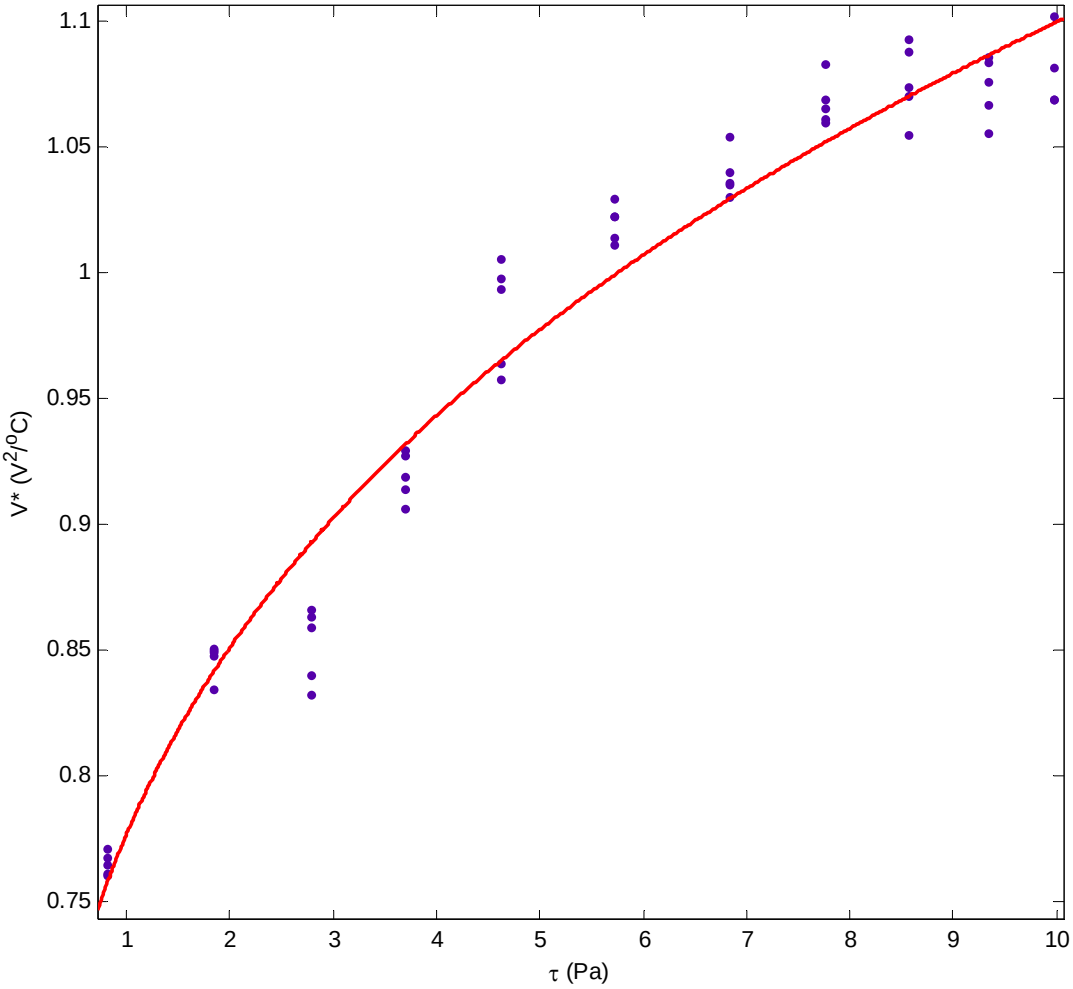


**Figure C.1. CTA calibration curve: 090209_Calibration 2.**

**090210_Calibration 2**
General model Power2:
f(x) = a*x^b+c
Coefficients (with 95% confidence bounds):
a = -0.6622 (-0.8646, -0.4599)
b = -0.2085 (-0.2851, -0.1319)
c = 1.296 (1.094, 1.497)

Goodness of fit:
SSE: 0.005564
R-square: 0.9896
Adjusted R-square: 0.9891
RMSE: 0.01045

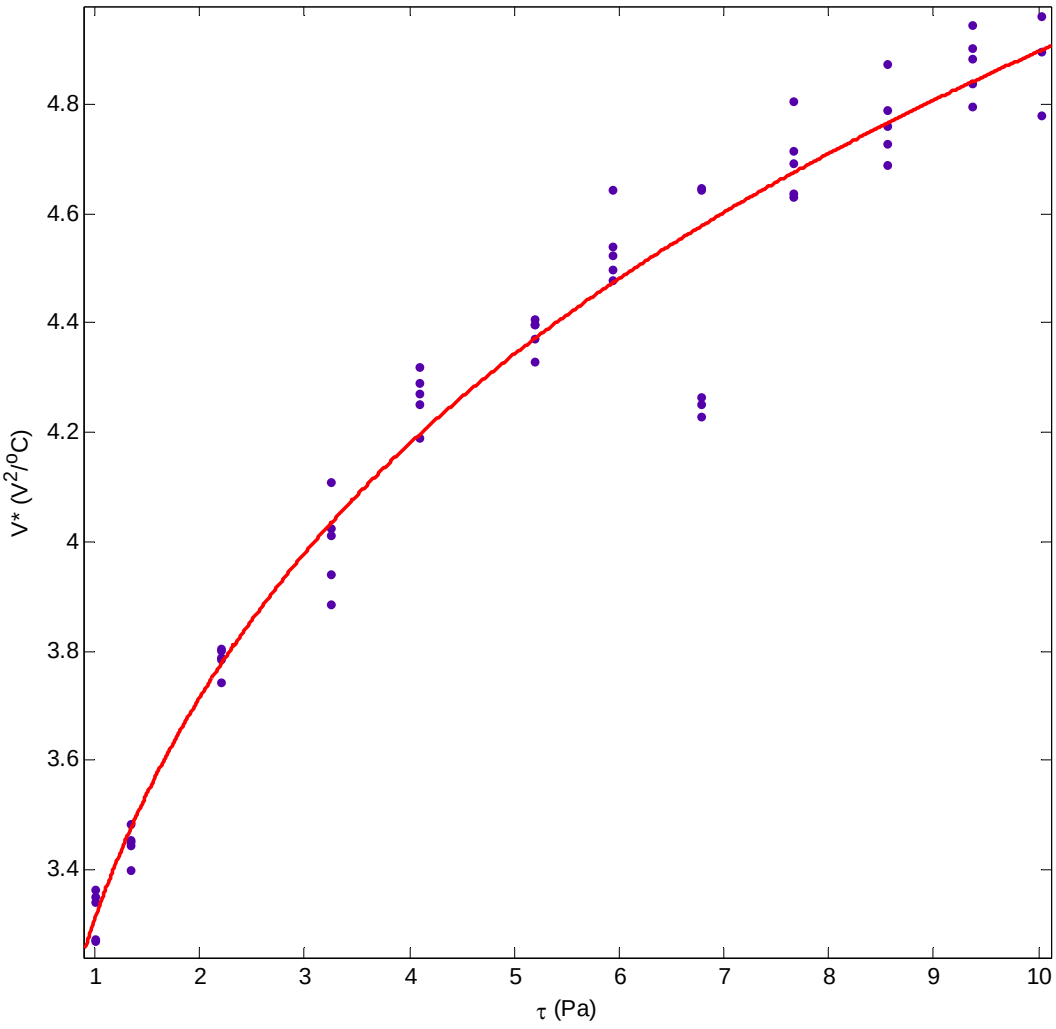


**Figure C.2. CTA calibration curve: 090210_Calibration 2.**

**090305_Calibration 1**
General model Power2:
f(x) = a*x^b+c
Coefficients (with 95% confidence bounds):
a = 43.75 (3.913, 83.59)
b = 0.1993 (0.05339, 0.3452)
c = -7.889 (-48.27, 32.49)

Goodness of fit:
SSE: 166.8
R-square: 0.9637
Adjusted R-square: 0.9624
RMSE: 1.71

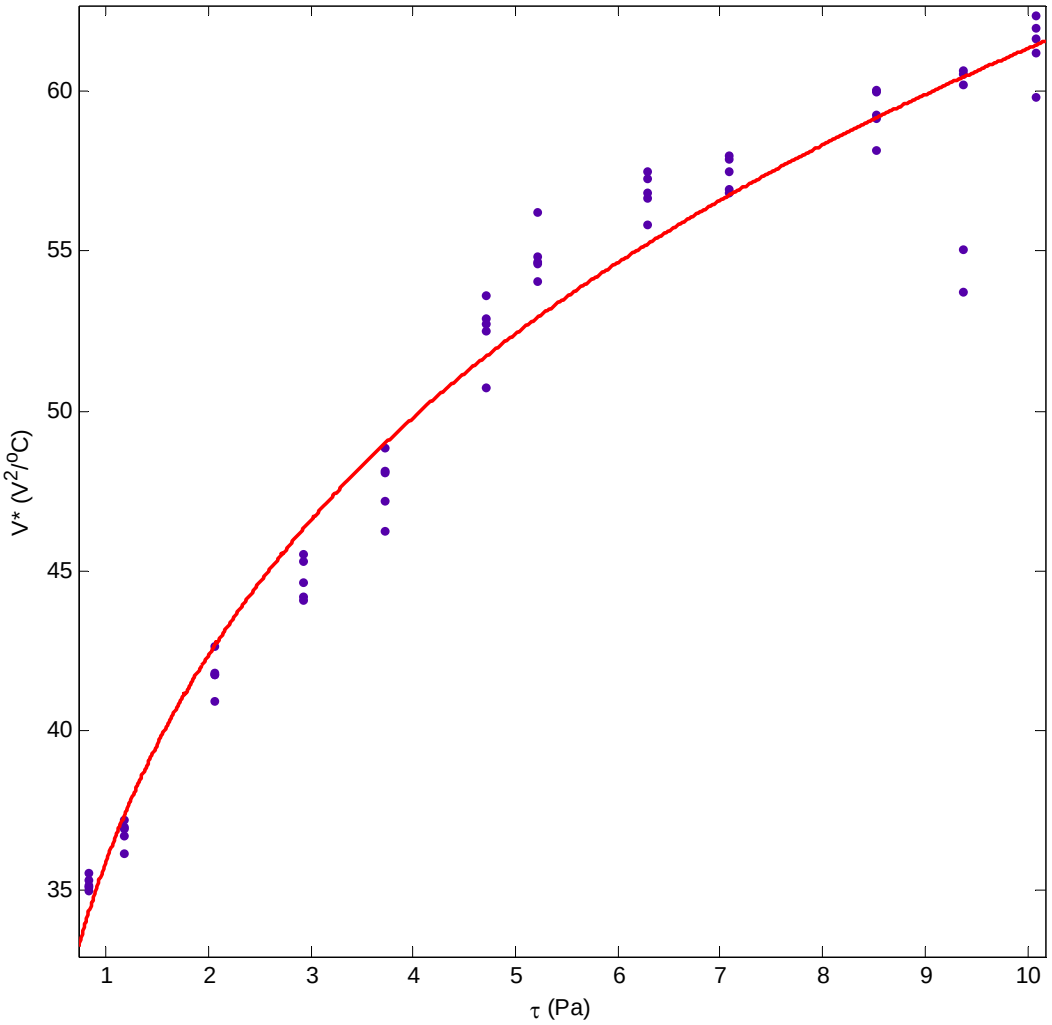


**Figure C.3. CTA calibration curve: 090305_Calibration 1.**

**090305_Calibration 2**
General model Power2:
f(x) = a*x^b+c
Coefficients (with 95% confidence bounds):
a = 24.06 (9.469, 38.65)
b = 0.1703 (0.0837, 0.2569)
c = -6.805 (-21.48, 7.865)
Goodness of fit:
SSE: 16.49
R-square: 0.984
Adjusted R-square: 0.9834
RMSE: 0.5379

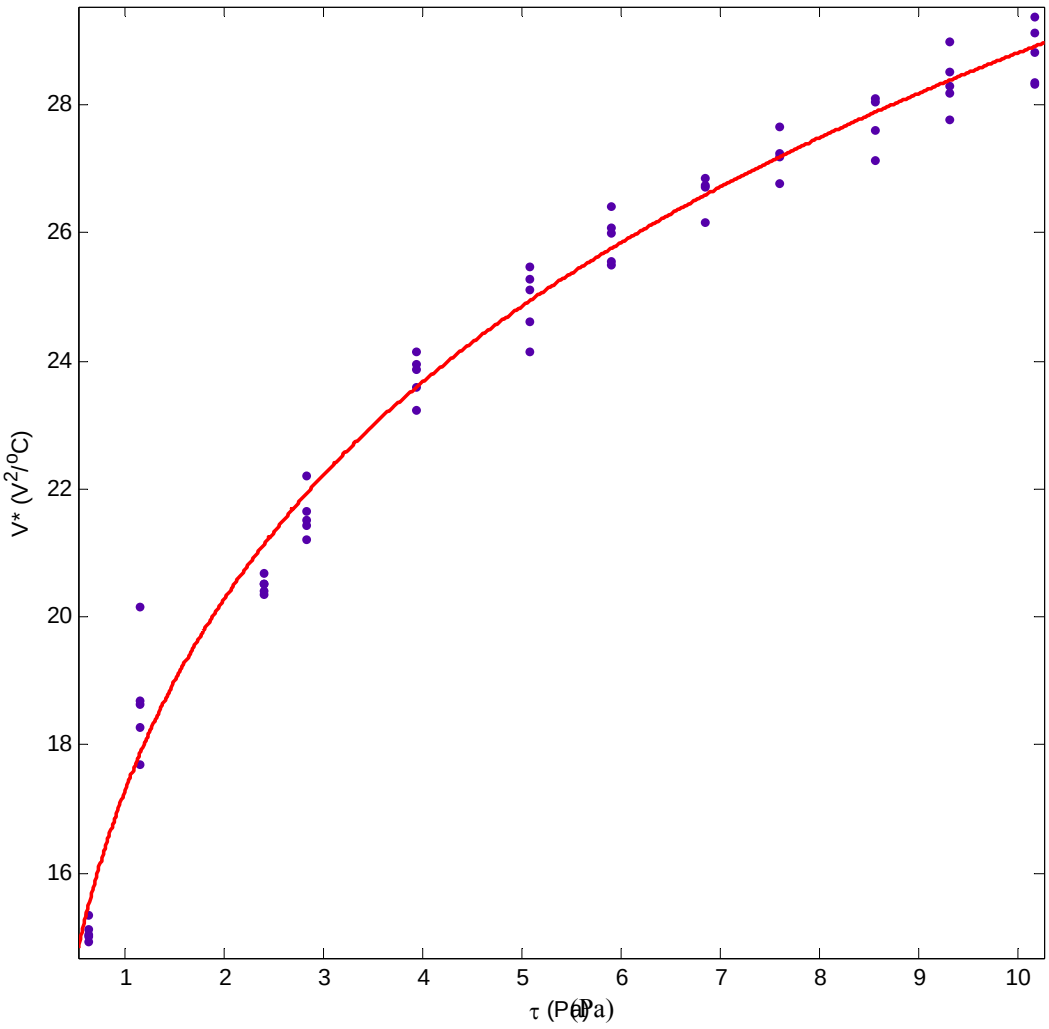


**Figure C.4. CTA calibration curve: 090305_Calibration 2.**

**090306_Calibration 2**
General model Power2:
f(x) = a*x^b+c
Coefficients (with 95% confidence bounds):
a = -9.977 (-36.32, 16.37)
b = -0.07803 (-0.3014, 0.1454)
c = 13.05 (-13.31, 39.41)
Goodness of fit:
SSE: 2.123
R-square: 0.9083
Adjusted R-square: 0.905
RMSE: 0.1965

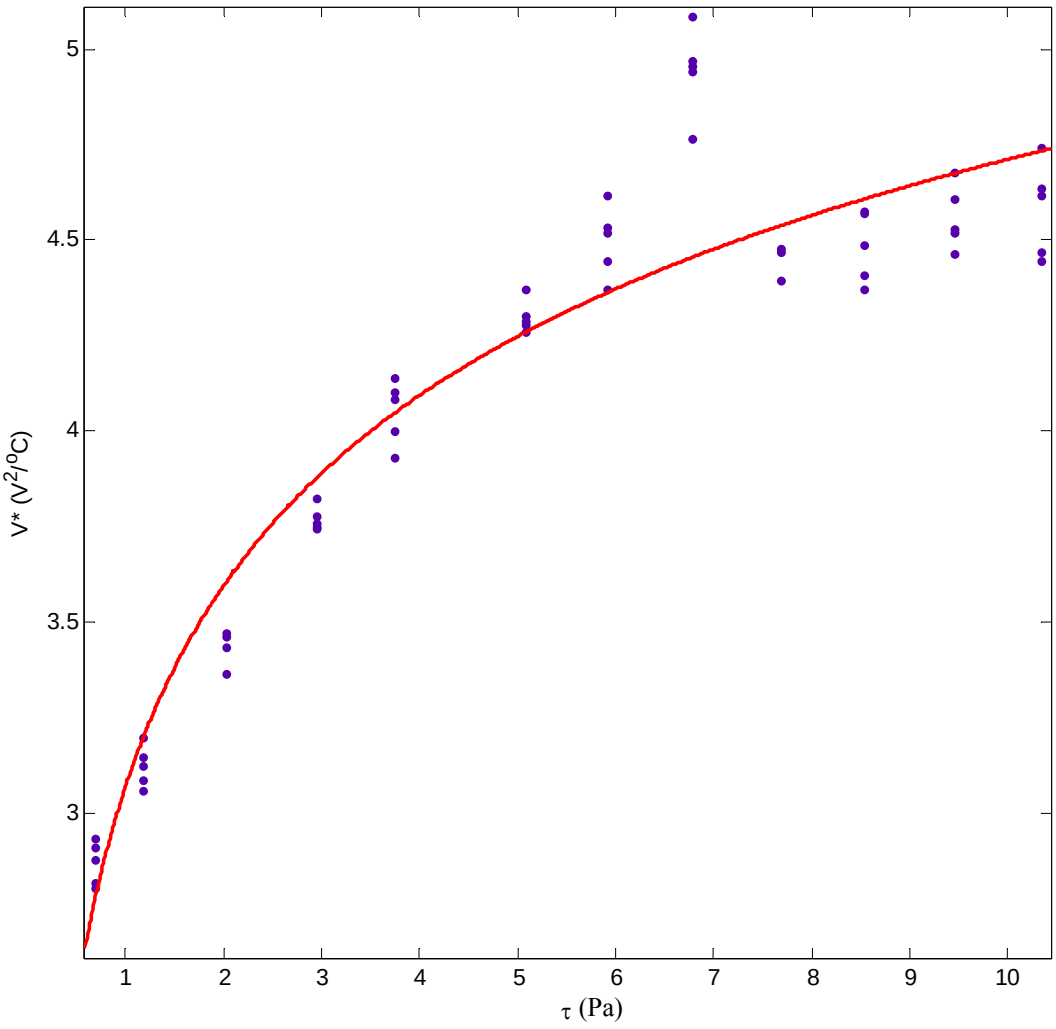


**Figure C.5. CTA calibration curve: 090306_Calibration 2.**

**090306_Calibration 3**
General model Power2:
f(x) = a*x^b+c
Coefficients (with 95% confidence bounds):
a = 1.19 (0.3747, 2.005)
b = 0.2901 (0.1455, 0.4347)
c = 0.6481 (-0.1922, 1.488)

Goodness of fit:
SSE: 0.3071
R-square: 0.9679
Adjusted R-square: 0.9668
RMSE: 0.0734

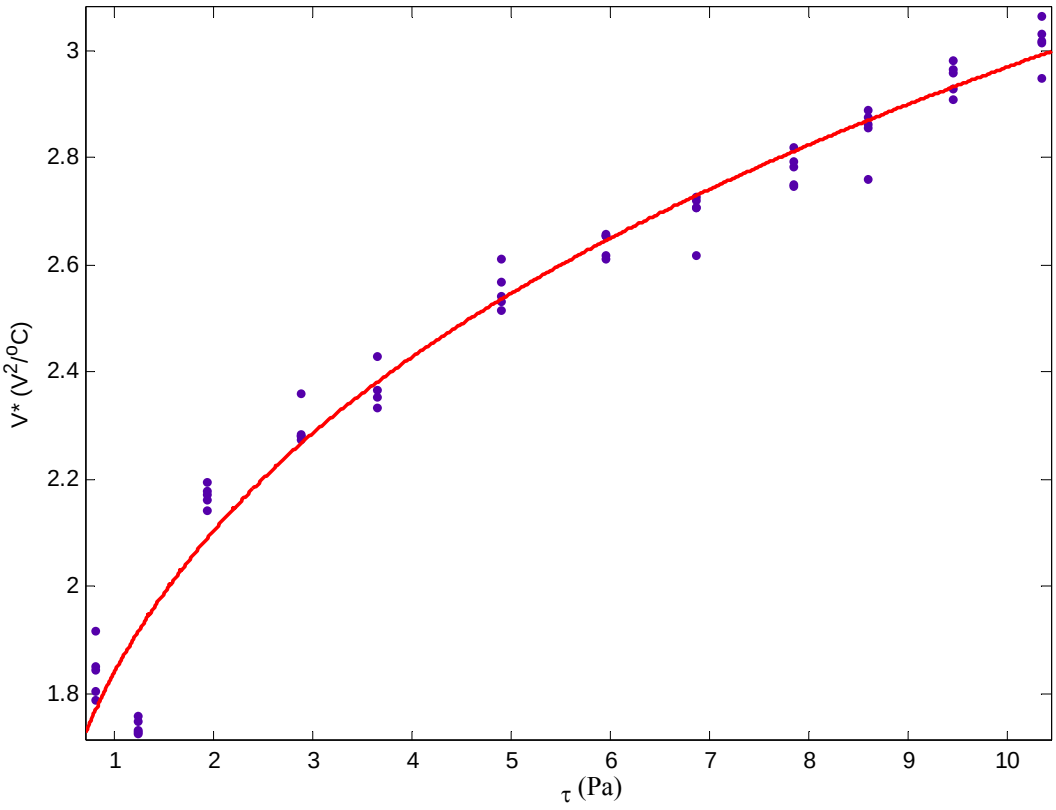


**Figure C.6. CTA calibration curve: 090306_Calibration 3.**

**090310_Calibration 1**
General model Power2:
f(x) = a*x^b+c
Coefficients (with 95% confidence bounds):
a = 1.34 (0.7193, 1.96)
b = 0.228 (0.1452, 0.3107)
c = 0.4072 (-0.2224, 1.037)

Goodness of fit:
SSE: 0.07985
R-square: 0.9874
Adjusted R-square: 0.9869
RMSE: 0.03743

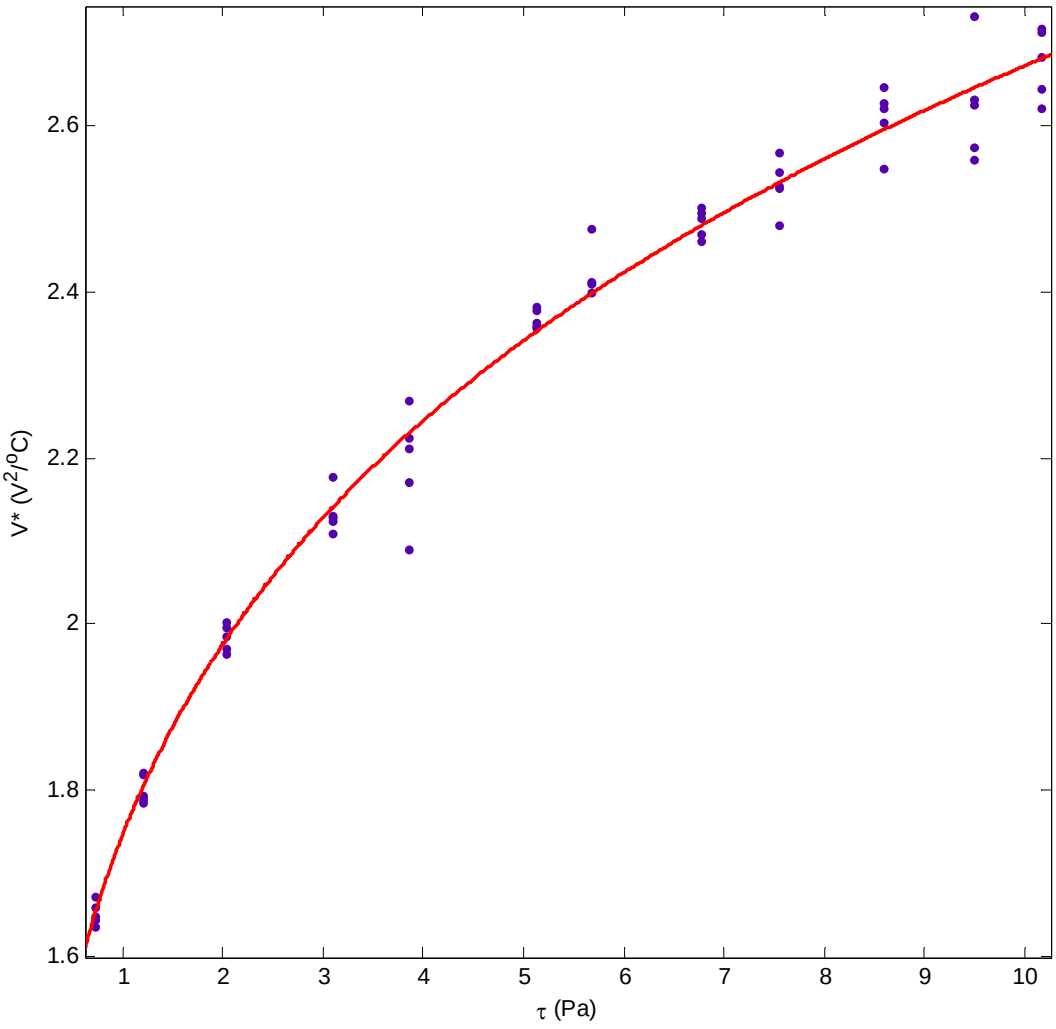


**Figure C.7. CTA calibration curve: 090310_Calibration 1.**

**090310_Calibration 1_repeat**
General model Power2:
f(x) = a*x^b+c
Coefficients (with 95% confidence bounds):
a = 1.777 (0.6487, 2.906)
b = 0.1177 (0.05042, 0.1849)
c = -0.4784 (-1.606, 0.6493)

Goodness of fit:
SSE: 0.02432
R-square: 0.99
Adjusted R-square: 0.9896
RMSE: 0.02163

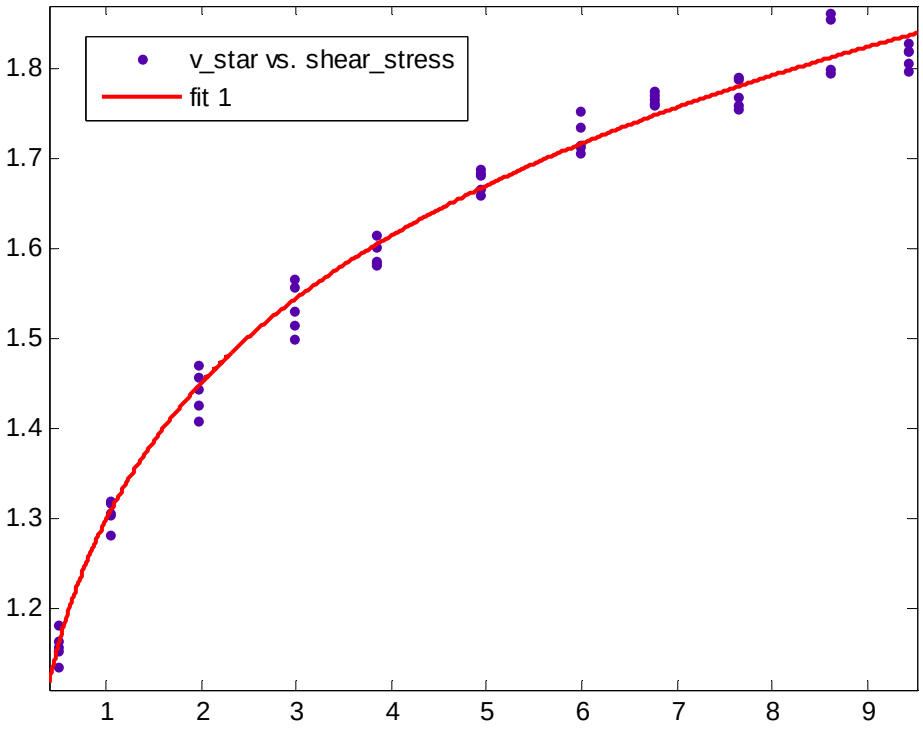


**Figure C.8. CTA calibration curve: 090310_Calibration 1_repeat.**

# Appendix D: Boundary shear stress to determine field method

**Table D.1. Boundary shear stress measured with the CTA and estimated with the law of the wall, Reynolds, and turbulent kinetic energy methods along the bare bank**

| | | | Boundary Shear Stress (Pa) | | | | | | | | | | |
|---|---|---|---|---|---|---|---|---|---|---|---|---|---|
| Location | x (cm) | y (cm) | $\tau_{CTA,Avg}$ | $\tau_{LOW, ADV}$ | $\tau_{LOW, ADV, 20\%}$ | $\tau_{LOW, MP}$ | $\tau_{LOW,MP,20\%}$ | $\tau_{uv}$ | $\tau_{uw}$ | $\tau_{vw}$ | $\tau_{uv, extrap}$ | $\tau_{uw, extrap}$ | $\tau_{vw, extrap}$ |
| A3 | 5 | 5.9 | 0.54 | 0.45 | 0.20 | 0.50 | 0.09 | 0.21 | 0.25 | 0.23 | 0.31 | 0.16 | 0.09 |
| B3 | 10 | 5.9 | 0.49 | 0.46 | 0.26 | 0.48 | 0.11 | 0.14 | 0.20 | 0.21 | 0.29 | 0.13 | 0.09 |
| C3 | 15 | 5.9 | 0.63 | 0.53 | 0.45 | 0.43 | 0.09 | 0.13 | 0.15 | 0.22 | 0.29 | 0.12 | 0.13 |
| D3 | 20 | 5.9 | 0.69 | 0.49 | 0.36 | 0.50 | 0.09 | 0.32 | 0.03 | 0.21 | 0.28 | 0.12 | 0.09 |
| E3 | 25 | 5.9 | 0.71 | 0.56 | 0.67 | 0.49 | 0.11 | 0.44 | -0.23 | 0.36 | 0.31 | 0.08 | 0.12 |
| A4 | 5 | 10.9 | 0.41 | 0.29 | 0.10 | 0.35 | 0.06 | 0.32 | 0.04 | 0.19 | 0.15 | 0.15 | 0.13 |
| B4 | 10 | 10.9 | 0.42 | 0.29 | 0.10 | 0.34 | 0.04 | 0.20 | 0.15 | 0.16 | 0.16 | 0.18 | 0.12 |
| C4 | 15 | 10.9 | 0.66 | 0.30 | 0.16 | 0.35 | 0.06 | 0.19 | 0.18 | 0.24 | 0.19 | 0.15 | 0.14 |
| D4 | 20 | 10.9 | 0.83 | 0.29 | 0.16 | 0.35 | 0.09 | 0.21 | 0.05 | 0.26 | 0.19 | 0.15 | 0.15 |
| E4 | 25 | 10.9 | 0.66 | 0.35 | 0.33 | 0.32 | 0.11 | 0.22 | 0.09 | 0.24 | 0.19 | 0.14 | 0.14 |
| A5 | 5 | 15.9 | 0.48 | 0.08 | 0.11 | 0.12 | 0.06 | -0.05 | 0.24 | 0.11 | -0.13 | 0.33 | 0.08 |
| B5 | 10 | 15.9 | 0.49 | 0.05 | 0.04 | 0.11 | 0.07 | -0.02 | 0.26 | 0.10 | -0.10 | 0.30 | 0.06 |
| C5 | 15 | 15.9 | 0.58 | 0.12 | 0.10 | 0.13 | 0.06 | -0.03 | 0.26 | 0.13 | -0.11 | 0.31 | 0.08 |
| D5 | 20 | 15.9 | 0.56 | 0.08 | 0.17 | 0.11 | 0.06 | -0.01 | 0.24 | 0.09 | -0.11 | 0.33 | 0.05 |
| E5 | 25 | 15.9 | 0.48 | 0.08 | 0.05 | 0.28 | 0.04 | 0.04 | 0.24 | 0.11 | -0.10 | 0.28 | 0.06 |
| A6 | 5 | 20.9 | 0.78 | 0.14 | 0.08 | 0.23 | 0.09 | 0.16 | 0.23 | 0.18 | 0.23 | 0.23 | 0.14 |
| B6 | 10 | 20.9 | 0.66 | 0.16 | 0.10 | 0.22 | 0.18 | 0.12 | 0.20 | 0.14 | 0.22 | 0.25 | 0.13 |
| C6 | 15 | 20.9 | 0.19 | 0.16 | 0.10 | 0.20 | 0.20 | 0.19 | 0.21 | 0.13 | 0.25 | 0.25 | 0.10 |
| D6 | 20 | 20.9 | 0.59 | 0.18 | 0.13 | 0.18 | 0.15 | 0.14 | 0.16 | 0.14 | 0.20 | 0.20 | 0.11 |
| E6 | 25 | 20.9 | 0.45 | 0.14 | 0.09 | 0.17 | 0.13 | 0.19 | 0.11 | 0.14 | 0.24 | -0.20 | 0.11 |

| | | | Boundary Shear Stress (Pa) | | | | | | | | | | | |
|---|---|---|---|---|---|---|---|---|---|---|---|---|---|---|
| Location | x (cm) | y (cm) | $\tau_{TKE}$ | $\tau_{TKE, extrap}$ | $\tau_{TKE, w}$ | $\tau_{TKE, w, extrap}$ | $\tau_{uv,2cm}$ | $\tau_{uw,2cm}$ | $\tau_{vw,2cm}$ | $\tau_{TKE,2cm}$ | $\tau_{uv,4cm}$ | $\tau_{uw,4cm}$ | $\tau_{vw,4cm}$ | $\tau_{TKE,4cm}$ |
| A3 | 5 | 5.9 | 0.25 | 0.25 | 0.46 | 0.49 | 0.27 | 0.10 | 0.09 | 0.22 | 0.26 | 0.16 | 0.07 | 0.23 |
| B3 | 10 | 5.9 | 0.22 | 0.25 | 0.42 | 0.48 | 0.20 | 0.20 | 0.08 | 0.22 | 0.30 | 0.10 | 0.08 | 0.22 |
| C3 | 15 | 5.9 | 0.21 | 0.24 | 0.45 | 0.50 | 0.21 | 0.10 | 0.12 | 0.20 | 0.30 | 0.07 | 0.10 | 0.21 |
| D3 | 20 | 5.9 | 0.22 | 0.23 | 0.42 | 0.47 | 0.24 | 0.14 | 0.06 | 0.20 | 0.27 | 0.04 | 0.06 | 0.22 |
| E3 | 25 | 5.9 | 0.27 | 0.24 | 0.72 | 0.51 | 0.29 | 0.13 | 0.11 | 0.22 | 0.36 | 0.02 | 0.05 | 0.23 |
| A4 | 5 | 10.9 | 0.19 | 0.21 | 0.40 | 0.47 | 0.00 | 0.24 | 0.16 | 0.19 | 0.15 | 0.26 | 0.07 | 0.23 |
| B4 | 10 | 10.9 | 0.18 | 0.21 | 0.36 | 0.44 | 0.08 | 0.27 | 0.16 | 0.23 | 0.18 | 0.15 | 0.09 | 0.19 |
| C4 | 15 | 10.9 | 0.21 | 0.21 | 0.44 | 0.47 | 0.24 | 0.13 | 0.12 | 0.19 | 0.20 | 0.12 | 0.07 | 0.20 |
| D4 | 20 | 10.9 | 0.20 | 0.21 | 0.44 | 0.47 | 0.26 | 0.11 | 0.15 | 0.20 | 0.14 | 0.17 | 0.09 | 0.20 |
| E4 | 25 | 10.9 | 0.21 | 0.20 | 0.41 | 0.46 | 0.17 | 0.13 | 0.12 | 0.19 | 0.12 | 0.23 | 0.10 | 0.21 |
| A5 | 5 | 15.9 | 0.18 | 0.21 | 0.28 | 0.36 | -0.08 | 0.31 | 0.04 | 0.20 | -0.06 | 0.31 | 0.03 | 0.21 |
| B5 | 10 | 15.9 | 0.18 | 0.20 | 0.31 | 0.34 | -0.10 | 0.27 | 0.05 | 0.19 | -0.10 | 0.30 | -0.02 | 0.19 |
| C5 | 15 | 15.9 | 0.18 | 0.20 | 0.34 | 0.37 | -0.06 | 0.25 | 0.05 | 0.18 | -0.08 | 0.28 | 0.02 | 0.19 |
| D5 | 20 | 15.9 | 0.17 | 0.21 | 0.28 | 0.36 | -0.04 | 0.33 | 0.03 | 0.22 | -0.19 | 0.30 | 0.04 | 0.22 |
| E5 | 25 | 15.9 | 0.17 | 0.19 | 0.30 | 0.32 | -0.12 | 0.30 | 0.05 | 0.20 | -0.18 | 0.27 | 0.04 | 0.20 |
| A6 | 5 | 20.9 | 0.24 | 0.24 | 0.42 | 0.42 | 0.20 | 0.15 | 0.10 | 0.21 | 0.05 | 0.17 | 0.04 | 0.15 |
| B6 | 10 | 20.9 | 0.19 | 0.23 | 0.38 | 0.41 | 0.18 | 0.21 | 0.09 | 0.19 | 0.09 | 0.12 | 0.04 | 0.13 |
| C6 | 15 | 20.9 | 0.20 | 0.23 | 0.36 | 0.38 | 0.18 | 0.16 | 0.07 | 0.18 | 0.17 | 0.16 | 0.02 | 0.17 |
| D6 | 20 | 20.9 | 0.19 | 0.21 | 0.34 | 0.35 | 0.17 | 0.21 | 0.07 | 0.19 | 0.03 | 0.18 | 0.04 | 0.14 |
| E6 | 25 | 20.9 | 0.19 | 0.22 | 0.35 | 0.39 | 0.15 | 0.17 | 0.08 | 0.18 | 0.14 | 0.17 | 0.02 | 0.17 |

**Table D.2. Boundary shear stress measured with the CTA and estimated with the law of the wall, Reynolds, and turbulent kinetic energy methods along the tree bank**

| | | | Boundary Shear Stress (Pa) | | | | | | | | | | |
|---|---|---|---|---|---|---|---|---|---|---|---|---|---|
| Location | x (cm) | y (cm) | $\tau_{CTA,Avg}$ | $\tau_{LOW, ADV}$ | $\tau_{LOW, ADV, 20\%}$ | $\tau_{LOW, MP}$ | $\tau_{LOW,MP,20\%}$ | $\tau_{uv}$ | $\tau_{uw}$ | $\tau_{vw}$ | $\tau_{uv, extrap}$ | $\tau_{uw, extrap}$ | $\tau_{vw, extrap}$ |
| **A3** | 5 | 5.9 | 0.07 | 0.08 | 0.16 | 0.00 | 0.00 | 0.16 | 0.19 | 0.23 | 0.16 | 0.04 | 0.10 |
| **B3** | 10 | 5.9 | 0.16 | 0.08 | 0.19 | 0.07 | 0.07 | 0.14 | 0.24 | 0.20 | 0.09 | 0.05 | 0.09 |
| **C3** | 15 | 5.9 | 0.14 | 0.07 | 0.22 | 0.09 | 0.09 | 0.17 | 0.19 | 0.27 | 0.16 | 0.11 | 0.11 |
| **D3** | 20 | 5.9 | 0.14 | 0.07 | 0.20 | 0.11 | 0.11 | 0.18 | 0.21 | 0.24 | 0.16 | 0.11 | 0.12 |
| **E3** | 25 | 5.9 | 0.37 | 0.08 | 0.20 | 0.10 | 0.10 | 0.14 | 0.20 | 0.28 | 0.15 | 0.10 | 0.11 |
| **A4** | 5 | 10.9 | 0.56 | 0.00 | 0.05 | 0.05 | 0.05 | 0.24 | 0.04 | 0.17 | 0.14 | -0.12 | 0.10 |
| **B4** | 10 | 10.9 | 0.58 | 0.00 | 0.06 | 0.05 | 0.05 | 0.19 | 0.08 | 0.13 | 0.14 | -0.12 | 0.08 |
| **C4** | 15 | 10.9 | 0.48 | 0.00 | 0.08 | 0.04 | 0.04 | 0.22 | 0.03 | 0.18 | 0.13 | -0.11 | 0.09 |
| **D4** | 20 | 10.9 | 0.48 | 0.00 | 0.06 | 0.05 | 0.05 | 0.18 | 0.12 | 0.17 | 0.14 | -0.09 | 0.10 |
| **E4** | 25 | 10.9 | 0.49 | 0.00 | 0.06 | 0.05 | 0.05 | 0.17 | 0.05 | 0.16 | 0.16 | -0.11 | 0.08 |
| **A5** | 5 | 15.9 | 0.04 | 0.00 | 0.04 | 0.00 | 0.00 | 0.21 | -0.01 | 0.14 | 0.21 | -0.14 | 0.13 |
| **B5** | 10 | 15.9 | 0.06 | 0.00 | 0.04 | 0.03 | 0.03 | 0.25 | -0.02 | 0.12 | 0.24 | -0.10 | 0.13 |
| **C5** | 15 | 15.9 | 0.08 | 0.00 | 0.04 | 0.04 | 0.04 | 0.23 | -0.04 | 0.14 | 0.20 | -0.11 | 0.13 |
| **D5** | 20 | 15.9 | 0.09 | 0.00 | 0.03 | 0.01 | 0.01 | 0.32 | -0.07 | 0.14 | 0.26 | -0.14 | 0.13 |
| **E5** | 25 | 15.9 | 0.07 | 0.00 | 0.06 | 0.01 | 0.01 | 0.20 | -0.01 | 0.13 | 0.23 | -0.12 | 0.13 |
| **A6** | 5 | 20.9 | 0.49 | 0.04 | 0.02 | 0.02 | 0.02 | 0.22 | -0.03 | 0.08 | 0.22 | -0.01 | 0.11 |
| **B6** | 10 | 20.9 | 0.72 | 0.04 | 0.03 | 0.02 | 0.02 | 0.14 | 0.02 | 0.08 | 0.20 | -0.02 | 0.12 |
| **C6** | 15 | 20.9 | 0.65 | 0.04 | 0.01 | 0.08 | 0.08 | 0.13 | 0.01 | 0.06 | 0.19 | 0.01 | 0.09 |
| **D6** | 20 | 20.9 | 0.57 | 0.04 | 0.03 | 0.01 | 0.01 | 0.15 | 0.01 | 0.08 | 0.20 | -0.01 | 0.10 |
| **E6** | 25 | 20.9 | 0.55 | 0.05 | 0.02 | 0.04 | 0.04 | 0.23 | -0.01 | 0.09 | 0.20 | 0.01 | 0.10 |

| | | | Boundary Shear Stress (Pa) | | | | | | | | | | |
|---|---|---|---|---|---|---|---|---|---|---|---|---|---|
| Location | x (cm) | y (cm) | $\tau_{TKE}$ | $\tau_{TKE, extrap}$ | $\tau_{TKE, w}$ | $\tau_{TKE, w, extrap}$ | $\tau_{uv,2cm}$ | $\tau_{uw,2cm}$ | $\tau_{vw,2cm}$ | $\tau_{TKE,2cm}$ | $\tau_{uv,4cm}$ | $\tau_{uw,4cm}$ | $\tau_{vw,4cm}$ | $\tau_{TKE,4cm}$ |
| **A3** | 5 | 5.9 | 0.21 | 0.18 | 0.45 | 0.54 | 0.25 | 0.15 | 0.06 | 1.11 | 0.22 | -0.11 | 0.07 | 1.06 |
| **B3** | 10 | 5.9 | 0.21 | 0.17 | 0.42 | 0.53 | 0.16 | 0.14 | 0.07 | 0.94 | 0.20 | -0.09 | 0.04 | 1.02 |
| **C3** | 15 | 5.9 | 0.24 | 0.22 | 0.51 | 0.61 | 0.29 | 0.06 | 0.10 | 1.10 | 0.31 | 0.04 | 0.04 | 1.41 |
| **D3** | 20 | 5.9 | 0.23 | 0.20 | 0.45 | 0.58 | 0.26 | 0.05 | 0.11 | 1.15 | 0.22 | 0.01 | 0.06 | 1.09 |
| **E3** | 25 | 5.9 | 0.23 | 0.20 | 0.48 | 0.56 | 0.25 | 0.07 | 0.12 | 1.10 | 0.25 | -0.01 | 0.06 | 1.19 |
| **A4** | 5 | 10.9 | 0.17 | 0.17 | 0.36 | 0.55 | 0.20 | -0.08 | 0.10 | 0.18 | 0.15 | -0.20 | 0.03 | 0.18 |
| **B4** | 10 | 10.9 | 0.17 | 0.17 | 0.33 | 0.55 | 0.20 | -0.12 | 0.10 | 0.18 | 0.17 | -0.28 | 0.07 | 0.18 |
| **C4** | 15 | 10.9 | 0.17 | 0.16 | 0.39 | 0.54 | 0.24 | -0.11 | 0.11 | 0.17 | 0.18 | -0.16 | 0.06 | 0.19 |
| **D4** | 20 | 10.9 | 0.19 | 0.17 | 0.37 | 0.52 | 0.19 | -0.06 | 0.12 | 0.17 | 0.17 | -0.19 | 0.02 | 0.19 |
| **E4** | 25 | 10.9 | 0.15 | 0.16 | 0.34 | 0.52 | 0.23 | -0.09 | 0.09 | 0.16 | 0.16 | -0.19 | 0.00 | 0.17 |
| **A5** | 5 | 15.9 | 0.13 | 0.15 | 0.31 | 0.43 | 0.25 | -0.17 | 0.14 | 0.17 | 0.12 | -0.20 | 0.05 | 0.15 |
| **B5** | 10 | 15.9 | 0.15 | 0.15 | 0.32 | 0.42 | 0.25 | -0.14 | 0.09 | 0.15 | 0.20 | -0.16 | 0.05 | 0.15 |
| **C5** | 15 | 15.9 | 0.13 | 0.14 | 0.34 | 0.42 | 0.19 | -0.07 | 0.08 | 0.12 | 0.19 | -0.17 | 0.06 | 0.15 |
| **D5** | 20 | 15.9 | 0.16 | 0.16 | 0.33 | 0.43 | 0.22 | -0.13 | 0.12 | 0.14 | 0.19 | -0.20 | 0.08 | 0.15 |
| **E5** | 25 | 15.9 | 0.13 | 0.14 | 0.30 | 0.39 | 0.24 | -0.11 | 0.13 | 0.15 | 0.16 | -0.24 | 0.08 | 0.15 |
| **A6** | 5 | 20.9 | 0.11 | 0.11 | 0.22 | 0.25 | 0.18 | 0.02 | 0.10 | 0.11 | 0.13 | -0.03 | 0.09 | 0.10 |
| **B6** | 10 | 20.9 | 0.09 | 0.12 | 0.22 | 0.26 | 0.21 | 0.00 | 0.09 | 0.12 | 0.14 | -0.03 | 0.05 | 0.10 |
| **C6** | 15 | 20.9 | 0.09 | 0.11 | 0.19 | 0.23 | 0.22 | -0.04 | 0.06 | 0.11 | 0.10 | -0.02 | 0.05 | 0.10 |
| **D6** | 20 | 20.9 | 0.09 | 0.11 | 0.20 | 0.24 | 0.18 | -0.04 | 0.08 | 0.11 | 0.17 | -0.08 | 0.06 | 0.11 |
| **E6** | 25 | 20.9 | 0.11 | 0.11 | 0.21 | 0.24 | 0.14 | 0.02 | 0.06 | 0.10 | 0.17 | -0.06 | 0.06 | 0.12 |

**Table D.3. Boundary shear stress measured with the CTA and estimated with the law of the wall, Reynolds, and turbulent kinetic energy methods along the shrub bank**

| | | | Boundary Shear Stress (Pa) | | | | | | | | | | |
|---|---|---|---|---|---|---|---|---|---|---|---|---|---|
| Location | x (cm) | y (cm) | $\tau_{CTA,Avg}$ | $\tau_{LOW, ADV}$ | $\tau_{LOW, ADV, 20\%}$ | $\tau_{LOW, MP}$ | $\tau_{LOW,MP,20\%}$ | $\tau_{uv}$ | $\tau_{uw}$ | $\tau_{vw}$ | $\tau_{uv, extrap}$ | $\tau_{uw, extrap}$ | $\tau_{vw, extrap}$ |
| **A3** | 5 | 5.9 | 0.30 | 0.25 | 0.13 | 0.23 | 0.10 | 1.08 | -0.04 | 0.73 | 0.88 | -0.11 | 0.27 |
| **B3** | 10 | 5.9 | 0.28 | 0.27 | 0.18 | 0.26 | 0.25 | 1.28 | -0.11 | 0.64 | 1.07 | -0.18 | 0.25 |
| **C3** | 15 | 5.9 | 0.38 | 0.28 | 0.13 | 0.13 | 0.00 | 0.72 | 0.32 | 0.49 | 0.90 | -0.01 | 0.28 |
| **D3** | 20 | 5.9 | 0.29 | 0.34 | 0.31 | 0.27 | 0.22 | 1.25 | -0.16 | 0.61 | 1.03 | -0.05 | 0.28 |
| **E3** | 25 | 5.9 | 0.23 | 0.32 | 0.29 | 0.15 | 0.04 | 1.42 | 0.04 | 0.52 | 1.02 | -0.09 | 0.33 |
| **A4** | 5 | 10.9 | 0.28 | 0.50 | 0.05 | 0.54 | 0.07 | 0.35 | -0.04 | 0.20 | 0.63 | -0.43 | 0.18 |
| **B4** | 10 | 10.9 | 0.23 | 0.36 | 0.05 | 0.70 | 0.01 | 0.37 | -0.08 | 0.24 | 0.66 | -0.39 | 0.14 |
| **C4** | 15 | 10.9 | 0.20 | 0.37 | 0.03 | 0.64 | 0.08 | 0.47 | -0.26 | 0.36 | 0.86 | -0.41 | 0.20 |
| **D4** | 20 | 10.9 | 0.23 | 0.29 | 0.01 | 0.01 | 4.40 | 1.06 | -0.65 | 0.67 | 0.92 | -0.59 | 0.33 |
| **E4** | 25 | 10.9 | 0.28 | 0.38 | 0.01 | 0.43 | 0.00 | 0.85 | -0.39 | 0.59 | 0.83 | -0.41 | 0.24 |
| **A5** | 5 | 15.9 | 0.24 | 0.15 | 0.00 | 0.73 | 0.56 | 0.10 | -0.02 | 0.05 | -0.19 | -0.23 | 0.09 |
| **B5** | 10 | 15.9 | 0.20 | 0.15 | 0.00 | 0.16 | 0.00 | 0.07 | -0.04 | 0.07 | -0.30 | -0.21 | 0.08 |
| **C5** | 15 | 15.9 | 0.29 | 0.15 | 0.00 | 0.01 | 1.18 | 0.03 | 0.01 | 0.08 | -0.26 | -0.17 | 0.08 |
| **D5** | 20 | 15.9 | 0.21 | 0.16 | 0.00 | 0.04 | 5.64 | 0.07 | 0.01 | 0.14 | -0.18 | -0.16 | 0.13 |
| **E5** | 25 | 15.9 | 0.21 | 0.24 | 0.01 | 0.14 | 0.75 | 0.00 | -0.01 | 0.14 | -0.19 | -0.20 | 0.14 |
| **A6** | 5 | 20.9 | 0.19 | 0.01 | 0.00 | 0.95 | 0.56 | 0.06 | -0.03 | 0.05 | 0.02 | 0.00 | 0.05 |
| **B6** | 10 | 20.9 | 0.17 | 0.02 | 0.00 | 2.47 | 18.85 | 0.00 | 0.00 | 0.04 | -0.01 | -0.03 | 0.04 |
| **C6** | 15 | 20.9 | 0.21 | 0.01 | 0.00 | 3.83 | 11.99 | 0.04 | -0.02 | 0.05 | 0.04 | 0.07 | 0.03 |
| **D6** | 20 | 20.9 | 0.18 | 0.01 | 0.00 | 5.91 | 0.00 | 0.01 | -0.01 | 0.04 | 0.01 | -0.02 | 0.03 |
| **E6** | 25 | 20.9 | 0.16 | 0.01 | 0.00 | 3.22 | 1.27 | -0.03 | 0.06 | 0.06 | 0.00 | 0.06 | 0.07 |

| | | | Boundary Shear Stress (Pa) | | | | | | | | | | | |
|---|---|---|---|---|---|---|---|---|---|---|---|---|---|---|
| Location | x (cm) | y (cm) | $\tau_{TKE}$ | $\tau_{TKE, extrap}$ | $\tau_{TKE, w}$ | $\tau_{TKE, w, extrap}$ | $\tau_{uv,2cm}$ | $\tau_{uw,2cm}$ | $\tau_{vw,2cm}$ | $\tau_{TKE,2cm}$ | $\tau_{uv,4cm}$ | $\tau_{uw,4cm}$ | $\tau_{vw,4cm}$ | $\tau_{TKE,4cm}$ |
| **A3** | 5 | 5.9 | 0.61 | 0.58 | 1.31 | 1.69 | 0.99 | -0.37 | 0.26 | 0.57 | 1.42 | -0.34 | 0.12 | 0.70 |
| **B3** | 10 | 5.9 | 0.59 | 0.63 | 1.23 | 1.81 | 0.94 | 0.13 | 0.08 | 0.54 | 1.31 | -0.63 | 0.06 | 0.83 |
| **C3** | 15 | 5.9 | 0.52 | 0.60 | 1.27 | 1.80 | 0.98 | -0.08 | 0.24 | 0.61 | 1.08 | -0.35 | 0.17 | 0.69 |
| **D3** | 20 | 5.9 | 0.59 | 0.64 | 1.27 | 1.85 | 0.78 | 0.02 | 0.15 | 0.56 | 1.58 | -0.54 | 0.24 | 0.82 |
| **E3** | 25 | 5.9 | 0.68 | 0.63 | 1.07 | 1.75 | 0.72 | -0.05 | 0.33 | 0.59 | 1.17 | -0.29 | 0.25 | 0.68 |
| **A4** | 5 | 10.9 | 0.23 | 0.37 | 0.72 | 1.33 | 0.52 | -0.31 | 0.18 | 0.34 | 1.21 | -0.19 | 0.08 | 0.57 |
| **B4** | 10 | 10.9 | 0.25 | 0.41 | 0.85 | 1.50 | 0.57 | -0.08 | 0.02 | 0.39 | 1.03 | -0.32 | -0.07 | 0.56 |
| **C4** | 15 | 10.9 | 0.28 | 0.46 | 0.93 | 1.60 | 0.64 | -0.25 | 0.17 | 0.45 | 1.65 | -0.29 | 0.00 | 0.71 |
| **D4** | 20 | 10.9 | 0.44 | 0.49 | 1.10 | 1.64 | 1.12 | -0.48 | 0.27 | 0.55 | 1.35 | 0.01 | -0.16 | 0.64 |
| **E4** | 25 | 10.9 | 0.39 | 0.45 | 1.10 | 1.54 | 0.43 | -0.41 | 0.13 | 0.40 | 1.69 | -0.53 | 0.02 | 0.73 |
| **A5** | 5 | 15.9 | 0.07 | -0.06 | 0.20 | 0.06 | 0.12 | -0.03 | 0.06 | 0.11 | 0.16 | -0.04 | -0.01 | 0.15 |
| **B5** | 10 | 15.9 | 0.06 | -0.09 | 0.17 | -0.05 | 0.04 | -0.03 | 0.01 | 0.07 | 0.13 | 0.02 | 0.03 | 0.10 |
| **C5** | 15 | 15.9 | 0.07 | -0.08 | 0.18 | -0.01 | 0.05 | 0.00 | 0.03 | 0.09 | 0.10 | 0.00 | 0.03 | 0.12 |
| **D5** | 20 | 15.9 | 0.10 | -0.06 | 0.34 | 0.07 | 0.10 | -0.01 | 0.06 | 0.10 | 0.37 | -0.08 | 0.14 | 0.18 |
| **E5** | 25 | 15.9 | 0.10 | -0.04 | 0.36 | 0.20 | 0.10 | -0.10 | 0.23 | 0.14 | 0.34 | 0.16 | -0.07 | 0.19 |
| **A6** | 5 | 20.9 | 0.05 | 0.04 | 0.16 | 0.09 | 0.03 | 0.08 | 0.02 | 0.07 | 0.08 | 0.02 | 0.01 | 0.09 |
| **B6** | 10 | 20.9 | 0.04 | 0.01 | 0.10 | 0.06 | 0.06 | -0.01 | 0.00 | 0.04 | 0.05 | 0.04 | -0.02 | 0.05 |
| **C6** | 15 | 20.9 | 0.03 | 0.05 | 0.09 | 0.11 | 0.00 | -0.07 | 0.00 | 0.04 | 0.00 | 0.05 | 0.02 | 0.06 |
| **D6** | 20 | 20.9 | 0.04 | 0.03 | 0.08 | 0.06 | 0.00 | -0.01 | 0.02 | 0.03 | 0.03 | 0.02 | -0.01 | 0.04 |
| **E6** | 25 | 20.9 | 0.06 | 0.03 | 0.12 | 0.07 | 0.02 | 0.01 | 0.00 | 0.05 | 0.06 | 0.05 | -0.03 | 0.07 |

**Table D.4. Boundary shear stress measured with the CTA and estimated with the law of the wall, Reynolds, and turbulent kinetic energy methods along the grass bank**

| | | | Boundary Shear Stress (Pa) | | | | | | | | | | |
|---|---|---|---|---|---|---|---|---|---|---|---|---|---|
| Location | x (cm) | y (cm) | $\tau_{CTA,Avg}$ | $\tau_{LOW, ADV}$ | $\tau_{LOW, ADV, 20\%}$ | $\tau_{LOW, MP}$ | $\tau_{LOW,MP,20\%}$ | $\tau_{uv}$ | $\tau_{uw}$ | $\tau_{vw}$ | $\tau_{uv, extrap}$ | $\tau_{uw, extrap}$ | $\tau_{vw, extrap}$ |
| A3 | 5 | 5.9 | 0.94 | NaN | NaN | 3.39 | 0.75 | NaN | NaN | NaN | NaN | NaN | NaN |
| B3 | 10 | 5.9 | 0.80 | NaN | NaN | 0.00 | 0.20 | NaN | NaN | NaN | NaN | NaN | NaN |
| C3 | 15 | 5.9 | 0.82 | NaN | 0.12 | 0.37 | 25.47 | -0.01 | 0.01 | 0.02 | NaN | NaN | NaN |
| D3 | 20 | 5.9 | 0.71 | NaN | 0.07 | 1.49 | 10.12 | -0.01 | -0.06 | -0.02 | NaN | NaN | NaN |
| E3 | 25 | 5.9 | 1.04 | NaN | 0.02 | 2.29 | 2.64 | 0.00 | 0.00 | 0.00 | NaN | NaN | NaN |
| A4 | 5 | 10.9 | 2.15 | NaN | 0.03 | 0.53 | 25.05 | 0.04 | 0.26 | 0.00 | NaN | NaN | NaN |
| B4 | 10 | 10.9 | 1.48 | NaN | NaN | 0.94 | 3.59 | NaN | NaN | NaN | NaN | NaN | NaN |
| C4 | 15 | 10.9 | 1.18 | NaN | NaN | 0.81 | 5.64 | NaN | NaN | NaN | NaN | NaN | NaN |
| D4 | 20 | 10.9 | 1.49 | NaN | 0.32 | 0.03 | 1.38 | 0.15 | 0.50 | -0.08 | NaN | NaN | NaN |
| E4 | 25 | 10.9 | 1.52 | NaN | NaN | 0.20 | 4.23 | NaN | NaN | NaN | NaN | NaN | NaN |
| A5 | 5 | 15.9 | 1.90 | NaN | NaN | 0.34 | 17.37 | NaN | NaN | NaN | NaN | NaN | NaN |
| B5 | 10 | 15.9 | 1.75 | NaN | NaN | 1.98 | 0.00 | NaN | NaN | NaN | NaN | NaN | NaN |
| C5 | 15 | 15.9 | 1.94 | NaN | NaN | 1.02 | 16.69 | NaN | NaN | NaN | NaN | NaN | NaN |
| D5 | 20 | 15.9 | 1.55 | NaN | NaN | 0.36 | 20.10 | NaN | NaN | NaN | NaN | NaN | NaN |
| E5 | 25 | 15.9 | 1.63 | NaN | NaN | 1.55 | 8.76 | NaN | NaN | NaN | NaN | NaN | NaN |
| A6 | 5 | 20.9 | 2.14 | NaN | NaN | 4.57 | 1.25 | NaN | NaN | NaN | NaN | NaN | NaN |
| B6 | 10 | 20.9 | 2.04 | NaN | NaN | 0.45 | 0.96 | NaN | NaN | NaN | NaN | NaN | NaN |
| C6 | 15 | 20.9 | 1.90 | NaN | NaN | 5.91 | 0.30 | NaN | NaN | NaN | NaN | NaN | NaN |
| D6 | 20 | 20.9 | 1.69 | NaN | NaN | 0.04 | 0.15 | NaN | NaN | NaN | NaN | NaN | NaN |
| E6 | 25 | 20.9 | 1.59 | NaN | NaN | 4.28 | 7.47 | NaN | NaN | NaN | NaN | NaN | NaN |

| | | | Boundary Shear Stress (Pa) | | | | | | | | | | | |
|---|---|---|---|---|---|---|---|---|---|---|---|---|---|---|
| Location | x (cm) | y (cm) | $\tau_{TKE}$ | $\tau_{TKE, extrap}$ | $\tau_{TKE, w}$ | $\tau_{TKE, w, extrap}$ | $\tau_{uv,2cm}$ | $\tau_{uw,2cm}$ | $\tau_{vw,2cm}$ | $\tau_{TKE,2cm}$ | $\tau_{uv,4cm}$ | $\tau_{uw,4cm}$ | $\tau_{vw,4cm}$ | $\tau_{TKE,4cm}$ |
| A3 | 5 | 5.9 | NaN | NaN | NaN | NaN | NaN | NaN | NaN | NaN | -0.01 | 0.00 | 0.00 | 0.01 |
| B3 | 10 | 5.9 | NaN | NaN | NaN | NaN | -0.01 | -0.02 | 0.00 | 0.01 | -0.16 | -0.69 | -0.14 | 0.17 |
| C3 | 15 | 5.9 | 0.02 | NaN | NaN | NaN | -0.04 | -0.13 | -0.01 | 0.05 | -0.02 | -0.06 | -0.01 | 0.03 |
| D3 | 20 | 5.9 | 0.02 | NaN | NaN | NaN | 0.05 | 0.11 | -0.03 | 0.05 | 0.01 | 0.00 | -0.01 | 0.03 |
| E3 | 25 | 5.9 | 0.01 | NaN | NaN | NaN | -0.04 | -0.13 | -0.03 | 0.05 | 0.02 | 0.06 | 0.00 | 0.08 |
| A4 | 5 | 10.9 | 0.08 | NaN | NaN | NaN | NaN | NaN | NaN | NaN | 0.00 | 0.00 | 0.00 | 0.01 |
| B4 | 10 | 10.9 | NaN | NaN | NaN | NaN | NaN | NaN | NaN | NaN | 0.01 | 0.02 | -0.03 | 0.03 |
| C4 | 15 | 10.9 | NaN | NaN | NaN | NaN | 0.00 | 0.00 | 0.00 | 0.01 | 0.00 | 0.03 | -0.01 | 0.03 |
| D4 | 20 | 10.9 | 0.15 | NaN | NaN | NaN | 0.05 | 0.12 | -0.09 | 0.08 | 0.17 | 0.55 | -0.52 | 0.39 |
| E4 | 25 | 10.9 | NaN | NaN | NaN | NaN | NaN | NaN | NaN | NaN | -0.01 | -0.03 | -0.01 | 0.02 |
| A5 | 5 | 15.9 | NaN | NaN | NaN | NaN | NaN | NaN | NaN | NaN | NaN | NaN | NaN | NaN |
| B5 | 10 | 15.9 | NaN | NaN | NaN | NaN | 0.00 | 0.00 | 0.00 | 0.00 | 0.00 | 0.00 | -0.01 | 0.01 |
| C5 | 15 | 15.9 | NaN | NaN | NaN | NaN | NaN | NaN | NaN | NaN | NaN | NaN | NaN | NaN |
| D5 | 20 | 15.9 | NaN | NaN | NaN | NaN | NaN | NaN | NaN | NaN | NaN | NaN | NaN | NaN |
| E5 | 25 | 15.9 | NaN | NaN | NaN | NaN | NaN | NaN | NaN | NaN | NaN | NaN | NaN | NaN |
| A6 | 5 | 20.9 | NaN | NaN | NaN | NaN | NaN | NaN | NaN | NaN | NaN | NaN | NaN | NaN |
| B6 | 10 | 20.9 | NaN | NaN | NaN | NaN | NaN | NaN | NaN | NaN | NaN | NaN | NaN | NaN |
| C6 | 15 | 20.9 | NaN | NaN | NaN | NaN | NaN | NaN | NaN | NaN | NaN | NaN | NaN | NaN |
| D6 | 20 | 20.9 | NaN | NaN | NaN | NaN | NaN | NaN | NaN | NaN | NaN | NaN | NaN | NaN |
| E6 | 25 | 20.9 | NaN | NaN | NaN | NaN | NaN | NaN | NaN | NaN | NaN | NaN | NaN | NaN |

*NaN=not a number

## Appendix E: Boundary shear stress calculations using the ray-isovel method

**Table E.1. Shear stress calculated from velocity field measured by the MicroADV where A is the area between rays and isovels, $\delta_{pb}$ is the incremental length along the wetted perimeter, and BSS is the boundary shear stress.**

| | Bare | | | Tree | | | | | | Shrub | | | | | |
|---|---|---|---|---|---|---|---|---|---|---|---|---|---|---|---|
| Location | A $cm^2$ | $\delta p_b$ cm | BSS Pa | A $cm^2$ | $\delta p_b$ cm | $u_{ref}$ m/s | Total stress Pa | Vegetation stress Pa | BSS Pa | A $cm^2$ | $\delta p_b$ cm | $u_{ref}$ m/s | Total stress Pa | Vegetation stress Pa | BSS Pa |
| A1 | 18.90 | 5.63 | 1.65 | 16.51 | 5.94 | 0.15 | 1.36 | 0.04 | 1.32 | 16.03 | 5.63 | 0.13 | 1.40 | 1.04 | 0.36 |
| A2 | 24.21 | 6.56 | 1.81 | 20.81 | 6.56 | 0.15 | 1.55 | 0.04 | 1.51 | 10.81 | 1.56 | 0.08 | 3.39 | 0.91 | 2.48 |
| A3 | 11.09 | 3.13 | 1.74 | 29.30 | 6.56 | 0.15 | 2.19 | 0.06 | 2.13 | 21.02 | 5.31 | 0.05 | 1.94 | 0.23 | 1.71 |
| A4 | 16.63 | 4.38 | 1.86 | 4.60 | 2.19 | 0.13 | 1.03 | 0.02 | 1.01 | 26.10 | 8.13 | 0.03 | 1.57 | 0.05 | 1.53 |
| B1 | 19.29 | 5.63 | 1.68 | 17.14 | 6.25 | 0.15 | 1.34 | 0.04 | 1.31 | 18.43 | 5.63 | 0.13 | 1.61 | 1.19 | 0.41 |
| B2 | 27.10 | 6.56 | 2.02 | 22.40 | 6.56 | 0.15 | 1.67 | 0.05 | 1.63 | 10.42 | 3.75 | 0.08 | 1.36 | 0.36 | 1.00 |
| B3 | 15.12 | 3.75 | 1.98 | 8.38 | 3.75 | 0.13 | 1.09 | 0.02 | 1.07 | 14.88 | 3.75 | 0.05 | 1.94 | 0.23 | 1.71 |
| B4 | 15.73 | 4.69 | 1.64 | 9.62 | 2.50 | 0.13 | 1.89 | 0.04 | 1.85 | NA | NA | NA | NA | NA | NA |
| C 1 | 19.76 | 6.25 | 1.55 | 15.60 | 5.94 | 0.15 | 1.29 | 0.04 | 1.25 | 24.84 | 6.56 | 0.13 | 1.86 | 1.38 | 0.48 |
| C 2 | 25.90 | 6.56 | 1.93 | 18.41 | 6.56 | 0.15 | 1.37 | 0.04 | 1.34 | NA | NA | NA | NA | NA | NA |
| C 3 | 14.07 | 3.13 | 2.21 | 17.96 | 4.06 | 0.15 | 2.17 | 0.06 | 2.11 | NA | NA | NA | NA | NA | NA |
| C 4 | 12.31 | 2.81 | 2.14 | 24.19 | 1.31 | 0.13 | 9.03 | 0.17 | 8.86 | NA | NA | NA | NA | NA | NA |
| D1 | 20.15 | 5.63 | 1.75 | 16.08 | 5.63 | 0.15 | 1.40 | 0.04 | 1.36 | 15.14 | 4.69 | 0.13 | 1.58 | 1.18 | 0.41 |
| D2 | 24.95 | 6.56 | 1.86 | 18.34 | 6.56 | 0.15 | 1.37 | 0.04 | 1.33 | 9.93 | 3.13 | 0.10 | 1.56 | 0.74 | 0.82 |
| D3 | 11.54 | 3.13 | 1.81 | 25.35 | 6.25 | 0.15 | 1.99 | 0.05 | 1.93 | 16.78 | 5.63 | 0.05 | 1.46 | 0.17 | 1.29 |
| D4 | 12.63 | 3.13 | 1.98 | 13.49 | 3.75 | 0.13 | 1.76 | 0.03 | 1.73 | 13.92 | 5.94 | 0.03 | 1.15 | 0.03 | 1.11 |
| E1 | 19.94 | 5.94 | 1.65 | 16.15 | 5.94 | 0.15 | 1.33 | 0.04 | 1.30 | 16.72 | 5.00 | 0.13 | 1.64 | 1.22 | 0.42 |
| E2 | 26.49 | 6.56 | 1.98 | 17.96 | 6.56 | 0.15 | 1.34 | 0.04 | 1.30 | 7.99 | 2.50 | 0.08 | 1.57 | 0.42 | 1.15 |
| E3 | 12.83 | 3.13 | 2.01 | 21.72 | 6.25 | 0.15 | 1.70 | 0.05 | 1.66 | NA | NA | NA | NA | NA | NA |
| E4 | 18.38 | 4.69 | 1.92 | 8.06 | 2.50 | 0.13 | 1.58 | 0.03 | 1.55 | NA | NA | NA | NA | NA | NA |

*NA=not calculated

*$\alpha_{tree}$=0.1 $m^{-1}$

*$\alpha_{shrub}$=3.89 $m^{-1}$

**Table E.2. Shear stress calculated from velocity field measured by the miniature propeller where A is the area between rays and isovels, $\delta_{pb}$ is the incremental length along the wetted perimeter, and BSS is the boundary shear stress.**

| | | Bare | | | Tree | | | | | | Shrub | | | | | |
|---|---|---|---|---|---|---|---|---|---|---|---|---|---|---|---|---|
| Cross-section | Location | A $cm^2$ | $\delta_{pb}$ cm | BSS Pa | A $cm^2$ | $\delta_{pb}$ cm | $u_{ref}$ m/s | Total stress Pa | Vegetation stress Pa | BSS Pa | A $cm^2$ | $\delta_{pb}$ cm | $u_{ref}$ m/s | Total stress Pa | Vegetation stress Pa | BSS Pa |
| A | 1 | 27.08 | 5.63 | 2.36 | 17.74 | 5.94 | 0.15 | 1.46 | 0.04 | 1.42 | 13.85 | 4.06 | 0.13 | 1.67 | 1.24 | 0.43 |
| A | 2 | 36.48 | 6.56 | 2.72 | 12.22 | 4.06 | 0.15 | 1.47 | 0.04 | 1.43 | 9.11 | 3.13 | 0.08 | 1.43 | 0.38 | 1.05 |
| A | 3 | 16.71 | 3.13 | 2.62 | NA | NA | NA | NA | NA | NA | 42.90 | 5.94 | 0.05 | 3.54 | 0.42 | 3.12 |
| A | 4 | 16.72 | 3.13 | 2.62 | NA | NA | NA | NA | NA | NA | 12.76 | 4.06 | 0.03 | 1.54 | 0.05 | 1.49 |
| B | 1 | 25.68 | 5.63 | 2.24 | 16.26 | 5.63 | 0.15 | 1.42 | 0.04 | 1.38 | 14.50 | 4.69 | 0.10 | 1.52 | 0.72 | 0.79 |
| B | 2 | 33.19 | 6.56 | 2.48 | 19.07 | 6.56 | 0.15 | 1.42 | 0.04 | 1.38 | 14.92 | 3.13 | 0.05 | 2.34 | 0.28 | 2.06 |
| B | 3 | 17.93 | 3.13 | 2.81 | 9.53 | 5.00 | 0.13 | 0.93 | 0.02 | 0.92 | 28.67 | 3.75 | 0.05 | 3.75 | 0.45 | 3.30 |
| B | 4 | NA | NA | NA | 16.14 | 4.69 | 0.13 | 1.69 | 0.03 | 1.65 | 33.91 | 3.13 | 0.03 | 5.32 | 0.16 | 5.16 |
| C | 1 | 25.88 | 5.31 | 2.39 | 14.00 | 5.63 | 0.15 | 1.22 | 0.03 | 1.19 | 15.60 | 2.81 | 0.05 | 2.72 | 0.32 | 2.39 |
| C | 2 | 35.45 | 6.56 | 2.65 | 21.47 | 6.53 | 0.15 | 1.61 | 0.04 | 1.57 | 11.14 | 1.88 | 0.05 | 2.91 | 0.35 | 2.56 |
| C | 3 | 16.23 | 3.13 | 2.54 | 14.06 | 4.38 | 0.13 | 1.57 | 0.03 | 1.54 | 20.07 | 3.13 | 0.03 | 3.15 | 0.09 | 3.05 |
| C | 4 | 15.16 | 3.13 | 2.38 | 9.01 | 3.44 | 0.10 | 1.28 | 0.02 | 1.27 | 15.80 | 2.81 | 0.03 | 2.75 | 0.08 | 2.67 |
| D | 1 | 27.80 | 5.63 | 2.42 | 14.76 | 5.63 | 0.15 | 1.29 | 0.04 | 1.25 | 18.94 | 4.69 | 0.13 | 1.98 | 1.47 | 0.51 |
| D | 2 | 40.11 | 6.56 | 2.99 | 20.43 | 6.53 | 0.15 | 1.53 | 0.04 | 1.49 | 11.17 | 2.81 | 0.05 | 1.95 | 0.23 | 1.71 |
| D | 3 | 14.48 | 3.13 | 2.27 | 14.13 | 3.44 | 0.15 | 2.01 | 0.06 | 1.96 | 20.38 | 5.00 | 0.03 | 2.00 | 0.06 | 1.94 |
| D | 4 | 16.19 | 4.06 | 1.95 | 12.23 | 4.06 | 0.10 | 1.48 | 0.02 | 1.46 | 20.21 | 3.75 | 0.03 | 2.64 | 0.08 | 2.56 |
| E | 1 | 27.61 | 5.50 | 2.46 | 13.23 | 5.63 | 0.15 | 1.15 | 0.03 | 1.12 | 38.22 | 12.50 | 0.10 | 1.50 | 0.71 | 0.78 |
| E | 2 | 32.25 | 6.50 | 2.43 | 8.44 | 4.06 | 0.15 | 1.02 | 0.03 | 0.99 | NA | NA | NA | NA | NA | NA |
| E | 3 | 15.46 | 3.25 | 2.33 | 13.11 | 4.38 | 0.13 | 1.47 | 0.03 | 1.44 | NA | NA | NA | NA | NA | NA |
| E | 4 | 21.36 | 5.75 | 1.82 | 11.44 | 4.06 | 0.10 | 1.38 | 0.02 | 1.36 | NA | NA | NA | NA | NA | NA |

*NA=not calculated

*$\alpha_{tree}$=0.1 $m^{-1}$

* $\alpha_{shrub}$=3.89 $m^{-1}$